SEPTEMBER 2023

Ph.D. in Civil Engineering

SÜLEYMAN DEMİR

REPUBLIC OF TÜRKİYE

GAZİANTEP UNIVERSITY

GRADUATE SCHOOL OF NATURAL & APPLIED SCIENCES

EFFECT OF THE WASTE GLASS ON ENGINEERING PROPERTIES OF A BENTONITE

Ph.D. THESIS

IN

CIVIL ENGINEERING

BY

SÜLEYMAN DEMİR

EFFECT OF THE WASTE GLASS ON ENGINEERING PROPERTIES OF A BENTONITE

Ph.D. Thesis

in

Civil Engineering

Gaziantep University

Supervisor

Prof. Dr. Ali Fırat ÇABALAR

by

Süleyman DEMİR

©2023[Gaziantep University]

EFFECT OF THE WASTE GLASS ON ENGINEERING PROPERTIES OF A BENTONITE

submitted by **Süleyman DEMİR** in partial fulfillment of the requirements for the degree of Doctor of Philosophy in **Civil Engineering, Gaziantep University** is approved by,

Prof. Dr. Çiğdem AYKAÇ
Director of the Graduate School of Natural and Applied Sciences ………...............

Prof. Dr. Nildem TAYŞİ
Head of the Department of Civil Engineering ………...............

Prof. Dr. Ali Fırat ÇABALAR
Supervisor, Civil Engineering ………...............
Gaziantep University

Exam Date: 15.09.2023

Examining Committee Members:

Prof. Dr. Selim ALTUN
Ege University ………...............

Prof. Dr. Ali Fırat ÇABALAR
Gaziantep University ………...............

Assoc. Prof. Dr. Eyyüb KARAKAN
Kilis 7 Aralık University ………...............

Assoc. Prof. Dr. Talha EKMEKYAPAR
Gaziantep University ………...............

Assist. Prof. Dr. Özgür Yıldız
Malatya Turgut Özal University ………...............

I hereby declare that all information in this document has been obtained and presented in accordance with academic rules and ethical conduct. I also declare that, as required by these rules and conduct, I have fully cited and referenced all material and results that are not original to this work.

Süleyman DEMİR

ABSTRACT

EFFECT OF THE WASTE GLASS ON ENGINEERING PROPERTIES OF A BENTONITE

DEMİR, Süleyman
Ph.D. in Civil Engineering
Supervisor: Prof. Dr. Ali Fırat ÇABALAR
September 2023

210 pages

This thesis presents some engineering properties of bentonite-glass mixtures. The waste glass (WG) with two different sizes (Fine WG-FWG and Coarse WG-CWG) was mixed with bentonite at ratios of 0%, 10%, 20%, 30%, and 40%. A series of laboratory tests including compaction, fall-cone, consolidation, direct shear, crumb, double hydrometer, viscosity, unconfined compression (UC), and bender element (BE) tests were performed on the specimens. Testing results showed that WG additions increased the maximum dry unit weight (γ_{dmax}) of bentonite. Consolidation testing results showed decrement in void ratio with WG additions. Maximum unconfined compressive strength (q_u) value of the specimens was obtained at bentonite-30% CWG mixture. Angle of internal friction of bentonite increased until 30% WG content and then decreased. The dynamic viscosity and dispersion potential of bentonite decreased with WG additions. Shear wave velocity (v_s) and compressional wave velocity (v_p) values of bentonite increased with WG additions. The v_p to v_s ratio of the specimens varied between 2.0 and 2.5, thus, yielding Poisson's ratios (υ) from 0.33 to 0.40. Effect of a medium plastic silt (ML) at 0%, 10%, 20%, 30%, 40%, and 50% mixture ratios on the triaxial behavior of a sand were also presented. The undrained triaxial tests (CU) tests showed that addition of ML decreased the deviatoric stress of Narlı sand. Furthermore, mixtures with the ML showed more contractive behaviour.

Key Words: Waste glass, Sand, Clay, Geotechnical Properties.

ÖZET

ATIK CAMIN BENTONİTİN MÜHENDİSLİK ÖZELLİKLERİ ÜZERİNDEKİ ETKİSİ

DEMİR, Süleyman
Doktora Tezi, İnşaat Mühendisliği
Danışman: Prof. Dr. Ali Fırat ÇABALAR
Eylül 2023

210 sayfa

Bu tez, bentonit-cam karışımlarının bazı mühendislik özelliklerini sunmaktadır. İki farklı dane çapı dağılımına sahip (İnce atık cam-FWG ve kaba atık cam-CWG) atık cam (WG) %0, %10, %20, %30 ve %40 oranlarında bentonit ile karıştırılmıştır. Numuneler üzerinde sıkıştırma, düşen koni, konsolidasyon, direk kesme, dağılma, çifte hidrometre, serbest basınç (UC) ve bender eleman (BE) testlerini içeren bir dizi laboratuvar testi yapılmıştır. Test sonuçları, WG ilavelerinin bentonitin en büyük kuru birim ağırlığını (γ_{dmax}) arttırdığını göstermiştir. Konsolidasyon test sonuçları, WG ilaveleri ile bentonitin boşluk oranında azalma göstermektedir. Numuneler arasında en büyük serbest basınç dayanımı (q_u) değeri, bentonit-%30 CWG karışımında elde edilmiştir. Bentonitin içsel sürtünme açısı %30 WG içeriğine kadar artmış ve sonra azalmıştır. Bentonitin dinamik viskozitesi ve dispersiyon potansiyeli, WG ilaveleri ile azalmıştır. Bentonitin kayma dalgası hızı (v_s) ve sıkıştırma dalgası hızı (v_p) değerleri WG ilaveleri ile artmıştır. Numunelerin v_p/v_s oranı 2,0 ile 2,5 arasında değişirken, Poisson oranları (υ) 0,33 ile 0,40 arasında elde edilmiştir. Çalışmada ayrıca %0, %10, %20, %30, %40 ve %50 karışım oranlarında kullanılan orta plastik siltin (ML) bir kumun üç eksenli davranışı üzerindeki etkisi de sunulmuştur. Drenajsız üç eksenli (CU) testleri, ML ilavelerinin Narlı kumunun deviatörik gerilmesinin azalttığını göstermiştir. Bunun yanında ML ilaveleri ile karışımlar daha çok hacimsel daralma davranışı göstermiştir.

Anahtar Kelimeler: Atık cam, Kum, Kil, Geoteknik özellikler.

''Dedicated to my family''

ACKNOWLEDGEMENTS

I want to thank my supervisor, Prof. Dr. Ali Fırat ÇABALAR, for everything. I am grateful for the opportunity to collaborate with him. I owe him gratitude for his kind and patient attitude, long discussions about testing results, his constant encouragement, and his overall contribution to my Ph.D. thesis.

I must acknowledge the financial assistance of the Scientific research projects governing unit (BAPYB) of the Gaziantep University.

I would like to thank my family, my mother, father, and brother, for their continued encouragement throughout this journey. Thank you all for your patience and constant support during my Ph.D. research journey.

TABLE OF CONTENTS

LIST OF TABLES

Page

LIST OF FIGURES

Page*

LIST OF SYMBOLS

γ_{dmax}	Maximum dry unit weight (kN/m^3)
φ	Angle of internal friction ($^\circ$)
G_{max}	Maximum shear modulus (MPa)
LL	Liquid limit (%)
PL	Plastic limit (%)
PI	Plasticity index (%)
w_{opt}	Optimum water content (%)
c_c	Compression index (m^2/kN)
c_s	Swelling index (m^2/kN)
k	Hydraulic conductivity (cm/s)
c_v	Coefficient of consolidation (cm^2/s)
q_u	Unconfined compressive strength (kPa)
v_s	Shear wave velocity (m/s)
v_p	Compressional wave velocity (m/s)
M_{max}	Maximum constrained modulus (MPa)
L	Length between two BE tips (mm)
t	Wave travel time (ms)
υ	Poisson's ratio
C_c	Coefficient of curvature
C_u	Coefficient of uniformity
D_{10}	Diameter corresponding to 10% passing (mm)
D_{30}	Diameter corresponding to 30% passing (mm)
D_{60}	Diameter corresponding to 60% passing (mm)
V	Volt
mV	Millivolt
s	Second
ms	Millisecond
e_g	Intergranular void ratio
e_{max}	Maximum void ratio

$\mathbf{e_f}$	Interfine void ratio
$\mathbf{e^*}$	Equivalent void ratio
$\mathbf{M_{CS}}$	Stress ratio at the critical state
$\boldsymbol{\phi_{CS}}$	Friction angle at critical state

LIST OFABBREVIATIONS

CO_2	Carbon dioxide
EU	European union
SEM	Scanning electron microscope
UC	Unconfined compression
CBR	California bearing ratio
ECS	Effective consolidation stress
CU	Consolidated undrained triaxial test
CD	Consolidated drained triaxial test
CWG	Coarse waste glass
FWG	Fine waste glass
BE	Bender element
WG	Waste glass
NS	Narlı sand
ML	Medium plastic silt
LVDT	Linear variable differential transformer
LDS	Linear displacement sensor
RD	Relative density
EDX	Energy dispersive x-ray

CHAPTER 1
INTRODUCTION

1.1 Motivation of Study

There are numerous soil types encountered in the field. The grain size of the soil generally plays an important role in the suitability of the soil for engineering designs. Fine-grained soils (e.g., clay) in general have a lower bearing capacity, high compressibility and swelling (i.e., deformation), and lower permeability than those of coarse-grained soils (gravel, sand). As a result, coarse-grained soil, rock or stabilized-fine-grained soils are preferred in the foundation of the engineering designs.

In the field, coarse-grained soils are typically employed to stabilize fine-grained soils. Although coarse-grained soils are a safe type of soil for engineering designs, coarse-grained soils are typically obtained by grinding natural resources such as mines and quarries. There are so many natural resources used around the world that there is a concern that natural resources will be depleted soon (Arulrajah et al. 2012a). Therefore, numerous researchers have investigated reducing the demand for natural resources by incorporating sustainable and environmentally friendly materials into engineering designs.

Waste materials can be characterized as materials that are unused after an application or manufacture. If a waste is not recycled or reused, it is usually stored or burned in landfills. However, these types of actions have a negative impact on the environment, such as air and water pollution, and climate change (Tan and Khoo, 2006; Brooks et al., 2010; Modarres and Nosoudy, 2015). First of all, landfills have been a source of hazardous gases such as carbon dioxide (CO_2) and methane. Meanwhile, landfills are thought to produce 10%-15% of total metal emissions which are more dangerous than carbon dioxide (Rawat et al. 2008). Second, waste degradation could have major environmental consequences (Demirbas, 2011). Additionally, several contaminants are created during trash incineration (Tan and Khoo, 2006). Aside from these negative environmental impacts, waste management, which includes waste collection, deposition, transportation, landfilling, and incineration, is associated with a significant economic challenge (Tan and Khoo, 2006; Geng et al. 2012; Pan et al. 2015). Despite the negative environmental impact of waste materials, multiple studies suggest that the production of waste materials is increasing.

Many researchers have investigated ways to incorporate waste materials into various engineering designs, and it is well known that waste recycling and reuse are prioritized by policies. Using waste materials in engineering designs reduces (i) the need for natural aggregates and thereby the use of natural resources in the designs, (ii) the amount of landfilling and thereby the adverse environmental effects, and (iii) the substantial financial burden of disposing of waste materials. Tan and Khoo (2006) conducted a life cycle assessment on waste materials and concluded that recycling is the best solution for waste materials. Engineering designs are one of the many areas where waste materials are recycled and used. Waste materials have been studied in a variety of engineering principles, including structures (concrete, foundation), retaining structures, and road pavements. Because some waste materials have similar engineering properties to natural aggregates, waste materials are commonly used in concrete instead of aggregates. Waste materials, on the other hand, can be used in soil mechanics in a variety of ways, including as an additive material to stabilize problematic soils and as a backfill material in retaining walls.

Stabilizing problematic soils with waste materials reduces the demand for traditional stabilizing chemicals such as lime and cement. Cement, for example, works as a binder in concrete or soil as a result of the chemical reaction it undergoes with water. It binds the soil grains together, reduces voids, and so increases bearing capacity. However, because CO2 emissions from cement production account for 5 to 8% of global emissions, researchers have been investigating sustainable materials in recent years (Miller et al. 2018; Mohammed et al., 2019; Pillai et al. 2019). As a result, one of the objectives of using waste materials in engineering fields such as geotechnical engineering is to reduce the demand for cement.

Glass is well-known for being one of the most sustainable products in the world (Khatib, 2016). Furthermore, the waste of glass known as waste glass (WG) is one of the most easily produced and recyclable waste materials in the world. WG can be a municipal waste as well as construction and demolition waste. WG is estimated to account for about 5% of all waste globally (Kaza et al., 2018). There has been a rise in the utilization of glass waste in recycling and engineering applications in recent years. WG is extensively employed in concrete and asphalt pavements, according to the literature. Aside from these areas, studies on the use of WG in some technical applications such as ground improvement, deep mixing, road paving, and retaining walls have been conducted (Kazmi et al., 2020).

Mixing two different materials for soil development requires substantial investigation and the possible identification of a transition zone between the two materials. A variety of factors influence the engineering properties of such a binary mixture. For example, Lupini et al. (1981) divides the behavior of a mixture consisting of round and platy particles into three zones. When round particles dominate the behavior, the shear strength of the mixture is primarily controlled by the inter-particle coefficient and round particle shape parameters. When the platy particles control the overall behaviour of the soil mixture, the sliding mode governs the overall behavior of the platy (i.e., the particle with a low inter-particle coefficient). The behavior is primarily governed by mineralogy, pore water chemistry, and platy particle inter-particle friction. Finally, transition zones exist when no single soil type dominates soil behavior. Several studies have been conducted to study the mixing of two different soil types that may be found in the field (Kuerbis and White 1989, Thevanayagam, 1998; Thevanayagam, 2000; Thevanayagam and Mohan, 2000; Simoni and Houlsby, 2006; Monkul and Ozden, 2007; Rahman et al., 2008; Cabalar, 2011; Cabalar et al., 2013). The concept of intergranular void ratio explains the optimal fine content that fills the void ratio of granular materials. According to the hypothesis, the transition fine content is determined by the intergranular void ratio (e_g) of the mixture is equal to the maximum void ratio (e_{max}) of the host material. The boundary between different soil combinations, such as sand-clay, sand-silt, and clay-silt, has been the subject of numerous research. These experiments demonstrated that the testing outcomes are significantly influenced by the transition zone of the mixtures.

1.2 Aim of the Thesis

The following are the objectives of this thesis:

1. Suggesting and investigating the use of an alternative sustainable admixture material, Waste glass (WG), with bentonite.

2. Investigating the effect of the size of WG on the engineering properties of bentonite-WG mixtures.

3. Investigating the transitional behaviour of a sand-silt mixture with the Consolidated undrained (CU) triaxial tests.

1.3 Organization of the Thesis

This thesis presents six chapters namely; introduction, literature review, materials and method, results and discussion, conclusions and recommendation for future works. The introduction presents an overview of the thesis, focused on the research questions. The literature review provides the number of studies and their results related to the research subject of this thesis. Within the literature review, the use of WG, bentonite in engineering applications, and triaxial testing of sand-silt mixtures are presented. The materials and method section provides the detailed procedure of testing methods and some properties of the materials used in this study. The results and discussion section gives the testing results of the thesis and a discussion of the results. Each test result is presented in a rationale section which goes over the reason for employing such a test in the study, results and discussion. The conclusion section of the thesis presents the main conclusions from the study. Finally, the recommendation for future works section suggests some research ideas for researchers.

CHAPTER 2
LITERATURE REVIEW

2.1 Generation of Waste Materials

Waste production is increasing in many parts of the world in direct proportion to the global population, economic development, and urbanization (Blanchard, 1992; Singh et al., 2014; Cole et al., 2019). Figure 2.1 depicts the total amount of waste produced globally, according to Eurostat numbers (Kaza et al., 2018). Waste production reached 2.01 million tons worldwide in 2016. According to Kaza et al. (2018), in 2030, this amount is projected to rise to 2.59 million tons, and by 2050, it is expected to reach 3.4 million tons.

Figure 2.1. Amount of waste generation in 2016 and predictions for 2030 and 2050 (redrawn from Kaza et al., 2018).

2.2 Waste Composition

To reduce waste production, it is necessary to first examine the various types of waste generated around the world. Waste materials are classified as industrial, agricultural, construction and demolition, hazardous, medical, or electronic waste (Kaza et al., 2018). Various amounts of waste materials are produced in the world as a result of various activities. Figure 2.2 depicts the global amount of various municipal solid waste types. Food, paper, plastic, and glass waste account for 78% of total solid waste. Metal and wood waste contribute 4% and 2%, respectively (Kaza et al., 2018).

2.3 Waste Management

Waste management refers to the actions that are taken to manage waste from its generation to its final disposal. Collection, transportation, disposal, and recycling are all aspects of waste management. Because of the growing amount of waste in the world, the European Union (EU) has launched a directive program to deal with waste materials. In this plan, the first stage is to reduce the formation of waste materials. Secondly, the reuse of waste is required. Thirdly, if waste material cannot be reused, it is proposed that recycled material. The final two steps are recovery and disposal. This section of the thesis presents some statistical data on waste disposal methods (Sakai et al., 2011).

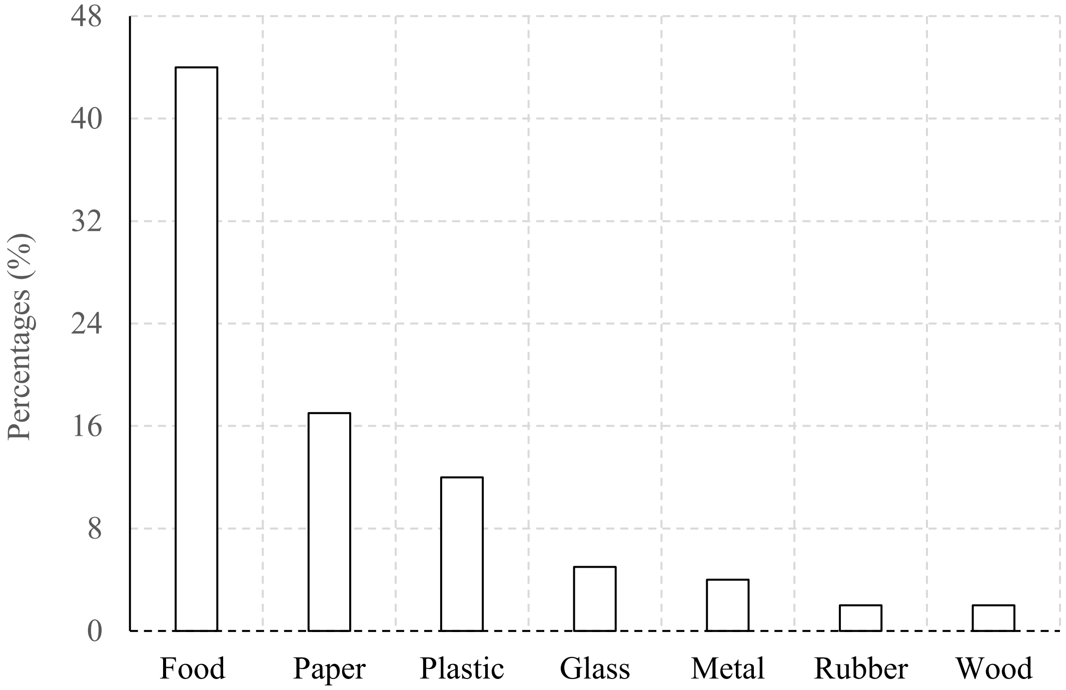

Figure 2.2. Percentages of different solid wastes generated in the world (redrawn from Kaza et al., 2018).

Figure 2.3 presents the global share of various waste disposal methods in 2016 (Kaza et al., 2016). Figure 2.3 shows that nearly one-third of the waste is dumped in the area openly. Furthermore, approximately 40% of waste is disposed of in landfills, while only 13.2% of waste is recycled or composted (7.7% is recycled, 5.5% is composted). Waste incineration accounts for 11% of all methods. This data shows that waste disposal is a major issue worldwide. Given that 76% of global waste is either held in landfills or discharged, roughly two-thirds of global waste has an environmental impact, as indicated previously in the thesis. Incineration is the second most hazardous waste disposal method shown in Figure 2.3. The controlled combustion of waste materials is known as incineration. Numerous studies have found that various harmful substances can emerge after combustion, causing negative effects on both nature and human health (Eriksson et al., 2005; Morselli et al., 2008). The open dump method, on the other hand, is one of the methods that take up unnecessary space in the world. These three methods (landfill, open dump, and incineration) account for approximately 87% of waste storage methods in the world. Recycling and composting account for about 13% of the remaining two methods. Recycling and composting are the most environmentally friendly methods. Composting is the process of decomposing waste from organic materials into a material that is a good fertilizer for plants. The second method is to recycle and reuse waste materials.

2.4 Waste Recycling

The process of transforming discarded material into a new material is known as recycling. If waste material creation cannot be avoided and waste material cannot be reused, the next best alternative is to recycle it and reuse it in another area. Due to a variety of environmental concerns, many countries attempt to recycle their waste production. Figure 2.4 depicts the total waste generated by the 32 countries, as well as the amount of waste recycled in thousand tones and recycling percentages (Kaza et al., 2016). Germany, France, Turkey, the United Kingdom, and Italy were the top five waste-producing countries in 2017, producing 51790, 35188, 34173, and 30911, 29572 thousand tons of waste, respectively. Four of the top five waste-producing countries rank in the top ten economies in the world, demonstrating that the most developed economies are responsible for the majority of the world's waste.

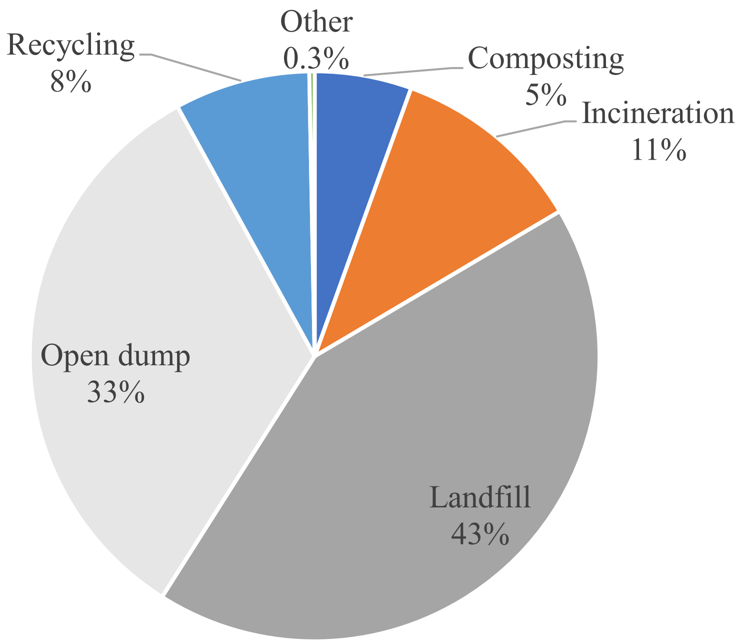

Figure 2.3. Percentages of different disposal methods of waste materials in 2016 (redrawn from Kaza et al., 2018

When it comes to recycling, Germany, Slovenia, Australia, Netherlands and Belgium rank first through fifth having the recycling ratio of 67.2%, 57.8%, 57.7%, 54.6%, and 53.9%, respectively. While four countries in the top ten economies generate the most waste in the world, only Germany appears in the top five countries that recycle the most waste. Serbia (0.3%), Malta (7.1%), Turkey (9.2%), Romania (14%), and Greece (18.9%) are the five countries with the lowest recycling rates in the world in 2017. This statistic also demonstrates that, while waste generation is proportional to the economic situation of the country, recycling is not (Kaza et al., 2016).

2.5 Using Waste Materials in Engineering Applications

Recycled waste material can be used in several engineering disciplines and applications including concrete, soil mechanics, transportation, and dams. In this section, a literature review on the use of one of WG is presented.

2.5.1 Using Waste Glass in Engineering Applications

Wartman et al. (2004a) presented the geotechnical properties of the clean WG with a grain size between 0.01 mm to 10 mm. According to their testing results, the specific gravity and maximum dry density (γ_{dmax}) value of the clean WG were found to be 2.49 and 16.6 kN/m^3, respectively. The angle of friction of WG from the direct shear test was found to be between 58 and 68˚ depending on the normal stress of the test, while the angle of friction in triaxial tests was found to be around 48°. The effective drainage properties of WG were demonstrated by a hydraulic conductivity test with k values of $1.6*10^{-4}$ cm/s.

Wartman et al. (2004b) investigated the compaction and direct shear properties of WG-kaolin and WG-Quarry fines mixtures at various WG ratios of 0%, 50%, 65%, 80%, 90%, and 100%. Figure 2.5 shows that until 60% WG additions, γ_{dmax} values of host material increased while w_{opt} values decreased, and then these trends reversed for subsequent WG contents. Furthermore, as WG additions increased from 0% to 100%, cohesion values decreased whereas the angle of internal friction values increased.

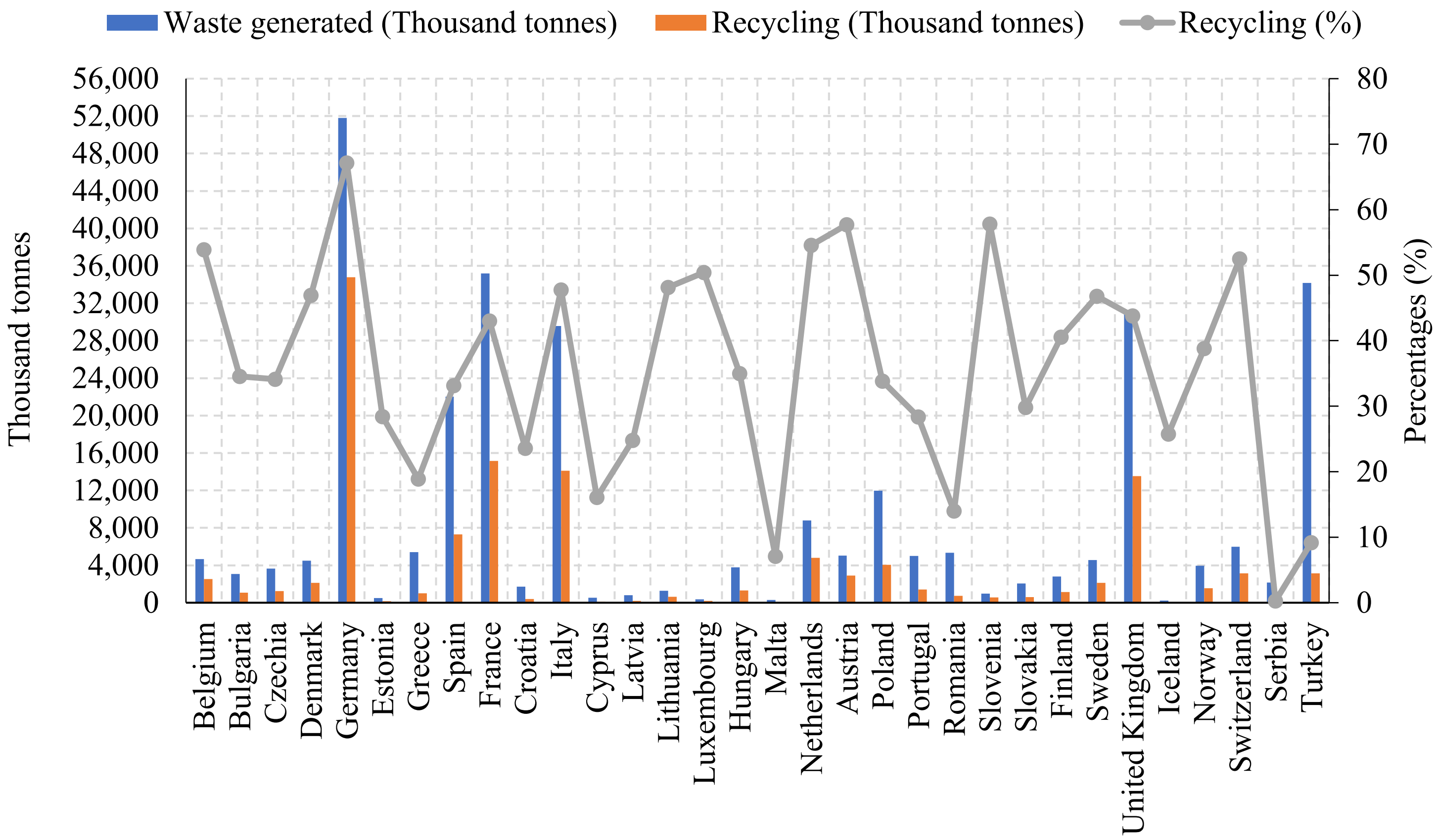

Figure 2.4. Waste and recycling statistics in 32 different countries in 2017 (data obtained from Eurostat).

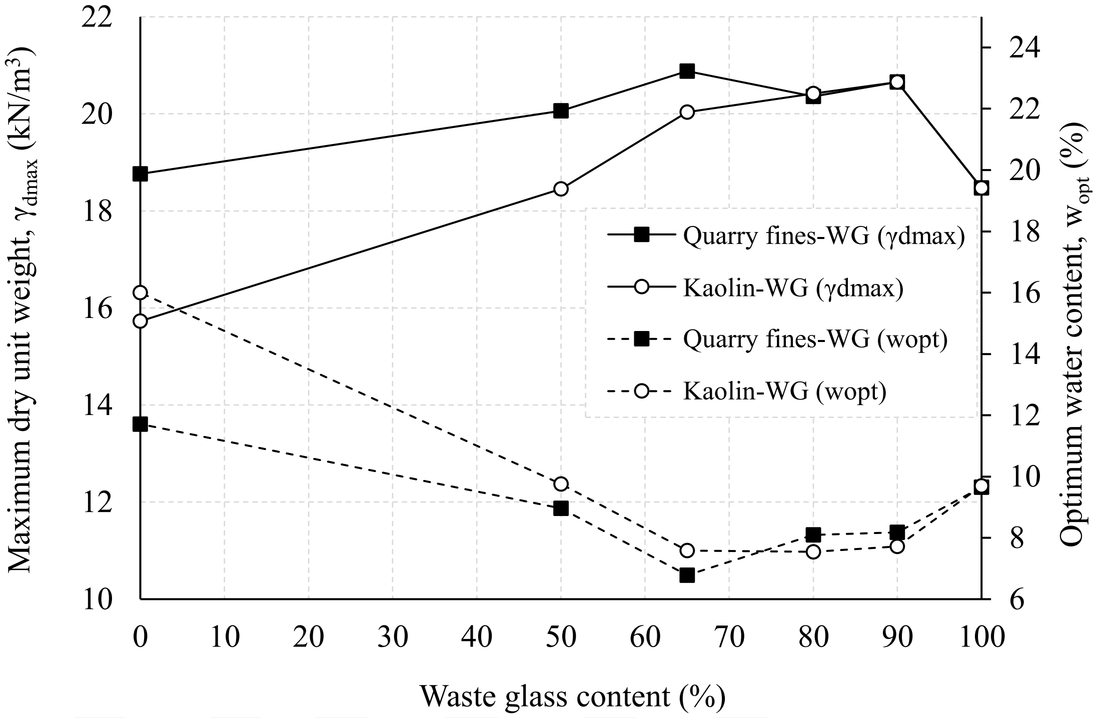

Figure 2.5. Compaction results of WG mixed with two types of soil namely kaolin and Quarry fines (redrawn from Wartman et al., 2004b).

Grubb et al. (2006) conducted compaction, unconsolidated undrained (UU) triaxial and direct shear testing on WG-dredged material mixes. With the addition of 80% WG, the γ_{dmax} values increased from 10.8 kN/m^3 to 17.3 kN/m^3, while the angle of internal friction determined by the UU triaxial test values increased from 16% to 33%. Also, the addition of 80% WG caused a decrease in w_{opt} value of the DM from 29 to 14. Furthermore, the addition of WG increased hydraulic conductivity while decreasing the void ratio, compressibility index (c_c), and swelling index (c_s) values of clean DM. WG was used in cement mortars by Sobolev et al. (2007). Instead of clinker, the researcher used 50% WG and 10% super silica. The findings of the flexure and compressive tests performed on cement mortars include WG-clinker and those performed on pure clinker cement mortar were compared by the researchers. At the same curing time, the flexural strength of glass-clinker mortal samples at 28 days that contained 50% WG was marginally greater than that of clinker (7.2 MPa vs. 6.7 MPa). Furthermore, the q_u values of the same specimens were found to be higher in mortal samples containing WG (50.1 MPa vs 45.4 MPa). The reason for this behavior was attributed to pozzolanic reactions seen in the Scanning electron microscope (SEM) pictures of the paper. As a result, the researchers concluded that the mortal sample containing 50% WG would be more environmentally friendly and durable than pure cement.

Chidiac and Federico (2007) studied the effect of fine and coarse WG on brick production. The researchers used 0%, 5%, 10%, and 15% WG in the brick design. The brick samples were subjected to UC and freeze-thaw tests. The results showed that the size and content of WG had a significant impact on the bricks. WG, as well as the porosity and firing temperature of the brick, significantly increased the q_u values. According to the researcher, the best WG ratio for brick production would be 10% fine-grained WG or 15% coarse-grained WG.

Ooi et al. (2008) performed laboratory tests including compaction, direct shear, and California bearing ratio (CBR) on several waste materials: WG, waste concrete, waste asphalt, and basaltic virgin aggregate to determine the most appropriate waste material for geotechnical applications. According to the test findings of the researchers, the highest to lowest γ_{dmax} waste materials are waste asphalt, basaltic virgin aggregate, WG, and waste concrete. The highest to lowest CBR values were found in waste concrete, basaltic virgin aggregate, WG, and waste asphalt.

Disfani et al. (2009) investigated the behavior of a WG-biosolid mixture using compaction and direct shear tests. Their testing results showed that the WG additions increased the γ_{dmax} of the clean biosolid. Depending on the normal strength employed during the direct shear tests, the shear strength of the mixtures reached the peak value with 40-60% of WG addition and then decreased for subsequent additions (Figure 2.6). According to the findings of the study, biosolids with 40%, 50%, and 60% of WG can be used as an alternative to virgin aggregates.

Disfani et al. (2011) conducted geotechnical tests on WG in three different grain sizes (coarse, medium, and fine). The researcher used coarse, medium, and fine-grained glass wastes with maximum grain sizes of 19, 9.5, and 4.75 mm, respectively. The researcher demonstrated that the permeability and angle of internal friction values of these WG are very similar to those of sand. The study demonstrated that WG can be utilized in many geotechnical applications in place of aggregate, except for coarse WG.

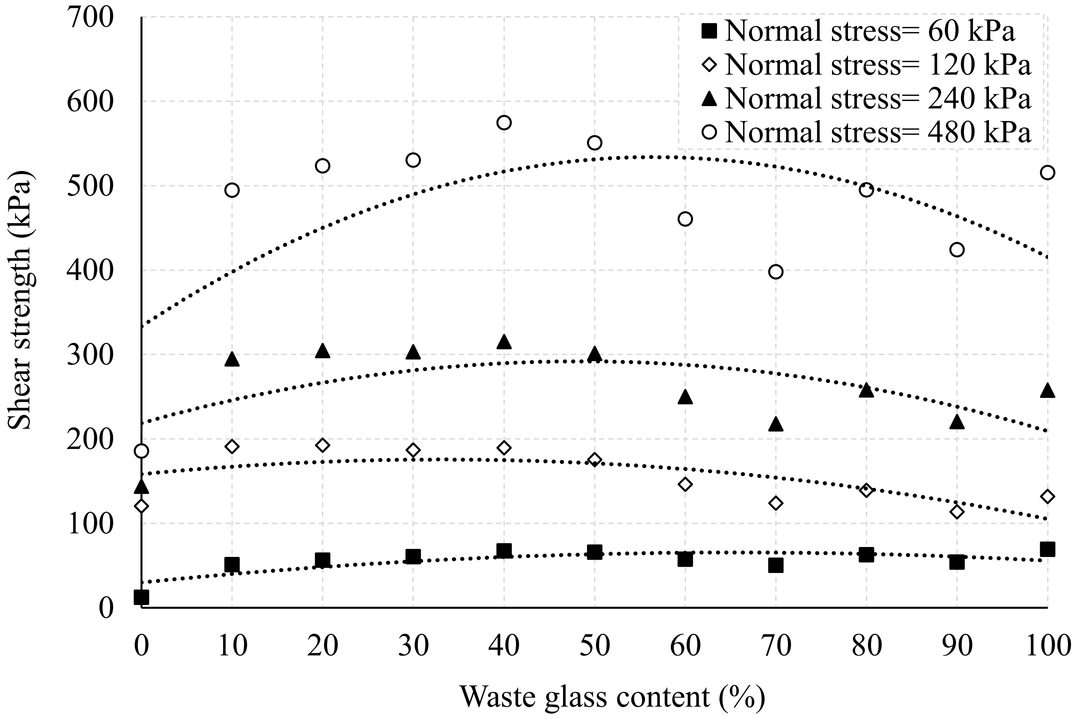

Figure 2.6. Shear strength values of biosolid-WG mixtures (redrawn from Disfani et al., 2009).

Arulrajah et al. (2012a) compared water absorption, compaction, Los Angeles abrasion, permeability, and CBR testing results of the five different construction and demolition waste types. According to their findings, the least water-absorbing waste material is found in WG. CBR results of WG revealed that another material is needed to use with WG to meet the requirements for a possible road project. Furthermore, among these waste types, WG has the lowest γ_{dmax} value.

To address the overuse of WG in engineering projects, Disfani et al. (2012) conducted some chemical and environmental tests, including total and leachate concentrations. A comparison with the US EPA revealed that using WG in road pavement projects posed no significant environmental risks.

Arulrajah et al. (2012b) investigated the usage of WG as a pathway base material. The researchers added 15% and 30% of WG to waste rock and conducted several laboratory tests, including CBR and compaction. The researchers concluded that a specimen of rock-WG mixture containing 15% WG would meet footpath base pavement requirements. The researchers suggested 15% as the optimal ratio of WG content.

Mujah et al. (2013) investigated the use of WG fibers as a sustainable and cost-effective geosynthetic material in sand, clay, and peat soils. Since WG fiber with 8-shaped is better for confining stress, the researcher developed WG fibers in that shape. The specimens were subjected to tensile and pullout tests. Tensile tests revealed that the fiber formed by WG significantly increased the tensile strength and cohesion values of the soils.

Olufowobi et al. (2014) investigated the influence of WG on cement-reinforced clay using several laboratory tests, including Atterberg limits CBR and direct shear. According to the results, the specimen containing 5% WG additions yielded the highest γ_{dmax} and CBR values, while the clay-10% WG additions had the highest cohesion and angle of internal friction values.

Ikara et al. (2015) investigated the effect of WG on the geotechnical characteristics of black cotton soil by performing compaction, CBR, and UCS tests on the specimens. The experimental findings showed that WG additives increased the γ_{dmax}, q_u, and CBR values of black cotton soil.

Fauzi et al. (2016) employed various amounts of WG grains (4%, 8%, and 12%) on cement-reinforced sand. The researchers performed compaction, CBR, and triaxial tests on the mixtures. The results showed that WG additions increased the γ_{dmax}, and CBR values of the cement-sand mixture while decreasing the cohesion w_{opt}, Atterberg's limits of the specimens. Arabani et al. (2012) performed a similar study and found that the γ_{dmax}, CBR, cohesion, and q_u values of the cement-sand mixture increased with WG while the w_{opt} value decreased.

Salamatpoor and Salamatpoor (2017) investigated the effect of WG on cement-reinforced sand using compaction, Unconfined compression (UC), CBR, and Consolidated drained (CD) triaxial tests. The researcher showed that the addition of WG reduces w_{opt} while increasing γ_{dmax}. Furthermore, with WG, cohesion, angle of internal friction and q_u increased. Direct shear tests showed that 30% of WG exhibited the maximum shear strength among all mixtures.

Patel and Singh (2017) investigated the effect of various amounts of glass fiber (Fc = 0.25%, 0.5%, 0.75%, and 1%) on the CBR testing results of silt. The testing results revealed that the presence of glass fibers increased the CBR values of silt.

Furthermore, the best CBR strength was obtained with 0.75% Fc (Figure 2.7) which was suggested as the optimum fiber ratio by the researcher.
Wang et al. (2017a) studied the effects of WG additions on the permeability and consolidation properties of sand. According to the findings of the researcher, the specimen with 20% WG had the highest permeability, while the specimen with 20-30% WG had the highest degree of consolidation.

The objective of Consoli et al. (2018) was to obtain the geotechnical characteristics of sand stabilized with green materials (WG and carbide lime). The compacted specimens were subjected to UC and pulse velocity tests. The testing results of the study showed that WG additions increased both the q_u and the maximum shear modulus (G_{max}) values. The study emphasized the application of WG and carbide lime in a wide range of engineering projects, such as pipelines and pavements.

Bilondi et al. (2018) investigated the geotechnical properties of clay soil mixed with WG and calcium carbide residue. According to the researcher, SEM pictures revealed that WG and calcium carbide residue formed a geopolymer, which could be used for soil improvement. The study suggests the optimum WG and calcium carbide residue mixing ratios as 7% and 15%, respectively.

Khan et al. (2018) investigated the geotechnical properties of local fine-grained soil mixed with WG. The researchers mixed 4%, 8%, and 12% of WG into the soil and performed CBR, UCS, Atterberg Limits, and direct shear tests. The experimental results revealed that WG grains reduced the Liquid limit (LL) of the clean soil. The highest and lowest angle of internal friction values were obtained at specimens containing 8% WG.

Attom (2018) worked on a cement-different-sized WG mixture to investigate the swelling potential of the mixtures. The researcher concluded that coarse glass grains were more effective at stabilizing bentonite. The addition of WG decreases the swelling potential of bentonite. The most effective stabilization was obtained with 5% glass-10% cement additions.

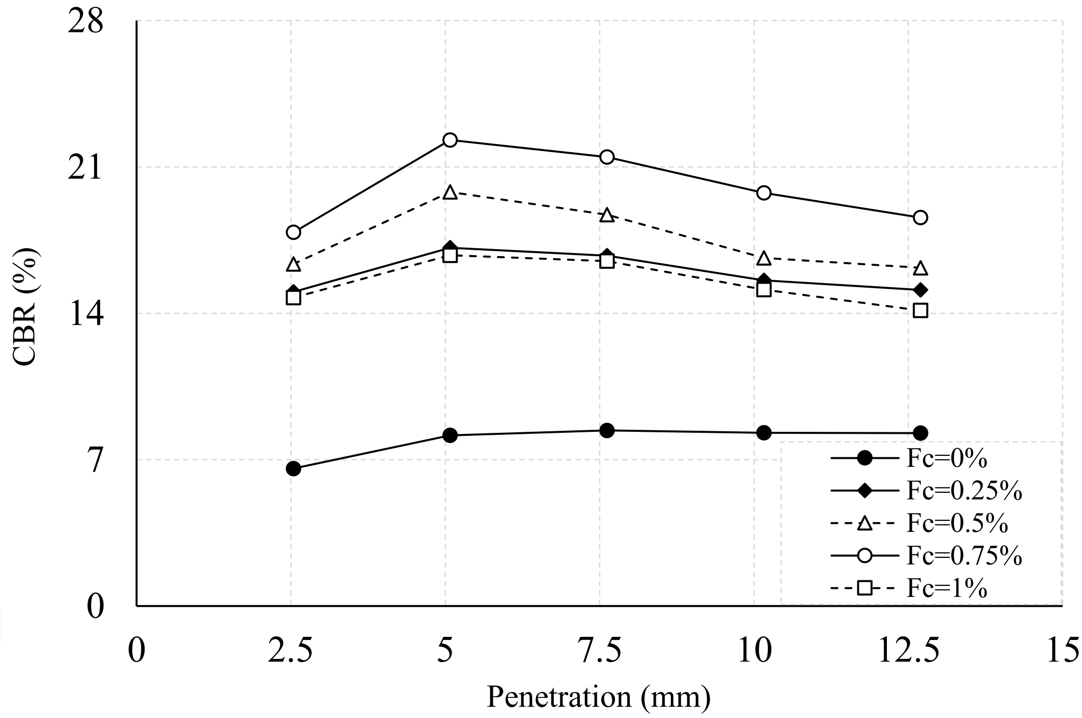

Figure 2.7. Effect of WG fibre on unsoaked CBR values of cohesive soil (redrawn from Patel and Singh, 2017).

Asl and Taherabadi (2018) investigated the performance of WG mixed with silty soil with varying WG ratios (0%, 10%, 15%, and 20%). After varying numbers of freeze-thaw cycles (0, 3, 6, 9), compression and tensile tests were performed on silty soil. Without freeze-thaw cycles, WG grains significantly increased the q_u value of silt. Adding 20% WG increased the q_u value of the silt by 56%. Tensile strength also increased with WG. During freeze-thaw cycles, the q_u values of the specimens decreased with WG additions.

Ibrahim et al. (2019) performed Atterberg limits, UC, free swell, and consolidation tests on clay stabilized with various percentages of WG (6%, 12%, 18%, 27%, 36%). The experimental results revealed that WG decreased the LL, PL, free swelling, and w_{opt} values while increasing the γ_{dmax}. Furthermore, the sample with 27% WG exhibited the highest q_u value. Consolidation results showed that WG additions reduced the void ratio, c_c, and c_r.

Adedokun et al. (2019) aimed to improve cement-reinforced laterite soil with WG additions at 0%, 2%, 4%, and 6%. The specimens were subjected to compaction, Atterberg Limits, UCS, and CBR tests. The testing results showed that the CBR values of mixtures increased with WG additions. Furthermore, WG additions increased the γ_{dmax} and q_u values up to 8% additive content and then decreased with additional additions. Overall, the researcher concluded that the best mixtures would contain 8% of WG additions.

Patel and Singh (2019) conducted triaxial tests on the sand with various lengths (10, 20 and 30 mm), and varying proportions (Fc = 0.5, 1, 2, 3 and 4%) of glass fibre. The testing results showed that glass fiber additions increased deviator stress at a given density of the specimens. The deviator stress of a mixture prepared with 4% glass fiber additive is approximately 140% higher than that of clean sand. Furthermore, the optimal fiber length was found to be 20 mm.

Bilgen (2020) investigated the effect of WG on some engineering properties of bentonite and two clay types, Alapli and Eregli clay. With the addition of the WG, the γ_{dmax} values increased. With 28 curing days, WG additions increased q_u and CBR values up to five times.

Mukherjee and Mishra (2020) investigated the feasibility of using WG in a bentonite-sand barrier in landfills. Various contents of glass fibres including 0.5%, 1%, and 1.5% were added to the specimen with an 80:20 sand: bentonite ratio. The specimens were subjected to CU triaxial tests. The testing results showed that glass fibers increased maximum deviatoric stress and peak frictional angle values while decreasing excess pore water pressure of the bentonite-sand mixture.

Yaghoubi et al. (2020) compared the geotechnical properties of waste foundry sand and WG. The direct shear test and CD triaxial tests revealed that the angle of internal friction of WG was 39.1 and 36.9, respectively. A comparison of the CBR and deviatoric stress showed that WG has higher CBR and deviatoric stress at all strain levels than waste foundry sand.

Consoli et al. (2021) employed carbide lime and WG as a binder in three different types of silica sand. The compacted specimens were subjected to UC and ultrasonic pulse velocity tests to correlate the q_u and G_{max} values of tested specimens. The testing results revealed that increasing the binder content increased both q_u and G_{max}. Between q_u and G_{max}, a linear relationship was observed by the researchers. The improvement was attributed by the researcher to a possible reaction between Ca^{2+} in carbide lime and silica in WG in alkaline pore fluid.

Kazmi et al. (2021) investigated some geotechnical properties of the waste glass in comparison to natural and manufactured sand. The results of direct shear tests revealed that the angle of internal friction of CWG in dry and saturated conditions was 35.5˚ and 39.0˚, respectively, while the values of natural sand in dry and saturated conditions were 36.9˚ and 34.4˚, respectively. In dry and saturated conditions, manufactured sand produced values of 44.9˚ and 43.0˚, respectively. The study concluded that Coarse waste glass (CWG) has chemical, shape, and geotechnical properties similar to sand and could be used in geotechnical engineering projects for environmental reasons. Mukherjee and Mishra (2021a) investigated the effect of 0.5%, 1.0%, and 1.5% glass fiber contents on a sand-10% bentonite mixture. With the addition of glass fiber, w_{opt}, void ratios, c_c, and c_s values of the sand-bentonite mixture decreased while q_u values increased. At a given effective stress, triaxial testing results showed that glass fiber additions increased deviatoric stress while decreasing pore water pressure. The hydraulic conductivity and c_v values of the sand-bentonite mixture increased with 0.5% glass fiber and then decreased at 1, and 1.5% fiber contents.

Saberian et al. (2019) investigated the various WG contents (1%, 3%, 5%) with a constant crumb rubber content of 1% in concrete aggregate and crushed rock. The addition of 1% rubber reduced the CBR and q_u values of both types of aggregates. WG additions increased the CBR and q_u values of the aggregates increased. The ductility of aggregates decreased as WG was added.

Mukherjee and Mishra (2021b) investigated the addition of 5%, 10%, and 15% waste tire fiber to a compacted bentonite-sand mixture (30% bentonite-70% sand). With waste tire additions, void ratios and settlement time of the bentonite-sand mixture decreased with tire fiber. The angle of internal friction values increased by 18.5 over the untreated bentonite-sand mixture and peaked at 15% glass fibre content. PWP of the bentonite-sand mixture decreased with waste tire additions at all strain levels. Maximum deviatoric stress was found at 15% waste tire addition, and this ratio was proposed as the optimum content.

Bilgen et al. (2022) performed Atterberg's limit, Standart Proctor and UC tests on clay with 5% lime mixed with 0%, 10%, 20%, and 25% WG. The specimens were saturated using tap water and seawater to see the effect of pore fluid on the testing results. At 1500 days of curing, the clean clay improved 22 times when compared to the clay with 25% WG-5% lime. The researcher attributed the improvement to the introduction of several cations, including Ca^{+2}, by the reaction between WG and pore fluid. The researcher attributes the long-term improvement to the CSH bods, which resulted from the interaction of Ca^{+2} cations with SiO_2 and Al_2O_3, respectively.

2.6 Bentonite-Based Materials

Drilling muds are one of the engineering applications that use bentonite. The main component of drilling mud is bentonite clay. Drilling mud is a viscous material used to aid drilling by cooling, lubricating, transporting drilling residues to the earth, protecting the walls, and preventing ejection. This material in the well helps with the drilling process. When drilling resumes, the material used as drilling mud must prevent drill holes from sinking to the bottom while also returning to fluidity. As a result, the material utilized must be thixotropic. Drilling mud is classified into three types: water-based, oil-based, and synthetic-based fluid. Because of its high viscosity, limited permeability, and thixotropic qualities, bentonite clay is utilized as a water-based drilling mud (Zhang et al., 2020).

Bentonite is also used in foundry bonds. Since it is a sustainable material, sand-clay mixtures are commonly used in foundry bond applications when shaping metals. Green-sand mixtures are commonly used in industrialized countries to cast steel and iron. Bentonite is used as a binder and to bind the sand grains together in this application. As a result, bentonite increases the cohesion and strength mixture (Murray, 1991).

Bentonite is also utilized in the disposal of nuclear waste. To allow radioactivity to pass, nuclear waste materials should be stored underground for a while before disposal. An impermeable layer is placed between the waste storage location and groundwater or rock to prevent nuclear waste leakage. The construction of a storage area in the bedrock is referred to as deep geological disposal. Because of its low permeability and superior water retention, compacted bentonite has been frequently employed as a buffer material in nuclear waste disposal. Sodium bentonite of various forms, such as MX-80, FEBEX, Kunigel V1, and Gao-Miao-Zi (GMZ), has been widely employed in nuclear waste disposal around the world (Wang, 2010; Xu et al., 2019; Villar et al., 2020). Furthermore, many researchers recommend incorporating a certain amount of sand into bentonite to improve thermal conductivity, long-term strength, and mechanical response. Some studies related to bentonite-based materials are summarized below.

Mollamahmutoglu and Yilmaz (2001) proposed using fly ash bentonite mixtures as a buffer in waste disposal areas. Compaction, permeability, and static triaxial tests were performed on fly ash containing 0, 10, 20, and 30% bentonite. The addition of bentonite increased the γ_{dmax}, c_c, and collapse potential of the fly ash while decreasing its hydraulic conductivity. With 30% bentonite, the angle of internal friction values increased from 33˚ to 42˚. The researchers suggested 20% bentonite content as the best ratio to use in fly ash.

Marcial et al. (2002) investigated the compressibility and compression behavior of three different types of bentonites: "Na Kunigel, Na-Ca MX80 Wyoming clay, and Ca Fourges clay". Figure 2.8 shows the testing results. Among the soil types tested, Na MX80 bentonite had the highest water retention capacity and void ratio. The initial void ratio of Ca bentonite slurry was roughly one-quarter that of Na bentonite. A significant difference in void ratios was observed at higher vertical stress levels of around 10 MPa. Na MX80 and Ca bentonite had compressibility index (c_c) values of 5.2 and 1.0, respectively.

Cokca and Yilmaz (2004) examined the geotechnical characteristics of fly ash mixed with rubber and bentonite. The results of the tests demonstrated that the hydraulic conductivity of fly ash increased with rubber concentration while its q_u values decreased. Maximum q_u values and γ_{dmax} were obtained with fly ash containing only 10% bentonite, which also produced the lowest hydraulic conductivity.

Delage et al. (2006) used Mercury Intrusion Porosimetry (MIP) and SEM tests to investigate the microstructural properties of statically compacted MX80 bentonite at curing days of 1, 30, and 90. A total of 12 specimens were tested, each with a different compaction condition. The compaction values of specimens ranged from 1.7 to 1.4

gr/cm^3 at water contents ranging from 8.2% to 28%. The findings revealed that density has a minor impact on the void ratio distribution. Large porosity values are similar at low water contents. In addition to the porosity, larger porosity decreased with curing at high water contents. Porosity after 90 days was found to be 31.7% higher than that of 1 day.

Gratchev et al. (2007) performed ring shear and dynamic triaxial tests on sand containing up to 15% bentonite. The cyclic testing results revealed that sand-bentonite mixtures were liquefied when the bentonite content was less than 11%, but mixtures with bentonite contents greater than 11% were found to be non-liquefied. According to the authors' interpretation, the high bentonite content resulted in a strong connection between sand particles. This increased packing density and thus liquefaction resistance. When the electrolyte concentration of the mixtures increased from 0.01M to 0.1M, the sand bentonite mixtures became more prone to liquefaction.

Cui et al. (2012) investigated the swelling behavior of bentonite-sand mixtures prepared at various initial densities with various contents from 0% to 50%. According to the results, maximum swelling pressure increased with dry density employed at the beginning of the test whereas they decreased with sand content. Maximum swelling pressure decreased with sand content up to 83% with the addition of 50% sand at a given initial density (Figure 2.9).

El Mohtar et al. (2014) performed resonant column, static triaxial compression, and cyclic triaxial tests on sand containing 3% and 5% bentonite. The resonant column tests revealed that the threshold shear strain at which excess PWP began to accumulate decreased with bentonite content. The excess PWP decreased as the bentonite content and curing days increased. Excess PWP testing results are shown in Figure 2.10a. The results of the tests revealed that the PWP of sand increased by 3% and then decreased by 5% bentonite. Ageing reduced the PWP at a given bentonite content. Cyclic triaxial testing results also showed that increasing bentonite content and curing increased sand liquefaction resistance. Figure 2.10b compares the excess PWP at each cycle to the number of cycles for clean sand and sand with 3% bentonite, demonstrating that the number of cycles required to reach liquefaction increased significantly with 3% bentonite.

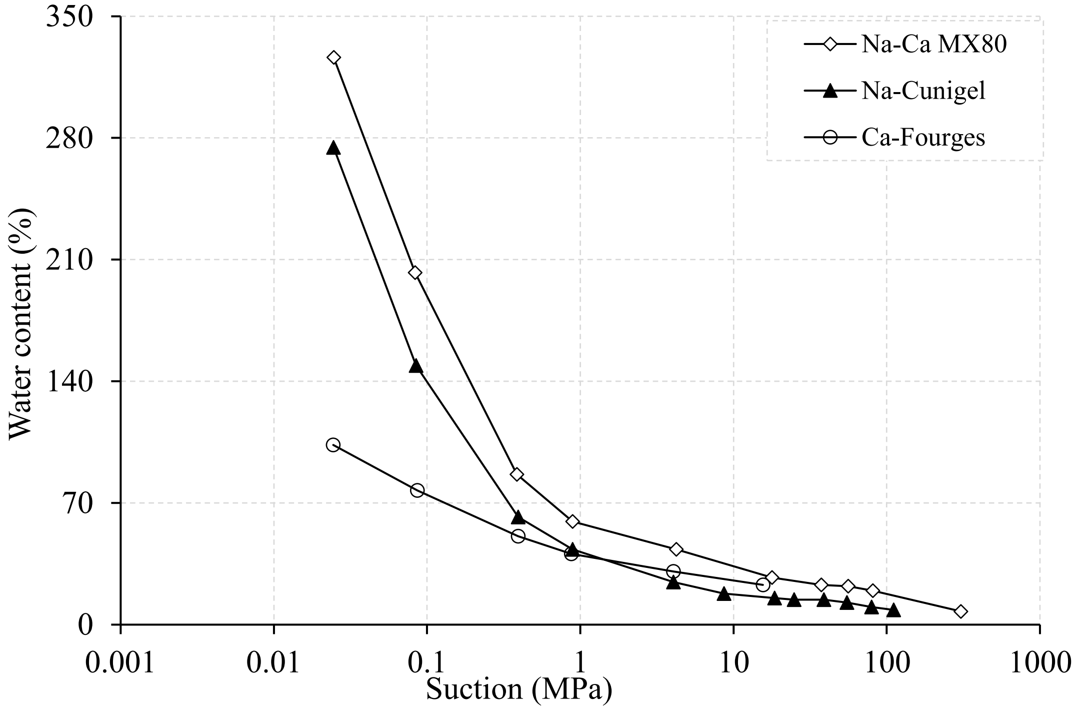

(a)

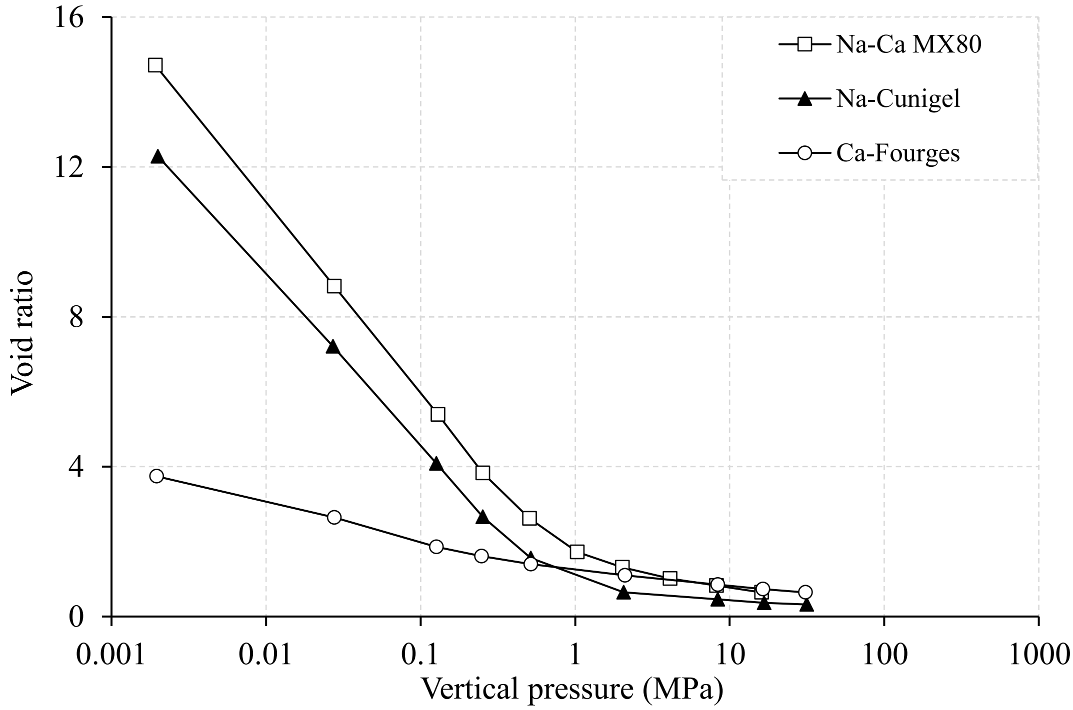

(b)

Figure 2.8. The comparison of (a) water retention and (b) compressibility of various types of bentonites prepared as a slurry (redrawn from Marcial et al. 2002).

Xu et al. (2014) investigated the hydraulic and thermal conductivity, as well as the swelling pressure, of bentonite at different sand contents ranging from 0% to 50%. With increasing sand content, the hydraulic conductivity of bentonite increases, and the ratio of this increase increases when the dry density of the mixture is low. Thermal conductivity also increased with sand content, but the ratio of increase in thermal conductivity of bentonite increased until 30% sand content and then decreased. Furthermore, swelling pressure decreased as sand content increased.

Sun et al. (2015) investigated the impact of sand content on the bentonite void ratio-vertical pressure relationship. When the sand content in the mixtures is less than 50%, a linear relationship between the void ratio of bentonite and vertical pressure is obtained, indicating that the void ratio of bentonite decreases with vertical pressure. However, when the sand content exceeds 50%, the relationship exhibits a nonlinear trend, which the authors refer to as "critical sand content." The vertical pressure did not affect the void ratio of bentonite above the critical sand content. According to the authors' interpretation, the external stress is carried by the bentonite grains below the critical sand content, whereas the external load is carried by the sand skeleton and bentonite once the content is exceeded.

Sabbar et al. (2017) mixed sand-bentonite mixture which included 3% bentonite with 2, 4%, and 6% slag contents. The clean sand prepared with a relative density of 10% exhibited static liquefaction and limited liquefaction at effective stresses of 100 and 150, respectively. 3% bentonite in sand reduced deviatoric stress while increasing PWP. The highest stress and lowest PWP were observed at the mixture of sand 3% bentonite and 4% slag.

Sharma et al. (2017) investigated the effect of bentonite on the various geotechnical properties of sand via compaction, UC and direct shear tests. The results of the tests revealed that the addition of bentonite increased the γ_{dmax}, cohesion, q_u, and Young's modulus of sand while decreasing the w_{opt}, hydraulic conductivity, and angle of internal friction of sand. The authors concluded that 50% bentonite in sand provides the optimum content for nuclear waste deposition.

Akgun and Kockar (2018) employed bentonite as an additive soil with additive contents ranging from 5% to 50% in the sand. The researcher performed compaction, direct shear tests, permeability, and UC tests on the compacted specimens. The laboratory testing results showed that the γ_{dmax} values incrased up to 30% bentonite additions, then decreased. The values of cohesion, Young's modulus, and qu increased steadily from 5% to 40% bentonite. Furthermore, bentonite additions decreased the coefficient of friction and hydraulic conductivity of the sand Finally, the researcher proposed a 30% bentonite content for use in nuclear waste disposal.

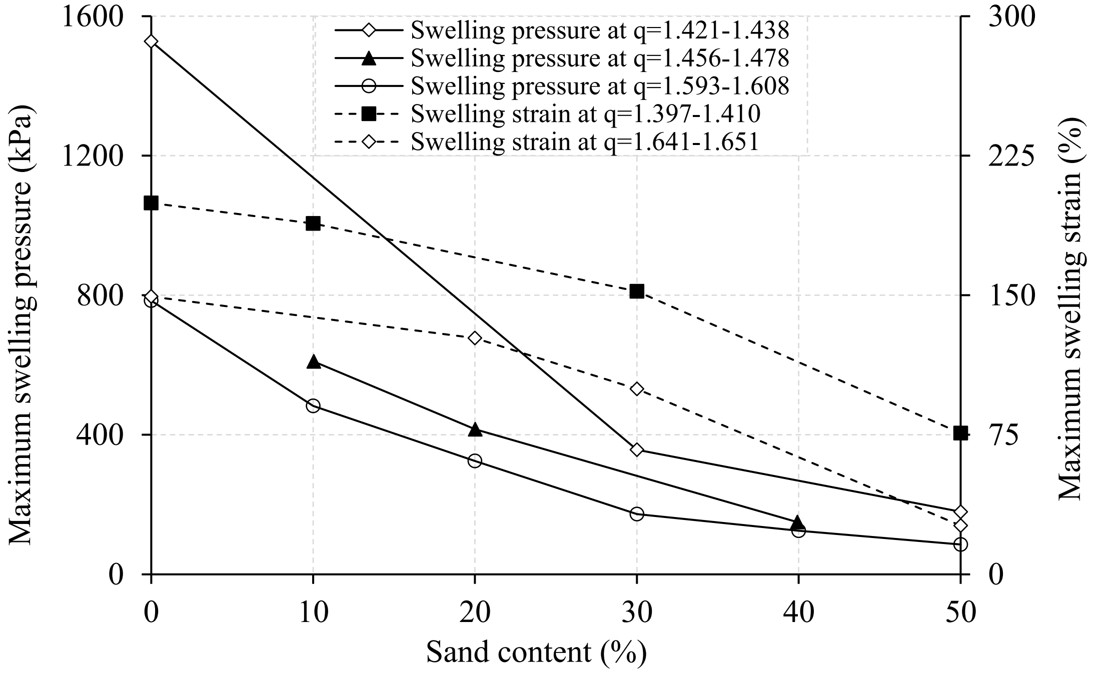

Figure 2.9. Effect of sand content on maximum swelling pressure and swelling strain (redrawn from Cui et al., 2012).

Bekhiti et al. (2019) investigated the effect of rubber fiber content (0, 0.5, 1, and 2% on the compaction, swelling, consolidation, and UC test behavior of cement-treated bentonite (cement ratios of 5, 7.5, and 10%). According to the testing results, rubber fiber reduced the liquid limit, swelling potential and swelling pressure of the bentonite cement mixture. Furthermore, the rubber fiber additions significantly increased the c_c, c_s and q_u values. The optimal mixture ratio for maximum q_u was found to be 2% rubber and 10% cement-treated bentonite.

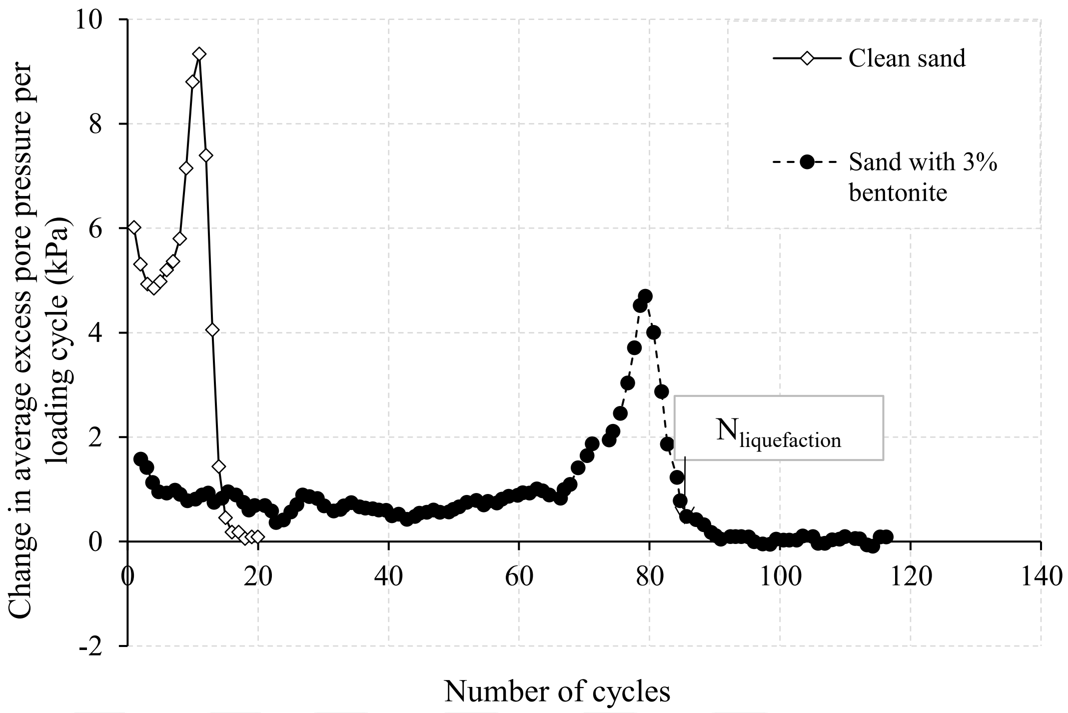

(a)

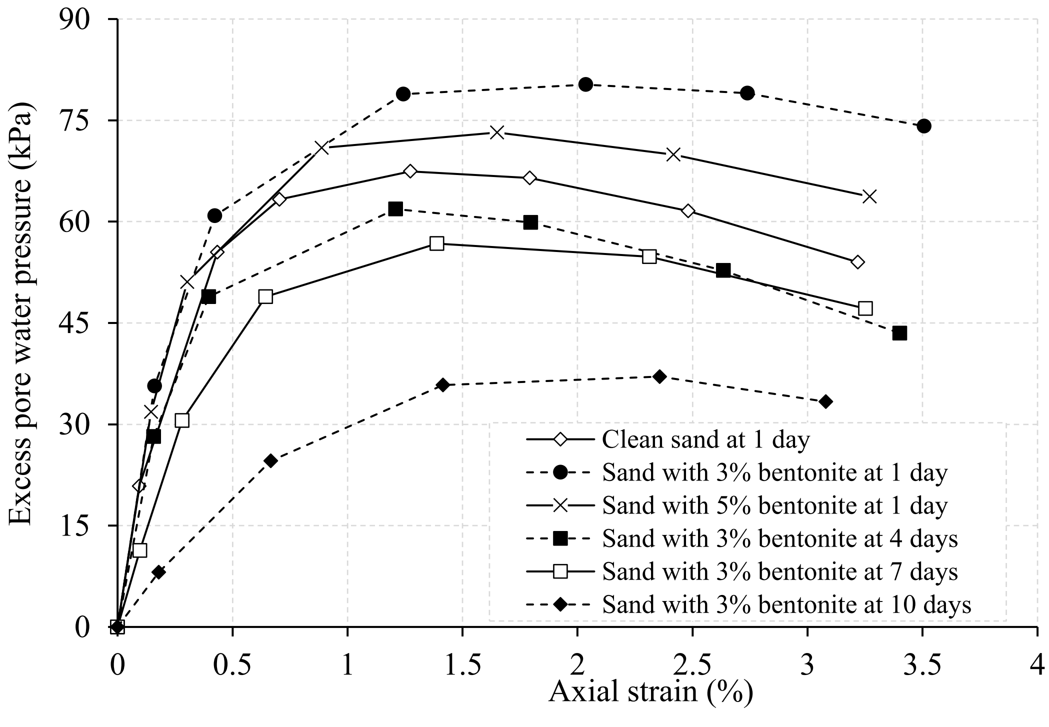

(b)

Figure 2.10. Excess PWP values of sand with bentonite at (a) cyclic triaxial test and (b) undrained static triaxial tests (redrawn from El Mohtar et al 2014).

Harrou et al. (2020) investigated the effect of two wastes, steel slag and phosphogypsum, on the UC test response of a bentonite-lime mixture containing 8% lime. The additions of 8% steel slag, 8% phosphogypsum, and 8% lime produced the highest q_u value at 28 days, which represents an increase of about 0.6 MPa over bentonite containing 8% lime at the same curing days. The researcher attributed such an improvement to the overall formation due to increased Ca^{2+} ion concentration and C-S-H formation.

Balagosa et al. (2020) performed resonant column tests to investigate the small strain response of compacted bentonite at different densities and correlated them with UC testing results. The initial dry density and water content of the compacted bentonite specimens ranged from 1.50 g/cm^3 to 1.77 g/cm^3, and from 8.7% to 11.5%, respectively. The results indicated that the v_s values ranged from 750 to 1100 m/s and the compressional wave velocity (v_p) values ranged from 1000 to 1600 m/s, with all values increasing with the dry density of the specimens. The υ values of the specimens ranged between 0.37 and 0.43. The maximum q_u values ranged from 3 to 13 MPa. Comparing the UC and resonant column testing results showed that Maximum constrained modulus (M_{max}) and elastic modulus (E_{max}) values increased with q_u values of the specimens. The values for small-strain damping ratios ranged from 2.5% to 4%.

Ozhan (2021) used polyacrylamides with mixture ratios of 1, 2, 5, 10, and 15% to improve the mechanical response of bentonite-sand mixtures (with bentonite contents of 10%, 15%, and 20%). Compaction, direct shear, UC, permeability, and swelling tests are performed on the compacted specimens. The addition of both anionic and cationic polyacrylamide increased cohesion, q_u, γ_{dmax}, and swelling index while decreasing internal frictional angle, permeability, and w_{opt}. Furthermore, the highest increment ratio was obtained at 2% polyacrylamides.

Xiang et al. (2021) investigated the swelling properties of GMZ01 bentonite with sand at various temperatures and electrolyte concentrations with mixing ratios of 70:30 and 30:70 by dry weights. According to the findings, the swelling deformation of the bentonite-sand mixture increases with temperature. The void ratio of bentonite reduces with increasing electrolyte concentration. The void ratio-vertical pressure trend is linear when the sand content is 30%, but nonlinear when the sand content is 70%.

Gupt et al. (2021) compared the UC testing results of bentonite with different types of fly ash, such as Farakka (FFA), Neyvelli (NFA), Badarpur (BFA), pond (PA), and bentonite with sand. The admixture contents ranged from 0% to 30%, 50% to 70%, and 100%. The q_u values of bentonite-fly ash mixtures increased with fly ash until 50% admixture content and then decreased (Figure 2.11). For bentonite-sand mixtures, however, the q_u values continued to decrease. The addition of 50% NFA resulted in a maximum improvement of 80%.

Zheng et al. (2022) performed direct shear tests on compacted bentonite specimens. Various pore fluids were employed in the study (0, 0.2, 0.5, and 1M sodium sulfate (Na_2SO_4) solutions. The testing results presented in Figure 2.12 showed that shear strength increased up to 180% at a given normal stress as the molarity of Na_2SO_4 increased. Figure 2.12 depicts the values of shear strength at various normal stress levels and cohesion values increased from about 40 kPa to 101 kPa and the angle of internal friction values increased from 12.1 to 32.2 with increasing Na_2SO_4 molarity in the solution.

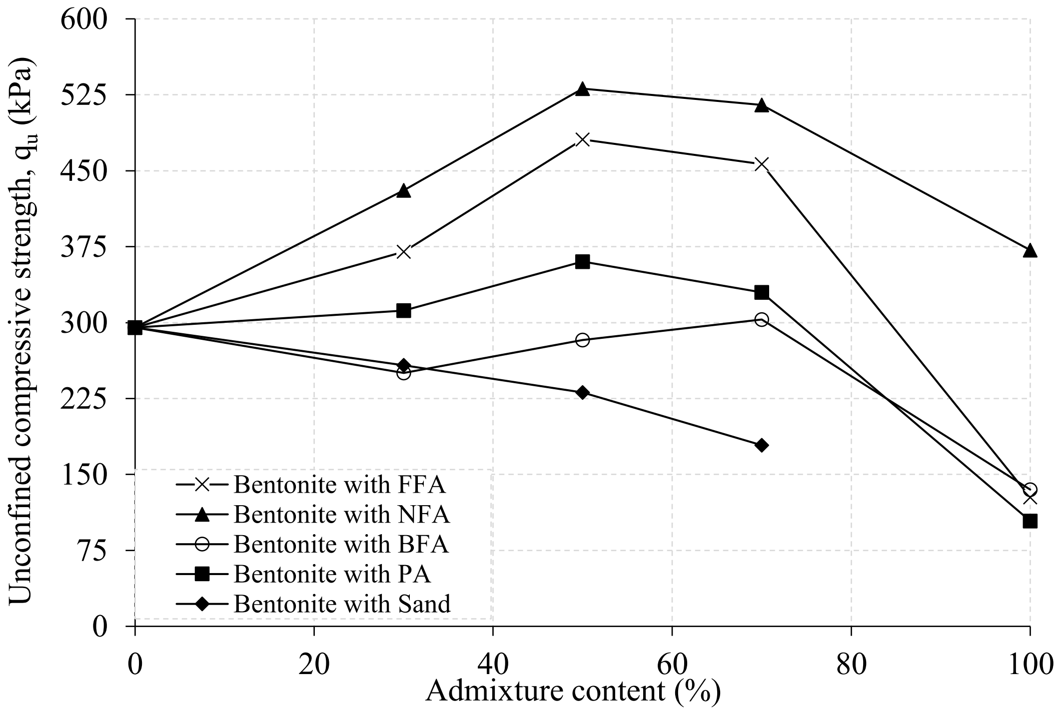

Figure 2.11. The q_u values of bentonite with various types of additions compacted at w_{opt} (redrawn from Gupt et al. 2021).

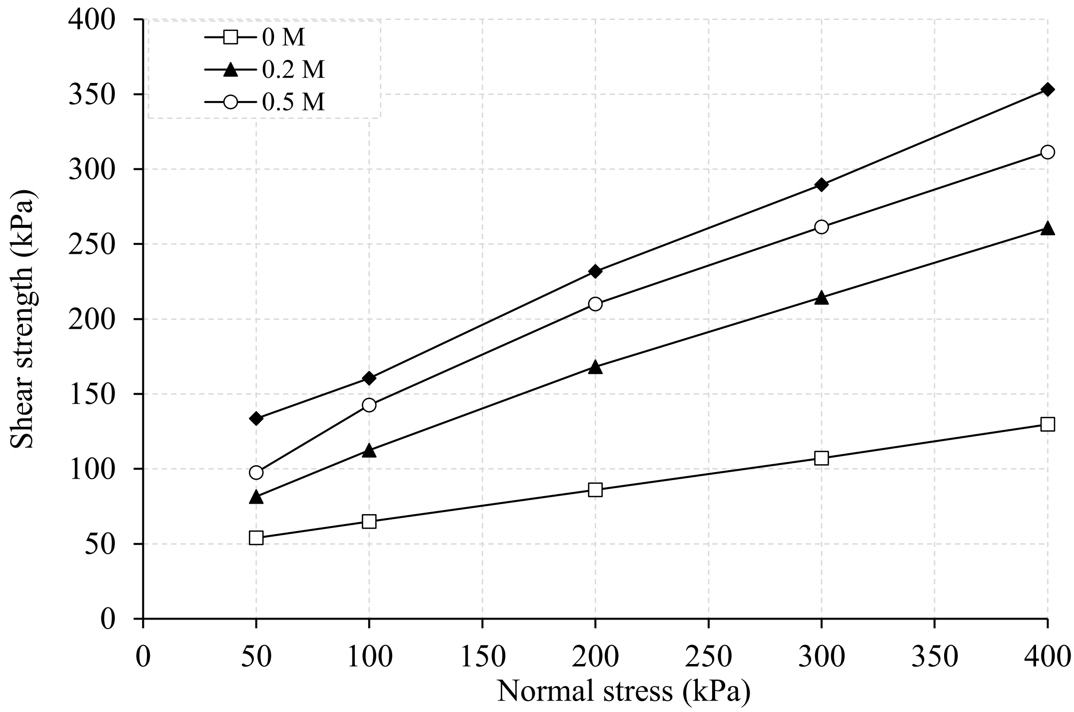

Figure 2.12. Direct shear testing results of compacted bentonite at different Na_2So_4 solutions (redrawn from Zheng et al. 2022).

2.7 Undrained Monotonic Behaviour of Clean Sands

Undrained behaviour of clean sands was first studied by the pioneer works conducted by Castro (1969, 1975), Ishihara et al. (1975), and Castro and Poulos (1977). The behaviour of the sands during undrained loading is determined by the two-state parameters; void ratio and effective consolidation stress (ECS).

According to Castro (1969), when the soil is loose and tested under low ECS (Specimen A in Figure 2.13), the behavior of sand is very contractive. The deviatoric stress reached a maximum and then decreased at high strain values. The researcher refers to this behavior as liquefaction. Some researchers refer to this behavior as flow liquefaction, static liquefaction, or unstable liquefaction (Yamamuro and Lade, 1998; Alarcon-Guzman et al., 1988). When the soil is dense (see Specimen B in Figure 2.13), the behavior is contractive at low strain levels and then dilative. At medium densities (Specimen C in Figure 2.13), the soil experiences an early peak deviatoric stress followed by softening. At high strain levels, such soil begins to dilate again and reaches higher stress levels. This is referred to as limited liquefaction.

Testing results of Mohamad and Dobry (1986) on clean sand are presented in Figures 2.14 and 2.15. Figure 2.14 shows the effect of ECS on a clean sand specimen at a similar void ratio following the consolidation stage. The findings revealed that increasing the ECS resulted in contractive and flow behavior. When it comes to the effect of void ratio, Figure 2.15 shows the testing results of clean sand with varied void ratios (after consolidation) at the same ECS. The results showed that when the soil is dense, the response is strongly dilative, and when the soil is loose, the response is contractive and unstable.

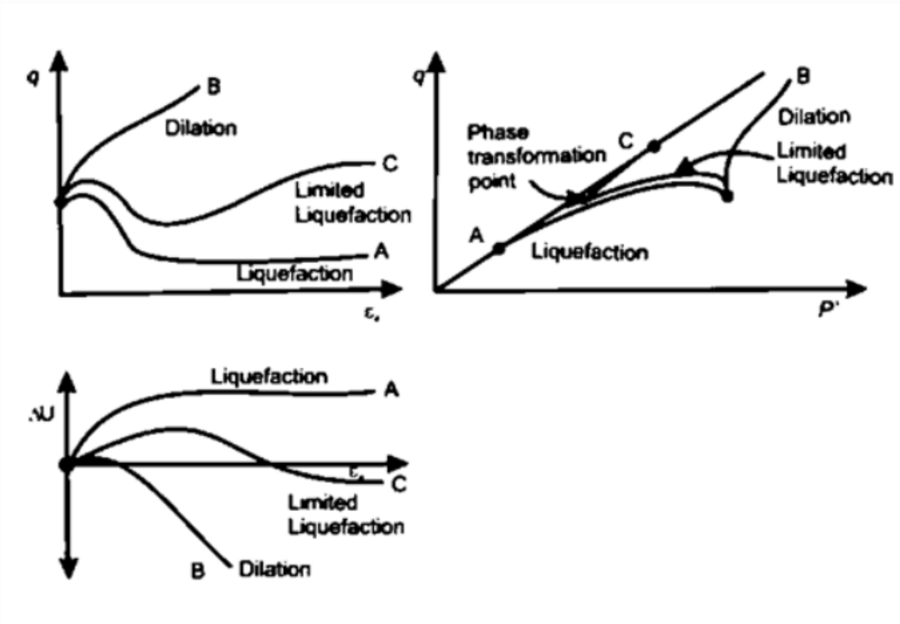

Figure 2.13. Typical undrained behaviour of sand at different initial states (Castro, 1969).

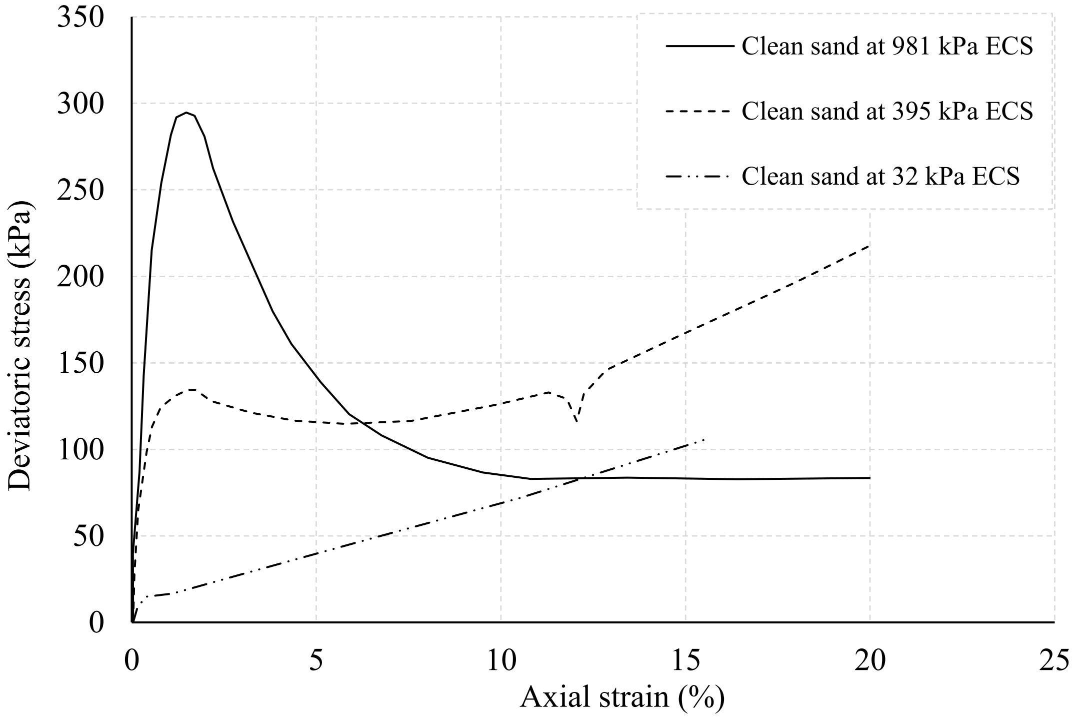

(a)

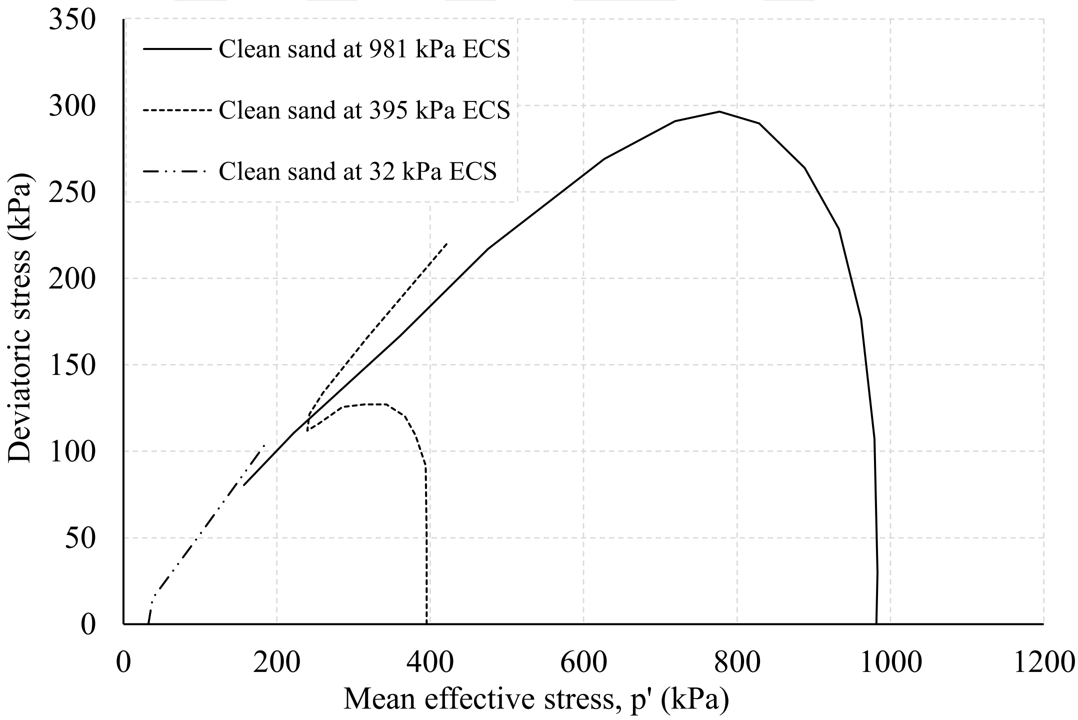

(b)

Figure 2.14. Effect of the ECS on the behaviour of sand (redrawn from Mohamad and Dobry, 1986)

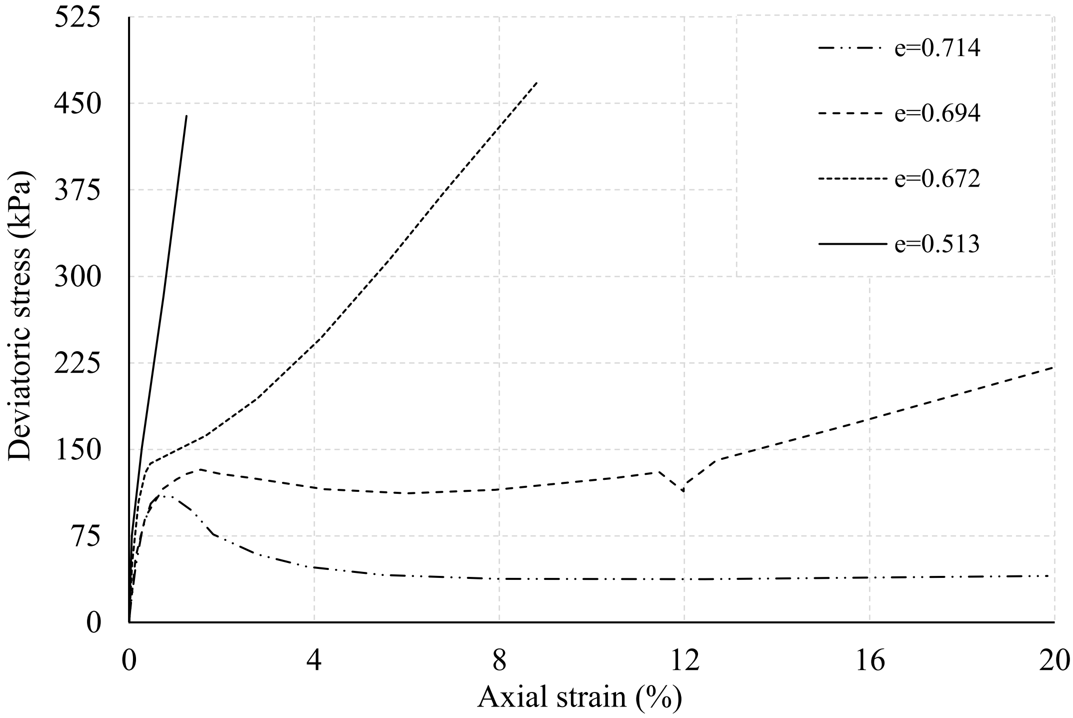

(a)

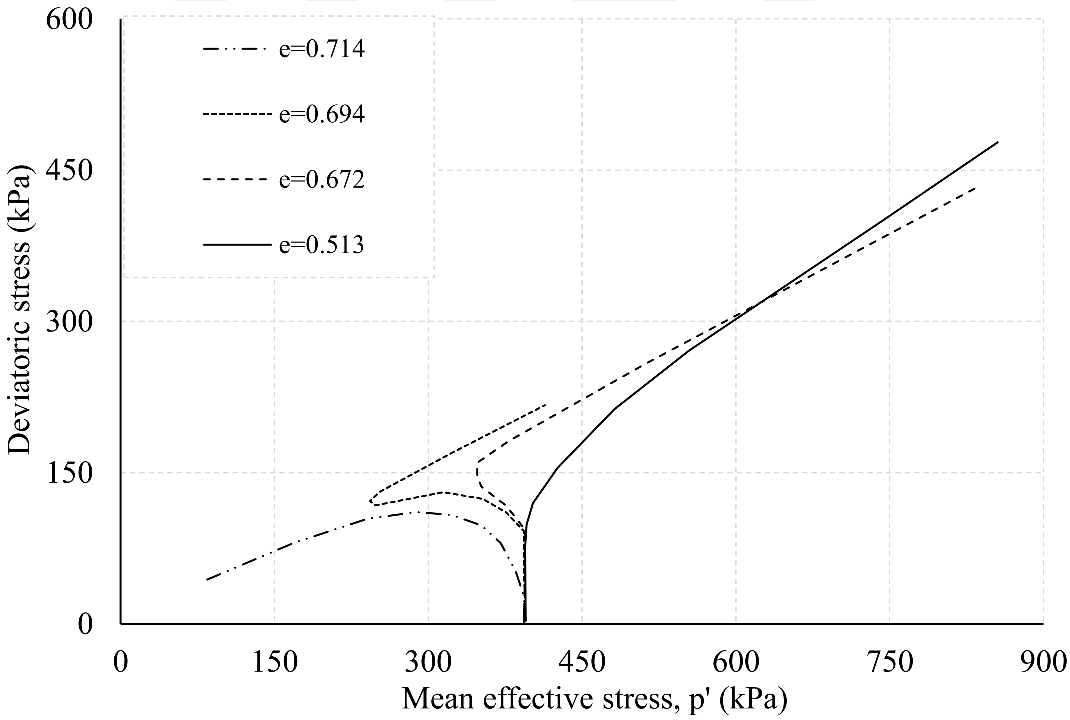

(b)

Figure 2.15. Effect of void ratio on the undrained behaviour of the sand (redrawn from Mohamad and Dobry, 1986)

2.8 Effect of Fines content on the Undrained Behaviour of Sands

Pitman et al. (1994) conducted a series of CU tests on the sand with changing fine concentrations. Ottowa sand was used as a host soil and fines contents of 10%, 20%, 30%, and 40% of kaolin or non-plastic crushed silica fines. The testing results showed that increasing fine content led to more dilatant behaviour compared to clean sand. Deviatoric stress increased with increasing both the plastic and non-plastic fines content.

Zlatović and Ishihara (1995) performed the CU tests on the sand and non-plastic silt mixtures at a 350 kPa effective confining pressure. The results presented in Figure 2.16 showed that the deviatoric stress of clean sand decreased while contractiveness increased with increasing silt content from 0% to 30%. However, the mixture with 40% silt showed less contractiveness and more dilatancy than that of 30% silt. The researchers also found that both the QSSL and SSL move downwards with increasing silt content.

Yamamuro and Lade (1997) performed both CD and CU tests on Two types of sand (Nevade sand and Ottawa sand) prepared using the dry funnel deposition method. The testing results presented in Figure 2.17 showed that both soil types exhibited static liquefaction at low confining pressures (up to 125 kPa for Nevade sand and 25 kPa for Ottawa sand) and loose states, whereas only limited liquefaction was observed at the high ECS. Furthermore, it was observed that the increasing relative density of soil increased the resistance against static liquefaction.

Lade and Yamamuro (1997b) performed the CU tests on loose and different-sized sand with varying fine content at a constant confining pressure of 25 kPa. The testing results showed that clean sand did not exhibit static liquefaction whereas all the mixtures with fines (fines content of 20, 50, and 100%) exhibited static liquefaction at all relative densities used in the study.

Thevanayagam (1998) performed CU tests on silty sands. The results showed that clean sand prepared at different void ratios exhibited similar undrained shear strength at the steady state despite testing at different effective confining stress whereas the undrained shear strength of silty sands depended on confining stress. The authors developed other parameters for evaluating the behavior of sand with particles, which will be briefly discussed later in this research. When comparing the testing results at similar e_g, the undrained shear strength values of the specimens were found to be similarly provided that the e_g<maximum void ratio of host sand (e_{max-hs}).

Yamamuro and Lade (1998) performed the CU tests on Navada sand mixed with 6% Navada fines prepared at 30% initial relative density at various effective confining pressures ranging from 25 kPa to 1000 kPa. The results presented in Figure 2.18 indicated that the stability of silty sand increased with increasing confining pressure. The authors named such behaviour as “reversed behaviour”. Such behaviour is opposite to the typical behaviour of loose sand which is increasing confining stress and decreasing the stability. The tests performed using varying strain rates from 0.011 %/min to 4.84%/min at constant confining stress of 200 kPa showed that increasing strain rate increased the deviatoric stress and stability of sand silt mixtures. Therefore, it was concluded that an increased strain rate increases the dilatancy of the sand silt mixtures.

Georgiannou (2006) investigated the effect of the particle shape of fine materials on the undrained response of clean sand. Kaolin, silt-sized mica as a platy fines and fine silica silt used as an additive soil with a maximum additive content of 2.5%. The testing results showed that the addition of kaolin or silt-sized mica decreases the stability of sand whereas the addition of silt-sized silica increases the stability of sand.

Murthy et al. (2007) performed CU tests on sand with 0%, 5%, 10%, and 15% non-plastic silt. The testing results revealed that increasing silt content decreases the contractiveness and deviatoric stress of sand. The silty sands reach the critical state earlier than the clean sand, showing that silt particles move the critical state line downwards. All the specimens prepared at different soil preparation methods including slurry deposition, dry pluviation, and moist tamping reached a unique critical state line. The critical state angle of sand increased with increasing silt content.

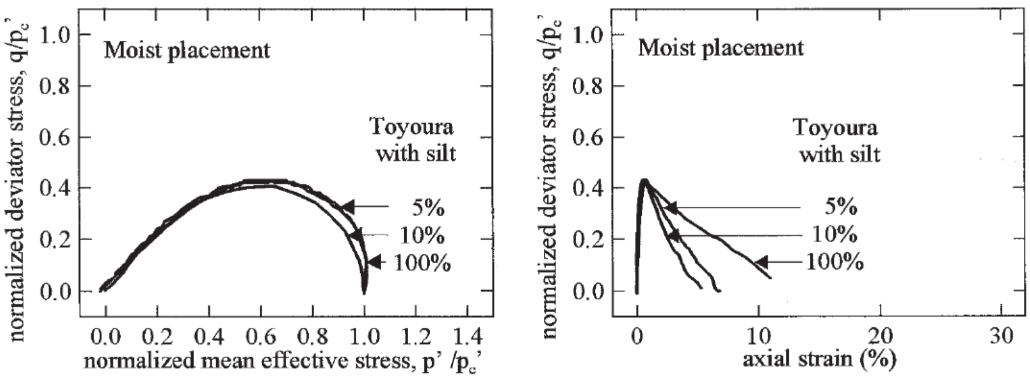

(a)

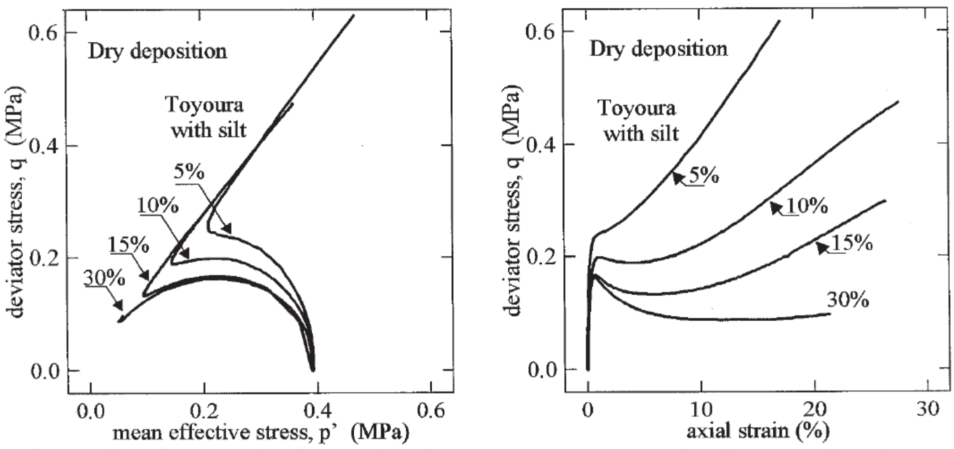

(b)

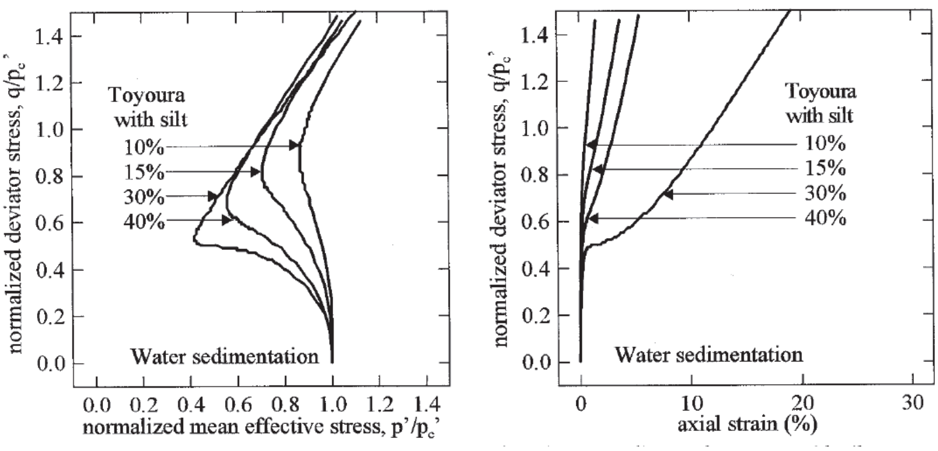

(c)

Figure 2.16. Effect of non-plastic silt content on the undrained shear response of sand (a) moist specimens (b) dry deposition specimens (c) water sedimentation specimens (Zlatović and Ishihara, 1995)

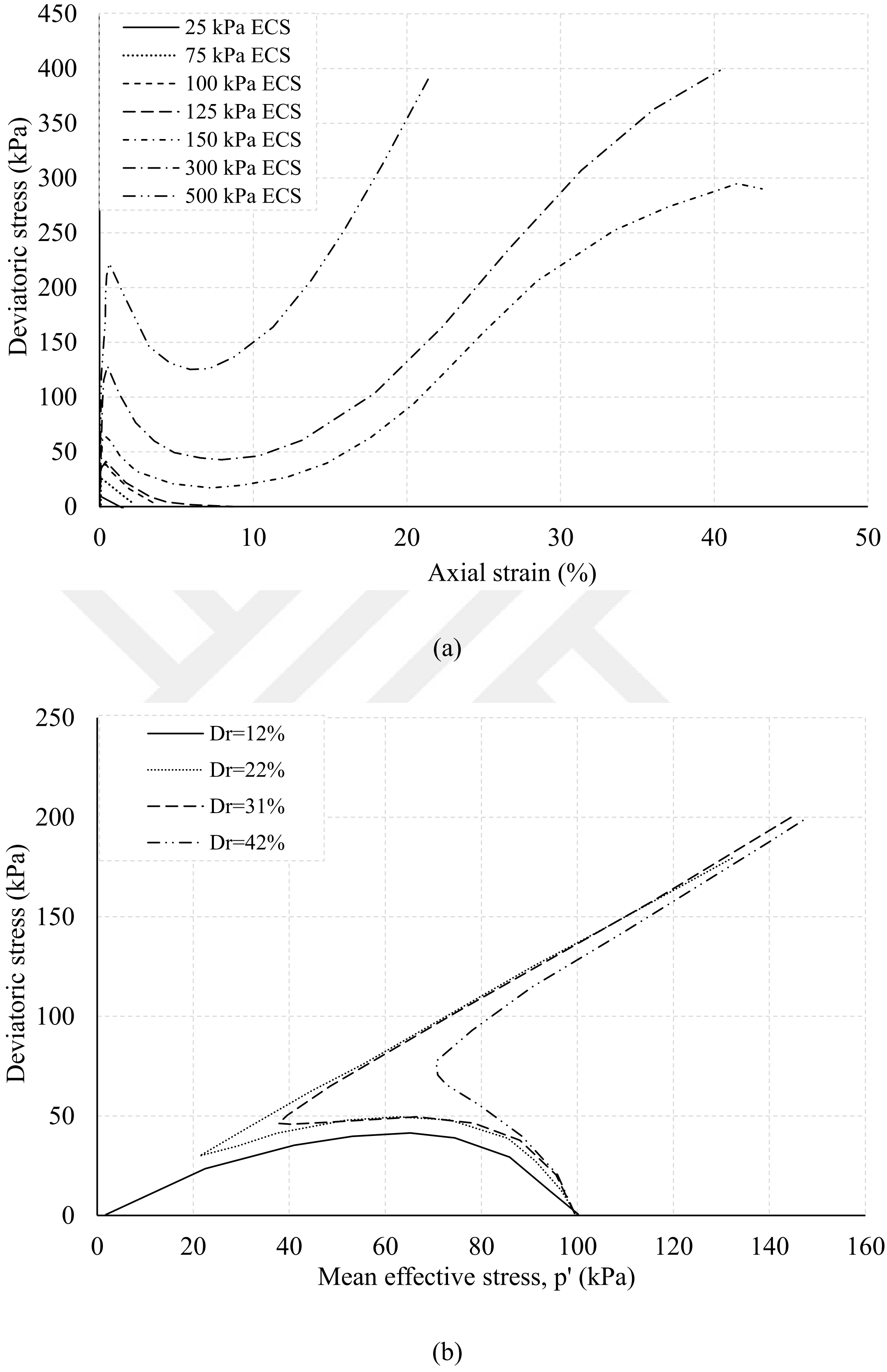

Figure 2.17. Undrained response of Nevada sand; (a) Effect of ECS on a Nevade sand at 12% RD (b) effect of different RD on a constant ECS of 100 kPa (redrawn from Yamamuro and Lade, 1997).

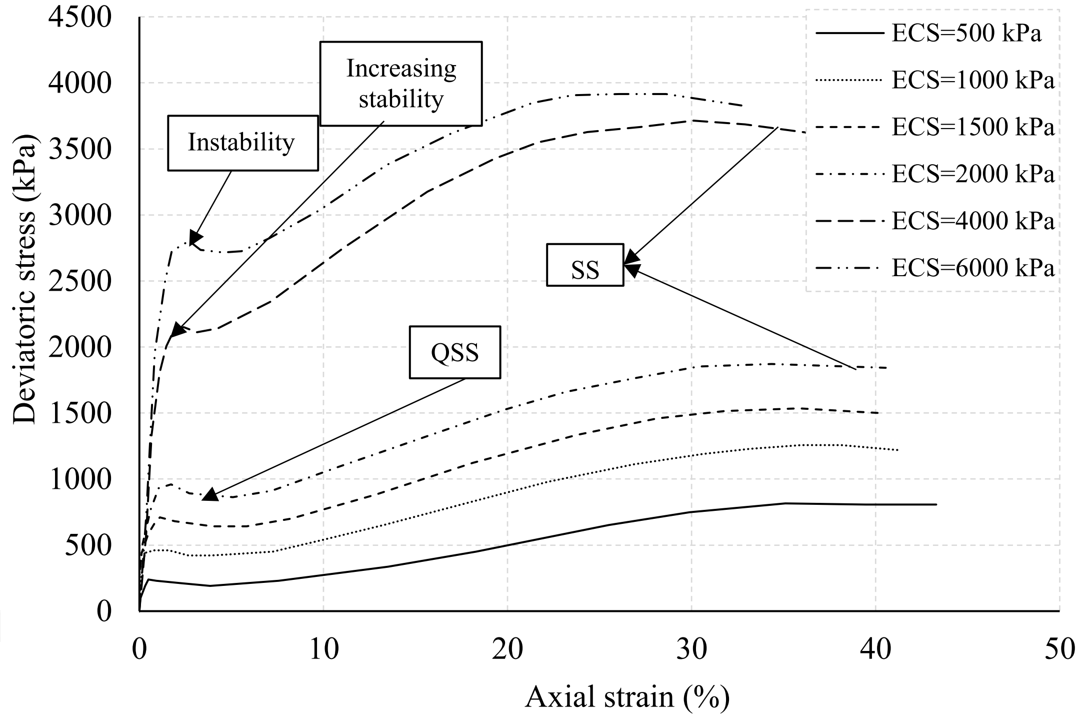

(a)

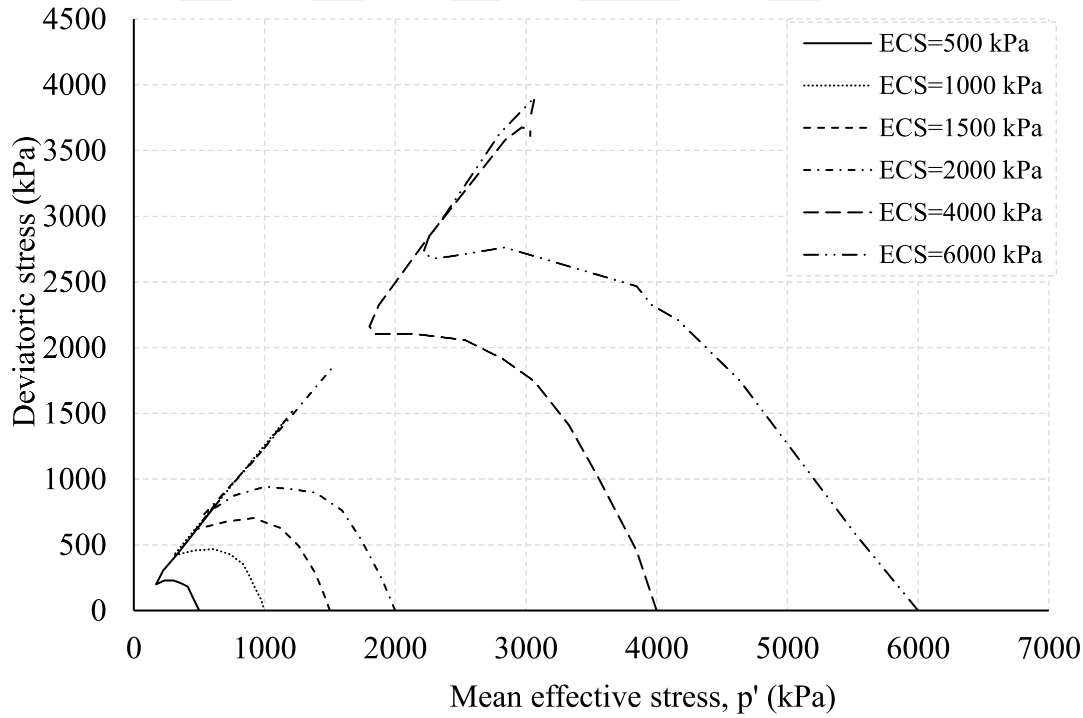

(b)

Figure 2.18. Effect of silt on the undrained response of sand at different ECS (redrawn from Yamamuro and Lade, 1998)

Lade et al. (2009) performed the CU tests at 25 kPa effective confining stress on sand silt mixtures prepared at varying relative densities. Figure 2.19 shows an example of their testing results of sand with 20% silt additions. The figure shows that the specimens with relative density lower than 53% exhibited static liquefaction while 53% and 56% exhibited limited liquefaction. Figures 2.19b and 2.19c indicated their testing results. The results show that 56% show dilatancy after a mean effective stress of around 7 kPa.

Yang and Wei (2012) investigated the effect of the shape of the fine particles on the undrained response of sand. Fine glass beads and angular crushed mixed with two different sands having different shapes. The testing results at similar void ratios showed that adding both types of fines decreased the undrained shear strength and the dilative tendency of both types of sand. Comparing the effect of the shape of the fines into Toyoura sand (angular sand), the addition of round glass beads reduced the strain-softening response of clean sand compared to that of angular silica fines. In contrast, comparing the effect of the shape of the fines on Fujian sand (round sand), the addition of round glass beads increased the strain-softening response of clean sand compared to that of angular silica fines. The critical state of clean sand increases with the addition of angular silica silt while it decreases with the round glass beads. According to the author, the round-round mixtures of fine and coarse soil are more unstable whereas angular-angular mixtures are more stable mixtures.

Belkhatir et al. (2012) performed CU tests on sand silt mixtures prepared at 20% and 90% relative density. The testing results of the authors showed that at a given density all silt contents from 0% to 50% decreased the deviatoric stress of the sand. Moreover, increasing silt content led to an increase in the contractiveness of the mixtures.

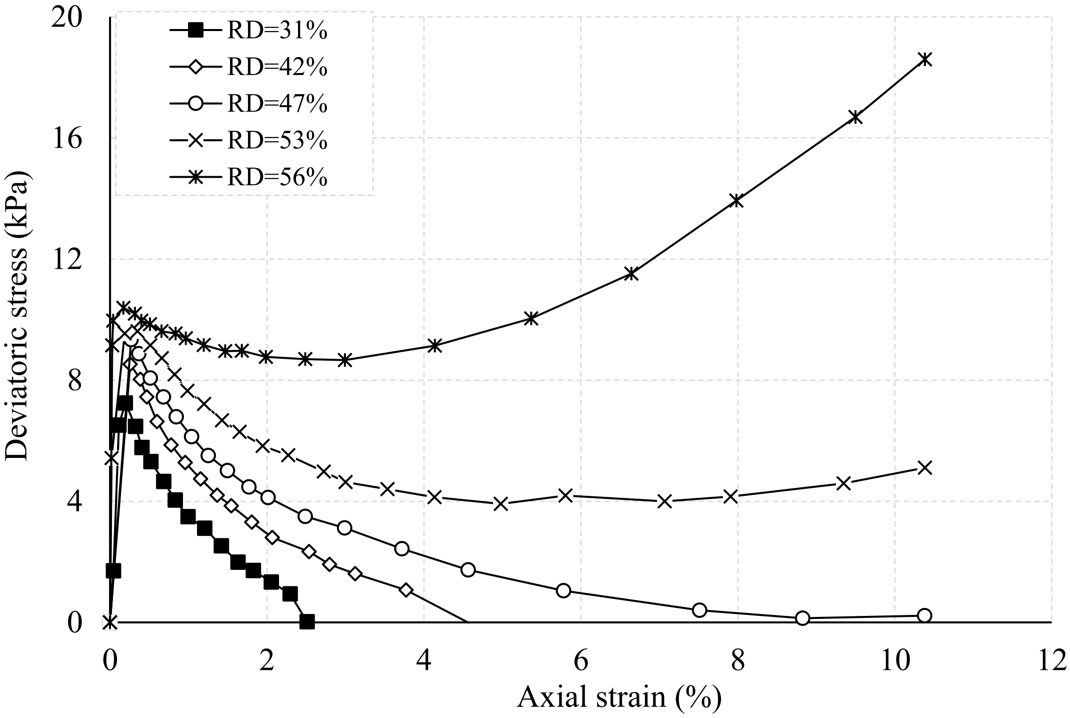
RD=31%
RD=42%
RD=47%
RD=53%
RD=56%
Deviatoric stress (kPa)
Axial strain (%)
0
4
8
12
16
20
0
2
4
6
8
10
12

(a)

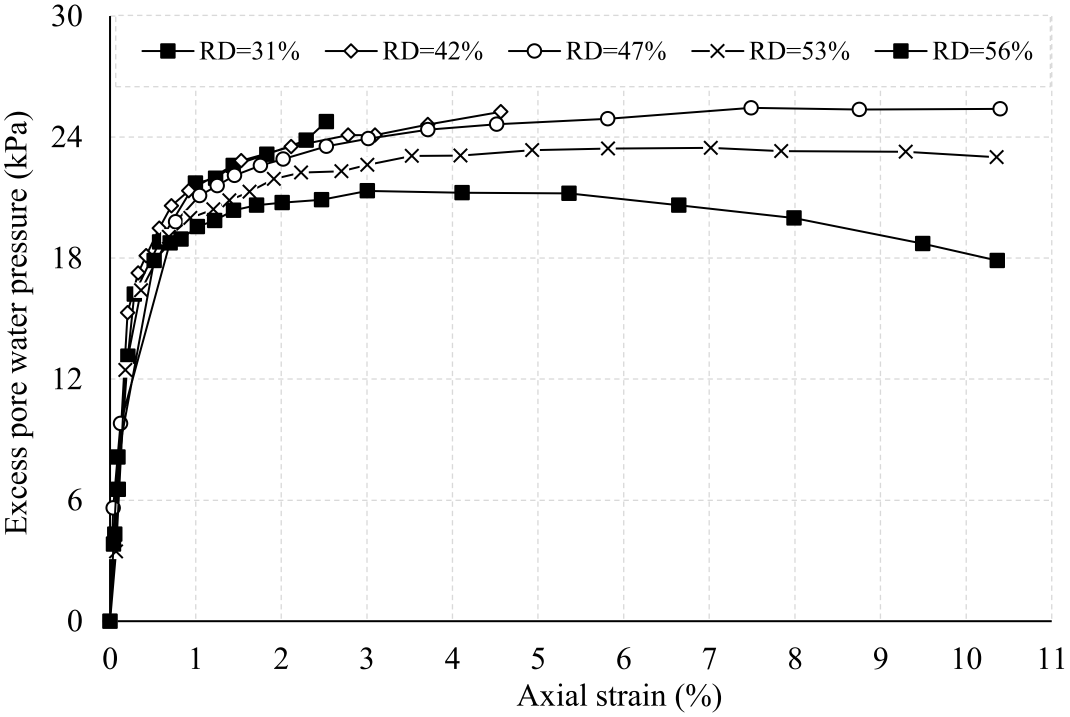
RD=31%
RD=42%
RD=47%
RD=53%
RD=56%
Excess pore water pressure (kPa)
Axial strain (%)
0
6
12
18
24
30
0
1
2
3
4
5
6
7
8
9
10
11

(b)

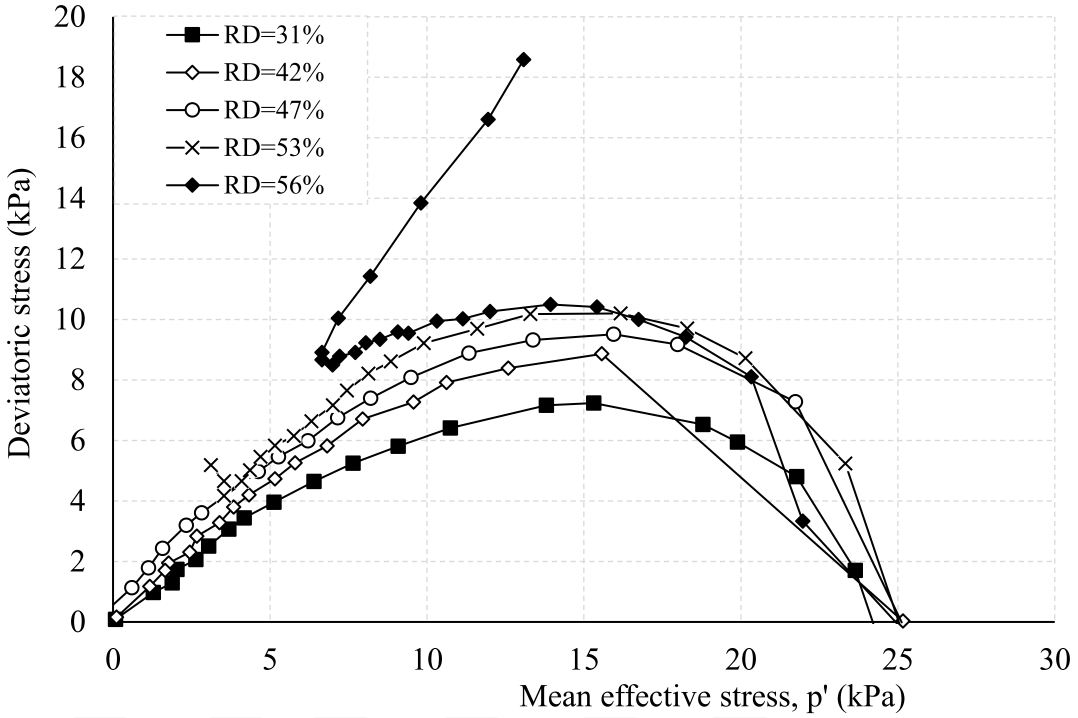

(c)

Figure 2.19. Effect of relative density on the undrained behaviour of sand with 20% silt mixture (redrawn from Lade et al. 2009)

Yang et al. (2015) performed CU tests on the three types of sand mixed with fine silica silt. The testing results were compared at constant void ratio, constant e_s, and constant equivalent void ratio (e*). The testing results showed the following three conclusions; (a) when the specimens were compared at the constant void ratio, the contractiveness of sand increased, therefore, peak deviatoric stress decreased with the increasing fines content, (b) when the specimens were compared at the similar e_s, the dilatancy and peak deviatoric stress increased with the increasing fines content, (c) when the specimens compared at the similar e*, The testing results fall in a narrow band with a slightly differing from each other. The conclusion of this study was to suggest the global void ratio in order to most accurately characterize the stress-strain response of mixed soils.

Taiba et al. (2016) performed the CU test on two types of sand with different shapes mixed with various ratios (0, 10, 20, 30, and 40%) of non-plastic silt. The silt additions decreased the peak undrained shear strength and the dilative tendency of the clean sand specimens. Comparing the mixtures at a given clay content showed that the mixtures with coarse sand grains exhibited greater undrained shear strength.

Mahmoudi et al. (2018) performed CU tests on sand silt mixtures prepared at similar relative densities and different consolidation ratios. The testing results showed a continuous decrement in the undrained shear strength of clean sand with silt additions. When it comes to the over-consolidation ratio effect, increasing OCR led to an increase in the deviatoric stress of all mixtures.

Goudarzy et al. (2021) performed CU tests on the sand with two different plastic clays namely kaolin and bentonite prepared at various void ratios. The testing results showed that both the fine additions decreased the undrained shear strength and the dilative tendency of sand grains. Comparing the effect of different clay types presented in Figure 2.20 showed that the mixtures with kaolin exhibited greater undrained shear strength and dilatancy than that of bentonite at a given clay content. Furthermore, bentonite additions increased the limited liquefaction susceptibility.

Mahmoudi et al. (2022a) performed CU tests on sand silt mixtures prepared at similar void ratios. Silt contents of 0, 10, 20, 30, 40, and 50% were mixed with sand at three different void ratios. The results showed that the specimens prepared using the dry pluviation method at a given void ratio showed a transitional fines content of 40% whereas this ratio decreased to 10% when the authors employed moist tamping specimens.

Mahmoudi et al. (2022b) performed CU tests on sand silt mixtures prepared at similar relative densities. Silt contents of 0, 10, 20, 30, and 40% were mixed with sand at a constant relative density of 52%. The testing results showed that dry pluviated specimens showed dilative response up to a maximum silt content of 20%, however, the contractive response was observed at 30% and 40%. The moist prepared specimens exhibited contractive response. When the specimens were prepared using the dry pluviation method, a continuous decrease in the deviatoric stress of clean sand was obtained with silt additions. However, when the specimens were prepared using the moist tamping method, silt additions resulted in a continuous increase in the deviatoric stress of clean sand.

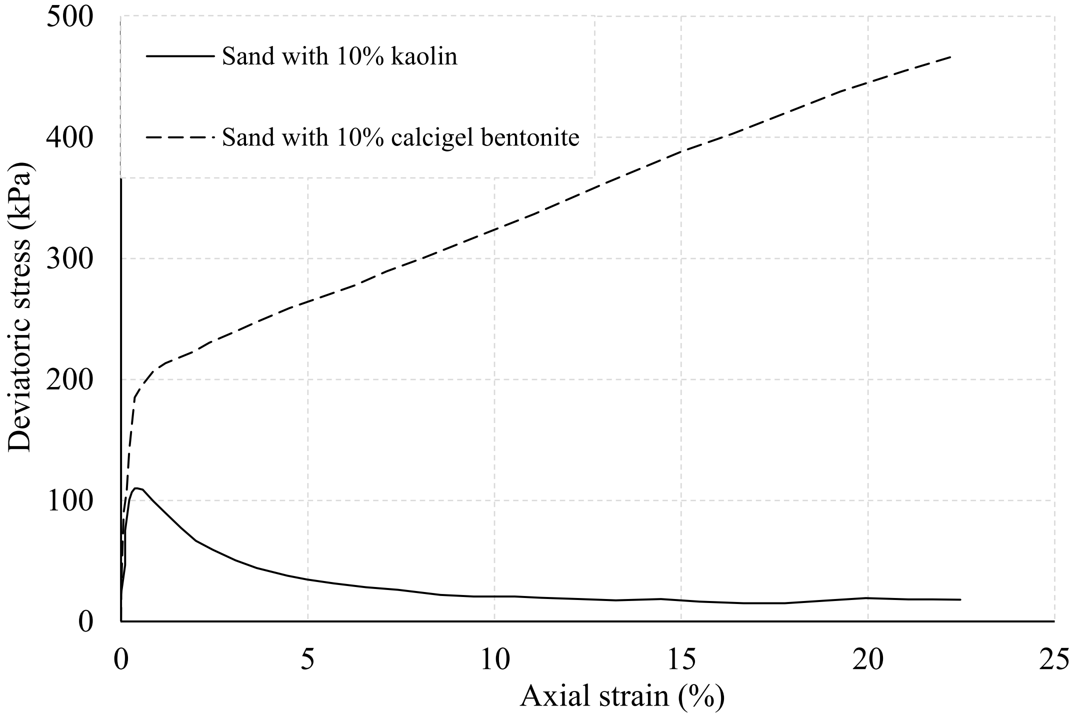

Deviatoric stress (kPa)
Axial strain (%)
Sand with 10% kaolin
Sand with 10% calcigel bentonite
500
400
300
200
100
0
0
5
10
15
20
25

(a)

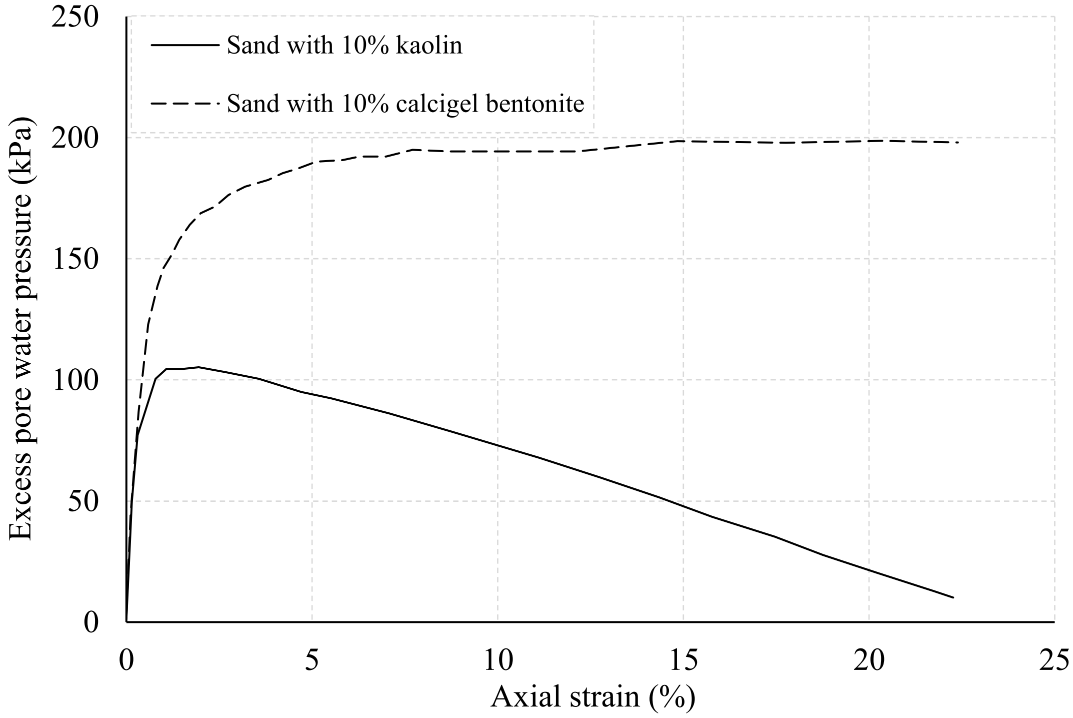

Excess pore water pressure (kPa)
Axial strain (%)
Sand with 10% kaolin
Sand with 10% calcigel bentonite
250
200
150
100
50
0
0
5
10
15
20
25

(b)

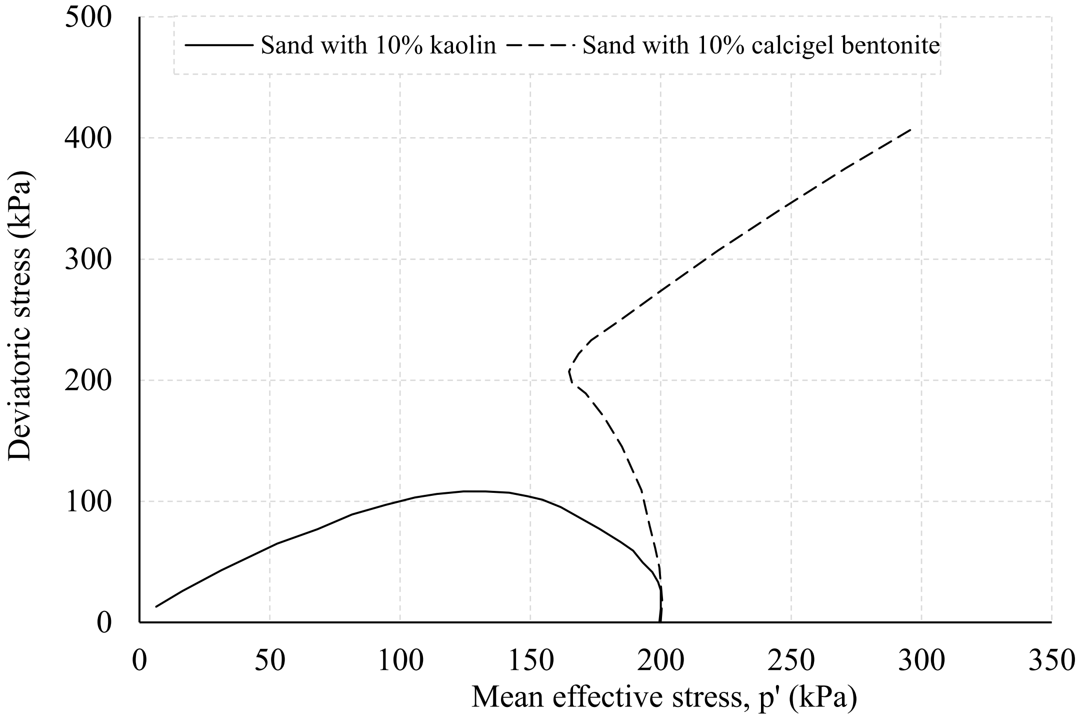

Sand with 10% kaolin
Sand with 10% calcigel bentonite
Deviatoric stress (kPa)
Mean effective stress, p' (kPa)
0
100
200
300
400
500
0
50
100
150
200
250
300
350

(c)

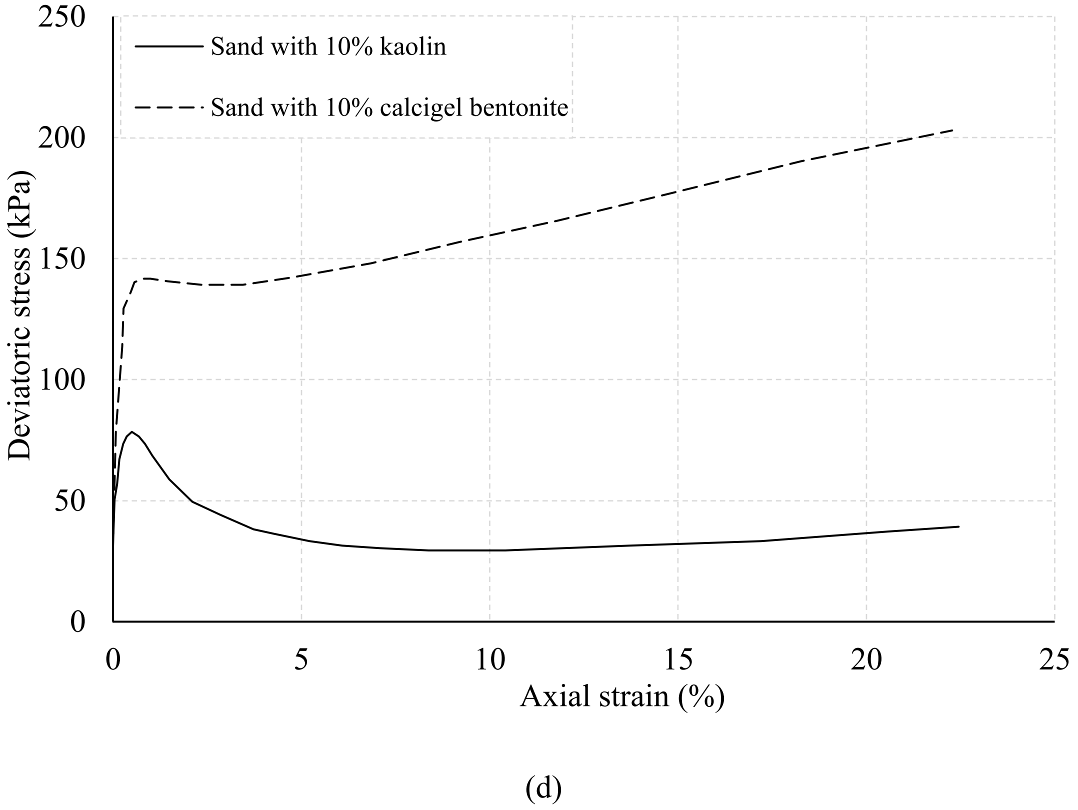

Sand with 10% kaolin
Sand with 10% calcigel bentonite
Deviatoric stress (kPa)
Axial strain (%)
0
50
100
150
200
250
0
5
10
15
20
25

(d)

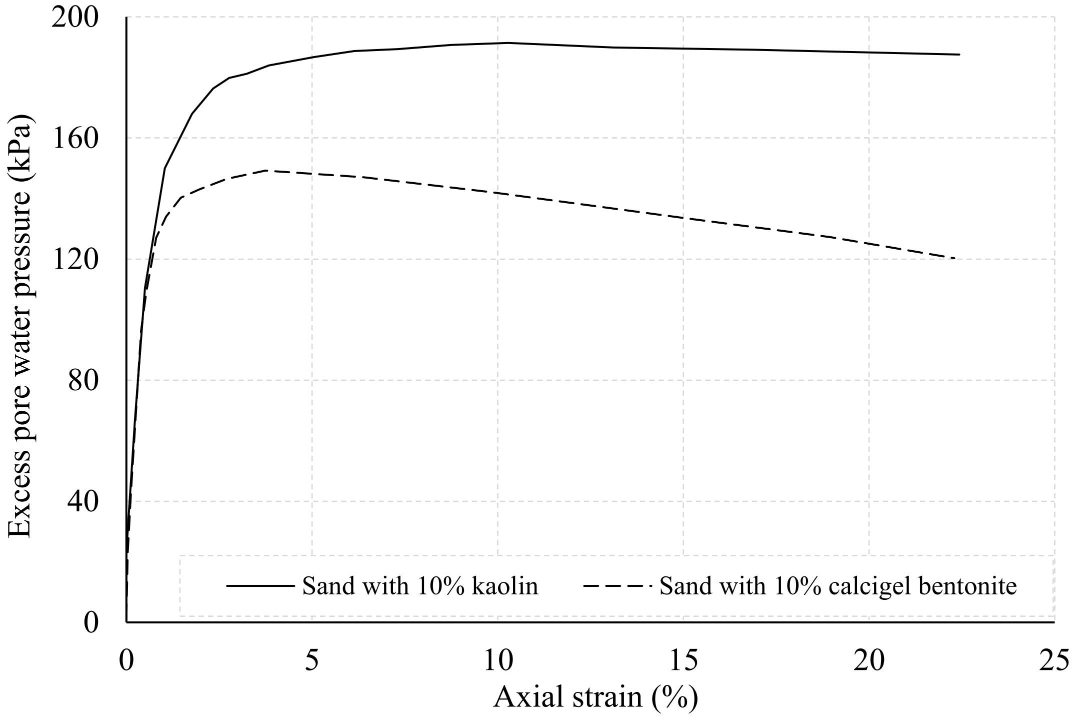

(e)

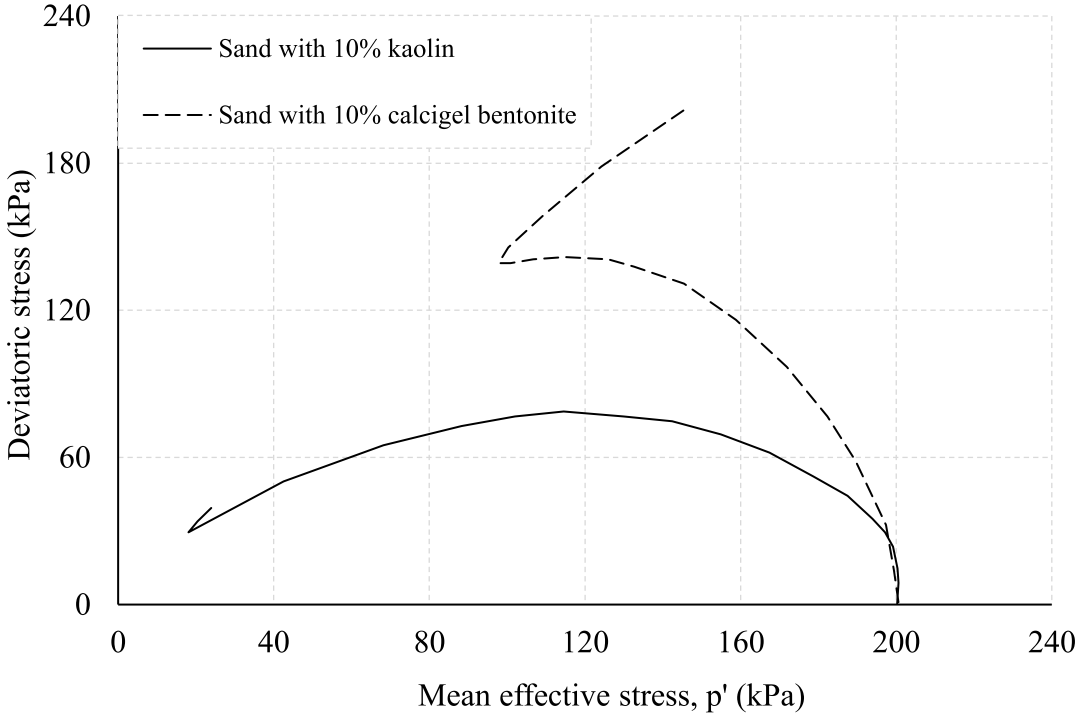

(f)

Figure 2.20. Effect of plasticity of the fine-grained soil on the undrained response of sand; (a), (b), (c) the testing results for the sand with 10% kaolin and calcigel bentonite (d), (e), (f) the testing results for the sand with 10% kaolin and calcigel bentonite (Goudarzy et al. 2021).

2.9 Intergranular Void Ratio

When obtaining the critical state line with void ratio, several studies showed that each mixture requires a unique critical state rather than having a single one for the mixtures independent of fines content. This is caused by the void ratio that was used as a comparison base in soil mechanics. Using void ratio to estimate critical state line or the response of soil could be useful however fines-coarse soil mixtures are complicated.

Theveneyagam (1998) divided the behaviour of fines-coarse soil mixtures into three states (Figure 2.21). When the fines content is low (stage 1) the fines float in the voids of coarse-grained soil and therefore do not contribute to the force chain. This requires instead of void ratio using e_s concept which regards fines as voids until a specific fines content. According to the author increasing fines content up to the e_{max} of host granular soil, fines additions decrease the compressive strength and increase the contractiveness of the mixture. Increasing the fines lead to a point where fines start contact with each other and thus contribute to the mechanical response of mixtures whereas the coarse grains float in the voids of fines in this stage. The mechanical response of mixtures improved with fines content in this stage. The authors suggested using the interfine void ratio in this stage as an accurate comparison base. Intergranular and interfine void ratio is defined as follows:

$$e_g = \frac{e + f_c}{1 - f_c} \qquad e_f = \frac{e}{f_c} \tag{2.1}$$

Where e is the void ratio and the f_c is the fines content in decimal.

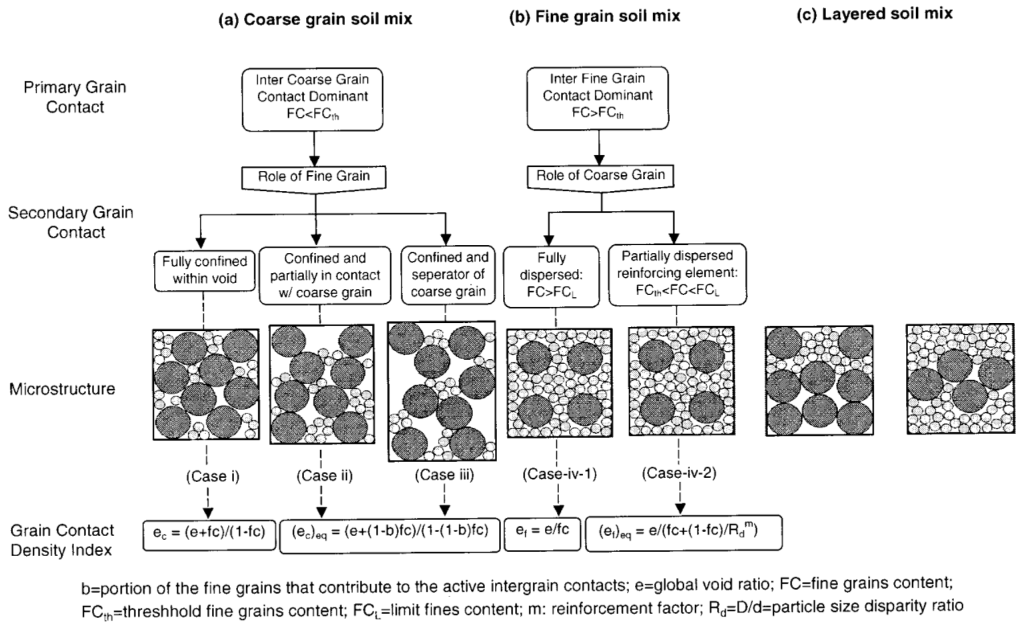

Figure 2.21. Concept of intergranular and interfine void ratios (Thevanayagam et al., 2002).

This concept was even updated as the fines could partially contribute to the force matrix. Thevenayagam (2000) introduces a "b" value to quantify the contribution of fines in mixtures. The "equivalent void ratio" equation was provided as follows:

$$e^* = \frac{e+(1-b)f_c}{1-(1-b)f_c} \tag{2.2}$$

Where e* is the granular void ratio and b (from 0 to 1) is the fraction of fine particles that are in contact. When the b value is 0, this means no fines contribute to the force chain. When it is between 0 and 1, it means the fines partially contribute to the force chain. When the b value is 1, it means all fines are in contact and contribute to the force chain. This concept led to a single trend in the e*-log p' space (Rahman, 2007).

The limiting fines content (or transitional fines content) and b value were further investigated by Rahman (2008) (Figure 2.22). The researcher investigated the testing results in the literature and suggested the following equations;

$$b = \left[1 - \exp\left(0.3 \frac{(f_c / f_{thre})}{k}\right)\right]\left(r \frac{f_c}{f_{thre}}\right)$$

$$f_{thre} = 0.4\left(\frac{1}{1+e^{0.5-0.13\chi}} + \frac{1}{\chi}\right)$$

$$\chi = \frac{D_{10}}{d_{50}} \tag{2.3}$$

$$r = \frac{1}{\chi}$$

$$k = 1 - r^{0.25}$$

Where f_{thre} is the threshold fines content, χ is the particle diameter ratio, D_{10} is the effective grain diameter of host grains, and d_{50} is the median diameter of fine particles.

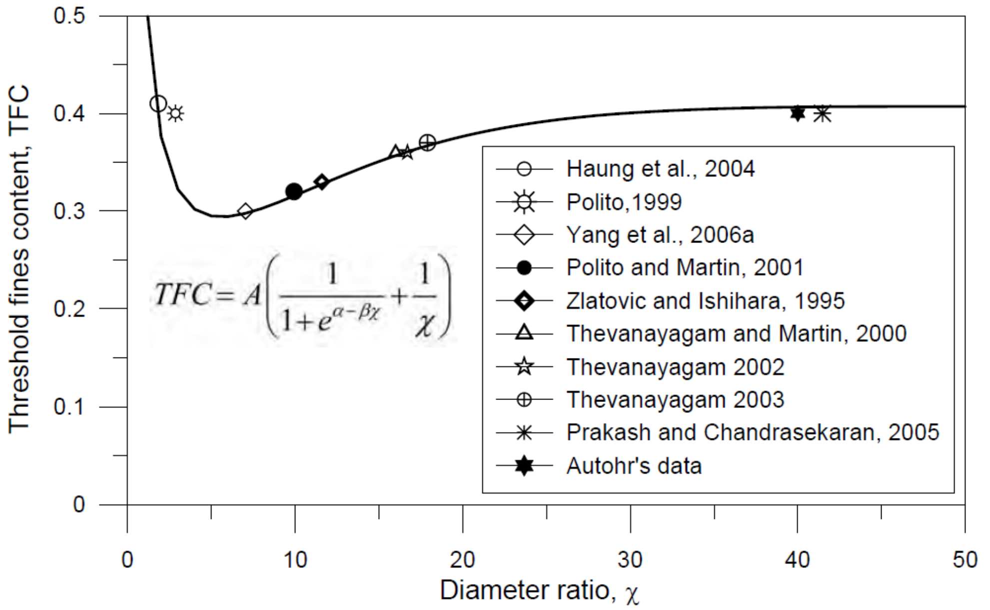

Figure 2.22. Variation of diameter ratio with threshold fines content (Rahman, 2009)

2.10 The Importance of Stiffness of Geomaterials at Small Strain Levels

The numerical studies conducted by Simpson et al. (1979) propose a non-linear stiffness model to accurately estimate the deformation and stiffness characteristics observed in field measurements. The numerical analysis divides the stiffness behavior of London clay into three ranges: (i.) elastic, where deformations are very small and the stiffness of the material is high, (ii.) intermediate, where both elastic and plastic strains can be observed in the lab, and (iii.) plastic, where large strains occur (>1%)

and is the strain range that the soil approaches its peak stress value. Such non-linear stiffness values were first confirmed by Costa-Filho, 1980, who conducted a UU test on clay with local measurements. Given that the majority of the deformation associated with tunnels, silos, and other structures occurs at deformation levels less than 0.1%, the use of the non-linear stiffness model proposed by Simpson et al. (1979) has grown in importance. Figure 2.23 shows a typical stiffness degradation curve that demonstrates that soil stiffness is constant and maximum at strain levels of 10^{-4}%. The stiffness then decreased until it reached around a constant value. The stiffness at a very small strain (10^{-3}%) is defined as the Maximum shear modulus (G_{max}). Soil stiffness at these levels is required in a wide range of engineering applications, including the modelling of soil behavior during earthquakes, winds, traffic vibrations, and other types of wave loading. Two laboratory tests are available to obtain G_{max} values from soil specimens: the BE and resonant column tests. The figure also shows that local strain gauges are insufficient to provide stiffness values at very low strain levels.

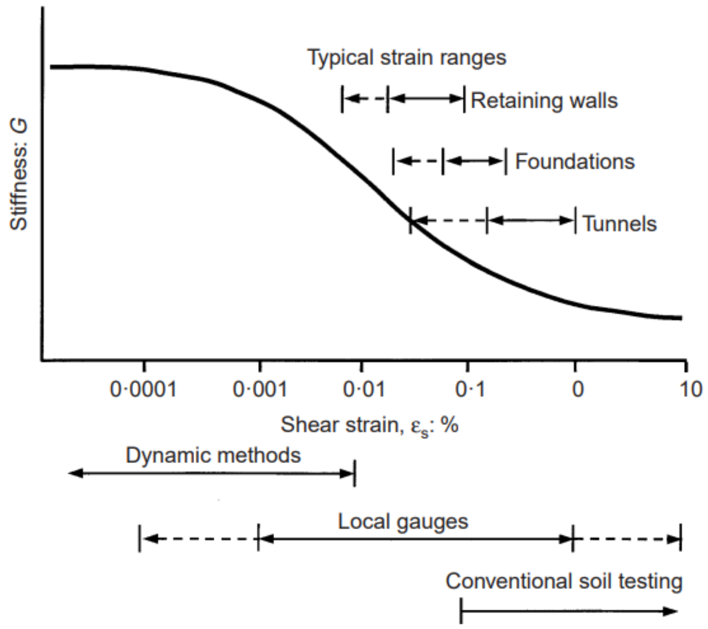

Figure 2.23. Soil stiffness variation with strain ranges for laboratory tests and structures (Atkinson, 2000).

2.10.1 Improvement of Local Strain Instrumentation in Triaxial Testing

Burland (1989) discussed the deformation of a silo that is located on chalk. The tank deformation test and large-scale plate loading test were compared to Young's modulus-

SPT relationship suggested by Wakeling (1970). The comparison revealed that the E values obtained from the tank test were 5 to 20 times higher than those suggested by the E-SPT line suggested by Wakeling (1970). Furthermore, Cole and Burland (1972) present the deformation characteristics of the retaining wall during the excavation and construction of the Britannic House in London, UK, in a similar discussion. The E values found in this study were found to be 4-5 times higher than those obtained in lab tests. As a result, the researchers believed that the low stiffness values of the soil were caused by the sampling disturbance effect of the in-situ specimens. Burland's (1989) analysis gives rise to the development of more sophisticated stiffness measurements in the laboratory.

The incorrect measurements by the external triaxial instrumentation were thought to be caused by several factors, including the stiffness of the apparatus itself, which included the stiffness of the load cell, porous stones, end platens, and filter papers during compression, and several alignment errors, specific bedding between the specimen and the load cell (Daramola, 1978; Burland and Symes, 1982; Costa Filho, 1980; Costa Filho, 1985). Several studies were conducted to improve measurements to directly measure deformation on the specimen rather than an external device (Burland and Symes, 1982; Jardine et al., 1984; Clayton and Khatrush, 1986). Correct stiffness measurements were then performed using local strain instrumentation rather than external LDS.

Jardine et al. (1985) made a comparable observation. The UU testing results of the authors are shown in Figure 2.24. Figure 2.24a depicts a portion of the stress-strain relationship obtained using both local and external instrumentation. The ratio of secant modulus to C_u is shown in Figure 2.24b. The results showed that the stress values and stiffness at small strains (0.1%) measured by local LVDTs are much higher than those measured by external LDS. As described by Simpson et al (1979), the stress-strain relationship depicted in Figure 2.24a is non-linear at low strain as opposed to linear elasticity theory.

Once the stiffness values on the tested specimen were determined using local measurements, the laboratory testing results were compared to those obtained in-situ. Jardine et al. (1985) performed a study that compares the stiffness values of London clay obtained with the laboratory triaxial tests with the stiffness values of the footing and a plate that lies on London clay in situ. Figure 2.25 depicts the in-situ stiffness and laboratory testing results using LVDTs on London clay from Jardine et al. (1985). The in-situ stiffness values obtained from plate loading and footing tests on London clay are very close to the stiffness value range obtained from the laboratory triaxial test using local measurement instrumentation. These findings highlight the significance of local strain measurements in laboratory tests. With the development of local strain measurements in the laboratory, the problem of the difference between in situ stiffness and laboratory stiffness on soils was minimized. This led to further development in local strain measurement instrumentation. Various types of instrumentation including local deformation transducers (LDTs) (Goto et al., 1991), submersible/non-submersible linear variable differential transducers (LVDTs) (Brown and Snaith, 1974; Burland and Symes, 1982; Costa Filho, 1980; Cuccovillo and Coop, 1997), proximity transducers (Hird and Yung, 1989), Hall effect gauges (Clayton and Khatrush 1986; Jardine et al., 1985) were developed by numerous researchers.

Clayton and Khatrush (1986) were among the first to apply Hall effect strain transducers, as illustrated in Figure 2.26, in the construction of a local strain gauge that employs a Hall effect semiconductor with direct current (DC). The researchers used a local strain gauge that works on the Hall Effect principle. The Hall Effect makes use of Hall voltage, which is a type of voltage produced in the normal direction of current flow. Linear Hall gauges generate direct current output that varies linearly with magnetic flux density. Figure 2.26 shows the CD triaxial stress-strain values measured with a local strain gauge and an external displacement sensor on Leighton Buzzard sand. It was found that the stiffness measured with local strain transducers was greater than that measured with external LDS. Furthermore, the stiffness values of the loading and unloading parts are significantly different.

The working principle of the proximity transducers is the transducer that converts the deformation to the rotation of the capsule. Jardine et al. (1985) were the first to develop the hinge mechanism on such transducers to allow for easy mounting. The gauges are submersible and have been tested at pressures as high as 1500 kPa. Jardine et al. (1985) developed a transducer, which is depicted in Figure 2.27.

Figure 2.28 depicts a pair of LDTs on a specimen. Each LDT is flexible, and thin and has a strip and a pair of hinges. Two strain gauges adhered to the strip that sits between the two hinges. The axial deformation on the strain gauges was triggered by the change in distance between two hinges when the specimen was deformed. LDTs were developed to precisely measure the stiffness of soils at strain levels ranging from 10^{-6} to 10^{-2} %. There are several error sources, including the non-linear calibration line and membrane-to-sample deformation.

LVDTs are one of the most widely used transducer types in the world. Many researchers and industries used commercially available LVDTs to obtain soil strain response. The LVDTs are usually attached diametrically opposite to each other in the specimen. Costa Filho (1980) pioneered the use of fixed-base, non-submersible LVDTs to measure local strain in specimens. Figure 2.29 depicts the non-submersible LVDT developed by Costa Filho (1980) and miniature submersible LVDTs developed by Cuccovillo and Coop (1997).

Cuccovillo and Coop (1997) used an RDP model LVDT with a displacement range of 10 mm, which is sufficient to measure the entire stress-strain range of the soil. The LVDT is made up of a lower and upper mount that is directly glued to the membrane, an armature, and an LVDT. Moving the armature in an LVDT generates voltage, which can then be used to calculate the corresponding deformation using the calibration results. In confining stress of 2 MPa, the water submersible LVDT can be used effectively. The results of the kaolin tests using both internal LVDTs and external LDS were comparable. It should also be noted that external measurements from their study were calibrated using several tests on steel dummy specimens to overcome the compliance of the apparatus. In summary, these studies showed that considerable improvements in obtaining the small strain properties of soil specimens using local strain gauges have commonly been used by researchers

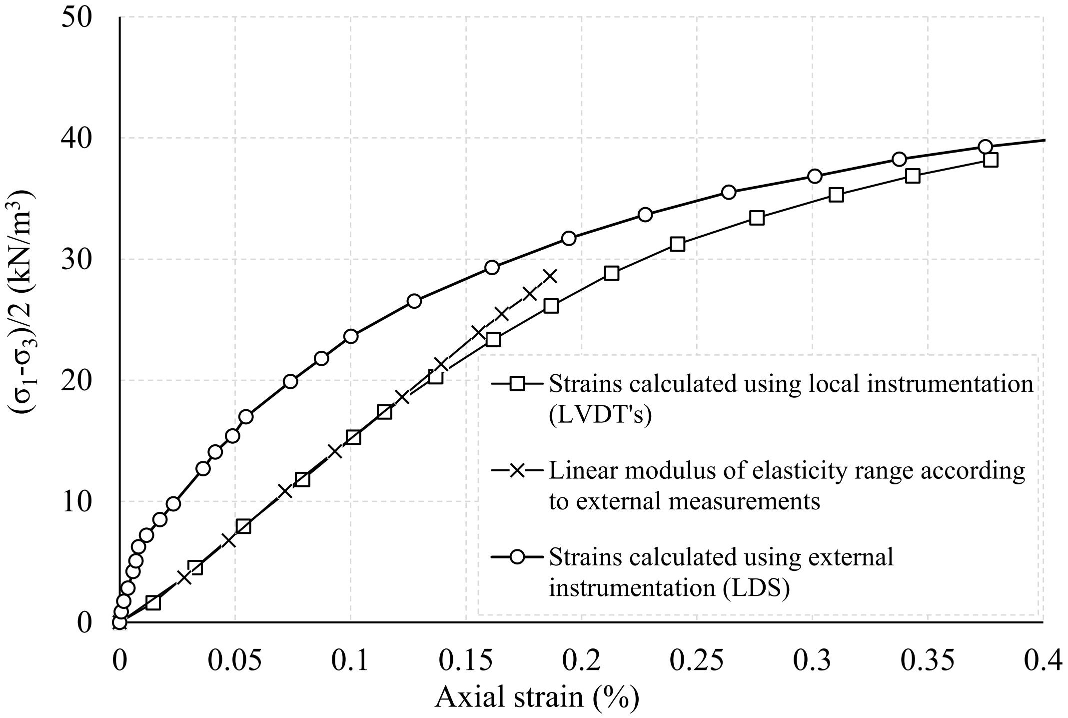

(a)

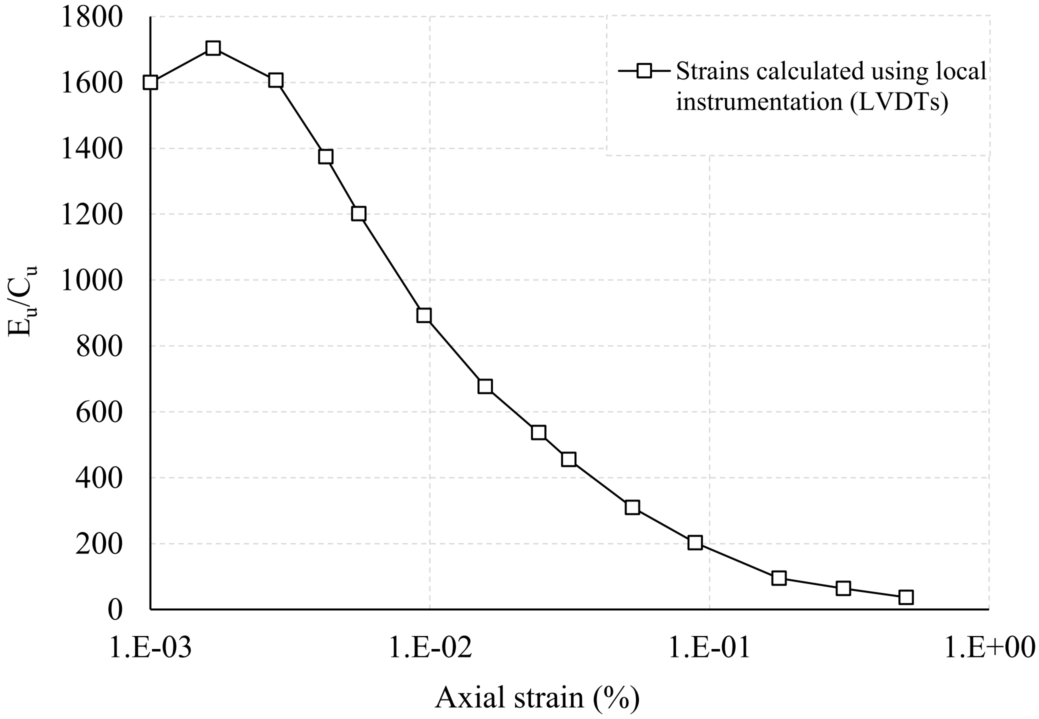

(b)

Figure 2.24. The UU triaxial testing results on London clay using the local LVDT's (a) stress-strain response (b) E_u/C_u ratio with axial strain (redrawn from Jardine et al., 1984).

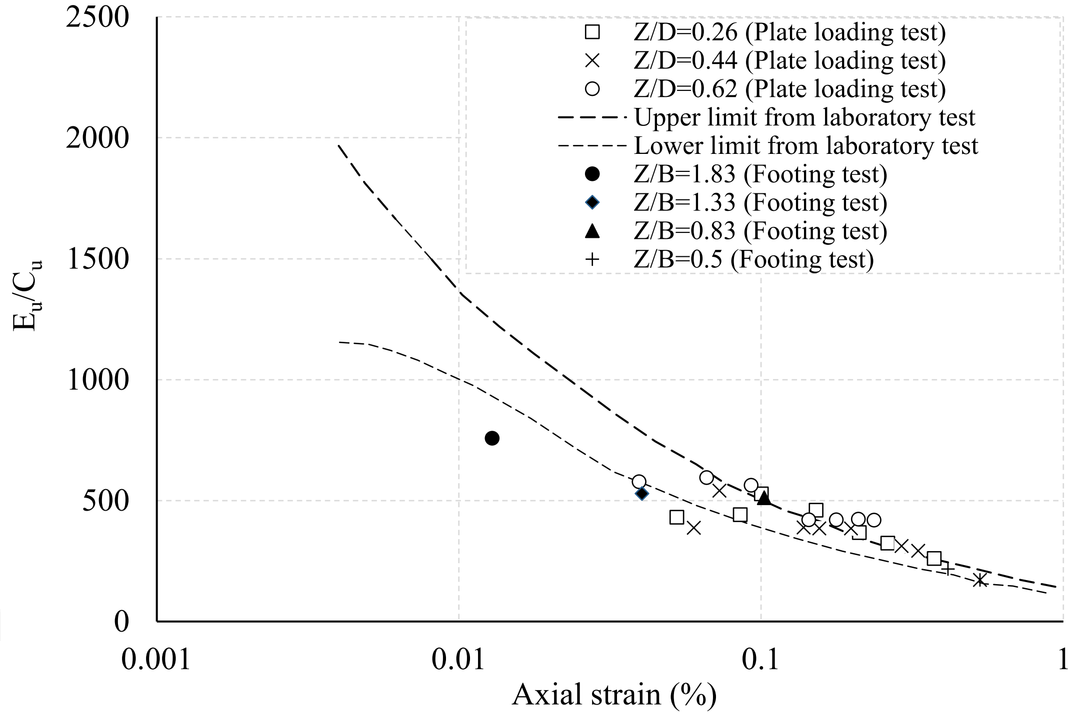

Figure 2.25. The comparison of in-situ tests and laboratory UU triaxial testing results on London clay using the local LVDTs (Z/D values are the plate loading testing results, Z/B values are footing testing results for the D and B values of 0.865 and 3 m respectively) (redrawn from Jardine et al., 1985).

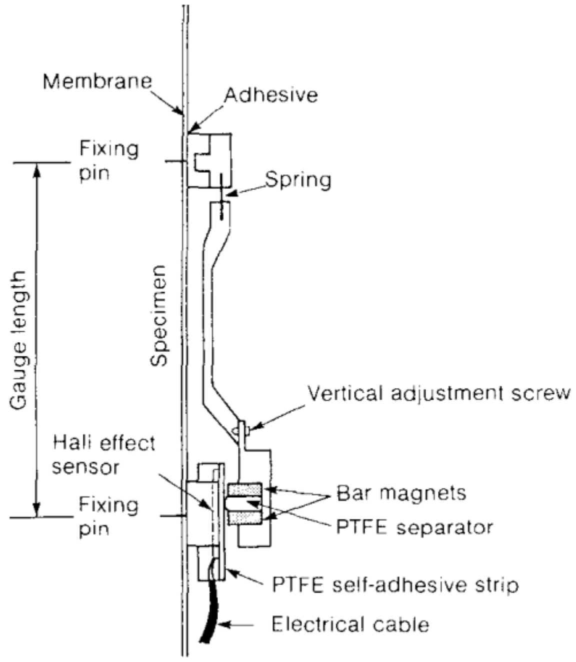

(a)

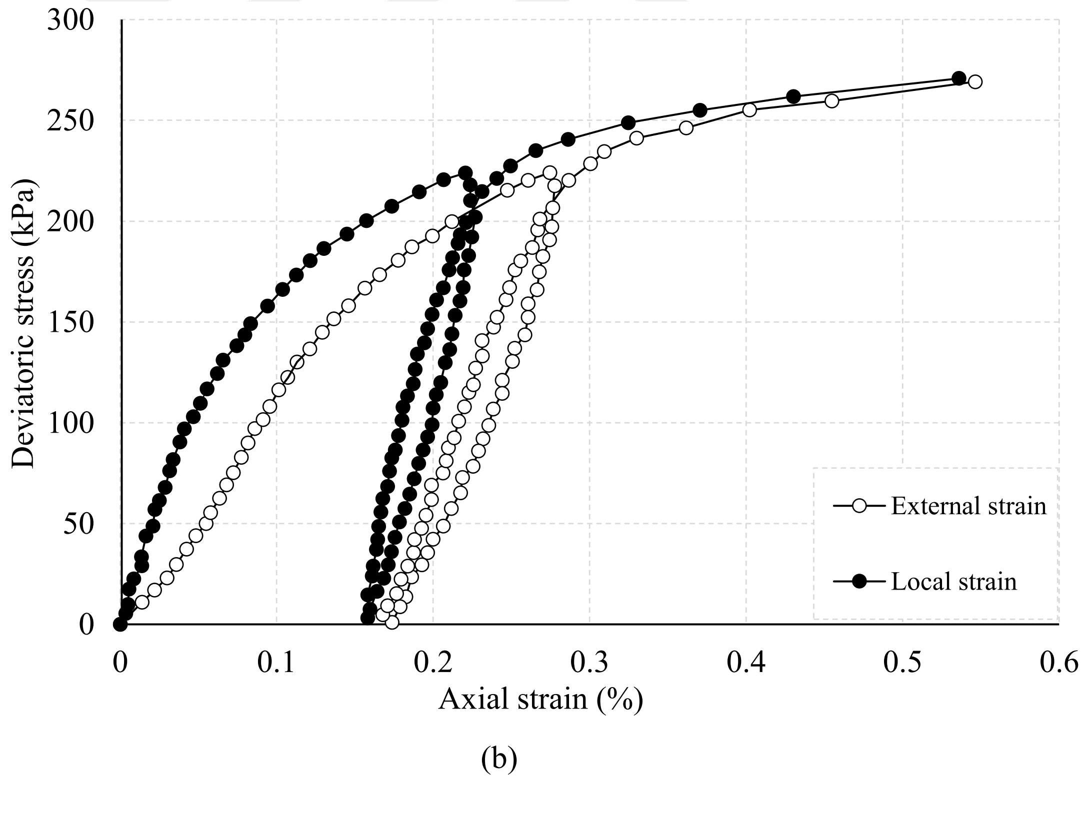

(b)

Figure 2.26. Hall effect local strain gauge: (a) Hall effect local strain gauge design (b) stress-strain graph of the CD triaxial test on Leighton Buzzard test using the local strain gauge and the external LDS (Clayton and Khatrush, 1986).

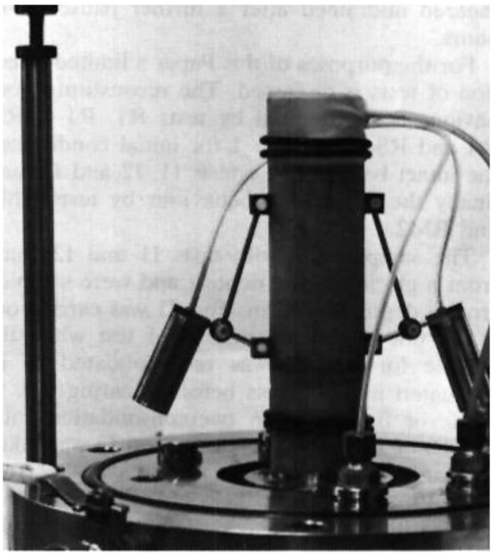

Figure 2.27. Electrolyte level transducers (Costa Filho, 1980).

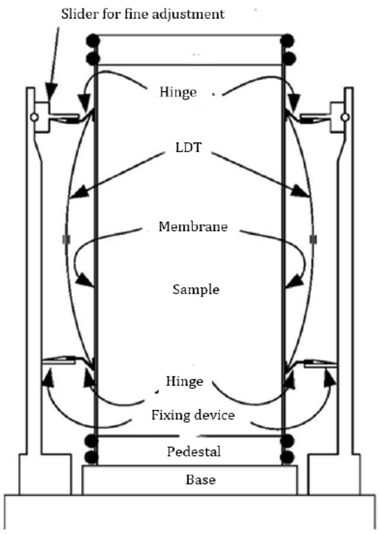

Figure 2.28. Local deformation transducers (LDTs) (Goto et al., 1991).

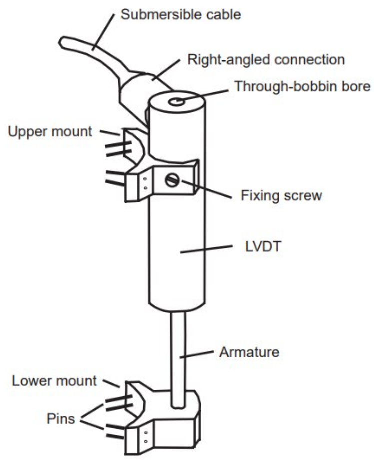

(a) (b)

Figure 2.29. Linear variable differential transducers (LVDTs) (a) Non-submersible LVDT design from Costa Filho (1980) (b) submersible LVDT design from Cuccovillo and Coop (1997).

2.10.2 Bender Element Test

Shirley (1978) proposed the Bender element (BE) testing equipment, which has long been recognized by numerous researchers. The BE tests allow researchers to employ both shear and compressional waves to determine both the v_s and v_p of the specimens tested. Because the BE is a small and compact instrument, it can be mounted in a variety of geotechnical testing equipment such as direct shear, consolidation (Dyvik and Olsen, 1989), resonant column (Dyvik and Madshus, 1985), and triaxial (Bates, 1989).

A BE testing setup consists of two components, one on each side of a soil specimen, one acting as a transmitter and the other as a receiver. Each embedded element is composed of two piezoceramic plates connected by a conductor. Applying a shear or compression wave causes the plates to extend or contract, resulting in a seismic wave (S wave or P wave) to be applied to the soil specimen in a strain magnitude level of 10^{-4}. When the wave reaches the opposite end of the specimen, the receiver element is distorted, resulting in a new voltage pulse (Figure 2.30). "Travel time" refers to the time difference between the two voltage pulses.

BE is made up of transmitter and receiver BE, function generator, power amplifier, and oscilloscope. The function generator is used to send electrical signals to the BEs to generate a wave that can be sinusoidal, sawtooth, or square. A power amplifier is used to amplify the output voltage to the BEs. Once the wave is fueled by the receiver BE the oscilloscope is used to accurately determine the travel time of the wave by transforming the voltage travelling in the soil to the waveform. The travel time is then calculated. Various geotechnical properties of the tested specimen including v_s, v_p, G_{max}, and M_{max} values can then be found. The υ value can also be determined in BE tests using both shear and compressional wave testing results.

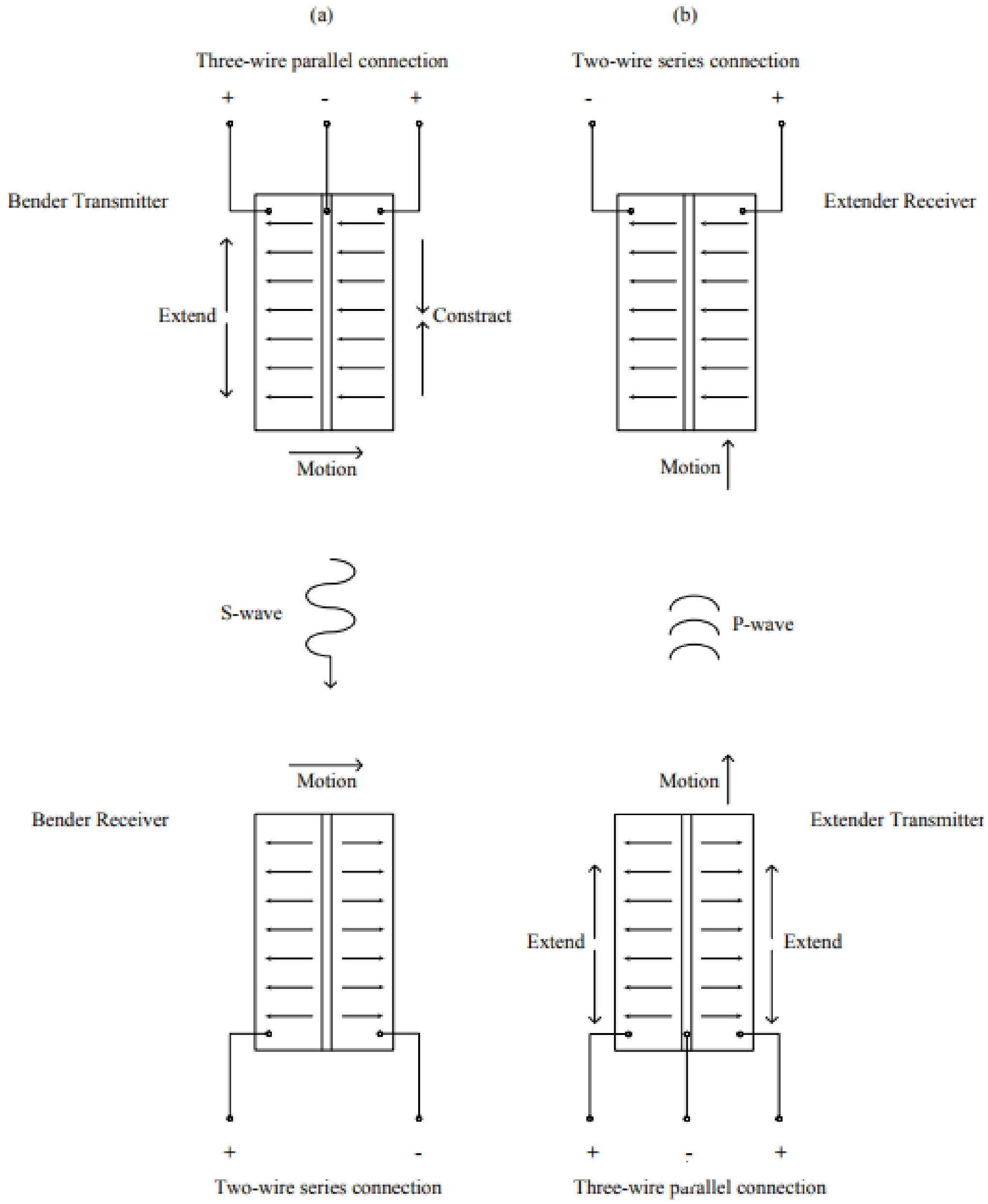

Figure 2.30. Diagram of the bender and extender connection: (a) S-wave transmission; (b) P-wave transmission (Lings and Greening, 2001).

CHAPTER 3
MATERIALS AND METHOD

3.1 Materials

The soil types used in this study were bentonite, Waste glass (WG) with two different sizes namely; Fine waste glass (FWG) and coarse waste glass (CWG), sand and silt. Bentonite type of clay has liquid and plastic limit values of; 279% and 165% respectively. The specific gravity of bentonite was 2.67. Several geotechnical properties of clean bentonite are presented in this thesis. The WG utilized in this study was the unused part of the glass after the manufacture of window profiles. The WG grains have a specific gravity (G_s) of 2.85. Figure 3.1 shows the grain size distribution of the two materials utilized in the studies. The median diameter (D_{50}), coefficient of curvature (C_c), and coefficient of uniformity (C_u) of bentonite clay were determined to be 0.035mm, 1.1, and 0.8, respectively. The D_{50}, C_c and C_u of the FWG were determined to be 0.037 mm, 1.9, and 0.84, respectively. D_{50}, C_c, and C_u of the CWG were measured to be 0.44 mm, 2.82 mm, and 0.96 mm, respectively. Figure 3.2 shows the images from Scanning Electron Micrographs (SEM) and Figure 3.3 depicts a photograph of the soils and the additives used in the study. Distilled water was used as a pore fluid in all laboratory tests. Table 3.1 presents the X-ray fluorescence (XRF) testing results of the materials used in the study.

3.2 Testing Apparatus and Sample Preparation

The amount of dry soil required for each soil type was calculated based on the γ_{dmax} of the mixtures. The amount of water used in the mixtures was determined by w_{opt} and then water was added to the dry soil specimens. The dry mixtures and water were then mixed until a homogeneous mixture was observed. The bentonite was mixed separately with FWG and CWG at mixing ratios of 0%, 10%, 20%, 30%, and 40% to prepare 9 different mixtures.

The testing program applied to the bentonite-WG mixtures is presented in Table 3.2. According to the test program, compaction, fall-cone, consolidation, direct shear, viscosity, crumb, double hydrometer, and unconfined compaction, and bender element tests were performed on the bentonite-WG mixtures. A second testing program used Narlı sand (NS) and medium plastic silt (ML). The ML was mixed with the NS with mixing ratios of 0%, 10%, 20%, 30%, and 40% and a series of the CU tests at three different ECS of 50, 100, and 150 kPa were performed on the specimens. The details for each test are presented in Table 3.2.

3.2.1 Compaction Test

In the compaction test, a sample base, mold, collar, and compaction hammer were used. The test was performed in a specially designed mold with a diameter of 43 mm, a height of 100 mm, and a 1.23 kg hammer. A hammer with a drop height of 0.23 m yielded an energy of around 2700 kJ/m^3 (Das and Sivakugan, 2016). Photograph of the test components are shown in Figure 3.4.

3.2.2 Fall-cone test

Figure 3.5 shows the picture of the fall-cone testing equipment used in the study. A 40 mm*55 mm cup was used for fall-cone tests. The soil was placed in the cup, and a penetration testing time of 5 seconds was allowed. Following the completion of the test, a piece of wet soil from the cone penetration region was obtained from the specimen to determine the water content. The undrained shear strength from fall-cone tests was obtained by the equation suggested by Hansbo (1957). developed Equation 1. where k is a constant of 0.85, w is cone weight (kN), and d (m) is the penetration of the cone.

$$s_u = \frac{k * w}{d^2} \tag{3.1}$$

Where k is 0.85 for a cone with a 30˚ apex angle, w is cone weight, and d is the penetration.

Table 3.1. XRF testing results of the materials used during the experimental study

Chemical compounds	Waste glass (%)	Bentonite (%)
Na_2O	12.31	3.17
SiO_2	69.42	61.2
Fe_2O_3	0.48	7.31
CaO	8.27	2.27
Al_2O_3	1.09	18.6
MgO	4.25	3.35

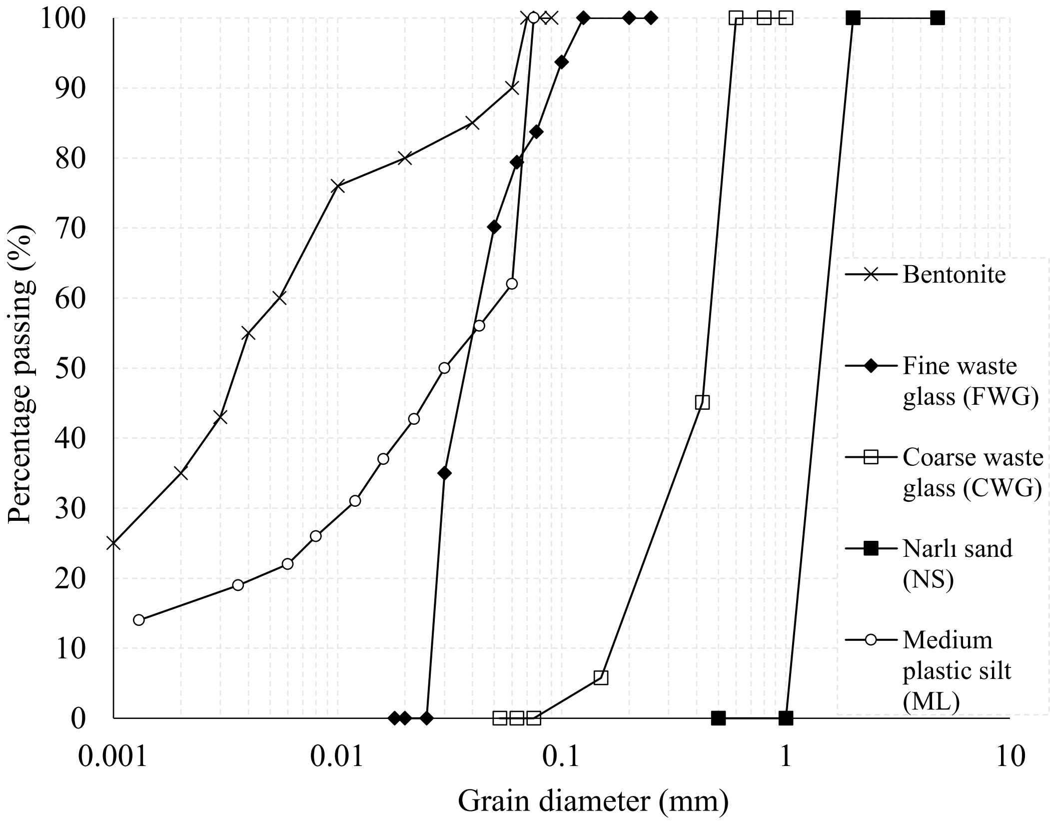

Figure 3.1. Grain size distribution of materials used in the study.

Table 3.2. Testing table of bentonite-waste glass mixtures

<table>
<tr><th>Host material</th><th>Admixture material</th><th>Admixture content (%)</th><th>Test program</th></tr>
<tr><td rowspan="9">Bentonite</td><td></td><td>0</td><td rowspan="9">Modified compaction test (ASTM D1557-12)
Fall-cone test (BS 1377-2)
Consolidation test (ASTM D2435)
Direct shear test (ASTM D6528-17)
Viscosity test (D2196 – 20)
Crumb test (ASTM D6572-21)
Double hydrometer test (ASTM D4221-18)
Unconfined compression test ASTM D2166-06
Bender element test (ASTM D8295-19)</td></tr>
<tr><td rowspan="4">FWG</td><td>10</td></tr>
<tr><td>20</td></tr>
<tr><td>30</td></tr>
<tr><td>40</td></tr>
<tr><td rowspan="4">CWG</td><td>10</td></tr>
<tr><td>20</td></tr>
<tr><td>30</td></tr>
<tr><td>40</td></tr>
</table>

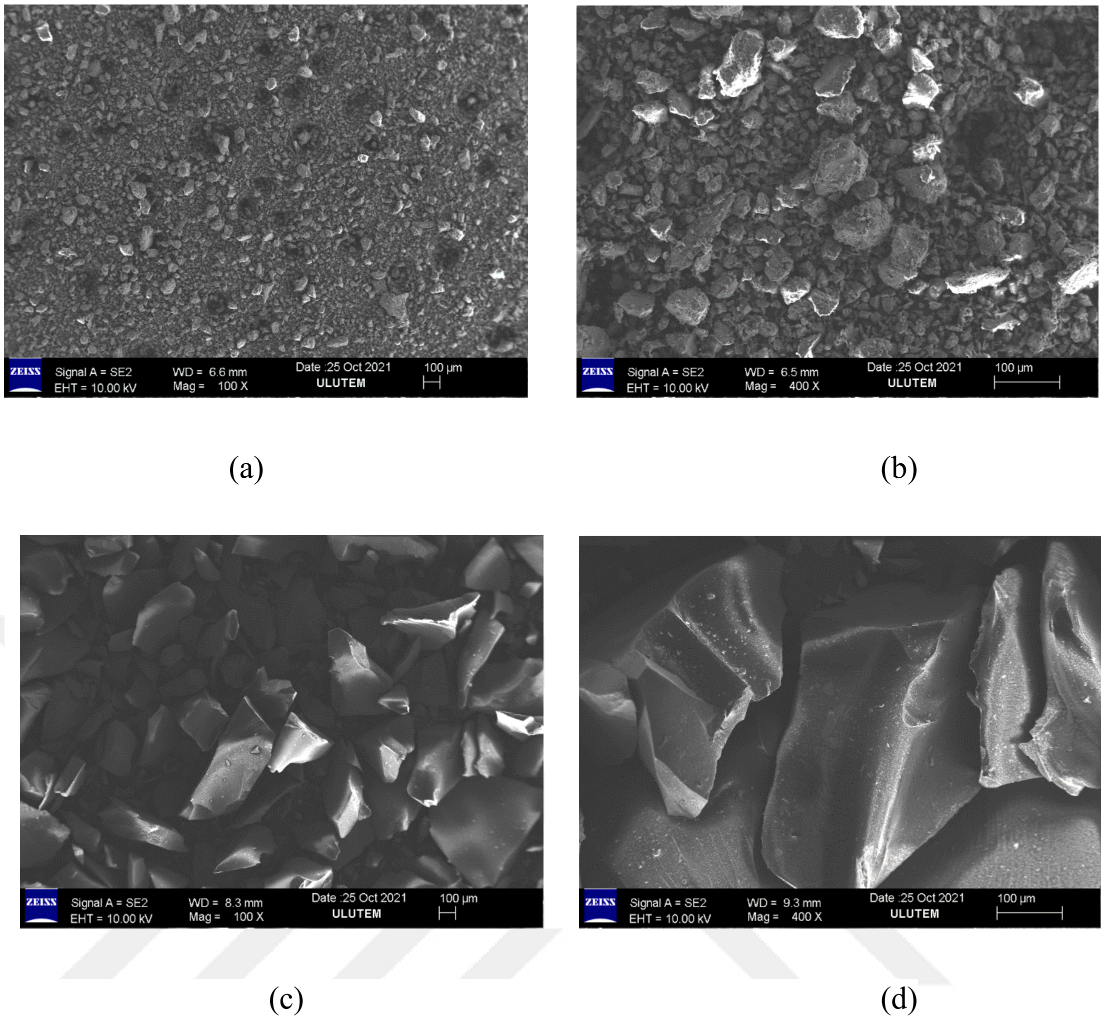

Figure 3.2. SEM pictures of (a, b) clean bentonite, and (c, d) clean WG.

3.2.3 Consolidation Test

The test setup of the consolidation test includes a consolidation cell, two porous discs, a sample ring, a top cap, two filter papers, an O-ring, three clumping nuts, and a locking ring. The specimen was placed into the sample ring using using static compaction method. The void ratio, c_c, and c_s values of the specimens tested were determined after the consolidation tests were completed. The specimens were put through a stress path that ranged from 22 kPa to 800 kPa, with the load being doubled at each step. After that, the unloading stage was carried out at the same stress levels as the loading stage. During the test, ASTM D2435/D2435M-11 (2020) was followed. Equation 3.2 was used to calculate the c_c and c_s of specimens in the consolidation test.

$$c_{c-s} = \frac{\Delta e}{\Delta \sigma'} \tag{3.2}$$

where c_{c-s} is the slope of the void ratio-pressure curve. The slope of the compression line gives c_c while that of the unloading line gives c_s. To find the c_v square time method was used in this study. Therefore, equation 3.3 was used during consolidation experiments.

$$c_v = \frac{0.848d^2}{t_{90}} \tag{3.3}$$

where c_v (cm^2/s) is the coefficient of consolidation, d is the height of the specimen (cm) and t_{90} (s) is the time when 90% of the settlement of the loading stage is completed.

3.2.4 Direct Shear Test

Direct shear tests were performed on the mixtures according to ASTM D6528-17. The tests were performed on square specimens 60 mm on each side under three normal stresses of 50, 100, and 200 kPa. The loading rate of 0.5 mm/min was employed during the test.

3.2.5 Crumb Test

Crumb and double hydrometer tests were used to obtain the dispersive potential of the specimens. A cubic specimen with 15 mm on each side was used for the crumb test. To prepare the cube at w_{opt}, ASTM D6572-21 was followed. The specimen was placed in a container filled with 250 ml of distilled water. The dispersive level was visually determined following the ASTM D6572-21 at 2 minutes, 1 hour, and 6 hours during the test. Figure 3.6 presents the cubes of bentonite-CWG mixtures for the crumb test.

3.2.6 Double Hydrometer Test

Double hydrometer tests were performed to calculate the dispersion potential of the samples. The producer detailed in the ASTM D4221-18 was followed in the tests. ASTM D7928 was followed to obtain chemically and mechanically dispersed samples. ASTM D4221-18 was followed to obtain specimens that were not mechanically or chemically dispersed. Some pictures of the specimens are presented in Figure 3.7. After completing these tests for each specimen, the dispersion potential was calculated as the ratio of 2-um passing of not dispersed samples to 2-um passing dispersed samples.

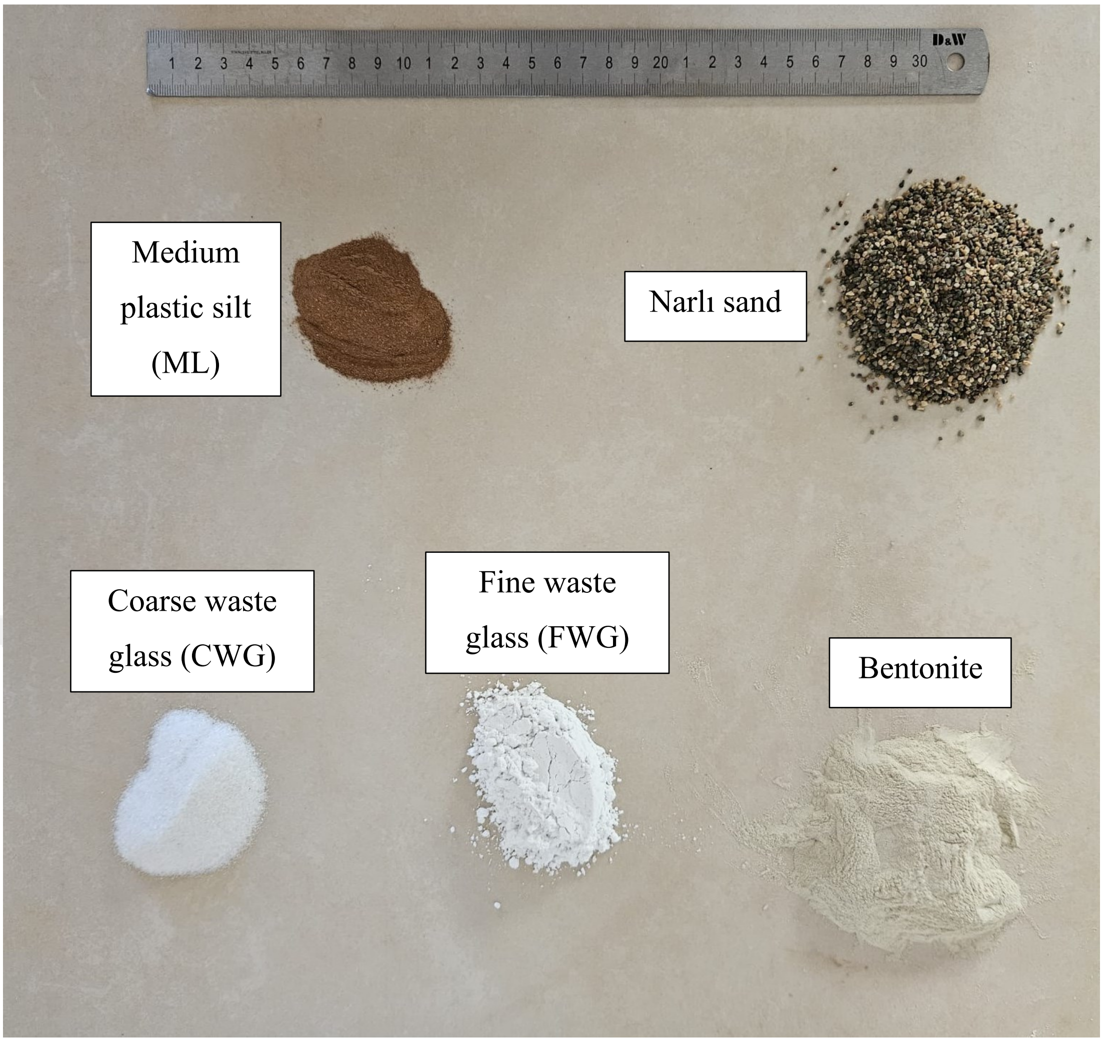

Figure 3.3. Photos of the soil types used in the study.

Figure 3.4. The compaction equipment used during the study.

(a) (b)

Figure 3.5. The fall cone test (a) picture of the test device (b) the cone used during the study.

3.2.7 Viscosity Test

The viscosity tests were performed on the slurry specimens. The specimens were mixed at water content equal to 1.5 times the liquid limit of each specimen. Such a method was used to avoid segregation, and air bubbles during the specimen preparation (Ahmadi-Naghadeh and Toker, 2018). A constant time of 24 hours to ensure homogeneity of the mixtures was applied to all mixtures. To eliminate sedimentation, wet mixtures were vigorously mixed before testing and then the specimen was directly tested using the viscometer device. The experiments were performed with a Brookfield DV3T viscometer, as illustrated in Figure 3.8. The Brookfield DV3T viscometer's Helipath stand was utilized during the viscosity test to obtain viscosity measurements of various parts of the specimens by moving lower and upward in the tested specimen (Figure 3.8). The testing results are automatically produced in.csv format (Brookfield Manual No. M13-2100-A0415).

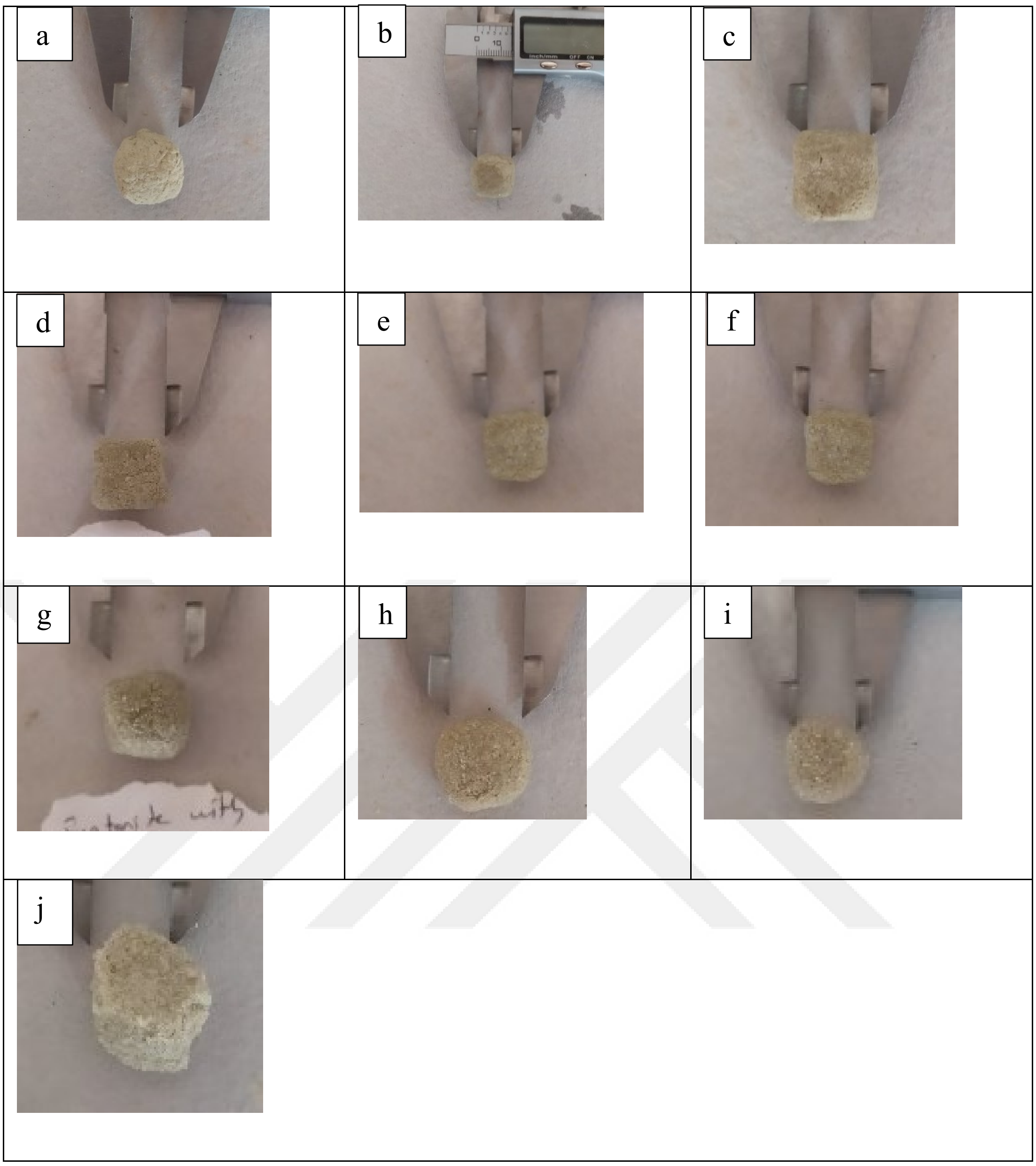

Figure 3.6. Soil specimens for crumb test: bentonite with (a) 0% (b) 10%, (c) 20, (d) 30%, (e) 40%, (f) 50%, (g) 60%, (h) 70%, (i) 80%, (j) 90% of CWG.

3.2.8 Minimum and Maximum Void Ratio Tests

The minimum and maximum void ratios of NS with 0, 10, 20, 30, 40, and 50% ML were obtained by following the ASTM D 4253 and ASTM D 4254, respectively. A vibratory table according to ASTM D4253 was used to find the minimum void ratios of the specimens. Regarding the maximum void ratio, ASTM D4254 Method A was followed during the test despite its limitation to the 15% fine content. Great care was given to prevent the segregation of the particles.

3.2.9 Bender Element and Unconfined Compression Tests

A triaxial device was used to perform both BE and UC tests on the same specimen. The BE testing instrument manufactured by Global Digital Systems Ltd (GDS) was used in the tests (Figure 3.9). The testing equipment shown in Figure 3.10 was employed for the BE and UC tests in a method. Before the test, the BEs were embedded in the soil to ensure the quality of the signal travelling between the soil particles. The specimens were subjected to S and P wave tests to determine v_s and v_p. A sinusoidal wave type was used in the test. The magnitude used in the test was 10 V while the period was 0.5 ms. It is well known that the presence of a near-field effect on the low-frequency levels caused some difficulties in accurately determining the characteristic points of the receiver wave (Cai et al., 2015). Also, input frequency depends on the resonant frequency of the material which is generally high for compacted stiff soils (Lee and Santamarina, 2005). Based on these facts and the material used during the experimental study, a minimum frequency of 30 kHz was chosen based on several studies (Lee and Santamarina, 2005; Camacho-Tauta et al., 2015; Wang et al., 2017b; Wang et al., 2021). The signals were quite clear at the range of input frequencies employed, and the travel time was easily and accurately determined without encountering any near-field effect (Figure 3.11). Furthermore, the frequency range was expanded to 50 kHz (30 kHz, 40 kHz, 50 kHz) to investigate the frequency effect. The testing results at 30, 40, and 50 kHz produced wavelength ratio (L_{tt}/λ) ratios of 16 to 30. These values were found to be similar to the literature (Lee and Santamarina, 2005; Wang et al., 2021).

Figure 3.11 presents a clean bentonite specimen with analyzed BE signals. Figures 11a and 11b show the analysis results during the test. The received signals were attenuated at the end of the sampling time of 5 ms. Figure 3.11c depicts the received signals from the S and P wave tests and an input signal. The correlation curves for the S and P waves are shown in Figure 3.11d. The travel time was calculated using the cross-correlation method (Wang et al. 2007).

In the BE test, the shear wave velocity (v_s) and compressional wave velocity (v_p) were calculated using equation 3.4.

$$v = \rho * \frac{L}{t} \tag{3.4}$$

Where ρ (g/cm^3) is the density of the tested specimen, v (m/s) is the velocity which can be either v_s or v_p, L (mm) is the length between two BE tips, and t (ms) is the wave travel time. Once the v_s and v_p were obtained, the maximum shear modulus (G_{max}), maximum constrained modulus (M_{max}), and υ of the specimen can be calculated using the equation below (Lee and Santamarina 2005; He et al. 2021).

$$G_{\max} = \rho * {v_s}^2 \tag{3.5}$$

$$M_{\max} = \rho * {v_P}^2 \tag{3.6}$$

$$\upsilon = \frac{(\mathrm{v_p} / \mathrm{v_s})^2 - 2}{2[(\mathrm{v_p} / \mathrm{v_s})^2 - 1]} \tag{3.7}$$

where v_s (m/s) and v_p (m/s) are the shear and compressional wave velocity values, respectively.

Following the completion of the BE tests, the UC tests were performed on the same specimens following ASTM D2166. The testing equipment for the UC test measurements includes a load cell and a linear displacement sensor (LDS), as shown in Figure 3.10. The loading rate of 0.7 mm/min was used in the UC tests. The maximum stress value obtained from the stress-strain curve during testing was accepted as the q_u value. The area beneath the stress-strain curve was used to calculate the energy absorption capacity.

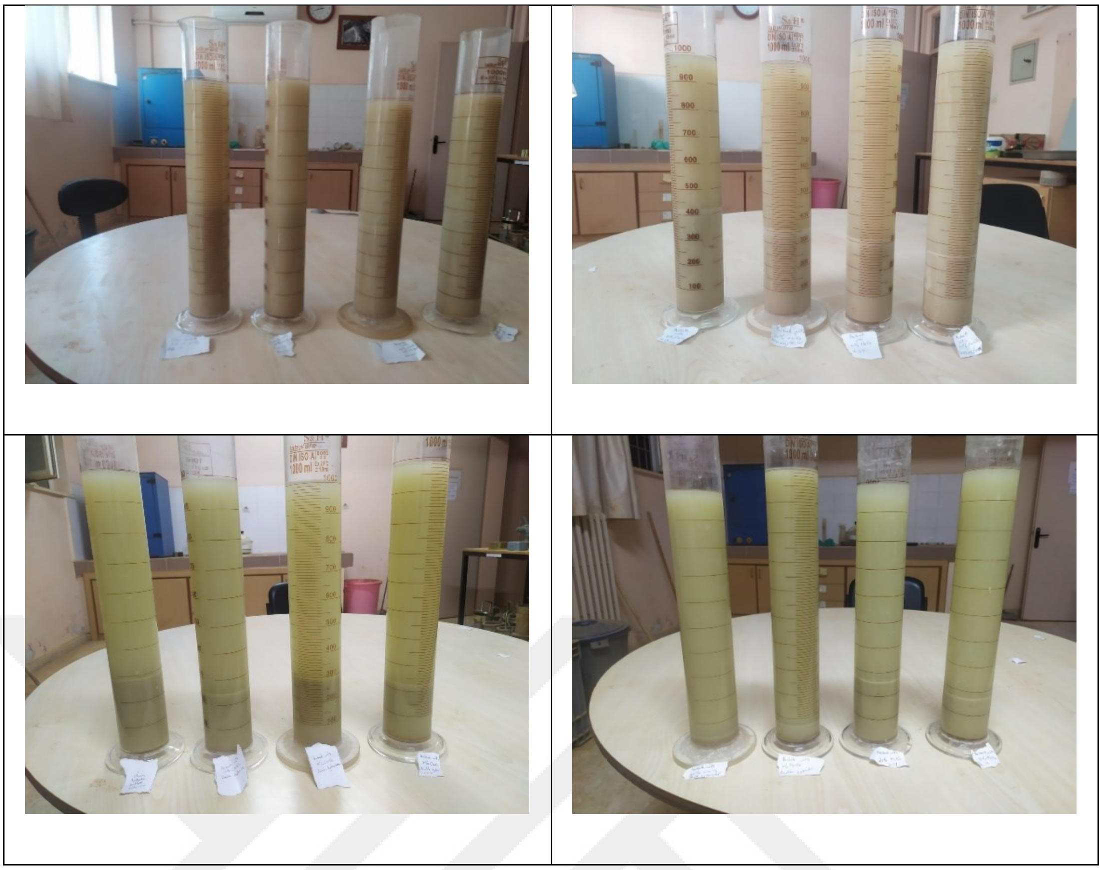

Figure 3.7. Double hydrometer test.

Figure 3.8. Some steps in the viscosity test: (a) viscosity test bentonite with 10% FWG specimen (b) spindle-specimen position during the test (c, d) running a viscosity test at various rotation speeds.

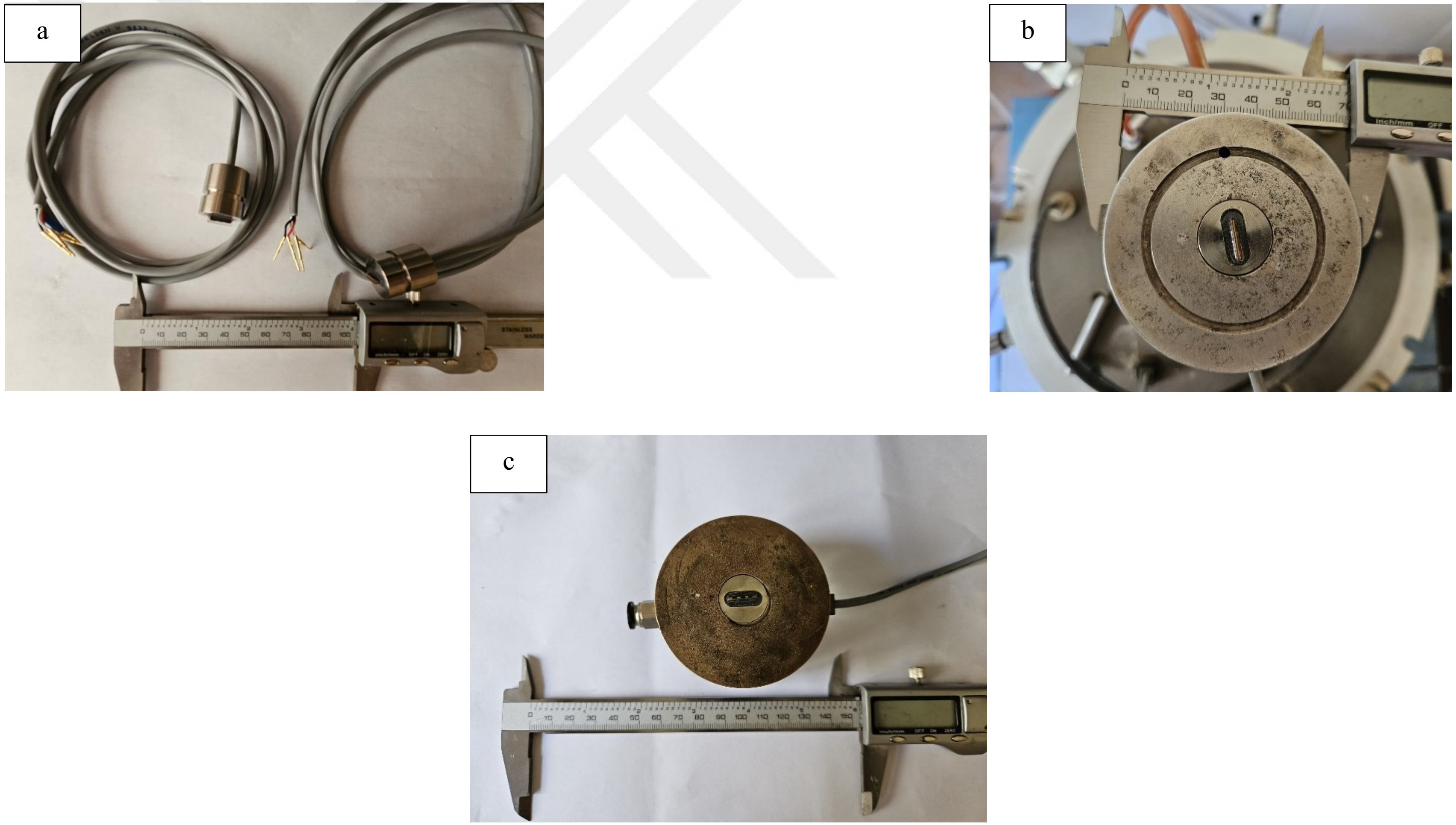

Figure 3.9. The bender elements used in the study (a) BE before the installation on the device (b) BE on the pedestal (c) BE on the top cap.

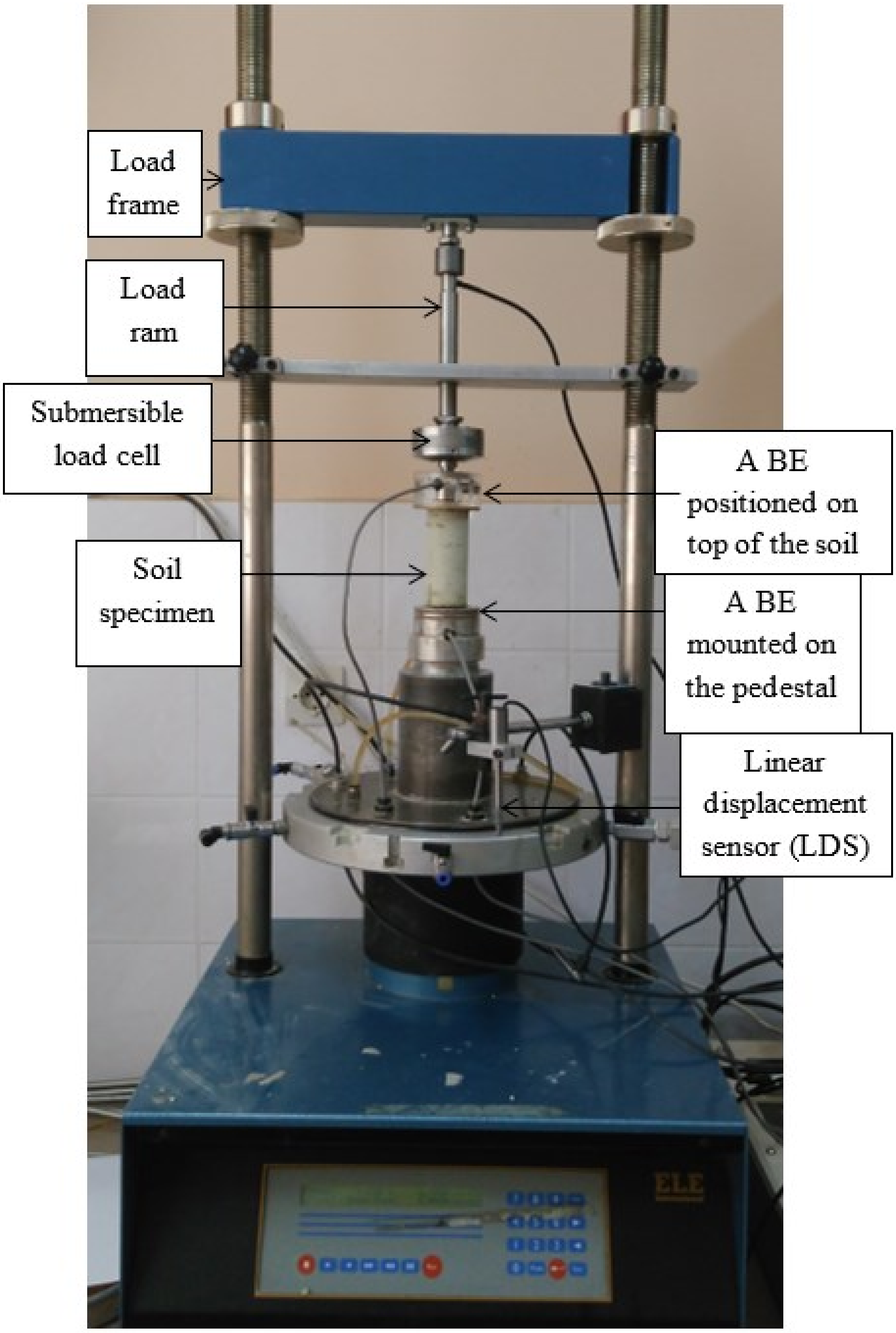

Figure 3.10. The testing apparatus used during UC and BE tests.

Pick 1: 0.12 ms Accept Pick 1? Pick 2: 0.84 ms Difference = 0.72 ms Velocity = 131.9 m/s
Offset Applied
Actual
4.97 mV
5.080 mV
0.11 mV
-4.97 mV
-4.860 mV
10 V
-10 V
0 ms
Fix First Trace
timebase (milliseconds)
5 ms
Test Setup
Current Gain (Auto)
x 500
RESET
Change to P Source
Change Source Details
Data Aquisition Options
kHz
mV
ms
<<
<
0.84
ms
>
>>
Re-Trigger
Test File saved
ADD TO STACK
Stack Count: 1
Filename:
BE_28071112_28
NEW TEST
Save Shot
GDS 2007

(a)

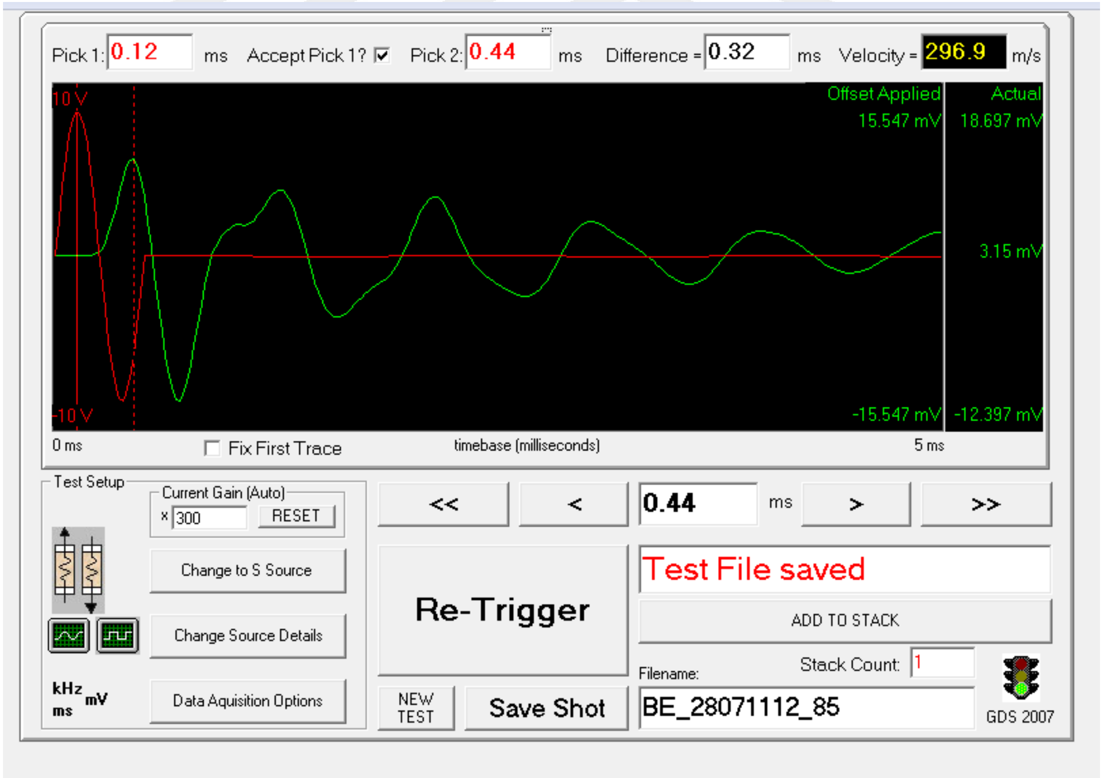

Pick 1: 0.12 ms Accept Pick 1? Pick 2: 0.44 ms Difference = 0.32 ms Velocity = 296.9 m/s
Offset Applied
Actual
15.547 mV
18.697 mV
3.15 mV
-15.547 mV
-12.397 mV
10 V
-10 V
0 ms
Fix First Trace
timebase (milliseconds)
5 ms
Test Setup
Current Gain (Auto)
x 300
RESET
Change to S Source
Change Source Details
Data Aquisition Options
kHz
mV
ms
<<
<
0.44
ms
>
>>
Re-Trigger
Test File saved
ADD TO STACK
Stack Count: 1
Filename:
BE_28071112_85
NEW TEST
Save Shot
GDS 2007

(b)

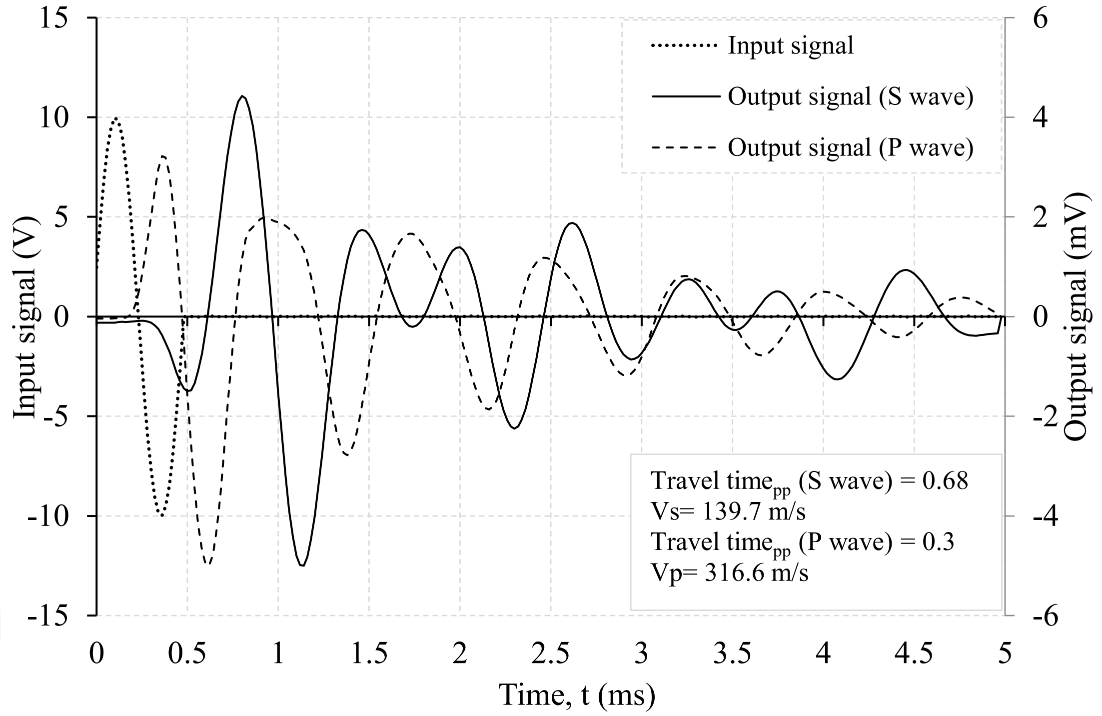

(c)

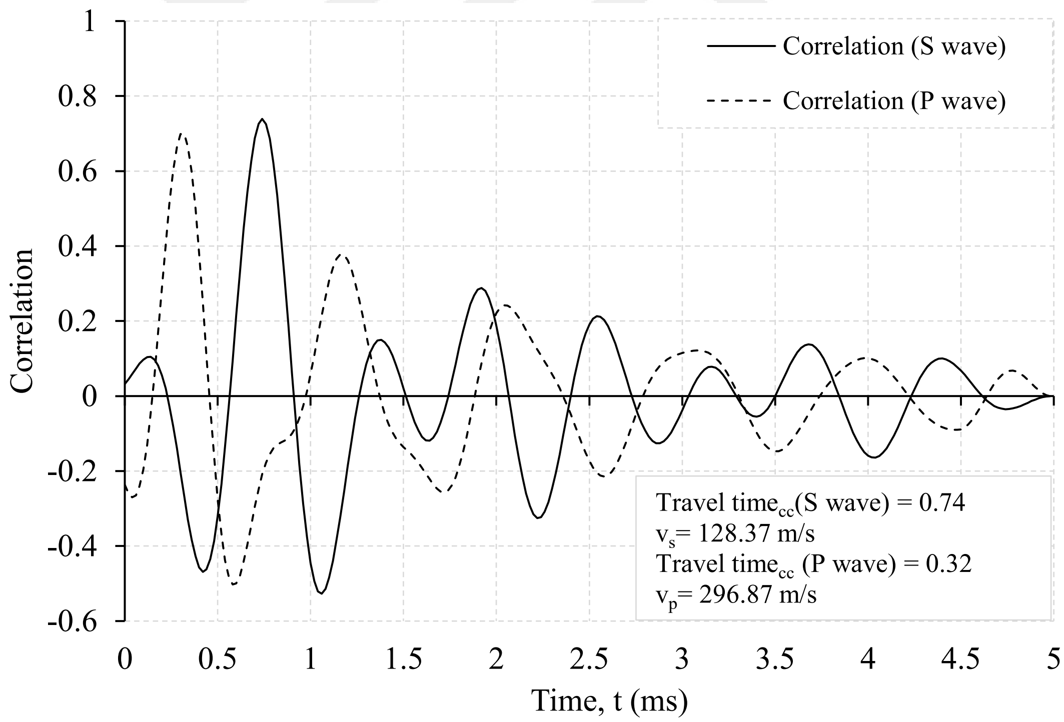

(d)

Figure 3.11. An example of BE testing results for clean bentonite: (a) transmitted and received signals during the S wave test (b) transmitted and received during the P wave test (c) comparing the received S wave and P wave signals, and (d) correlation curves for the tested specimen.

3.2.10 Triaxial Test

The testing program for CU tests is presented in Table 3.3. CU tests were performed on NS-ML mixtures at ECS values of 50 kPa, 100 kPa, and 150 kPa. A cylindrical specimen with a diameter of 70 mm and a height of 150 mm was tested with a loading rate of 0.02 mm/min. The height/diameter ratio of the test specimens was around 2.14, which is appropriate for triaxial testing (Baldi et al., 1988).

The triaxial testing device includes a load frame body with a capacity of 50 kN, and the frame motor was manufactured by ELE International company. The base of the device contains a stepper motor-driven unit that can be controlled manually via the screen at the base. The screen allows controlling the pedestal level and displacement ratio. The device was mounted on pneumatic mounts to prevent external vibrations. The frame has a crossbar whose height is determined by the height of the cell. The pedestal of the device enables to test of 38 mm, 50 mm, and 70 mm diameter specimens. The cell used in the study is made of acrylic plastic.

The pedestal of the machine is 70 mm in diameter. The base of the cell has four holes for four cables: two for local LVDTs and two for the BEs. The cell also has three holes on the top: one for the submersible load cell and two for venting any air that may have accumulated inside the specimen while filling the cell. The pedestal of the machine also has two vents that connect to the back-pressure and cell-pressure lines.

Volume-pressure controller produced by GDS was utilized to provide the desired pressure to the cell fluid. Each pressure controller was capable of producing a maximum pressure of 2000 kPa and holding 200 cm^3 of water. The volume-pressure controller was connected to the inside of the cell and applied cell pressure, while the other was a connected base of the specimen and applied back pressure. Axial displacements were externally measured by a linear displacement sensor. The sensor is attached to the top of the triaxial cell. Figure 3.12 shows the calibration graph of the LDS. The sensor has a 12 mm displacement capacity. To measure pore water pressure and cell pressure during the testing stages, two pore pressure transducers with a pressure range of 0-1000 kPa were used. Two submersible LVDTs manufactured by GDS Instruments Limited were used for measuring local axial deformation (Figure 3.13). Submersible LVDTs were directly glued to the membrane over a center of the gauge length of 50 mm. Figure 3.12 shows the calibration graphs for the two LVDTs.

Two transducers mounted diametrically opposite each other on the specimen using super glue.

Table 3.3. The testing program of the CU tests

Name of the specimens	Host material	Admixture material	Admixture content (%)	Test program
Clean NS	Narlı sand	ML	0	-Minimum void ratio -Maximum void ratio -Monotonic undrained triaxial test at three different ECS (50 kPa, 100 kPa, and 150 kPa) for each mixture
NS with 10% ML			10	
NS with 20% ML			20	
NS with 30% ML			30	
NS with 40% ML			40	
NS with 50% ML			50	

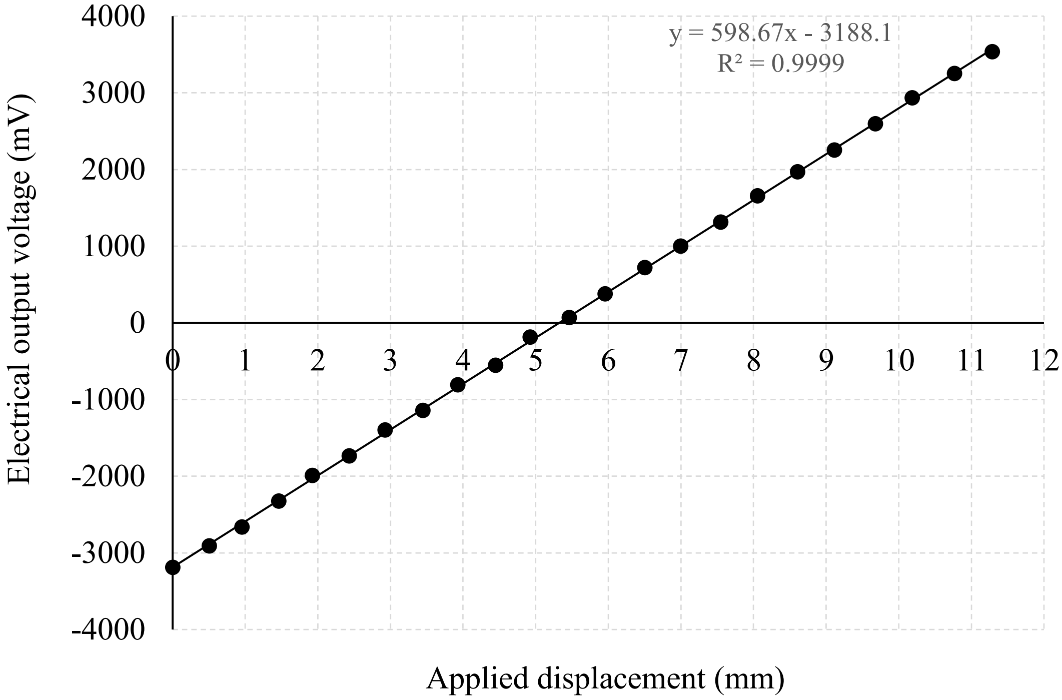
y = 598.67x - 3188.1
R² = 0.9999
Electrical output voltage (mV)
Applied displacement (mm)
4000
3000
2000
1000
0
-1000
-2000
-3000
-4000
0 1 2 3 4 5 6 7 8 9 10 11 12

(a)

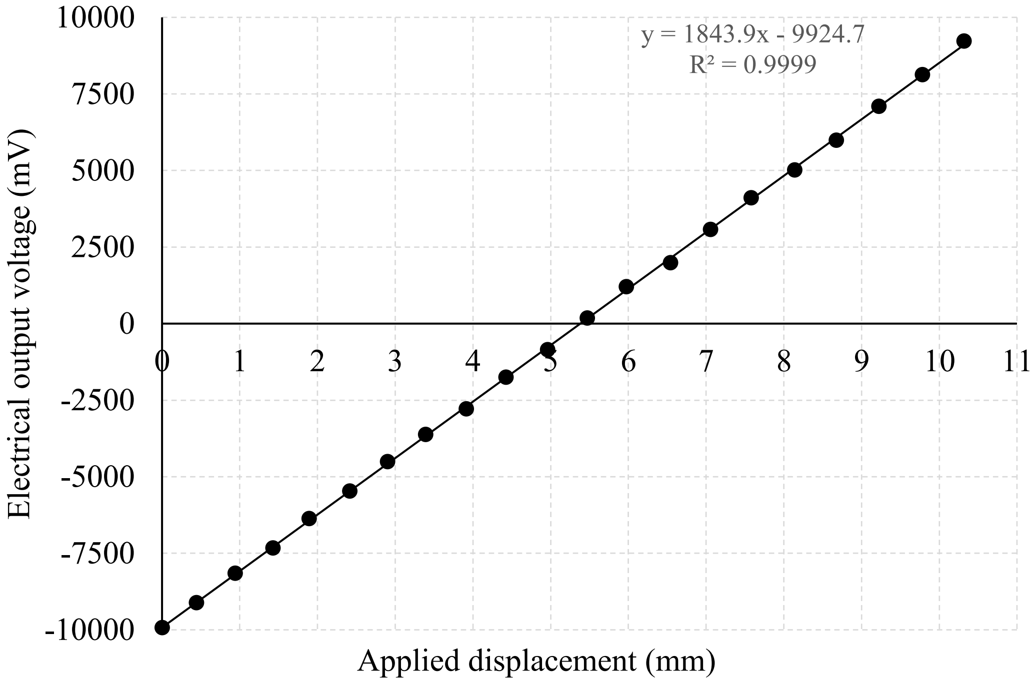
y = 1843.9x - 9924.7
R² = 0.9999
Electrical output voltage (mV)
Applied displacement (mm)
10000
7500
5000
2500
0
-2500
-5000
-7500
-10000
0 1 2 3 4 5 6 7 8 9 10 11

(b)

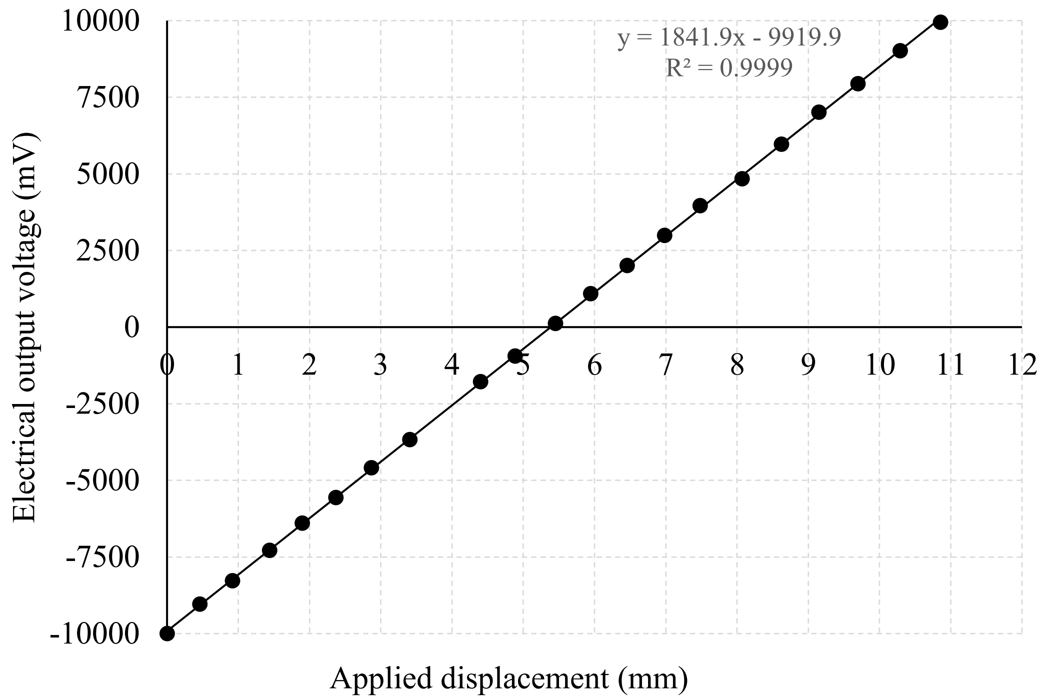

(c)

Figure 3.12. Calibration results of (a) LDS (b) LVDT 1 (c) LVDT 2.

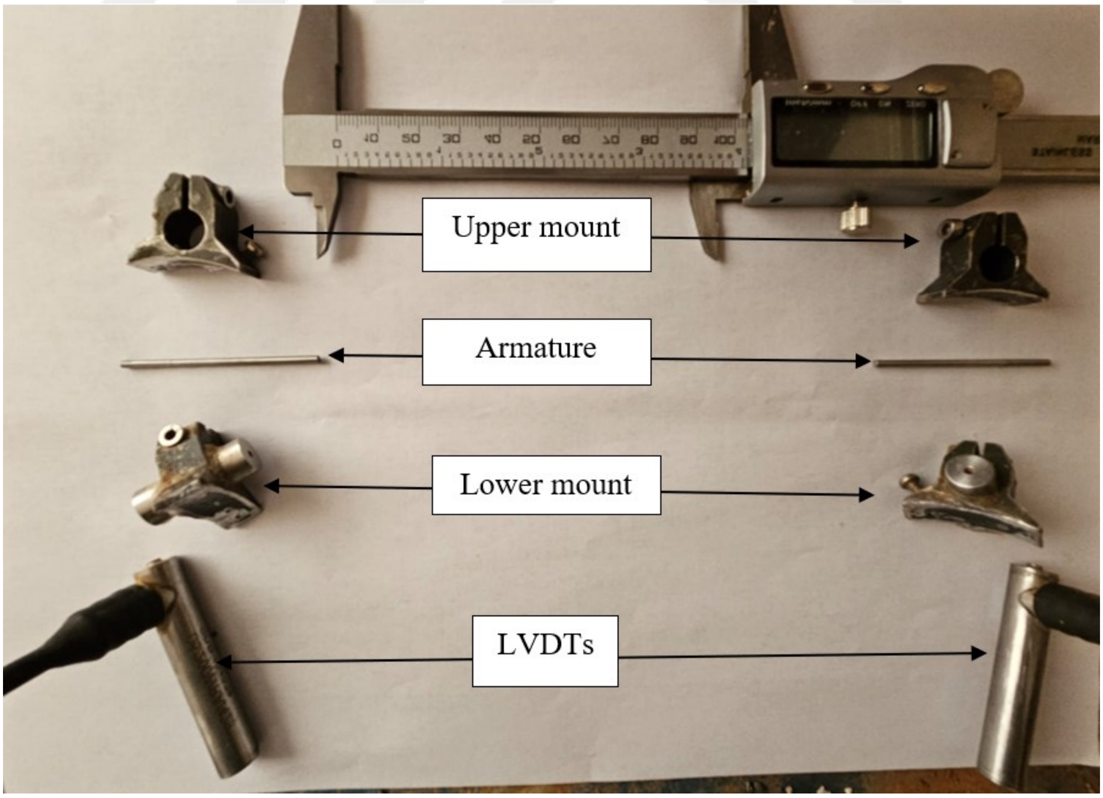

Figure 3.13. A picture of the LVDTs used in the study.

The data acquisition system of the triaxial apparatus contains three different data loggers. The data from the instruments were recorded using a 16-bit data logger with 8 channels. A second data logger was used to record the local LVDT measurements. The third data logger was used to record the signal from the BEs.

The following steps were followed during the specimen preparation stages of the CU tests.

1. The membrane was first placed on the pedestal. On the specimen base, two O-rings were installed.
2. Since cohesionless soil (i.e., NS) was tested, the specimen was prepared using a pair of split molds. After stretching the membrane over the mold, filter paper and specimen were placed into the membrane. Once the mold was filled with the specimen, a spatula was used to flatten the top of the specimen, giving it a uniform top and preventing any soil mass. A filter paper was then placed on the specimen.
3. The tested specimens were then covered with a top cap. During the tests, a special top cap with a flat end was used to accurately determine the stiffness values of the tested specimens at low strain levels. In the triaxial tests, to obtain accurate measurements at small strains, the load cell and top cap must be perfectly aligned and connected. As shown in Figure 3.14, many different types of connections have been proposed for triaxial testing. In Figures 3.14a and 3.14b, a halved steel ball was used to shape the specimen when it was first compressed. However, this may result in inaccurate measurements of displacement values when determining the start of the test. This can be improved by using a flat ram; however, misalignment and inaccurate determination of small strains remain. During the triaxial tests of this study, a flat top cap with a hemispherical end submersible load cell was used. At low strain levels, this type of connection provides an accurate measurement (Clayton, 2011).
4. On the top cap, two O-rings were installed. After that, a pair of split molds was removed by applying a -20 kPa effective stress to the soil via a back pressure channel.

5. Once the target stress was reached, the mold was removed. The diameter and height of the specimen were then measured at three different locations using a digital calliper and ruler.
6. To accurately measure the deformation of the soil during the test, the submersible LVDTs were directly glued to the membrane over a center of the gauge length of 50 mm.
7. The cell was then placed on the frame and filled with water.
8. After filling the cell with water, back pressure and cell pressure were simultaneously increased to ensure a minimum effective stress of 20 kPa following ASTM D4767-11. The B value test was then performed on the soil to check the B value of the specimens. To accomplish this, the back pressure valve was closed first, and after waiting for the PWP to become constant, the cell pressure was increased. The change in PWP and cell pressure recorded, as well as the B value, was calculated using the equation below, where U is the change in PWP and $\Delta\sigma_{cp}$. All specimens were subjected to a constant back pressure of 600 kPa to obtain a Skempton B value of at least 0.9.

$$B = \frac{\Delta U}{\Delta \sigma_{cp}} \tag{3.8}$$

9. The saturation phase was followed by the consolidation stage. During the consolidation stage, the cell pressure was increased to achieve the desired ECS. The target ECS was achieved by reflecting it on the specimen as a difference in cell pressure and back pressure (i.e., for 100 kPa ECS, 600 kPa back pressure and 700 kPa cell pressure were used).
10. After reaching the desired effective stress, the back pressure valve was closed and the specimen was subjected to the CU shear test. During the shear stage, a loading rate of 0.02 mm/min was used. Two LVDTs and an LDS were used to record displacement values, while a submersible load cell was used to measure the load values. Pore water pressure was measured at the back pressure line using a pore pressure transducer.
11. Once the test was completed, the back and cell pressures gradually and simultaneously decreased.

Some steps in the triaxial tests are shown in Figure 3.15.

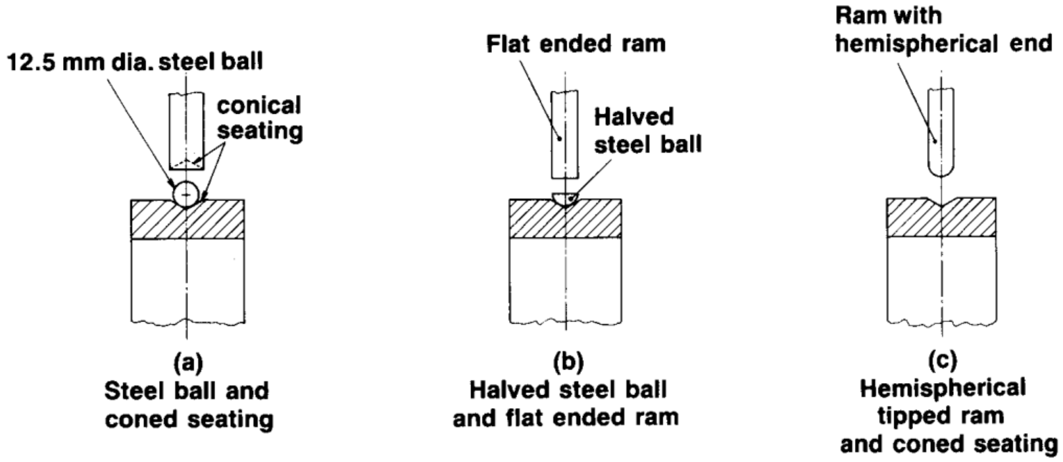

Figure 3.14. The typical connection between the top cap and load cell (Baldi et al., 1988).

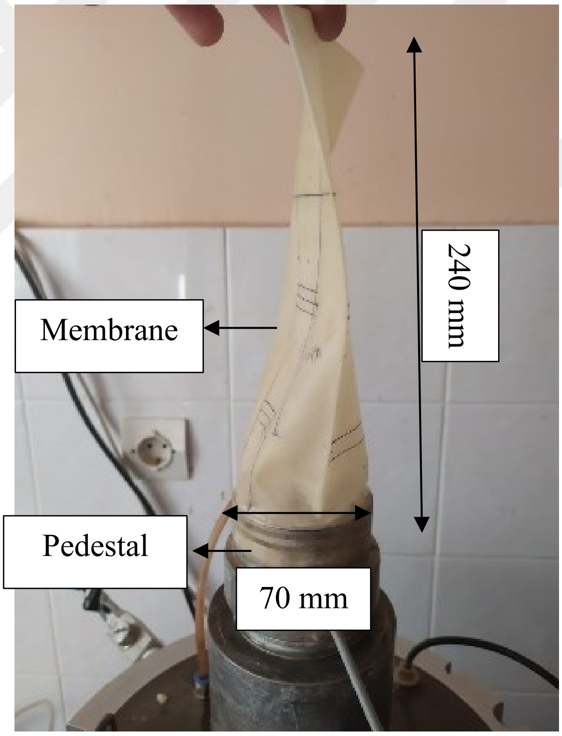

(a)

(b)

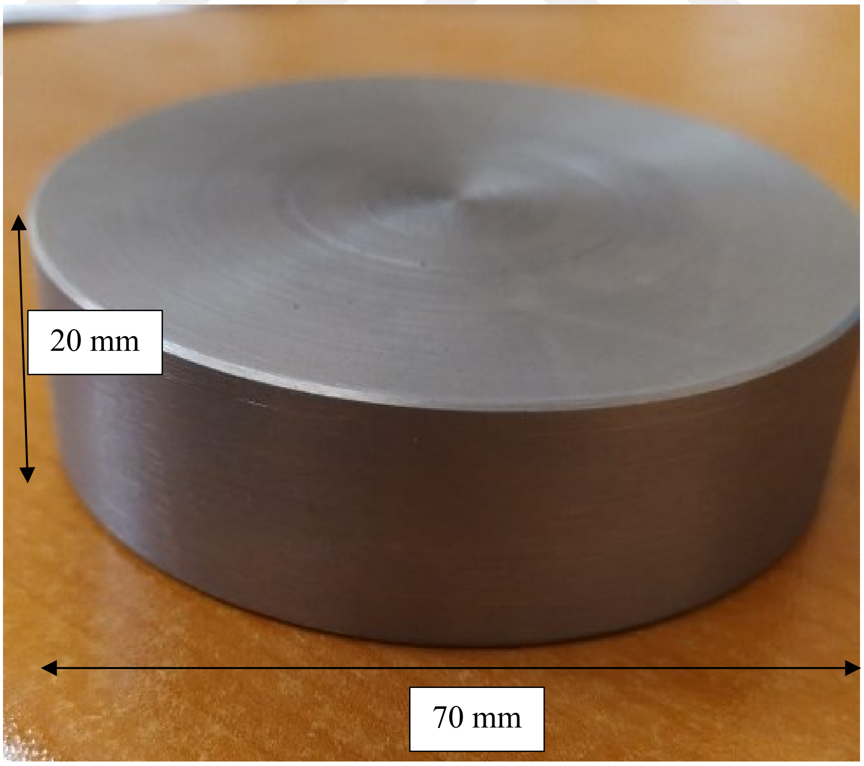

(c)

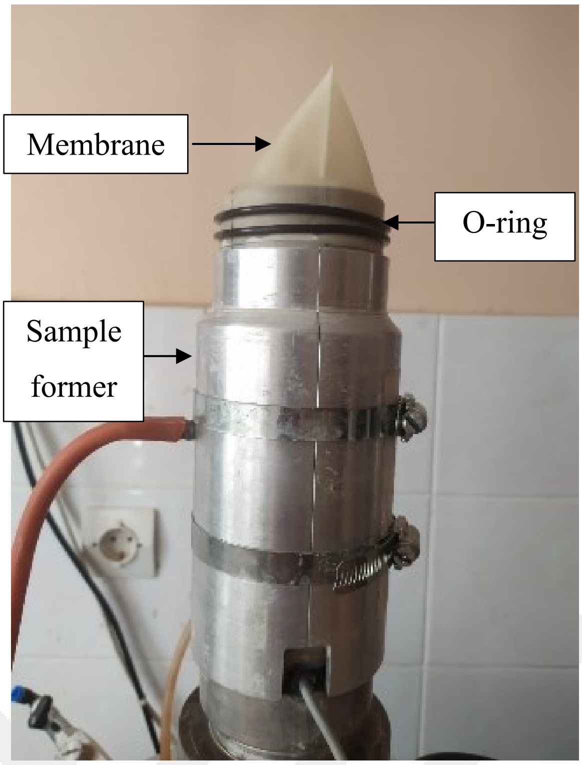

(d)

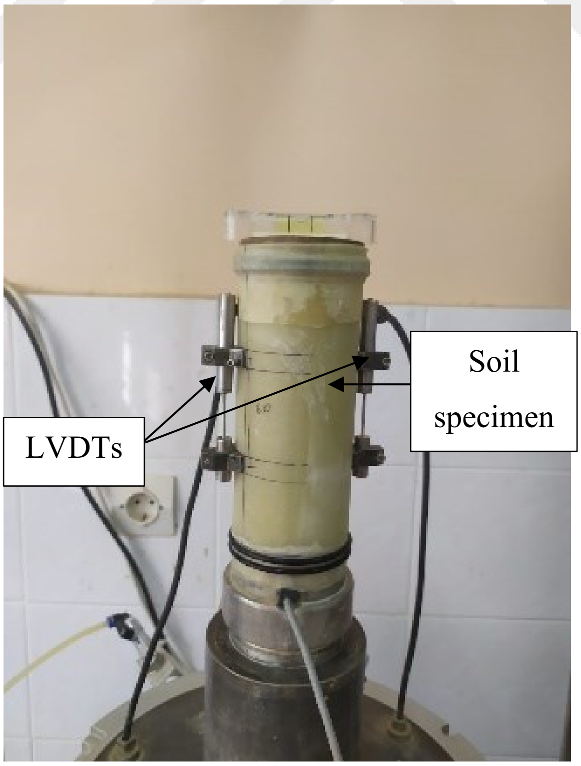

(e)

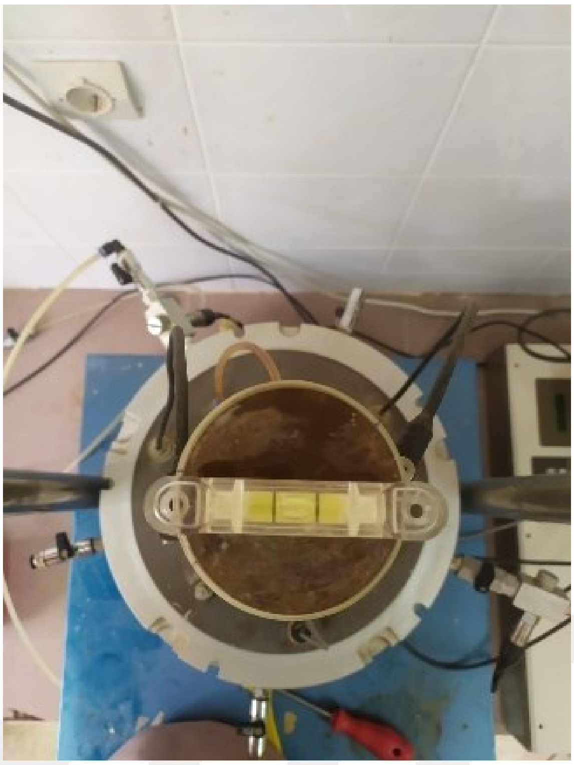

(f)

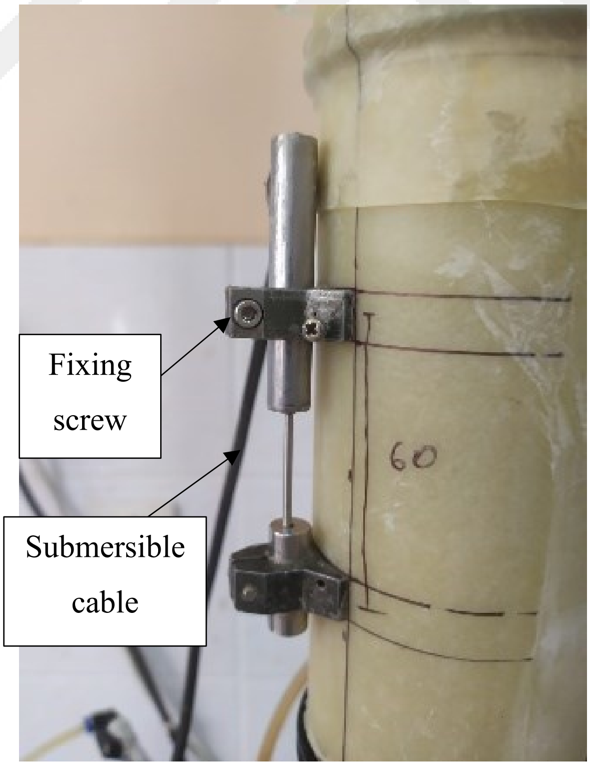

(g)

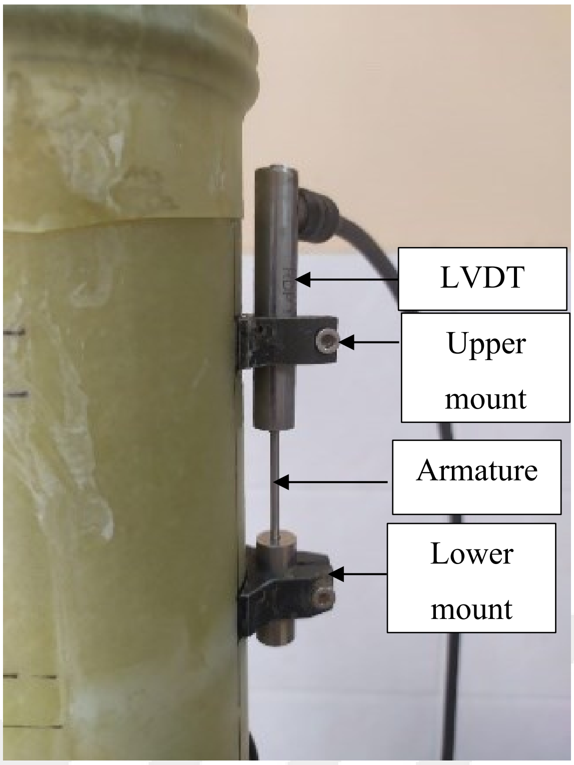

(h)

(i)

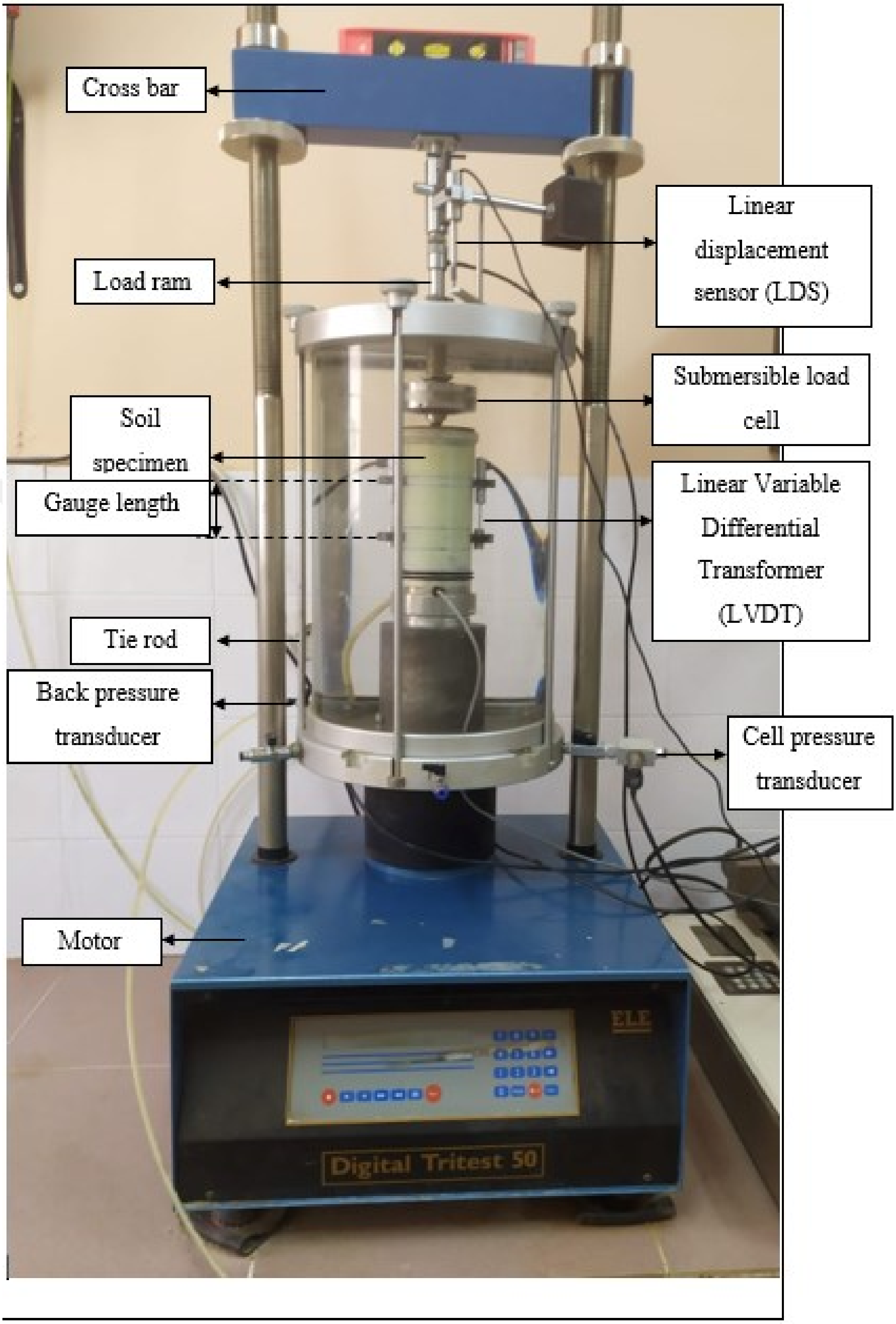

(j)

Figure 3.15. The preparation stages of the triaxial compression test: (from a to i) some pictures of the soil preparation stage, (j) the test components.

CHAPTER 4
RESULTS AND DISCUSSIONS

4.1 Introduction

The testing results of the mixtures are presented in this chapter. Firstly, the testing results of bentonite with 0%, 10%, 20%, 30%, and 40% of FWG and CWG were presented. The various laboratory tests including compaction, fall cone, consolidation, direct shear viscosity, crumb, double hydrometer, UC, and BE were performed on bentonite WG mixtures. The purpose of this test program was to suggest an alternative additive to be used with bentonite in bentonite-based mixtures. The testing results are summarized in Table 4.1 and detailed below.

4.2 Testing Results of Bentonite-Waste Glass Mixtures

4.2.1 Compaction Testing Results

The compaction test is generally the first step in proposing an alternative mixture for use in an engineering application. The compaction tests were performed on the mixtures according to the procedure detailed in the materials and method section.

Figure 4.1 and 4.2 presents the compaction curves of bentonite with (a) FWG and (b) CWG. The general shape of the compaction curves of the specimens exhibits a major peak in the γ_{dmax}, followed by a minor peak. The dry density of the minor peak was around 2%-5% lower than that of the major peak. For example, the first peak of bentonite was found to be at a water content of 21.53% with a dry density of 13.56 kN/m^3. The minor peak was found to be at a water content of 36.68% with a dry density of 12.80 kN/m^3. Such types of compaction curves were observed by several researchers in the literature (Das and Sivakugan, 2016). Lee and Suedkamp (1972) were among the first researchers who observed such a compaction shape named as an "irregular compaction curve". The researcher performed compaction tests on various types of soil. According to the researcher, four types of compaction curves namely bell-shaped, 1-1/2 peak, double peak, and odd-shaped were observed in their results. The shape of the compaction curve is determined primarily by the mineralogy, type, and liquid limit of the testing soil.

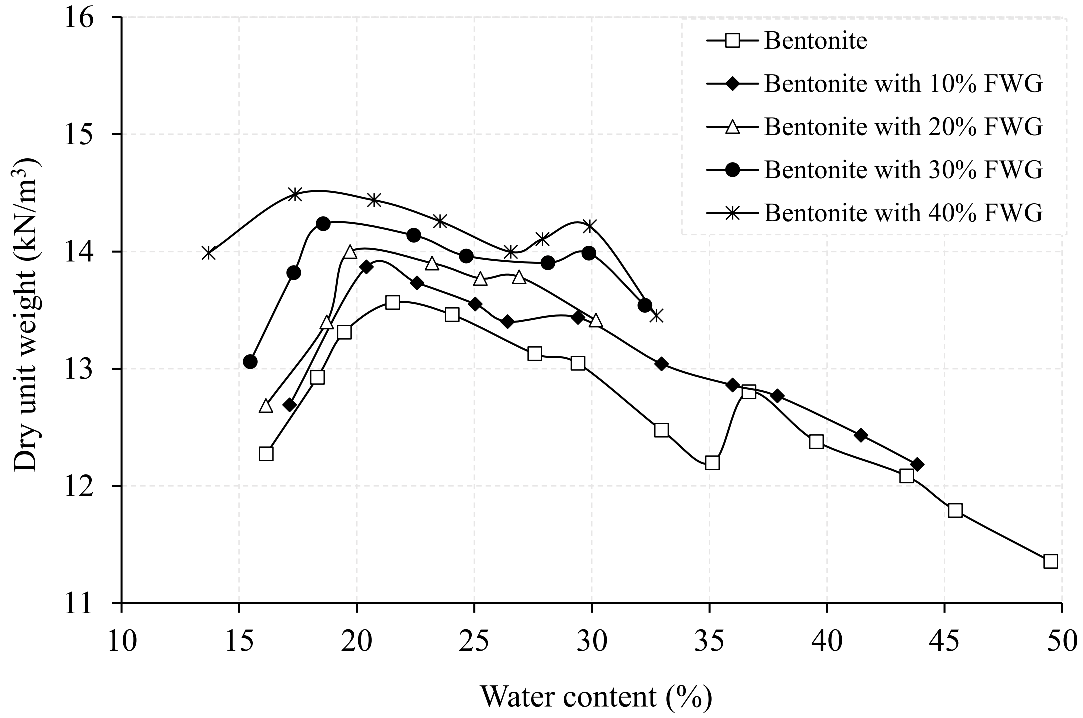

Figure 4.1. Compaction testing results of the bentonite-FWG mixtures.

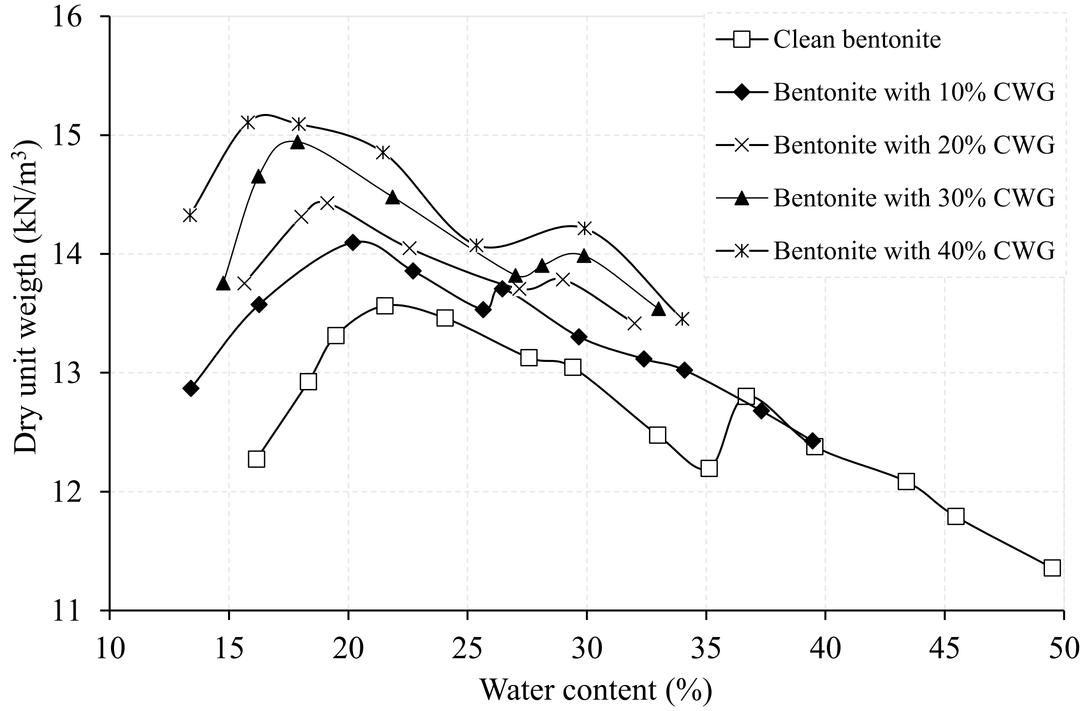

Figure 4.2. Compaction testing results of the bentonite-CWG mixtures.

Table 4.1. Summary of compaction, fall-cone, direct shear and consolidation testing results

Specimen	WG content (%)	γ_{dmax} (kN/m^3)	w_{opt} (%)	LL (%)	c_c (m^2/kN)	c_s (m^2/kN)	m_v (m^2/kN)	Cohesion (kPa)	Angle of internal friction (°)	c_v (cm^2/s)
Clean Bentonite	0	13.56	21.53	279	0.183	0.047	0.008	115.0	23.5	3.92E-05
Bentonite with FWG	10	13.87	20.40	259	0.133	0.036	0.006	115.3	32.0	5.90E-05
	20	14.00	19.72	233	0.107	0.031	0.005	110.5	35.2	9.88E-05
	30	14.24	18.58	204	0.090	0.026	0.004	103.0	38.8	2.16E-04
	40	14.49	17.38	186	0.076	0.018	0.004	88.0	35.8	7.93E-04
Bentonite with CWG	10	14.09	20.19	257	0.136	0.039	0.006	107.0	33.0	8.81E-05
	20	14.43	19.12	237	0.120	0.033	0.005	102.9	38.3	3.52E-04
	30	14.94	17.88	215	0.101	0.028	0.005	100.8	41.4	4.46E-04
	40	15.15	16.50	203	0.082	0.021	0.004	97.5	38.8	1.14E-03

The researcher also pointed out that soils containing montmorillonite minerals and those having a liquid limit greater than 70%, such as bentonite, may exhibit a double peak compaction curve. Their study showed that a bentonite type of clay with liquid and plastic limits of 310 and 244% exhibited compaction curves with a major and a minor peak. When it comes to this study, similar compaction curves were obtained in bentonite-based mixtures. A similarity between Atterberg's limit of the bentonite used in this study and the bentonite tested in the study of Lee and Suedkamp (1972) was realized. It should be noted that the liquid and plastic limits of bentonite (279% liquid limit and 162% plastic limit, respectively). Furthermore, several researchers reported in the literature some irregular compaction shapes for clay types having high liquid limits (Olson 1963; Lee and Suedkamp 1972; Lee and Hsu 1973; Lee 1976; Likos 2000; El Mountassir et al. 2014). Figures 4.3 and 4.4 present γ_{dmax} and w_{opt} values of the specimens obtained in the compaction curves. The graph shows that WG additions increased γ_{dmax} values while decreasing w_{opt} values of clean bentonite. For example, 40% of CWG additions increased the γ_{dmax} value of clean bentonite from 13.564 kN/m^3 to 15.107 kN/m^3, corresponding to around an 11% increase. The reason for this trend could be attributed to the higher specific gravity (2.85) of WG than that of bentonite (2.67). Furthermore, with CWG additions, w_{opt} value of clean bentonite (21.53%) decreased gradually (20.19%, 19.12%, 17.88%, 16.50% for bentonite with 10%, 20%, 30%, and 40% of CWG additions, respectively). This decrease in w_{opt} values with WG additions could be due to a difference in bentonite and WG water retention capacity. WG is well known for having a low water absorption capacity (Arulnahaj et al. 2012). Arulnahaj et al. (2012) investigated the water adsorption capacity of various waste materials. Among the waste materials tested, the researchers found that fine WG particles have the lowest water adsorption capacity. Similar trends related to the effect of WG grains on the w_{opt} values of the various soil types including clay, and biomass was also obtained by various researchers (Disfani et al. 2011; Wartman et al. 2004b; Grubb et al. 2006; Ibrahim et al. 2019; Bilgen 2020).

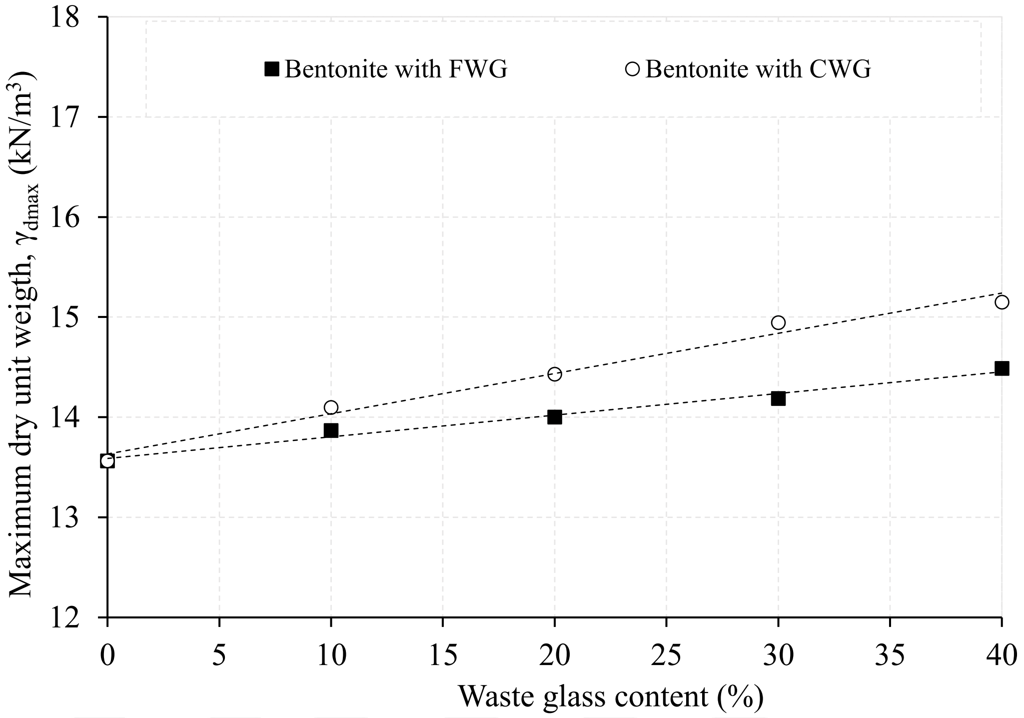

Figure 4.3. γ_{dmax} values of tested specimens.

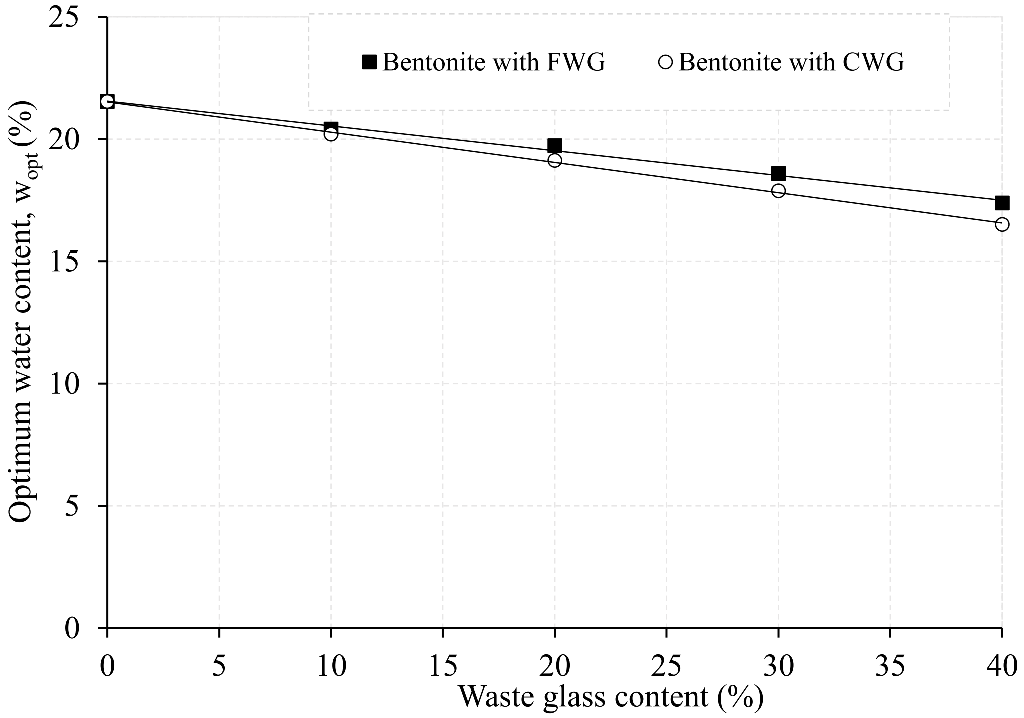

Figure 4.4. w_{opt} values of tested specimens.

Regarding the grain size effect of WG on compaction results, at a given content of WG, the mixture with CWG exhibited a higher γ_{dmax} and lower w_{opt} than bentonite with FWG. According to previous studies in the literature, the lower w_{opt} with CWG specimens can be explained by the fact that coarse particles generally have a lower specific surface area and a lower water adsorption capacity (Arulnahaj et al., 2012; Likos and Jaafar, 2014). The higher γ_{dmax} of the specimens with CWG grains can be explained by the denser packing of the larger grains compared to the small grains (Cho et al., 2006, Disfani et al., 2011, Disfani et al., 2012, Chang et al., 2018, Xu et al., 2019).

Figure 4.5 presents more visual information by showing a 3D surface of the γ_{dmax}-w_{opt} relationship with different CWG modifications. The plot was produced by applying a polynomial equation to the surface of the test data. The compaction curves of the specimens can be seen in this 3D surface.

4.2.2 Fall-cone Testing Results

The fall-cone test was used to investigate the liquid limit and undrained shear strength of soil mixtures. The liquid limit of bentonite is an important indicator for quantitatively demonstrating the water-holding/absorbent quality of bentonite with WG. Several researchers associate the liquid limit with the compressibility of fine-grained soils (Skempton and Jones, 1944; Sridharan and Nagaraj, 2000; Deng et al., 2018). Besides, undrained shear strength is a significant indicator of shear strength values in fine-grained soils with low permeability (Das and Sivakugan, 2016). These two indicators prompted the researcher to perform the fall-cone test to investigate the applicability of bentonite-WG mixtures.

Figures 4.6 and 4.7 show the fall-cone penetration and the s_u values of bentonite with both FWG and CWG at various water contents. The trend shows that the increasing water content of the tests leads to an increase in penetration values and thereby decreases the s_u values. For instance, increasing the water content from 160% to 190% led to an increase in penetration value from 17 mm to 20 mm in bentonite with a 40% FWG mixture. However, a similar amount of increase in water content in bentonite with 40% CWG (from 180% to 210%) caused an increase in penetration value from 15 mm to 23 mm. This shows that mixtures with CWG are more susceptible to changes in water content values. The effect of WG additions leads to an increase in the fall-cone penetration values at a given water content. For example, at 200% water content, the fall-cone penetration of 20% FWG was approximately 12 mm, while penetration values of 16.6 and 20 mm were obtained with the addition of 30% and 40% CWG, respectively. The increase in penetration values caused by WG additions resulted in a decrease in s_u values. The s_u value of bentonite with 20% CWG was found to be around 4.0 kPa at 200% water content, however, this value decreased to 2.22 and 1.66 kPa with the addition of 30% and 40% CWG, respectively. The possible difference in cohesion forces between WG and bentonite could justify the decrease in s_u values with the addition of WG. Figure 4.8 compares the fall-cone testing results of bentonite at 10% and 30% FWG and CWG contents. The figure shows that the fall-cone penetration and s_u values of the specimen with CWG are greater than those of the specimen Figure 4.9 presents the liquid limit values of the specimens. The addition of WG resulted in a decrease in liquid limit values. The addition of 40% CWG decreased the liquid limit value of clean bentonite from 279 to 203%, while the addition of the same amount of FWG decreased it to 186%.

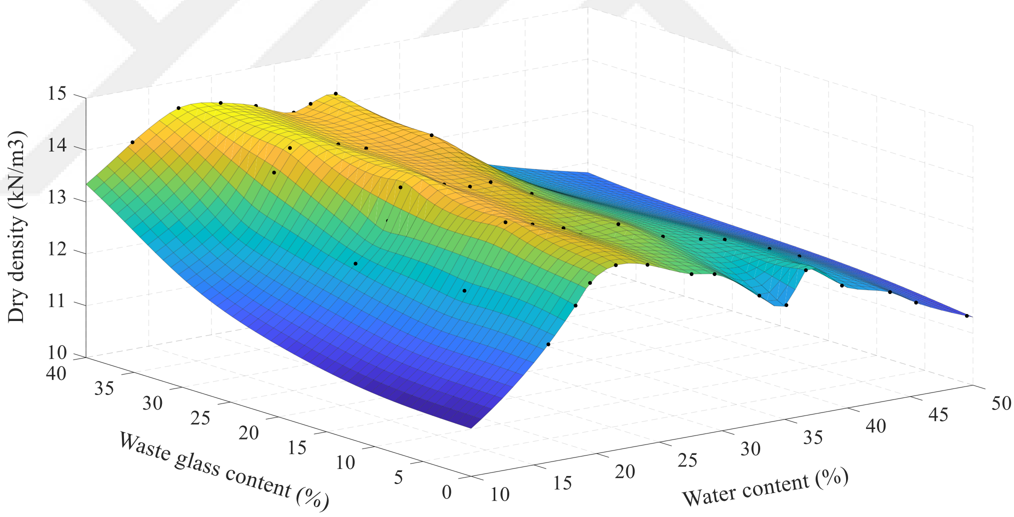

Figure 4.5. 3D surface of compaction results of bentonite with CWG.

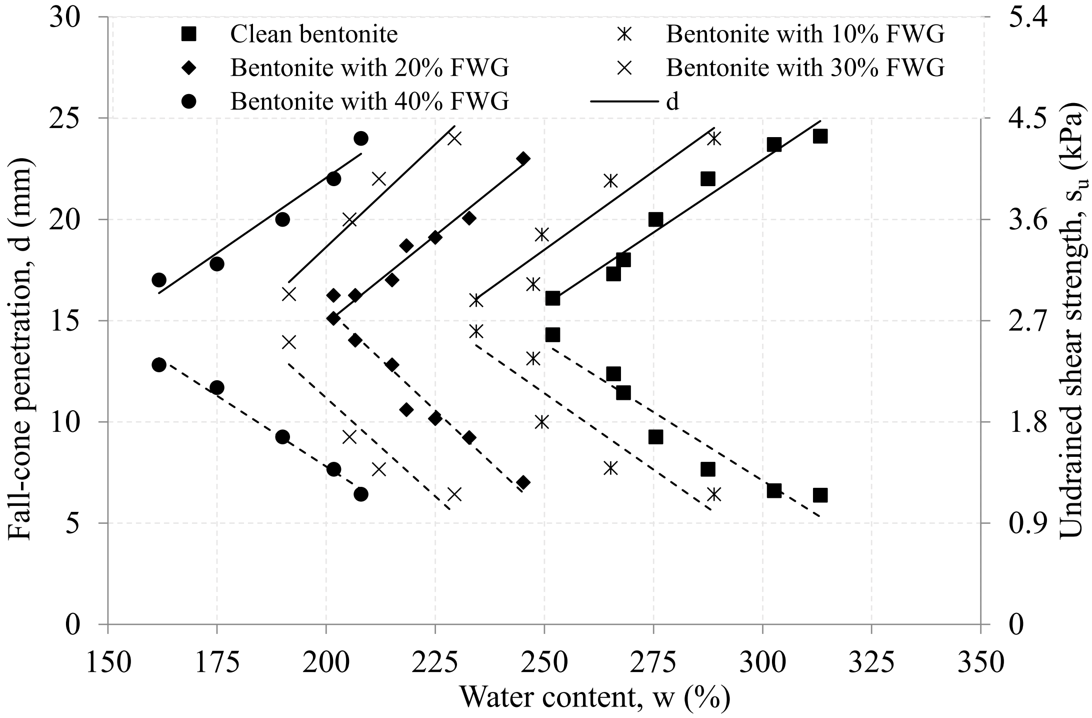

Figure 4.6. Fall cone testing results of bentonite-FWG mixtures

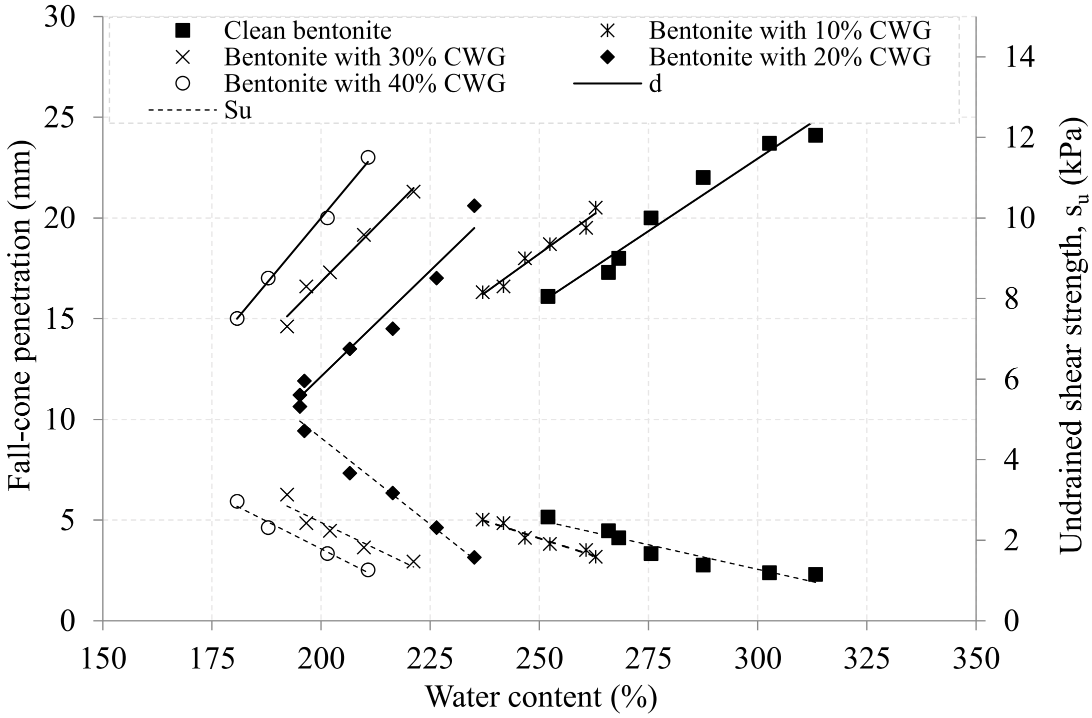

Figure 4.7. Fall cone testing results of bentonite-CWG mixtures

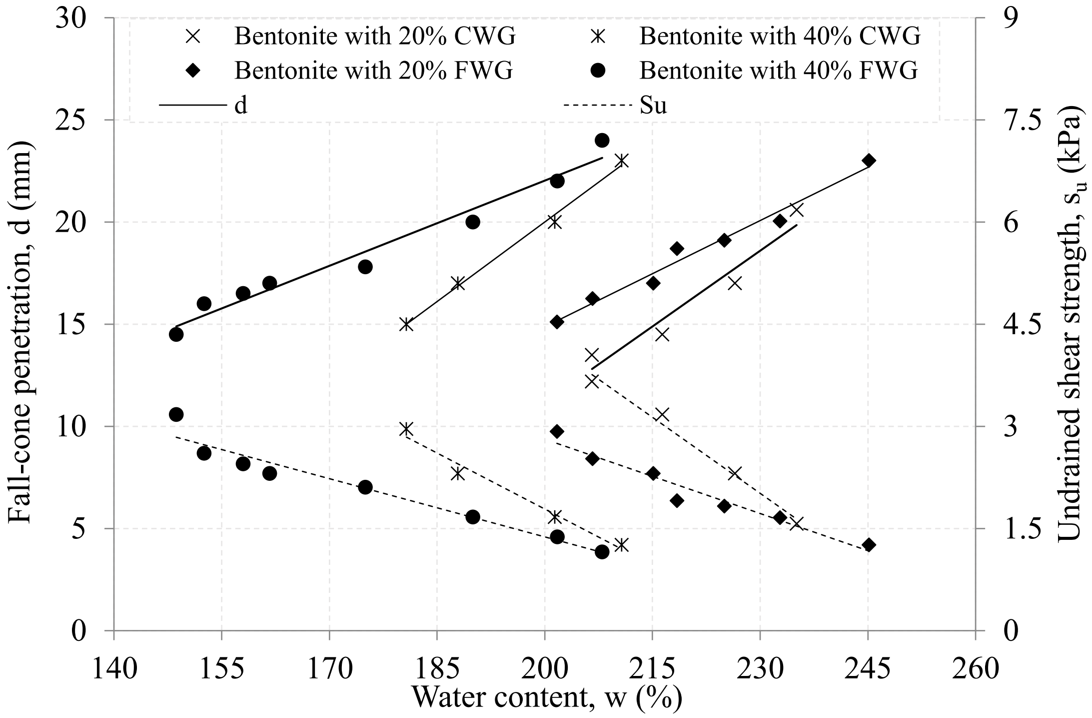

Figure 4.8. Effect of grain size of WG on the fall cone testing results.

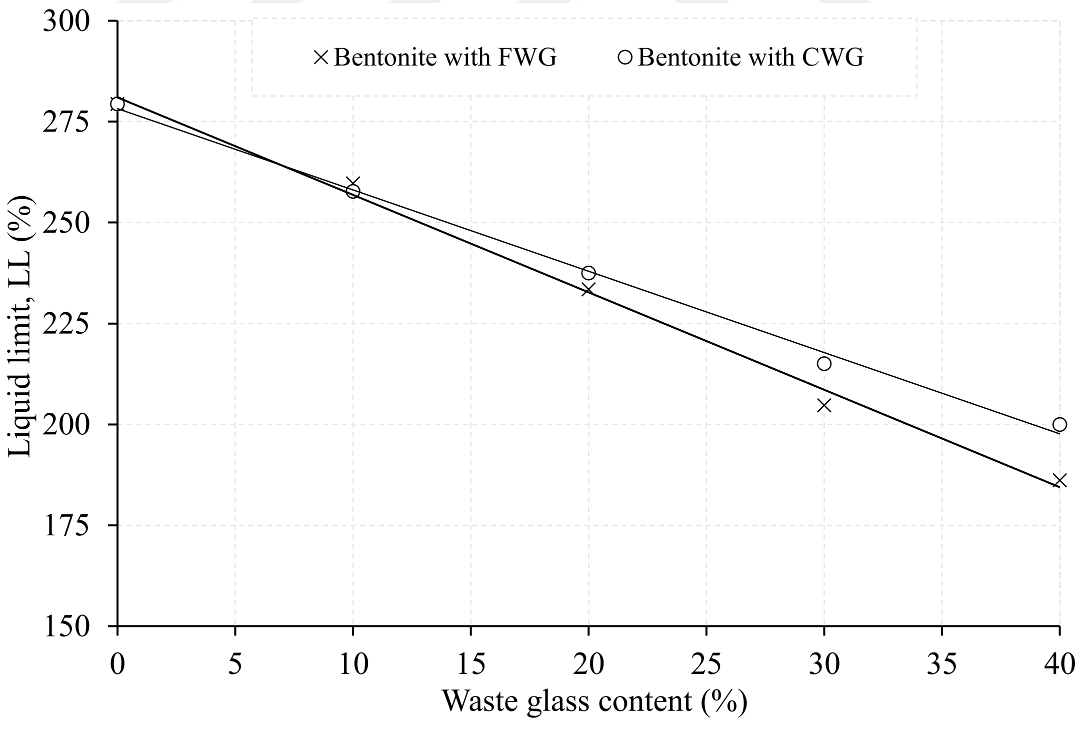

Figure 4.9. The liquid limit values of the specimens obtained from fall-cone tests

In the second series of fall cone tests different water contents from 5% to around 50% were performed on WG with 0%, 1%, 2% and 3% of bentonite. This part of the fall-cone tests investigated the effect of small bentonite additions on the fall-cone testing results of the WG. Figure 4.10 presents the fall-cone penetration values of the tested specimens at different water contents. The results showed that the water content of the specimens was the primary factor affecting the penetration values. The penetration values were observed to have three unique parts. When the water content is low, the penetration is comparatively high around 20 mm. Increasing water content leads to a decrease in the penetration values of the mixtures up to a water content range of 32%-37% with the lowest penetration value. Further, an increase in water content led to a continuous increase in penetration values. Such a trend between water content and penetration values was observed by several researchers (Likos and Jaafar 2014, Cabalar and Demir, 2019). According to numerous researchers working on the behaviour of soil in the unsaturated state, when the soil is saturated, the pore water pressure is positive negative pore water pressure was observed in the unsaturated case. According to the effective stress equation suggested by Bishop (1959), the negative pore water pressure contributes to the effective stress of the soil skeleton. Using this concept, the suction stress is zero when the soil is dry therefore the penetration is high. Increased water content caused negative pore water pressure to build up which led to an increase in the effective stress of the tested soil and penetration started to decrease. In the water content range where the minimum penetration value was observed, there was enough water in the pores of the soil grains to form a menisci bridge between them. In this case, the suction stress achieved its maximum value, resulting in the least amount of penetration (Likos and Jaafar, 2014). When the minimum penetration region is exceeded, the suction stress decreases with increasing water content. This increased penetration values. Several authors referred to these three areas as pendular, funicular, and capillary ranges (Cho and Santamarina, 2001; Fredlund et al., 2012; Yuan and Chareyre, 2022). Figure 4.11 depicts the undrained shear strength of the specimens. The s_u values of the specimens were low in dry conditions, then they increased with water content and reached maximum s_u value. Given that the s_u values are affected by the penetration values according to equation 1, the trend of s_u values was also influenced by the trend of penetration values. Figure 4.11 shows that bentonite additions increased the s_u values of clean WG at a given water content. This pattern could be explained by the contribution of bentonite cohesion forces to the effective stress of the soil matrix.

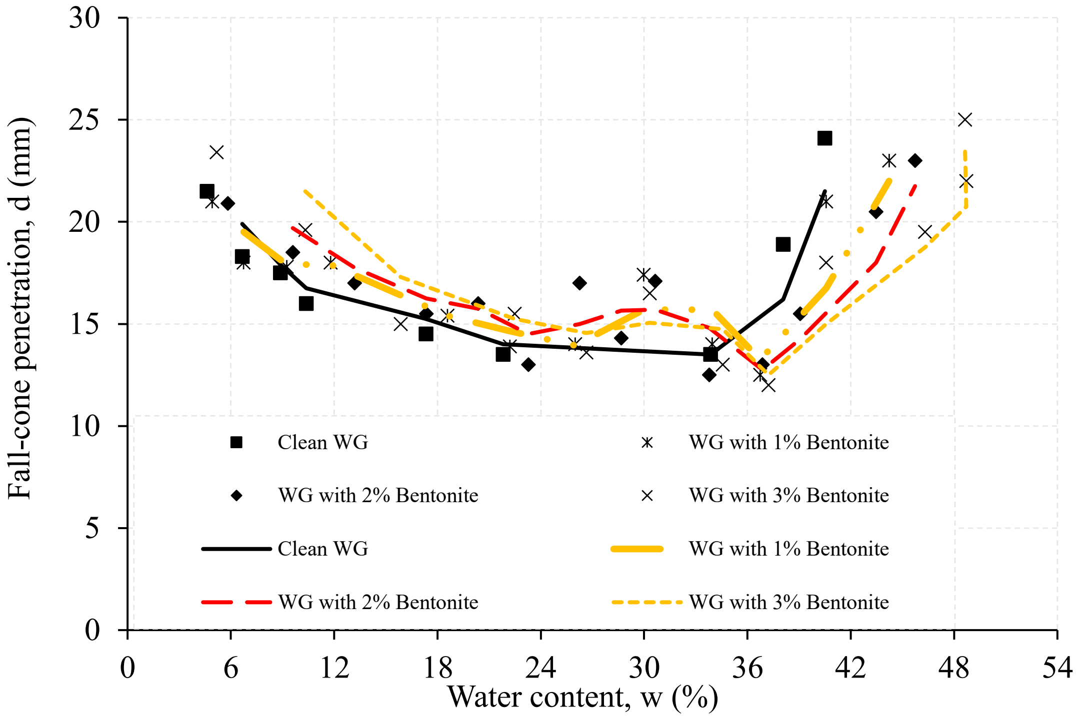

Figure 4.10. Fall-cone penetration values of WG-bentonite mixtures

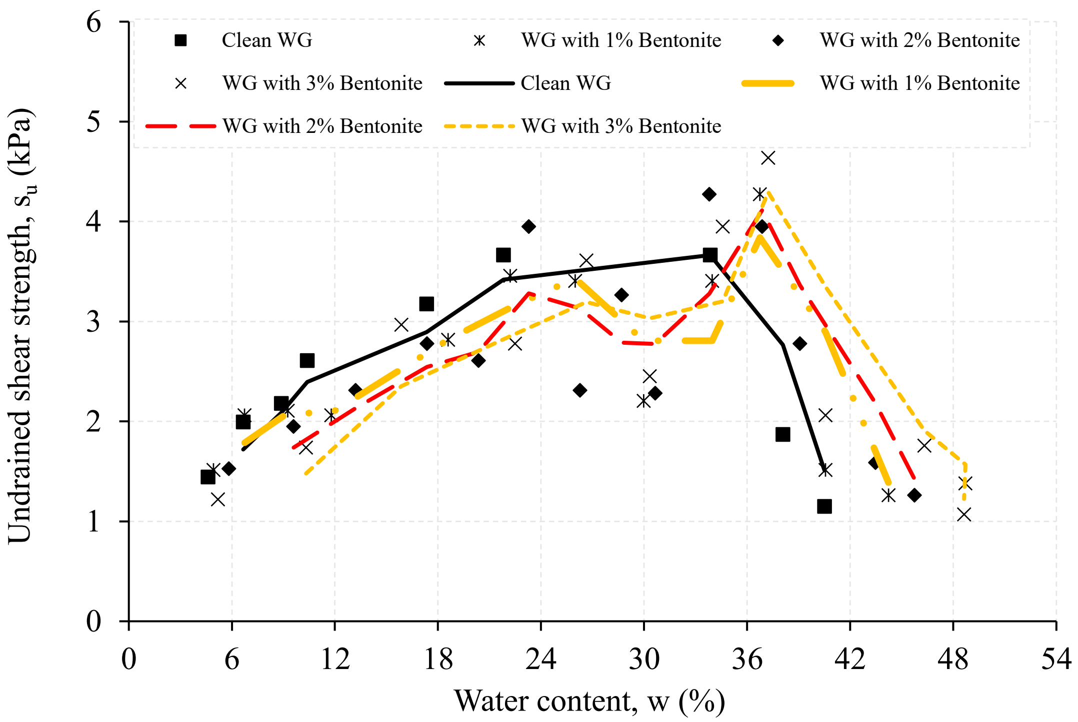

Figure 4.11. Undrained shear strength values of WG-bentonite mixtures

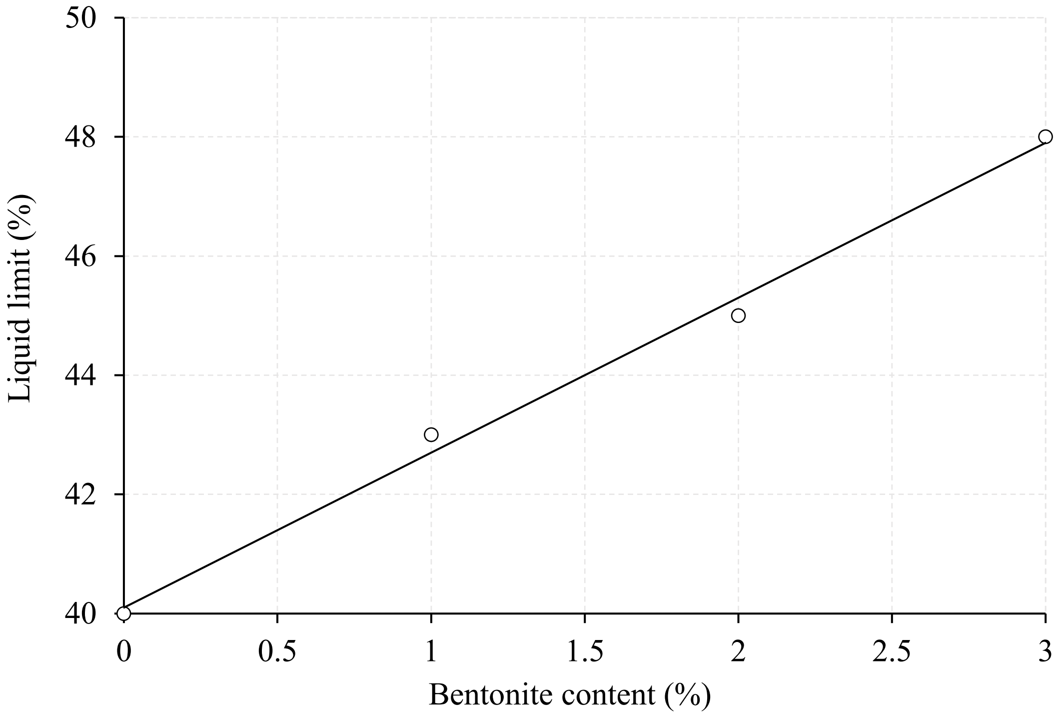

Figure 4.12. The liquid limit values of WG-bentonite mixtures.

It was realized that some researchers obtained similar results (Kumar and Wood, 1999; Cabalar and Mustafa, 2015; Karakan and Demir, 2018). Figure 4.12 shows the liquid limit values of the specimens. With the addition of 1%, 2%, and 3% bentonite, the liquid limit value of clean bentonite increased from 40% to 43%, 45%, and 48%. It was determined by the researchers that the liquid limit value of soil is related to water absorption capacity (Sridharan and Nagaraj, 1999). Therefore, increasing the liquid limit of bentonite is an indication of increasing the water absorption capacity of WG.

4.2.3 Consolidation Testing Results

Consolidation tests were performed to investigate the effect of WG on the mechanical response of the bentonite, such as compressibility and void ratio.

Figure 4.13 presents the change in void ratio values of mixtures at different normal stresses. The first noticeable point in Figure 4.13 is that WG additions reduce the initial void ratio of the specimens.

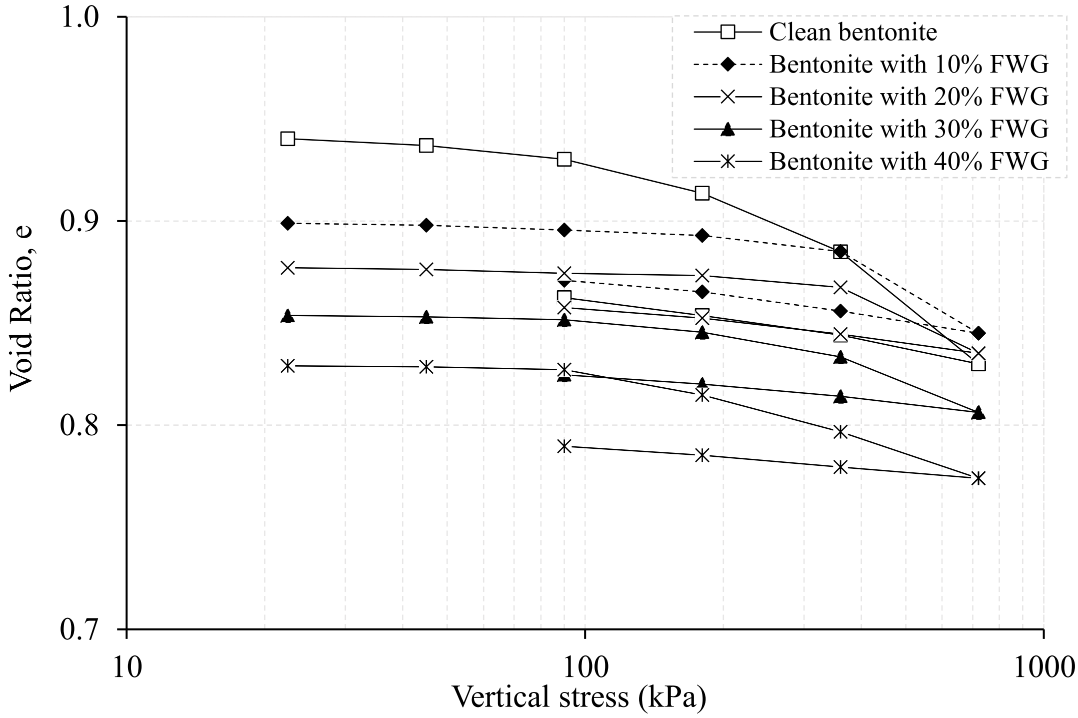

(a)

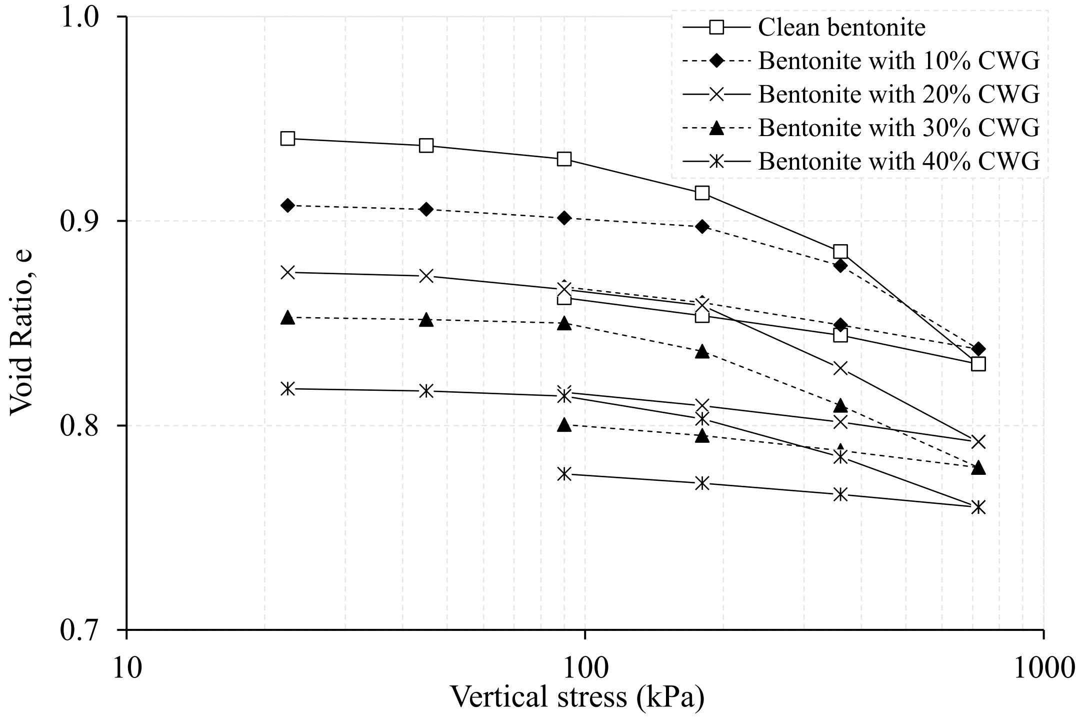

(b)

Figure 4.13. Variation of the void ratio of bentonite with (a) FWG and (b) CWG.

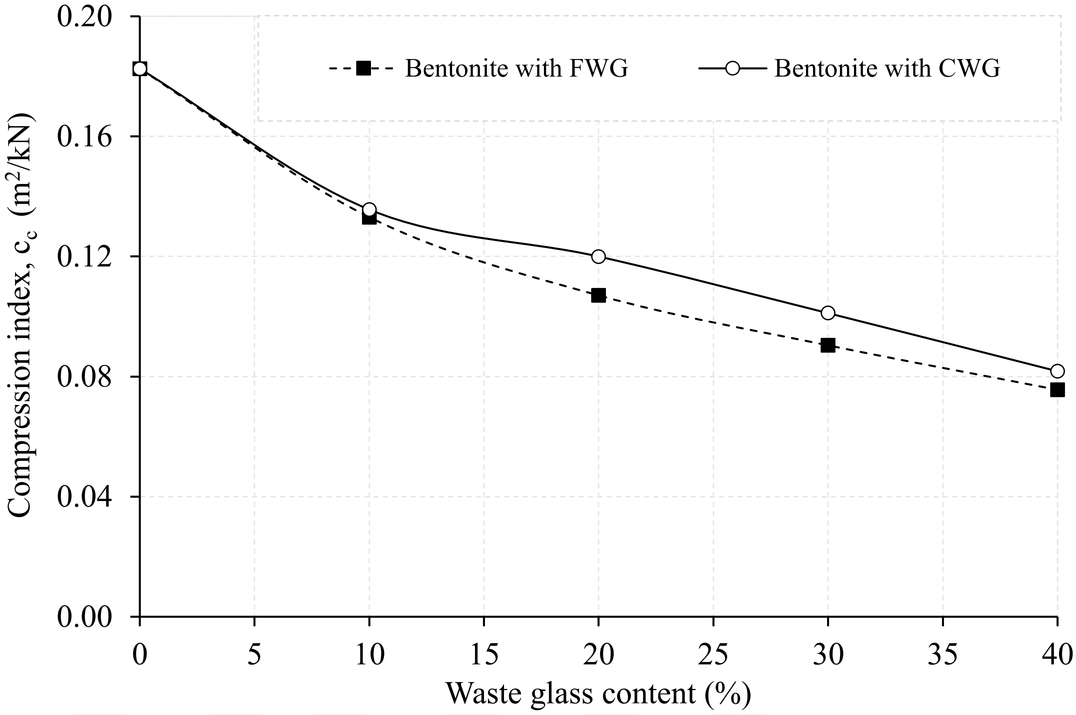

Figure 4.14. The c_c values of the bentonite-WG mixtures.

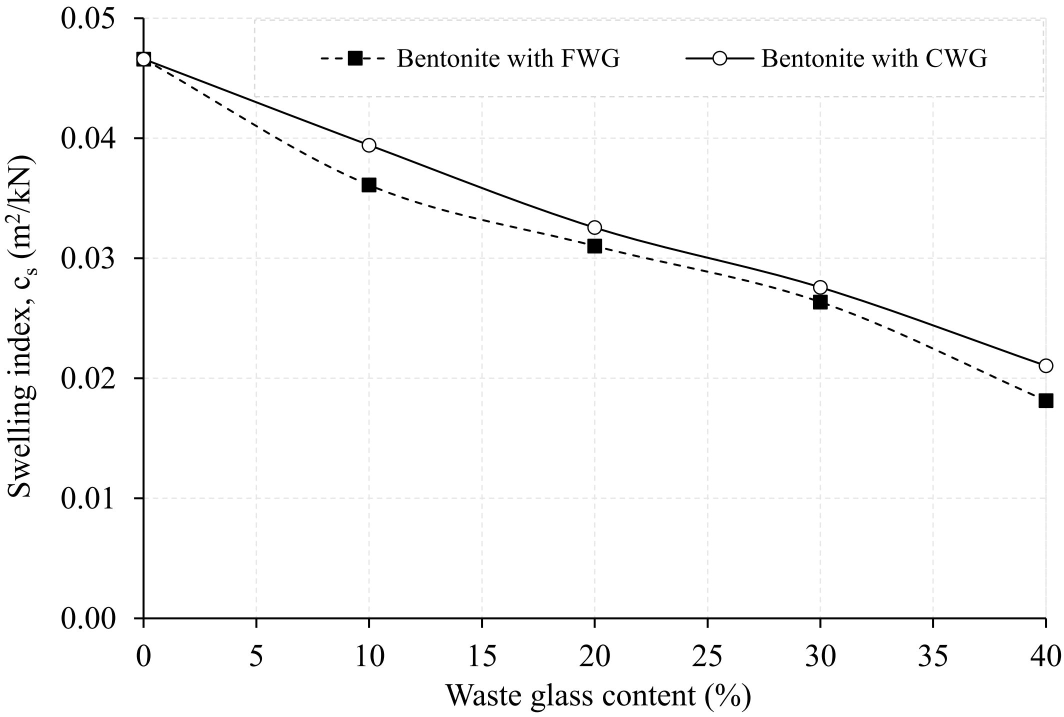

Figure 4.15. The c_s values of the bentonite-WG mixtures.

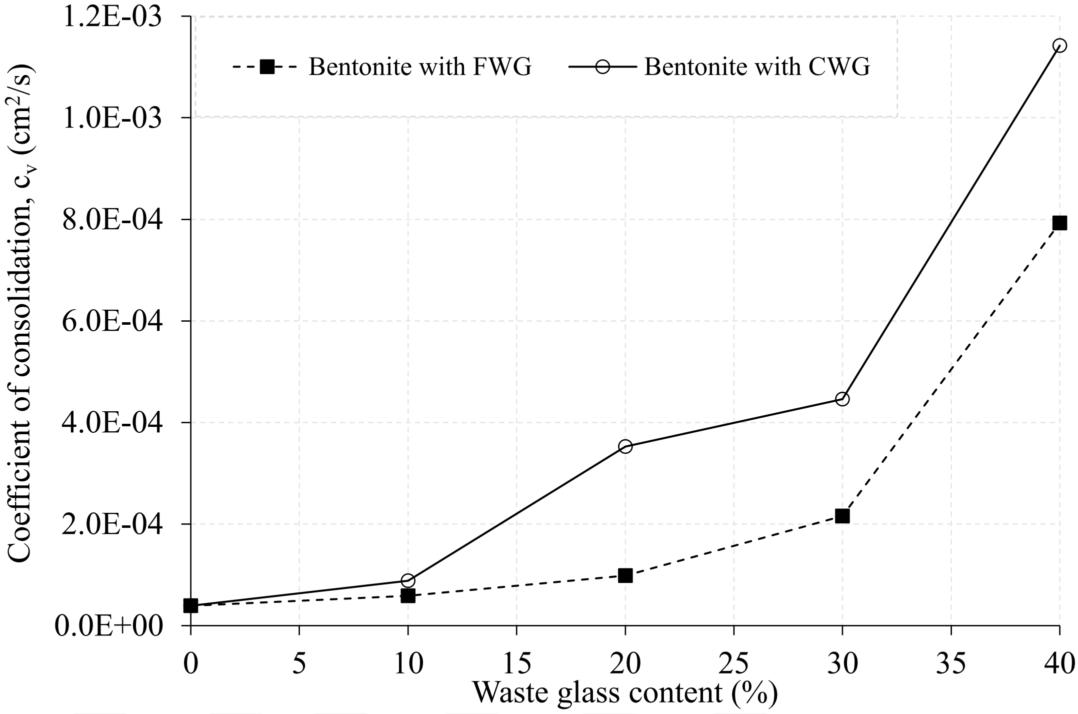

Figure 4.16. The c_v values of the bentonite-WG mixtures.

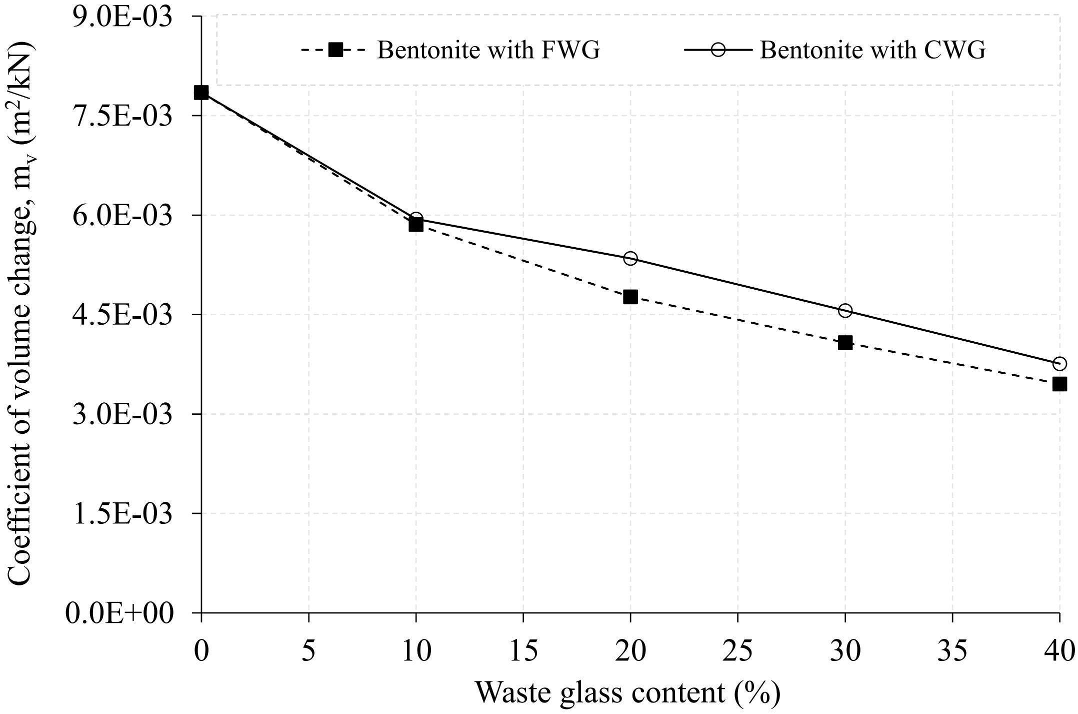

Figure 4.17. The m_v values of the bentonite-WG mixtures.

With additions of 10, 20, 30, and 40% FWG the initial void ratio of clean bentonite decreased from 0.94 to 0.90, 0.87, 0.85, and 0.81, respectively. This shows a 13% decrease in void ratio with 40% of FWG additions. Figure 4.14 and 4.15 presents the effects of FWG and CWG on the c_c and c_s coefficients. The results showed that WG additions caused a decrease in the c_c and c_s coefficients. The range of c_c values was from 0.18 to 0.09 m^2/kN while the c_s value was from 0.047 to 0.021 m^2/kN. The c_c value of 100% bentonite is 0.16 m^2/kN, while the value is reduced to 0.13, 0.12, 0.10, and 0.82 m^2/kN with 10%, 20%, 30%, and 40% CWG additions, respectively. Figure 4.14 and 4.15 also compares the different particle sizes of specimens to the results. The c_c and c_s values of CWG-containing specimens were found to be slightly higher than those of FWG-containing specimens. Similar results were obtained by several researchers (Vadlamudi and Mishra, 2018; Shen et al., 2018). Figure 4.16 presents the coefficients of consolidation (c_v) values of the mixtures. An increase in c_v values was obtained with WG additions. Figure 4.17 shows the m_v coefficients of the mixtures. The values ranged from 0.008 to 0.004 m^2/kN. The trend shows a decrease in m_v values with WG additions. As WG additions introduce cations to the soil mixture as discussed above, the compressibility of bentonite particles and therefore m_v values decreased. Several similar results were obtained by researchers (Dutta and Mishra, 2016; Jalal et al., 2021).

4.2.4 Viscosity Testing Results

The high viscosity and dispersion properties of clays caused several problems in the engineering designs. The high viscosity could cause undesirable time-dependent long-term deformation (Terzaghi, 1941; Bjerrum 1967, Garlanger 1972, Le et al., 2012; Ural, 2018; Sadeghi et al., 2019; Abbaslou et al., 2020). Therefore, viscosity tests were performed on the specimens.

Viscosity testing results can be seen in Figures 4.18 to 4.30. The test time was selected as 5 minutes with a data saving of 5 seconds. Figure 4.18 presents the viscosity values of clean bentonite at various rotational speeds. The results showed that the viscosity values decreased with increasing rotational speeds. Increasing the rotational speeds from 0.1 rpm to 0.4 rpm resulted in a decrease in viscosity values by 30%. Further, analysis from Figures 4.18 to 4.29 presents the dynamic viscosity values for all specimens. The graphs showed that the viscosity values decreased with both types of

WG additions. Also, the viscosity values of bentonite with CWG were found to be lower than that of FWG. Average viscosity values obtained from dynamic viscosity measurements are presented in Figure 4.19. The average viscosity value of clean bentonite decreased from 1040 Pa.s to 929 Pa.s, 825 Pa.s, and 723 Pa.s when increasing the rotational speed from 0.1 rpm to 0.4 rpm. At a constant speed of 0.1 rpm, the viscosity of clean bentonite was found to be 1040 Pa.s whereas this decreased to 850, 687, 521, and 316 Pa.s with the addition of 10%, 20%, 30%, 40% of FWG, respectively. Average viscosity values in Figure 30 also show that viscosity values decreased with both WG additions. Such a trend in viscosity values is trend is related to surface area, particle size, and viscosity difference between bentonite and the WG (Papo et al., 2010; Bentz et al., 2012; Ren et al., 2021).

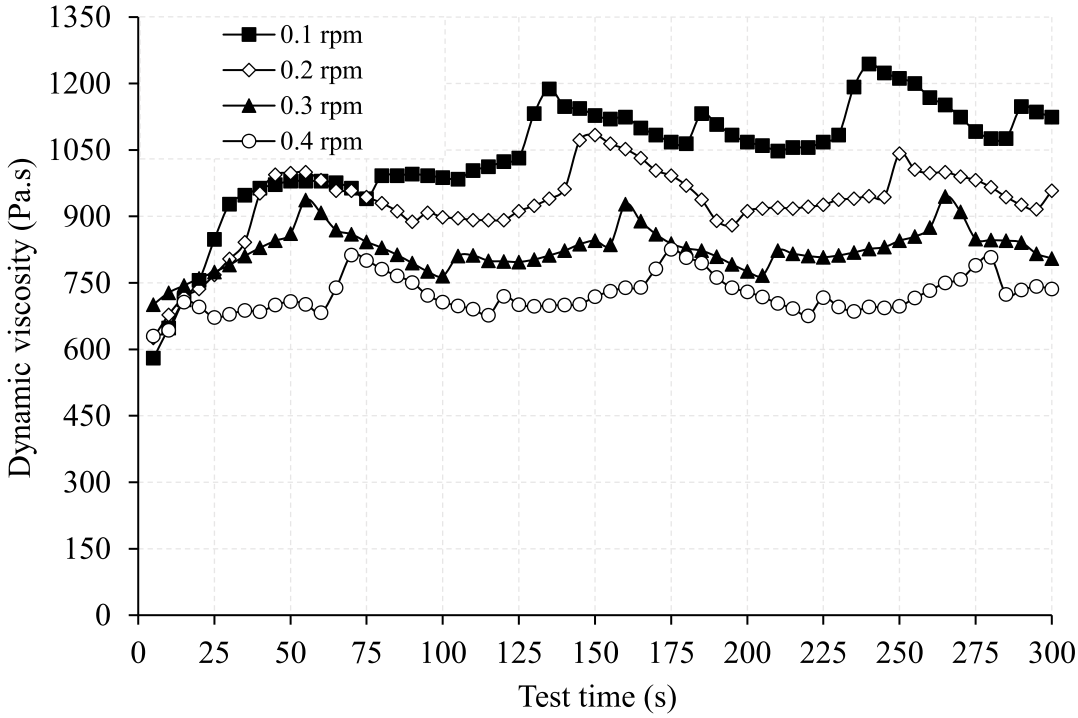

Figure 4.18. The viscosity values of clean bentonite at different rotational speeds.

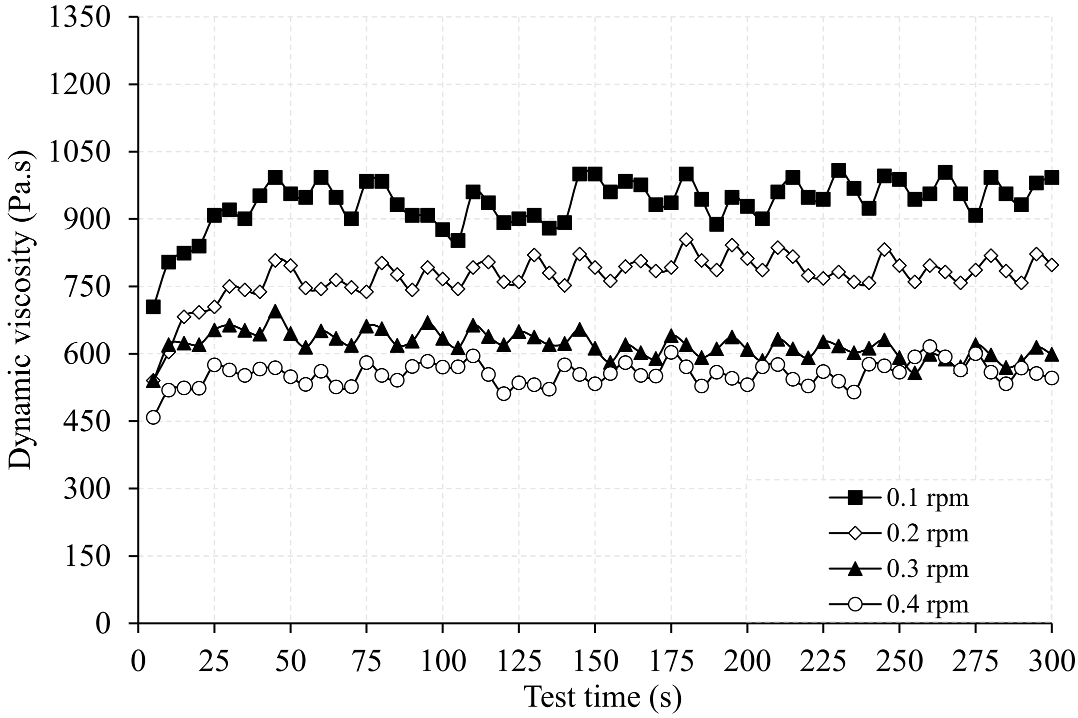

Figure 4.19. The viscosity values of bentonite with 10% CWG at different rotational speeds.

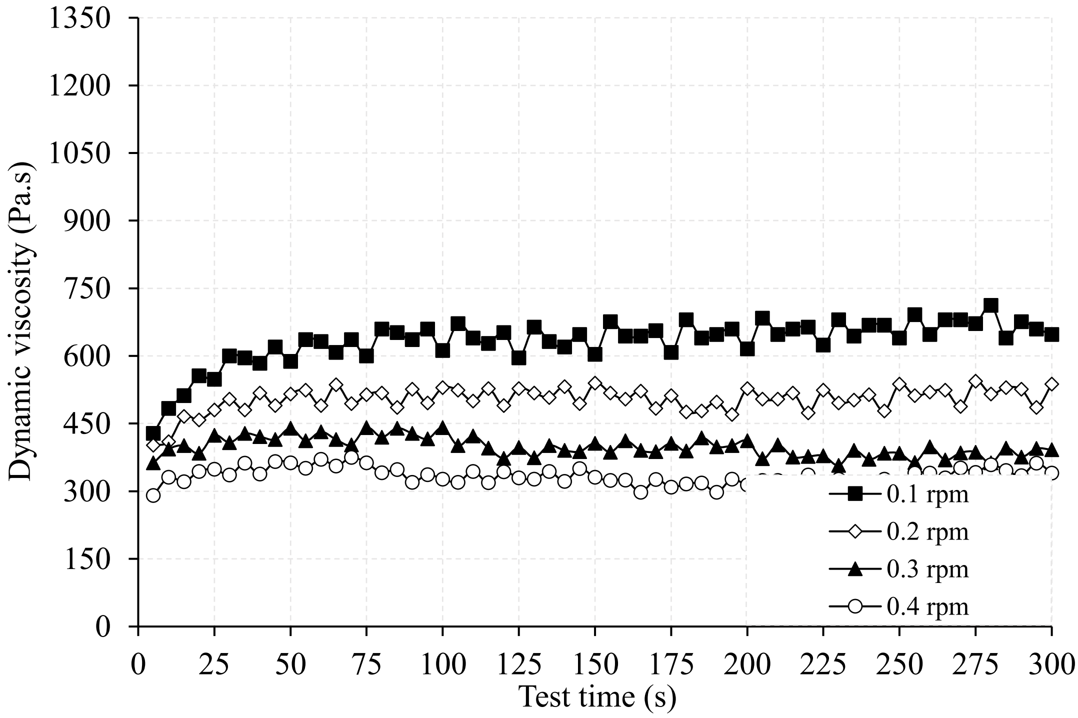

Figure 4.20. The viscosity values of bentonite with 20% CWG at different rotational speeds.

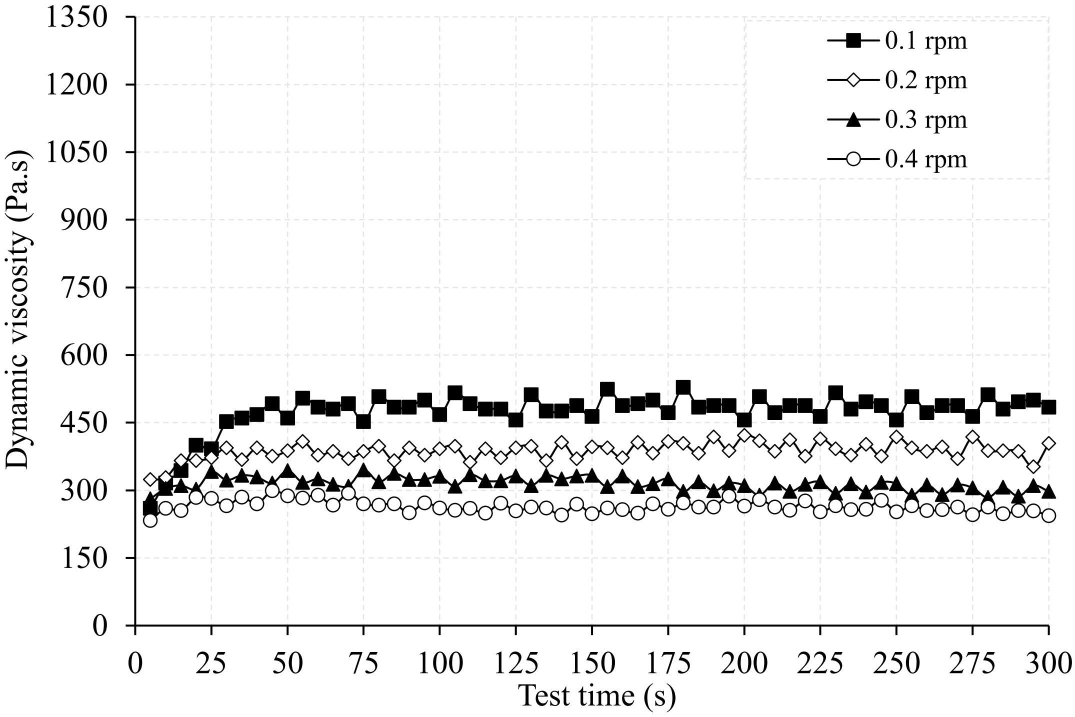

Figure 4.21. The viscosity values of bentonite with 30% CWG at different rotational speeds.

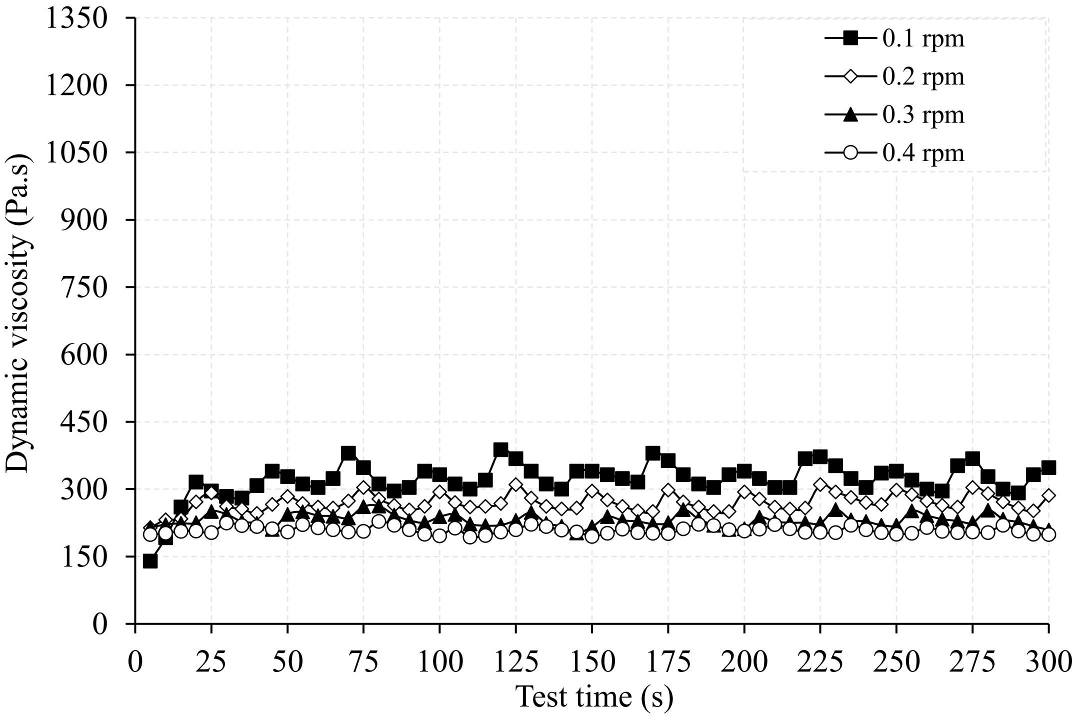

Figure 4.22. The viscosity values of bentonite with 40% CWG at different rotational speeds.

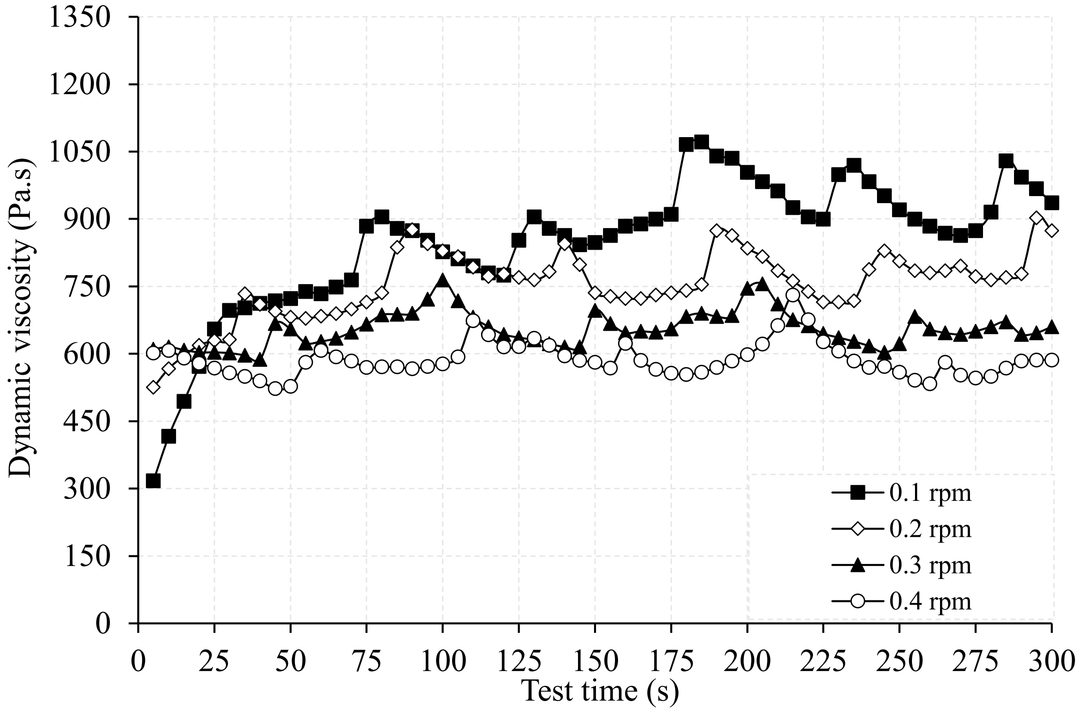

Figure 4.23. The viscosity values of bentonite with 10% FWG at different rotational speeds.

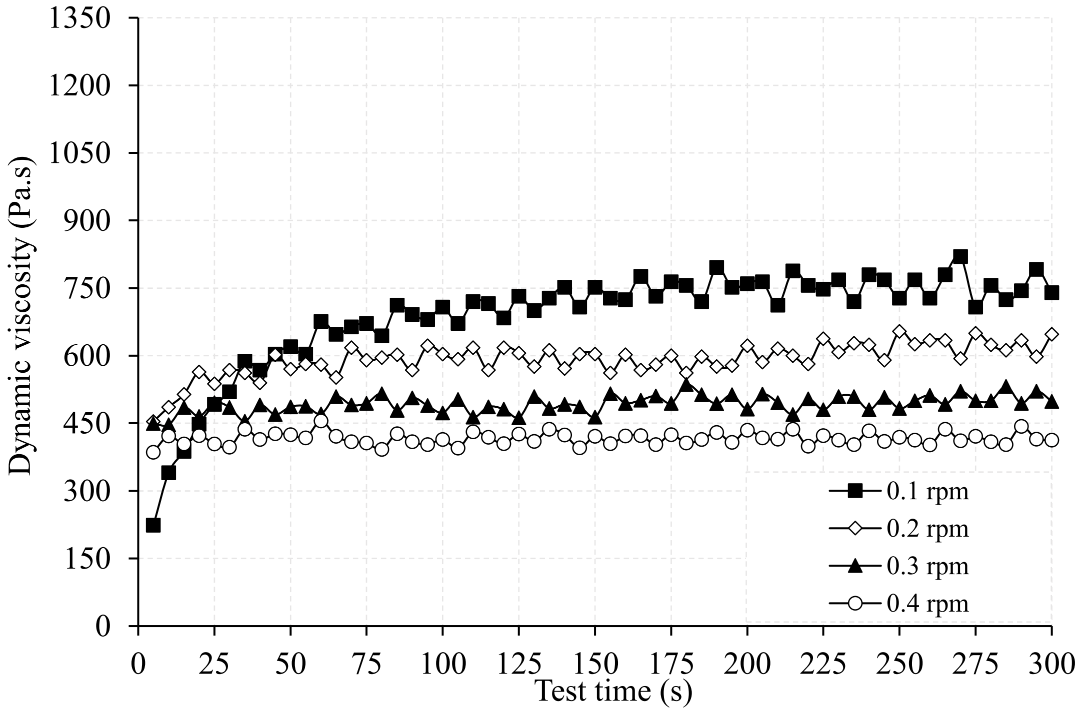

Figure 4.24. The viscosity values of bentonite with 20% FWG at different rotational speeds.

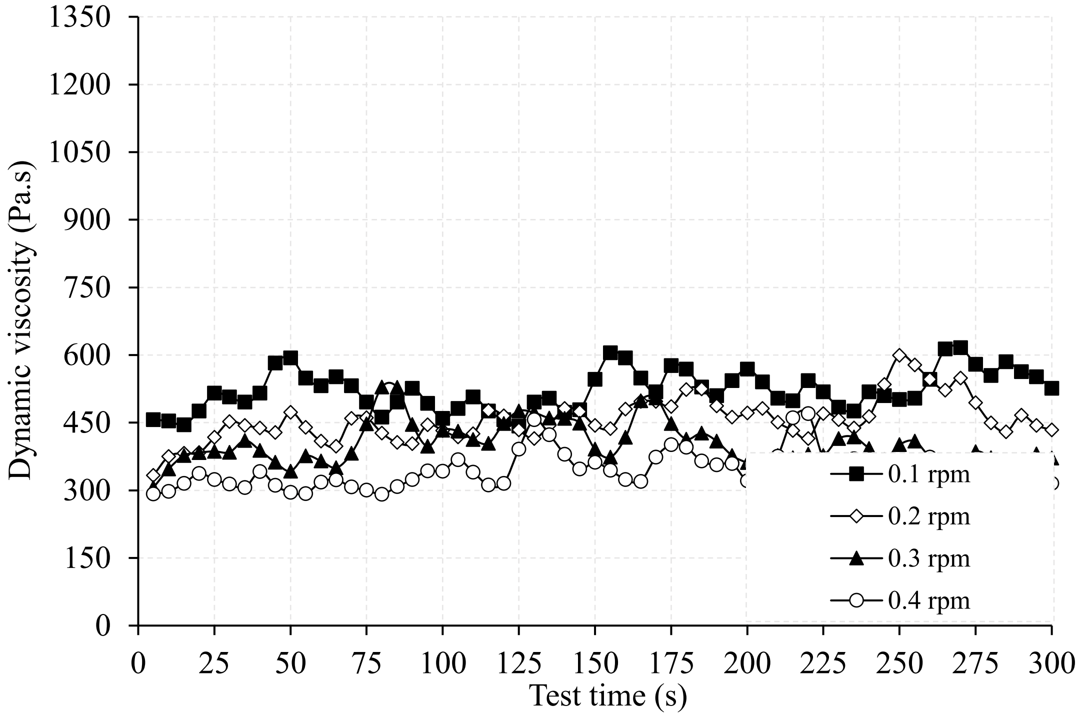

Figure 4.25. The viscosity values of bentonite with 30% FWG at different rotational speeds.

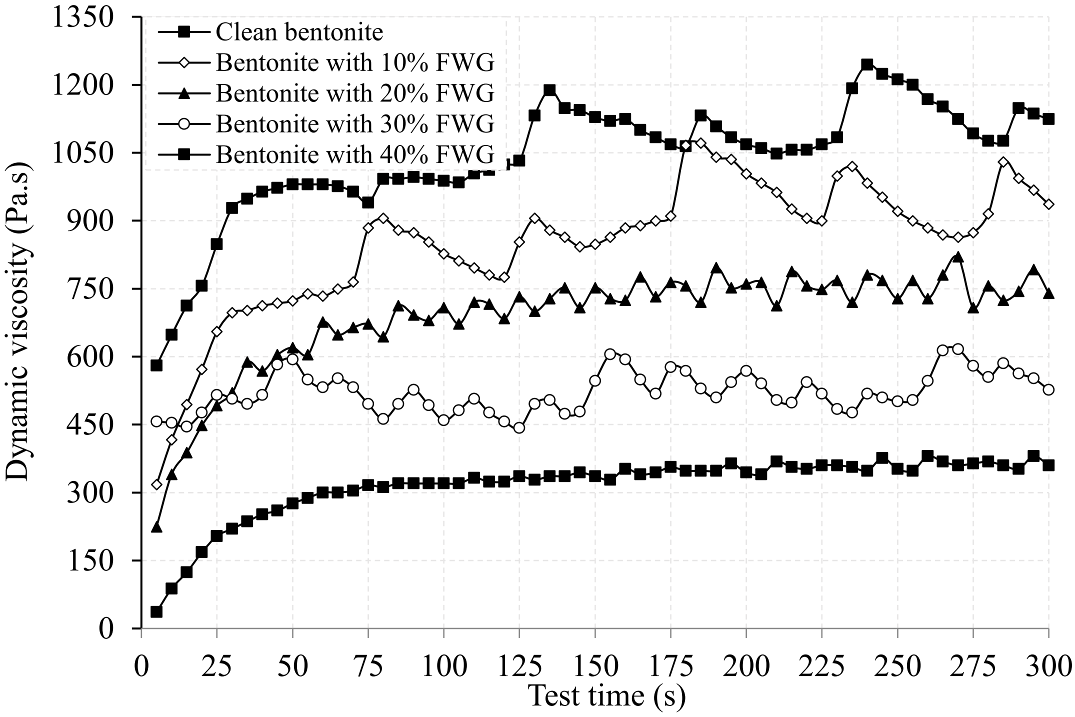

(a)

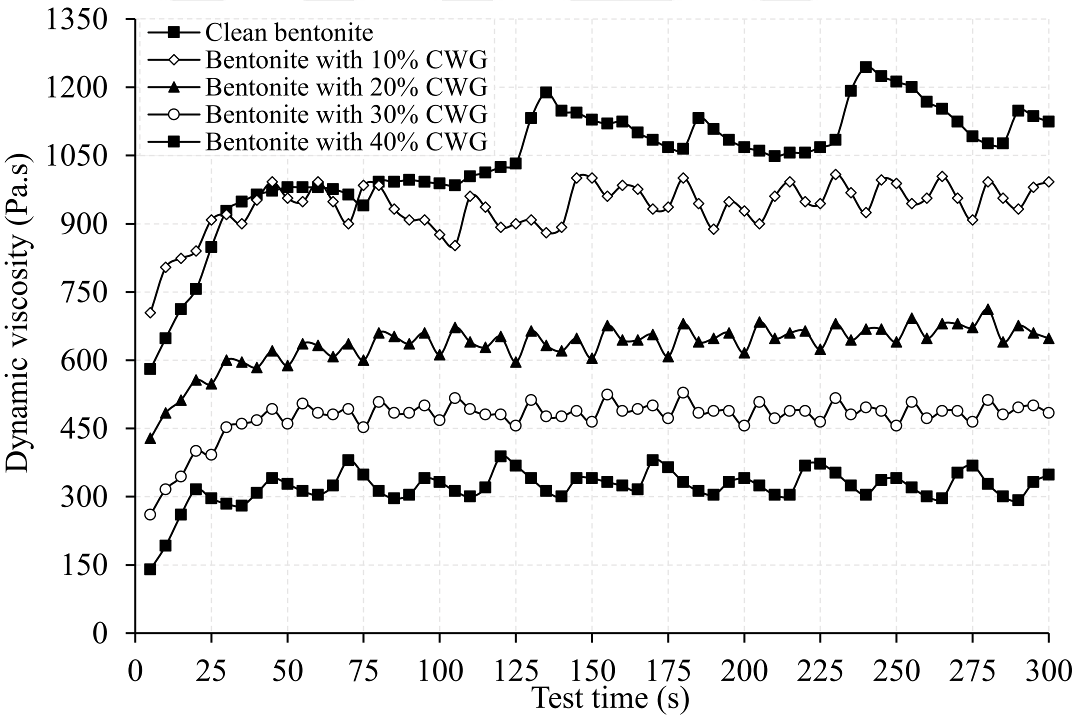

(b)

Figure 4.26. The dynamic viscosity values of the bentonite with various contents of (a) CWG and (b) FWG at 0.1 rpm rotational speed.

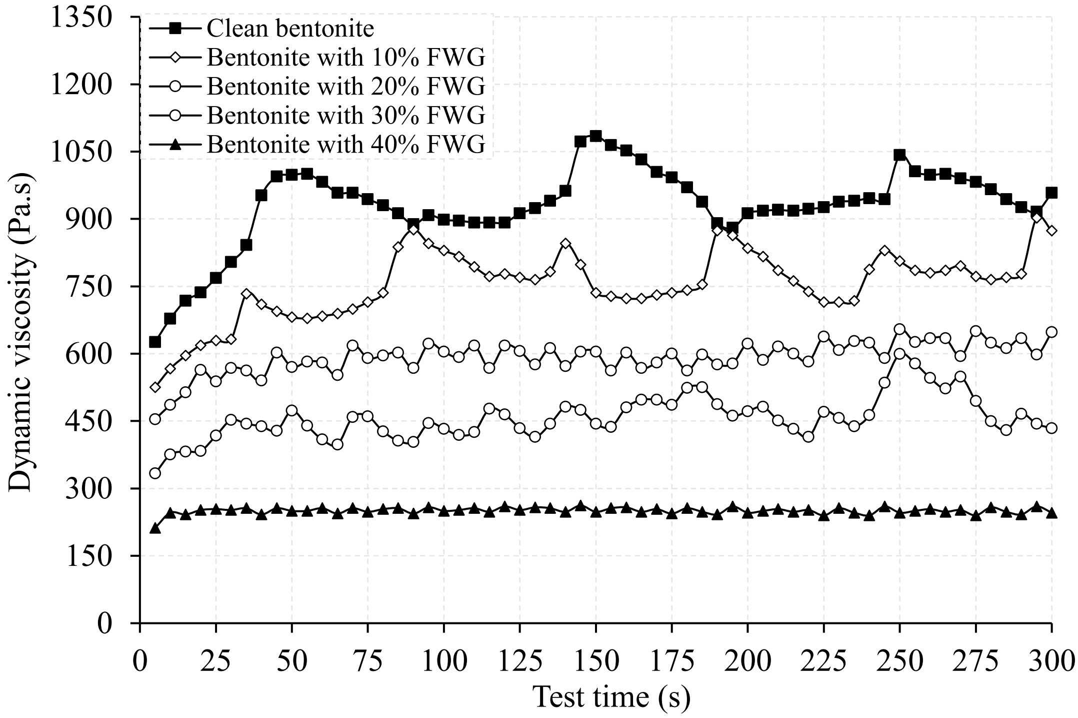

(a)

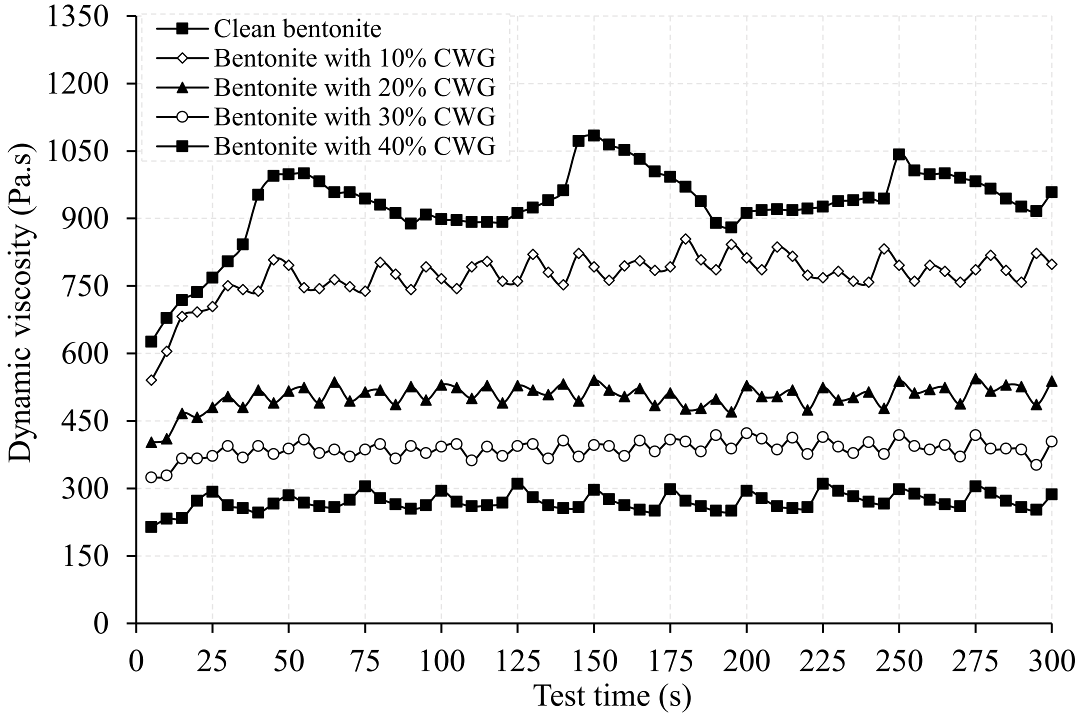

(b)

Figure 4.27. The dynamic viscosity values of the bentonite with various contents of (a) CWG and (b) FWG at 0.2 rpm rotational speed.

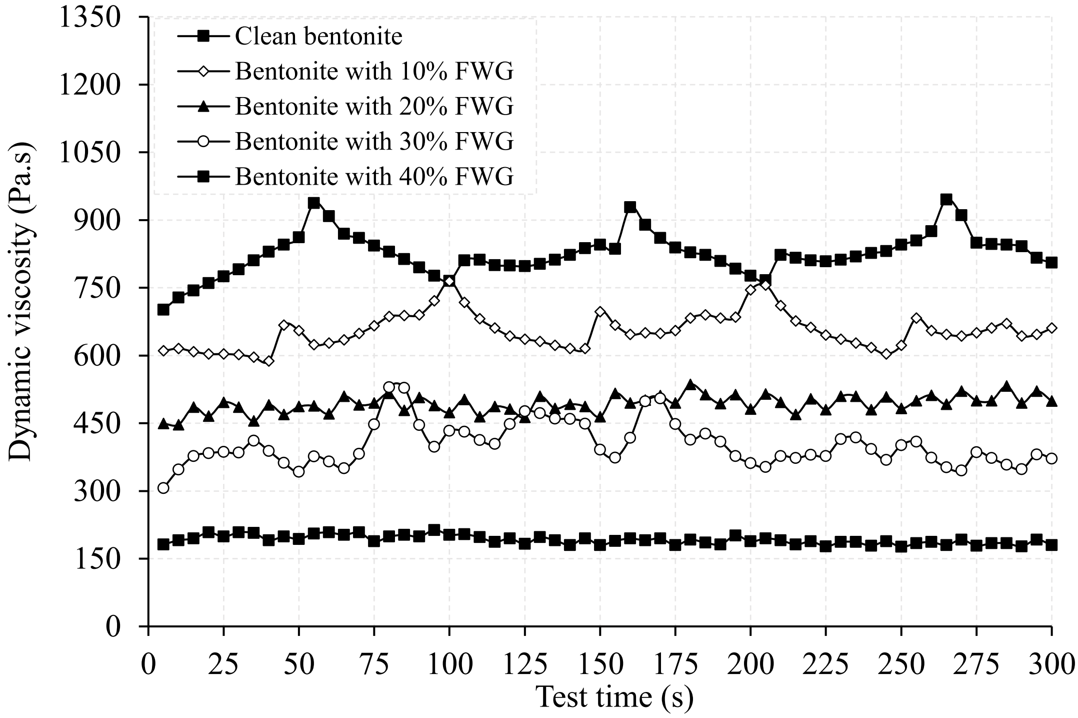

(a)

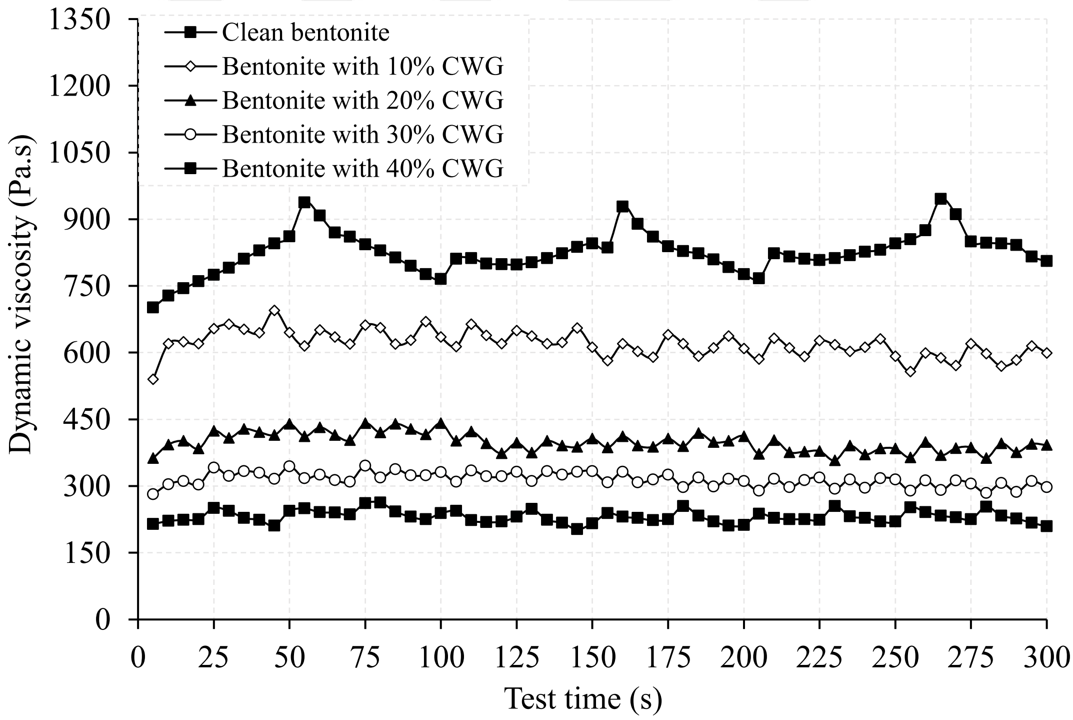

(b)

Figure 4.28. The dynamic viscosity values of the bentonite with various contents of (a) CWG and (b) FWG at 0.3 rpm rotational speed.

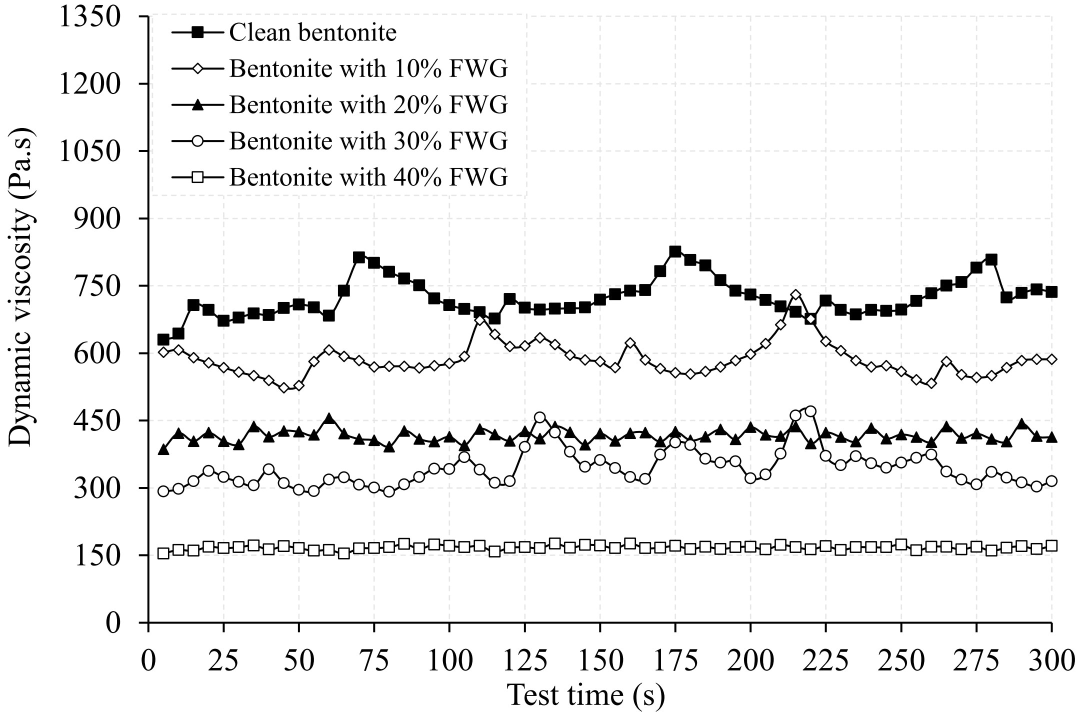

(a)

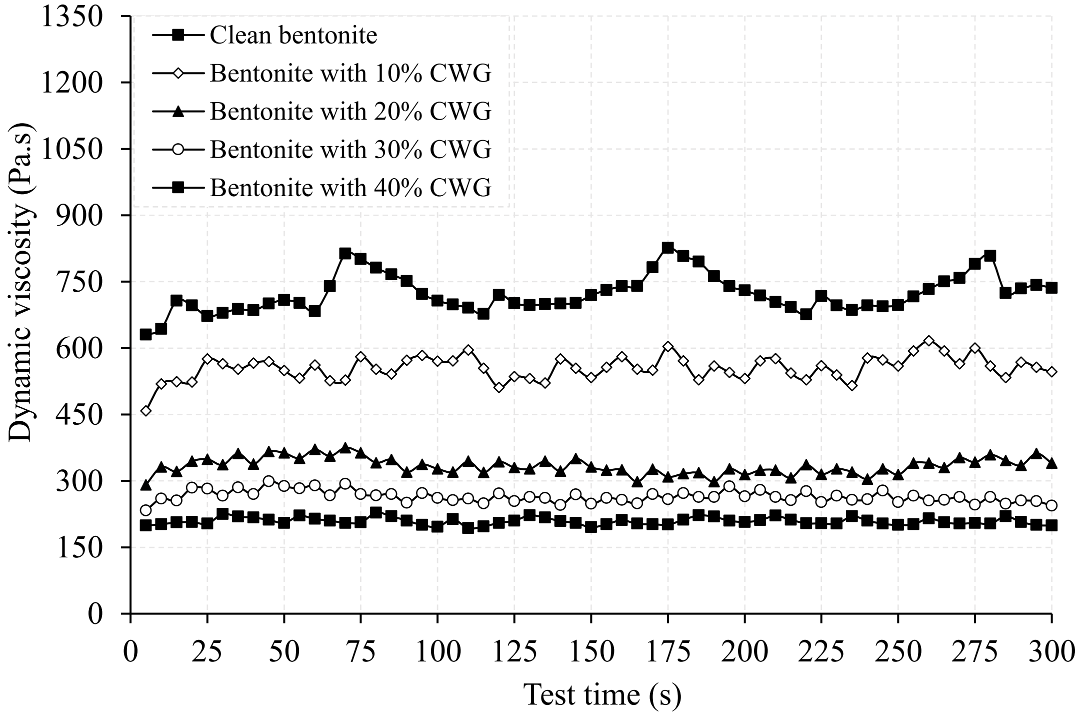

(b)

Figure 4.29. The dynamic viscosity values of the bentonite with various contents of (a) CWG and (b) FWG at 0.4 rpm rotational speed.

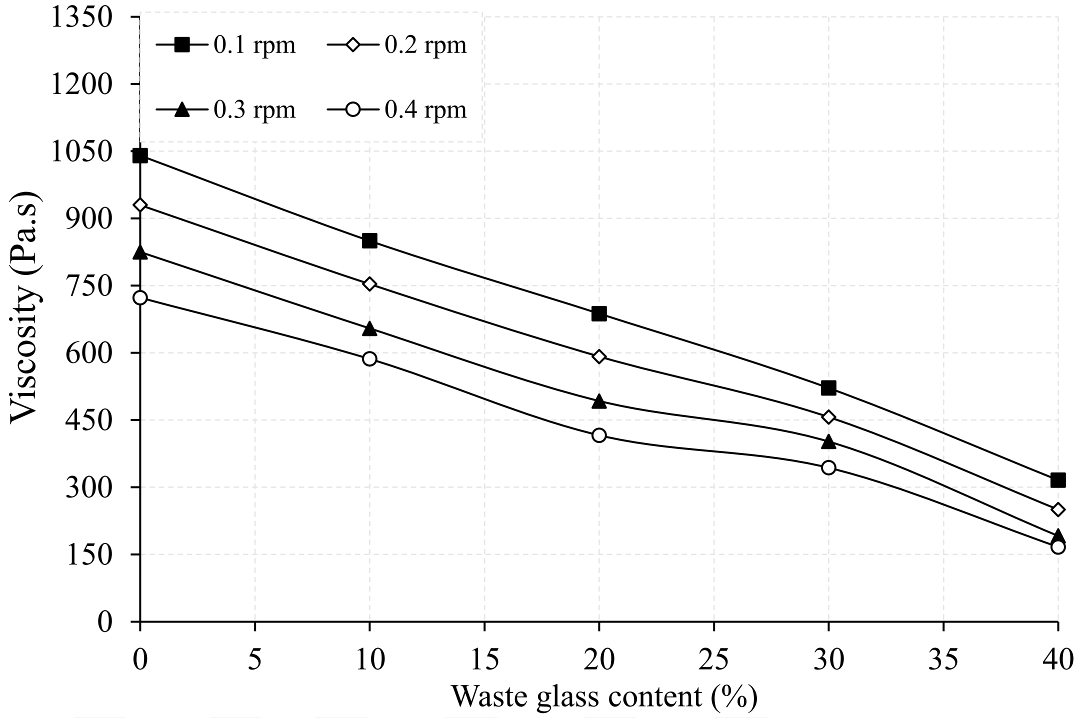

(a)

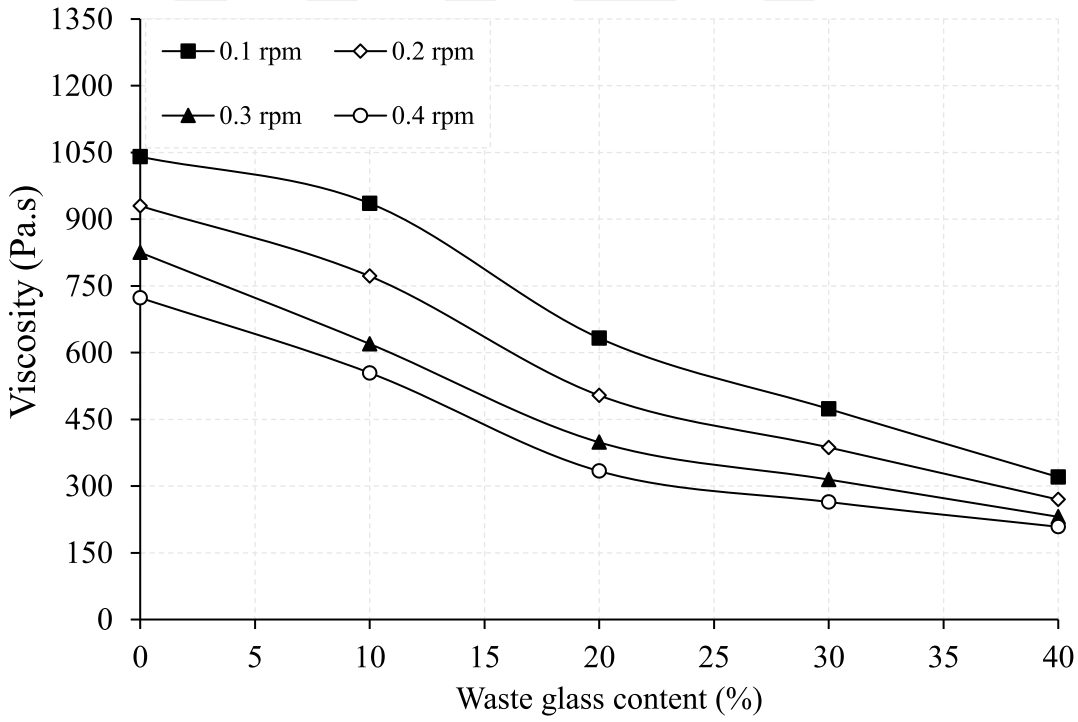

(b)

Figure 4.30. Average viscosity value of bentonite with (a) FWG (b) CWG at various rotational speeds.

4.2.5 Crumb Testing Results

Dispersibility is the tendency of soil particles to behave as separate particles rather than forming aggregations/flocs. The formation of high dispersibility causes several instability problems including the piping phenomena in earth dams (Fell et al., 1992, Richards and Reddy, 2007), deterioration of road pavements (Nevels, 1993, Quinonez Samaniego et al., 2023), and the erosion of the compacted soils of landfill clay liners (Ouhadi and Goodarzi, 2006; Sadeghi et al., 2019). Therefore, investigating the use of bentonite in engineering applications requires proper investigation of soil dispersibility. This thesis investigated the dispersibility of the soil mixtures through crumb and double hydrometer tests.

The crumb test is a preferable method in the literature to determine the dispersive properties of the soils due to its ease of performing. Therefore, several tests from clean clay to bentonite with 90% of WG were subjected to crumb tests to investigate the dispersive potential of the mixtures. Figures 4.31-4.36 present crumb testing results at 2 min, 1 hour, and 6 hours. The standard suggests obtaining dispersive potential at the above times of the test. If the dispersive potential at 1 hour and 6 hours are different the standard suggests assigning the dispersive potential according to the test result obtained at the 6th hour of the test.

Crumb testing results presented in Figures 4.31 to 4.36 show that the dispersive potential of the mixtures at 2 minutes is Grade 1 (No reaction). At 1 hour, the dispersive potential is Grade 2 (slightly dispersive). Grade 4 (Highly dispersive) potential is obtained at most of the mixtures at 6 hours. The dispersive potential of clean bentonite at 6 hours is Grade 4. Such a high dispersibility of bentonite could be attributed to the particle size and high repulsion force of bentonite particles (Shaikh et al., 2017). Increasing WG content up to 40% was not sufficient to reduce the dispersive potential of the bentonite. Therefore, WG additions were extended up to 90% for the crumb test. The results showed that 90% of WG decreased the dispersive potential of bentonite to Grade 1 (No reaction).

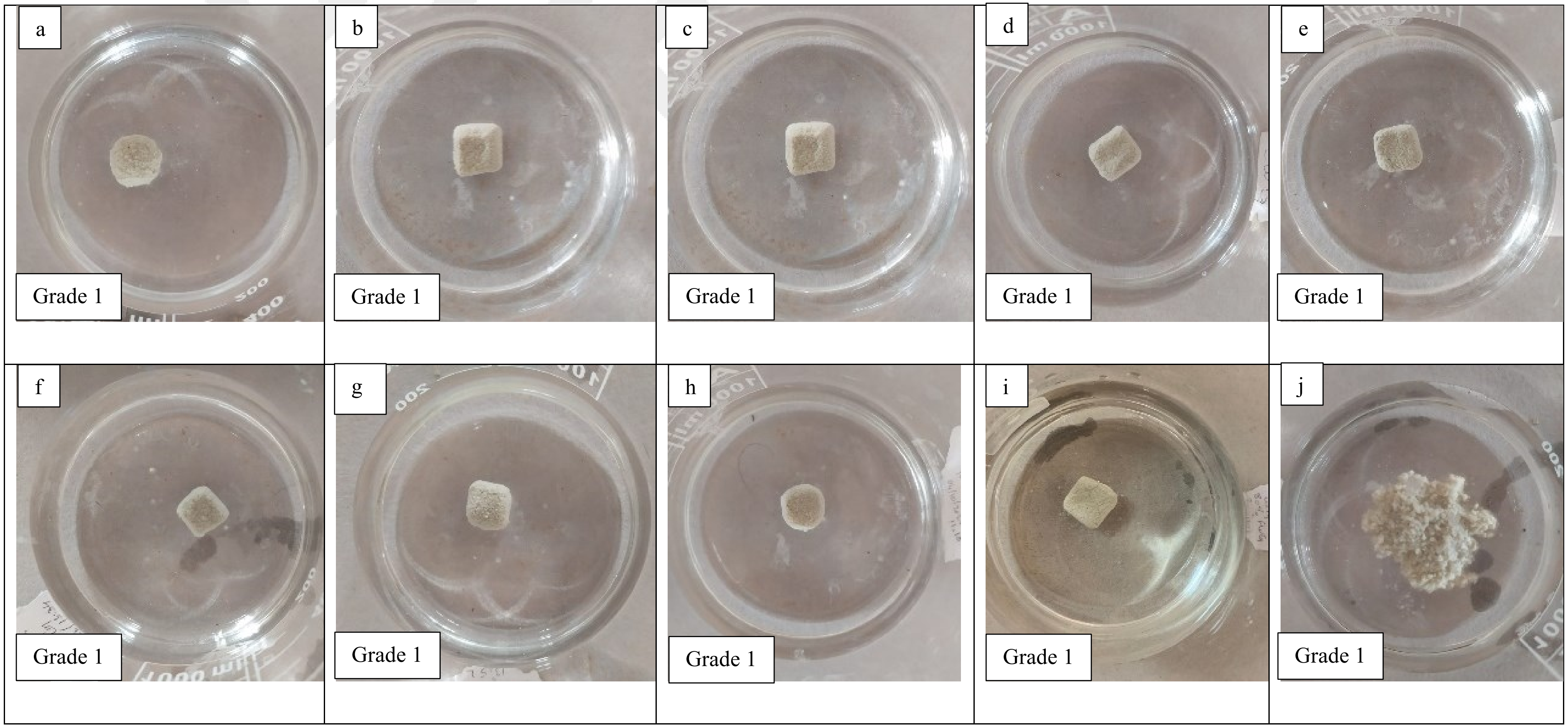

Figure 4.31. Crumb test on bentonite with (a) 0%, (b) 10%, (c) 20%, (d) 30%, (e) 40%, (f) 50%, (g) 60%, (h) 70%, (i) 80%, (j) 90% of CWG: the pictures at 2 minutes of the test.

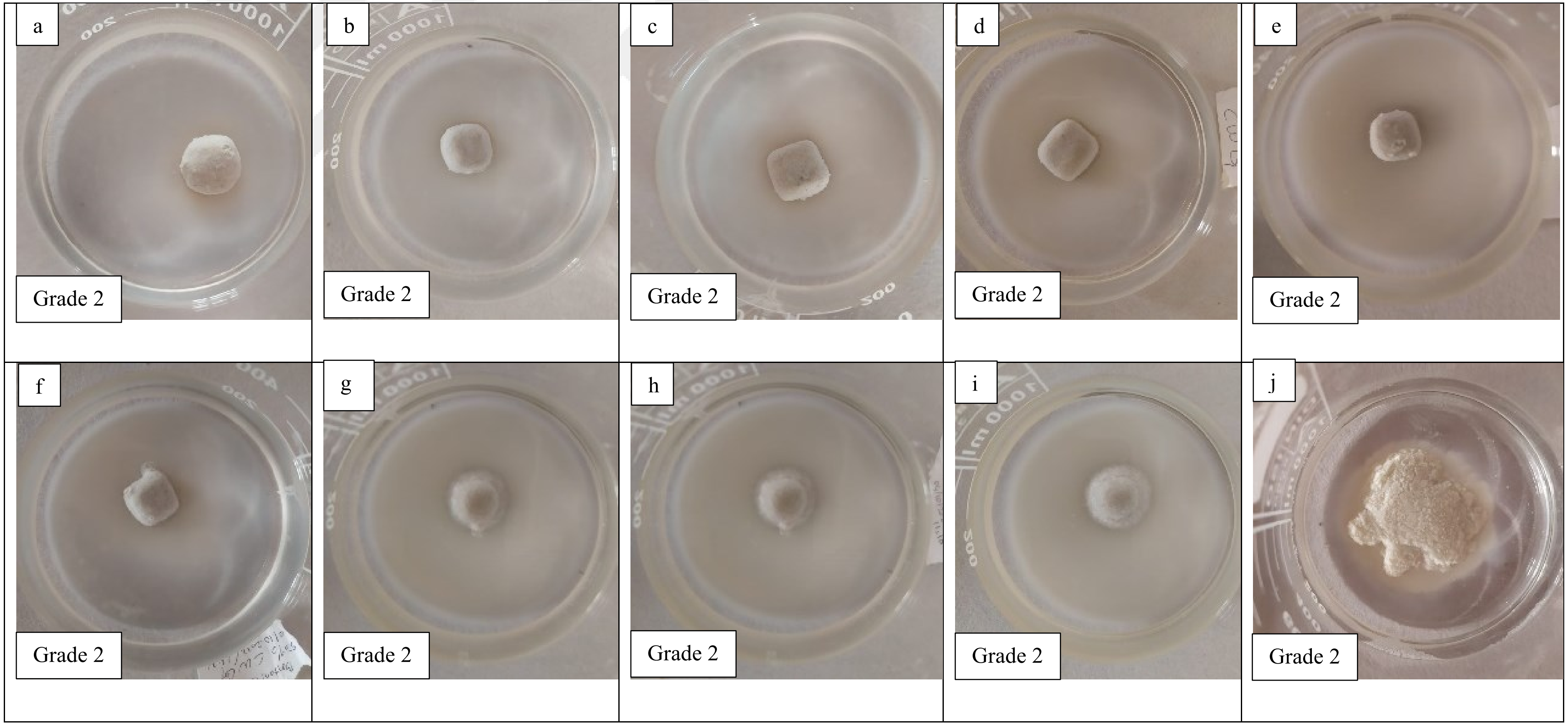

Figure 4.32. Crumb test on bentonite with a) 0%, (b) 10%, (c) 20%, (d) 30%, (e) 40%, (f) 50%, (g) 60%, (h) 70%, (i) 80%, (j) 90% of CWG: the pictures at 1 hour of the test.

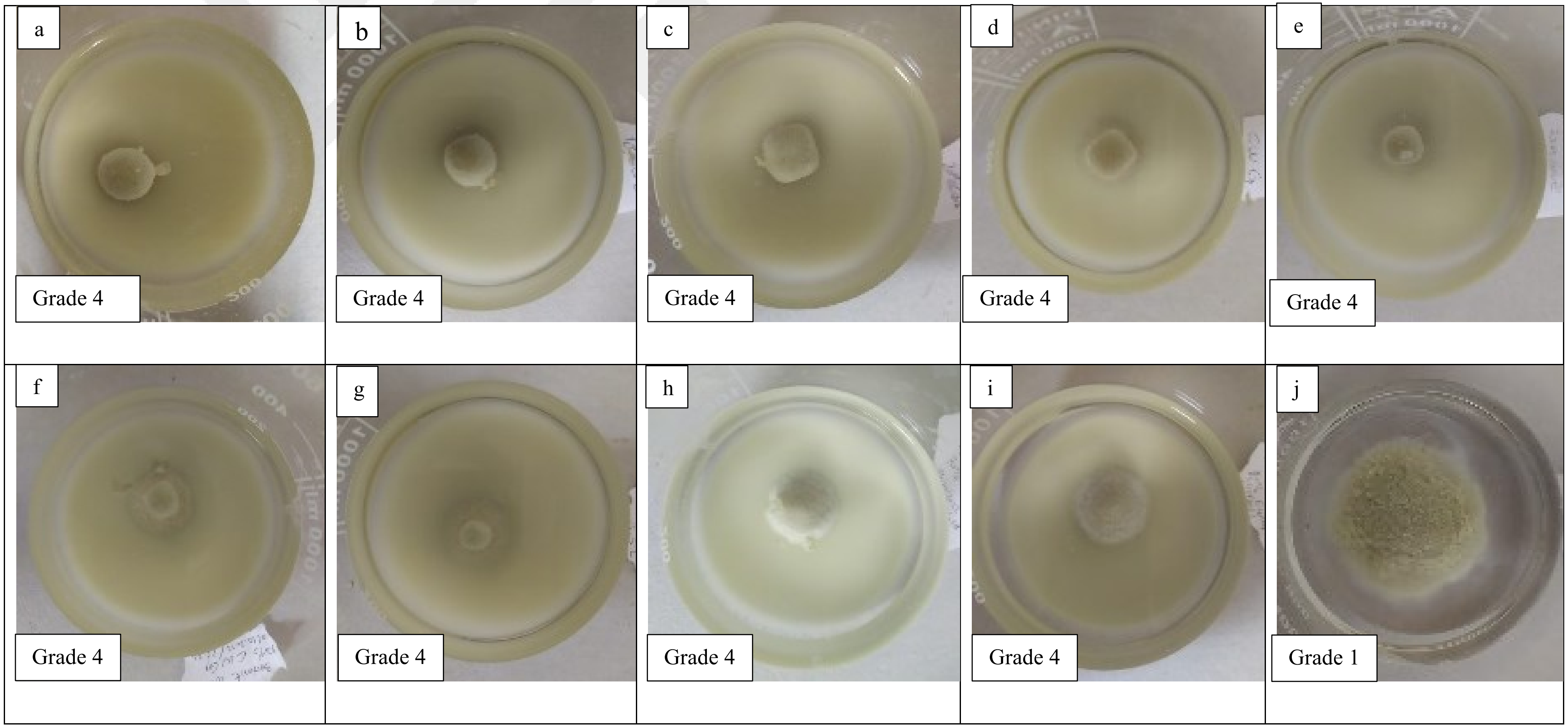

Figure 4.33. Crumb test on bentonite with a) 0%, (b) 10%, (c) 20%, (d) 30%, (e) 40%, (f) 50%, (g) 60%, (h) 70%, (i) 80%, (j) 90% of CWG: the pictures at 6 hours of the test.

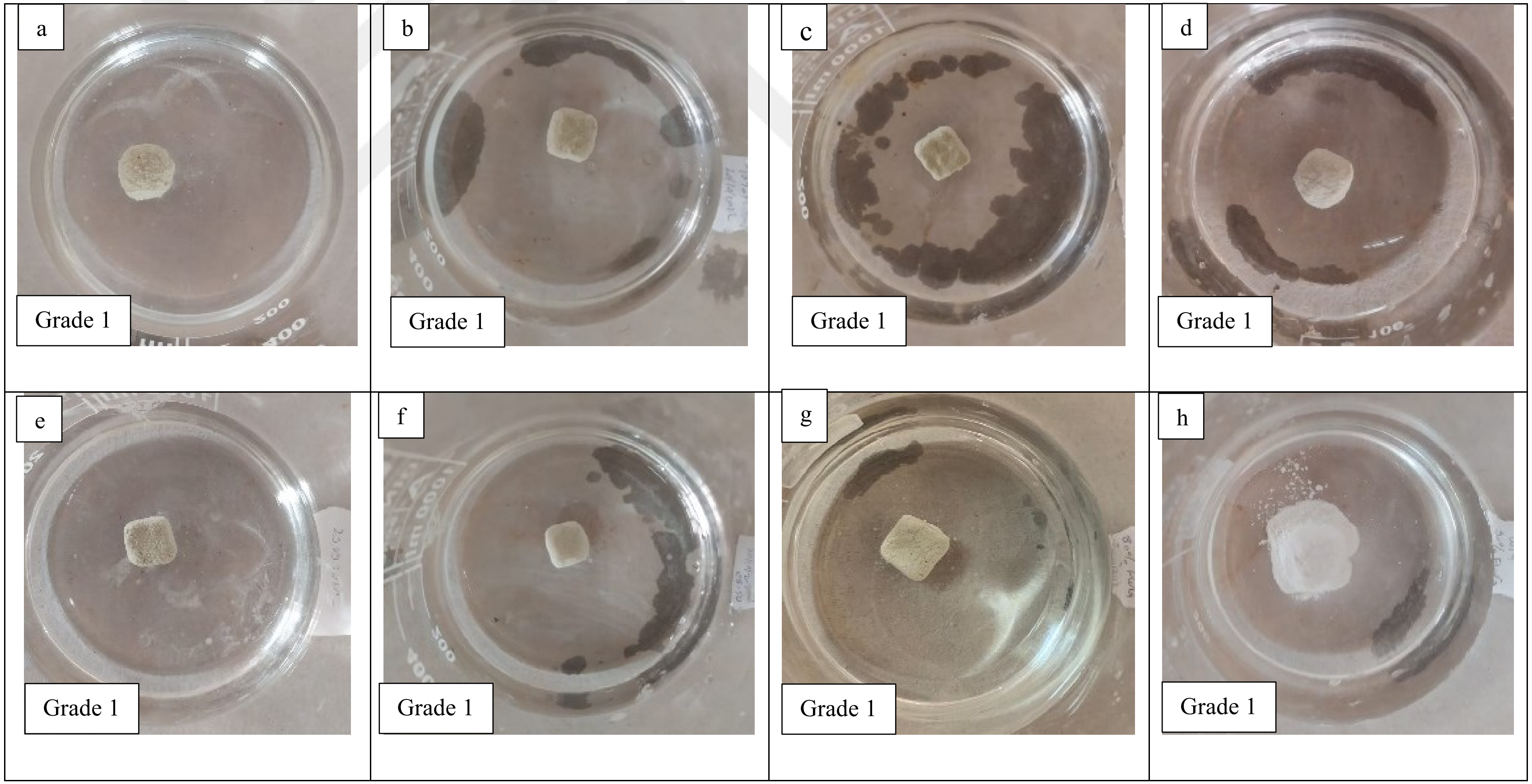

Figure 4.34. Crumb test on bentonite with (a) 0%, (b) 10%, (c) 20%, (d) 30%, (e) 40%, (f) 50%, (g) 80%, (h) 90% of FWG: the pictures at 2 minutes of the test.

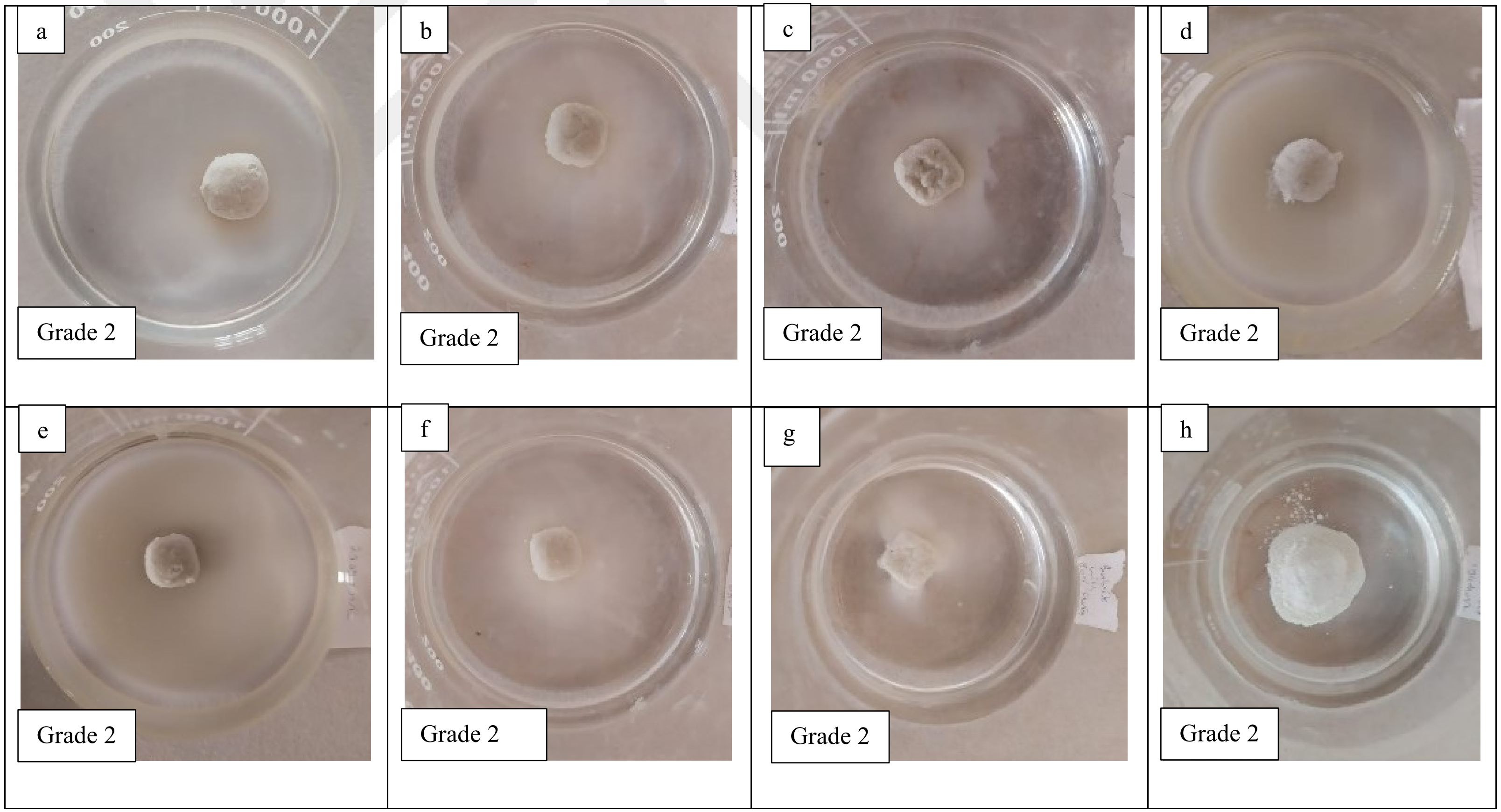

Figure 4.35. Crumb test on bentonite with (a) 0%, (b) 10%, (c) 20%, (d) 30%, (e) 40%, (f) 50%, (g) 80%, (h) 90% of FWG: the pictures at 1 hour of the test.

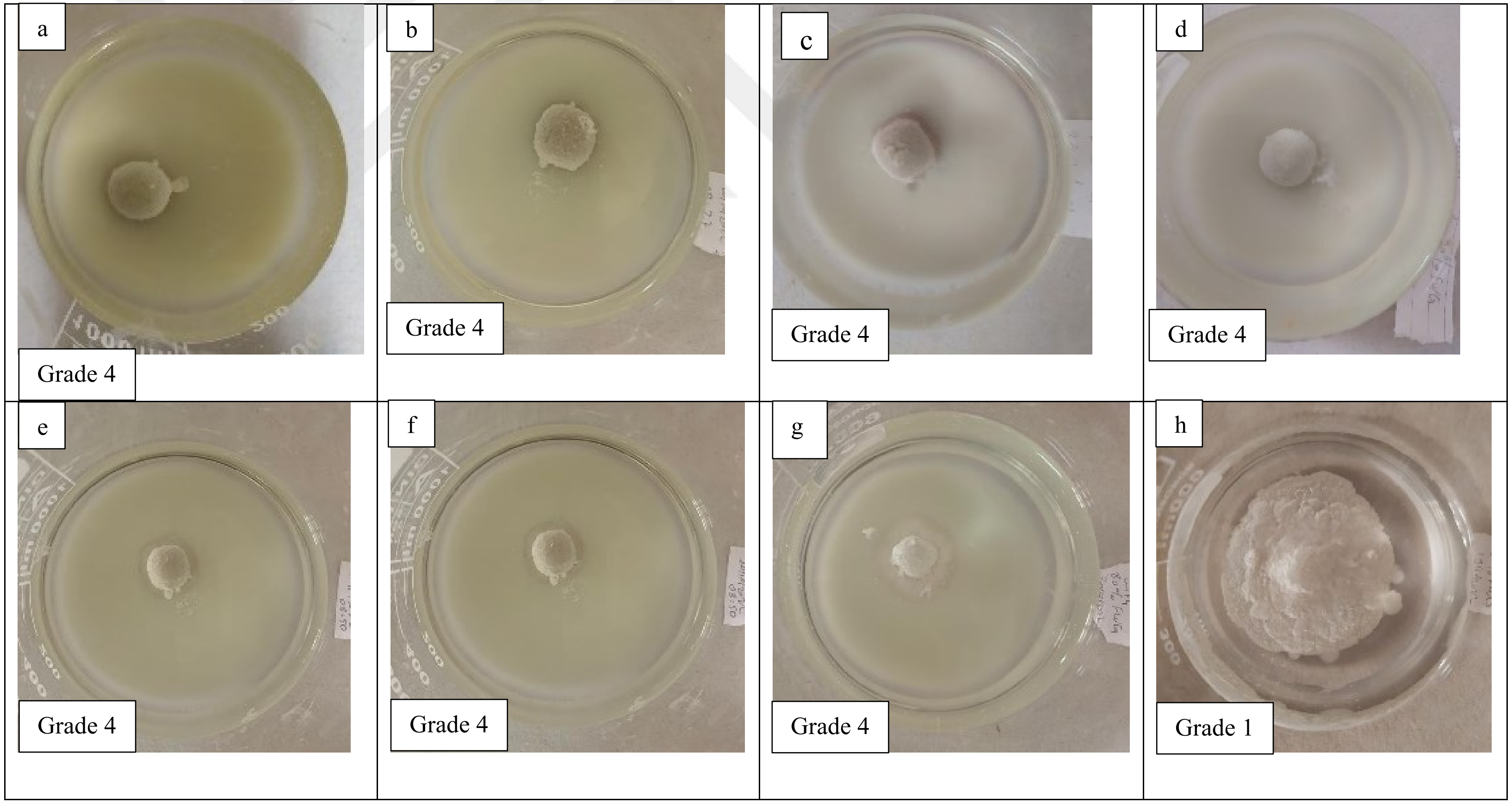

Figure 4.36. Crumb test on bentonite with (a) 0%, (b) 10%, (c) 20%, (d) 30%, (e) 40%, (f) 50%, (g) 80%, (h) 90% of FWG: the pictures at 6 hours of the test.

4.2.6 Double Hydrometer Testing Results

Crumb tests discussed above were combined with double hydrometer tests to quantitively obtain the dispersive potential of the mixtures. Figure 4.37 shows the dispersive potential of the mixtures. The dispersive potential of clean bentonite was found to be around 65% (i.e., dispersive), which agrees with the crumb testing results. The addition of both WG types caused a decrease in the dispersive potential of the bentonite. A minimum dispersive potential was obtained as 38% with bentonite-40% CWG. Therefore, according to the double hydrometer testing results, the dispersive potential of bentonite reduced from highly dispersive to medium dispersive with 40% of CWG additions.

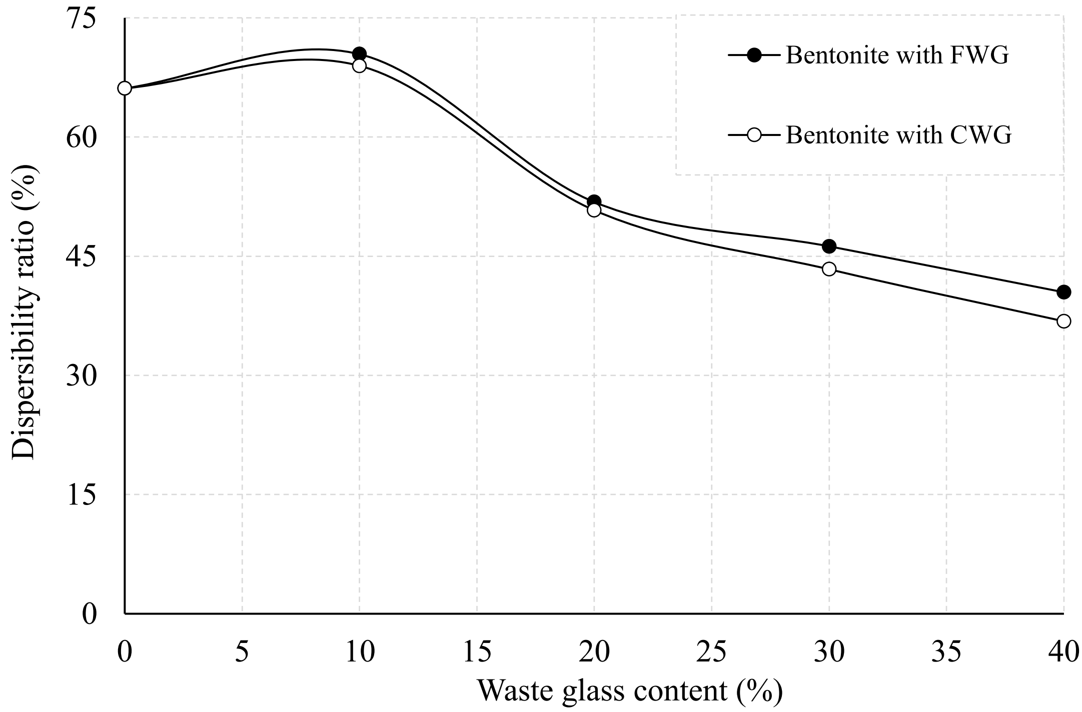

Figure 4.37. Dispersibility ratio of the specimens obtained from double hydrometer test.

4.2.7 Direct Shear Testing Results

Direct shear tests were also performed on the specimens to obtain cohesion and angle of internal friction of the specimens which are widely utilized to predict the response of soils under a given normal load.

Figure 4.38 depicts the effect of normal stress on bentonite shear stress. Shear strength increases with normal stress, as shown in the figures. The maximum shear stress (shear strength) cohesion and angle of internal frictions of bentonite with CWG are shown in Figures 4.39a and 39b. Shear strength increased with normal stress in all mixes. With the inclusion of CWG, the cohesive values of the specimen decreased. The addition of 40% CWG in bentonite resulted in a maximum 15% decrease in the cohesion value of clean bentonite. The angle of internal friction values of the mixtures increased with CWG additions until a 30% mixing ratio was reached, at which point they reduced. This demonstrates a transition between bentonite and WG, which will be studied further in the thesis. Figures 4.40a and 4.40b show the maximum shear stress (shear strength) cohesion, and angle of internal frictions of the bentonite with FWG. A continuous decrease in cohesion values with FWG values was observed. The angle of internal friction values shows similar trends to the CWG-contained mixtures, with the values peaking at a 30% mixing ratio. The values are also presented in Table 4.2. The testing results are similar to the Disfani et al. (2009).

4.2.8 Unconfined Compression Testing Results

Yong et al. (1986) and Villar (2021) developed general engineering criteria for bentonite-based mixtures for engineering applications. The researchers pointed out some insufficient properties of bentonite such as mechanical response and deformation characteristics. To address these insufficient engineering properties, numerous researchers have proposed additive materials. To evaluate the modification effect of WG grains on the maximum unconfined compressive value and the stiffness at small strain levels the UC and BE tests were performed on the mixtures. Furthermore, such an experimental program enables researchers to estimate the stiffness in a very small strain (G_{max}) as a function of unconfined compressive strength (q_u) using such an experimental program (Cabalar et al., 2018; Consoli et al. 2020; Yao et al. 2020; Consoli et al. 2021).

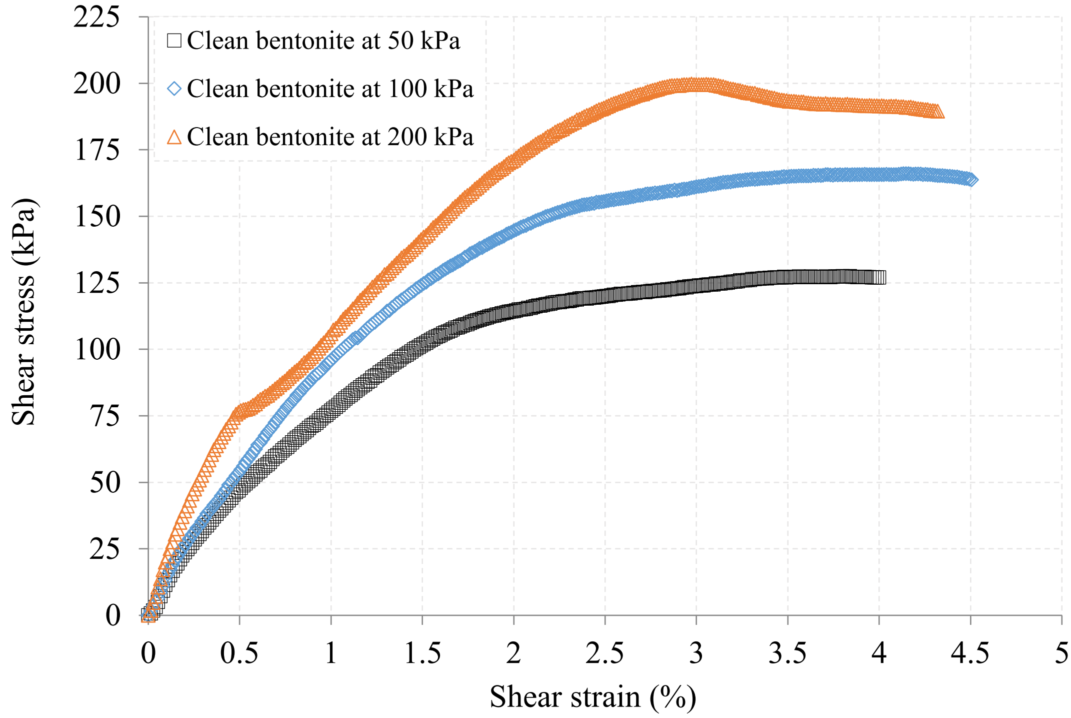

Figure 4.38. Effect of normal stress on the shear stress values of clean bentonite.

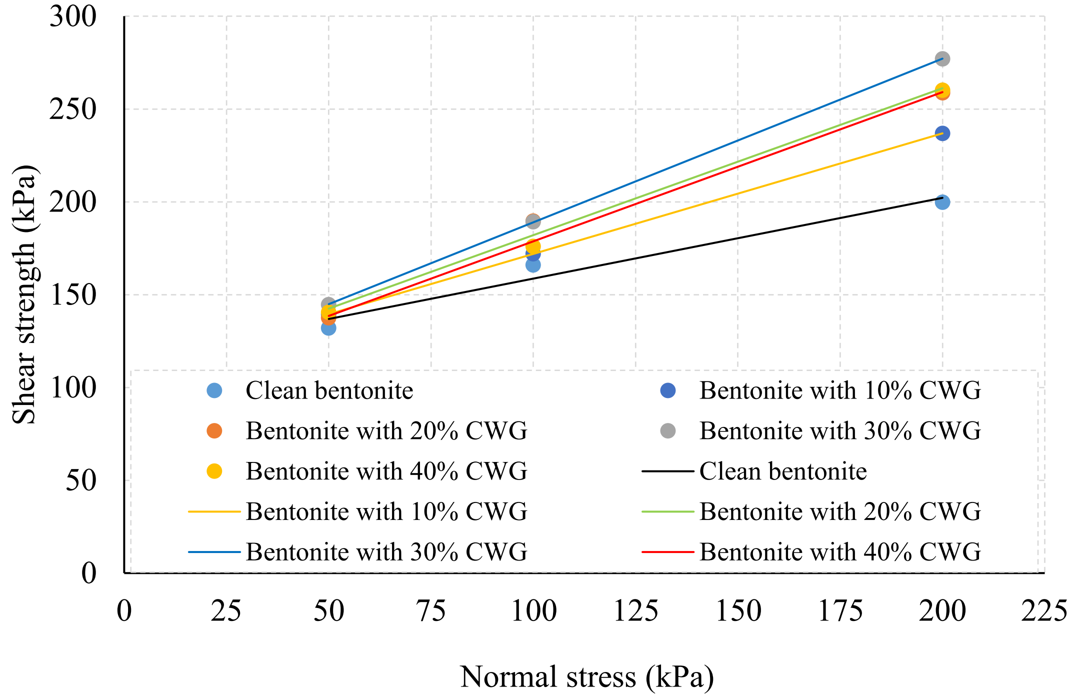

(a)

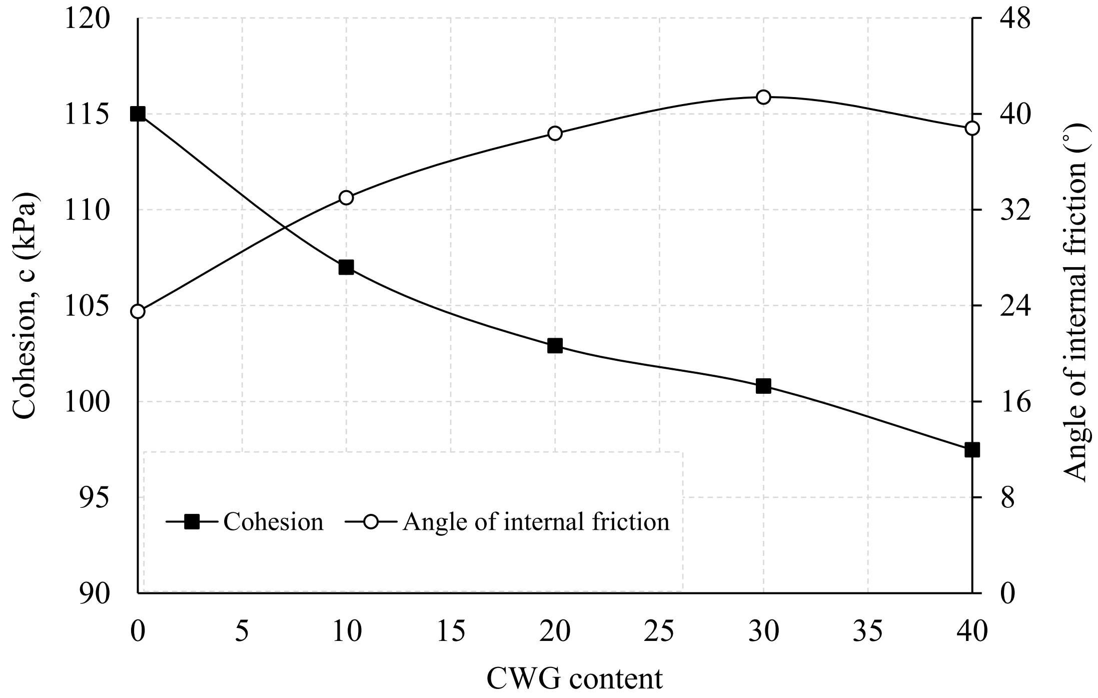

(b)

Figure 4.39. Direct shear testing results of bentonite with various amounts of CWG (a) peak shear stress values (b) cohesion and angle of internal friction values.

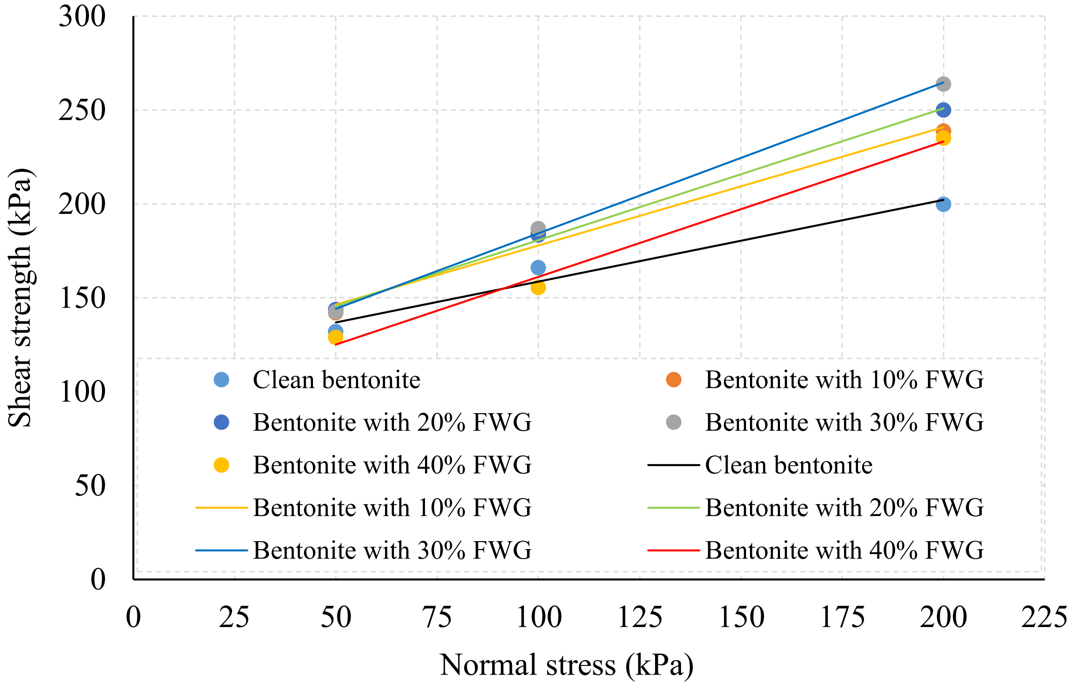

(a)

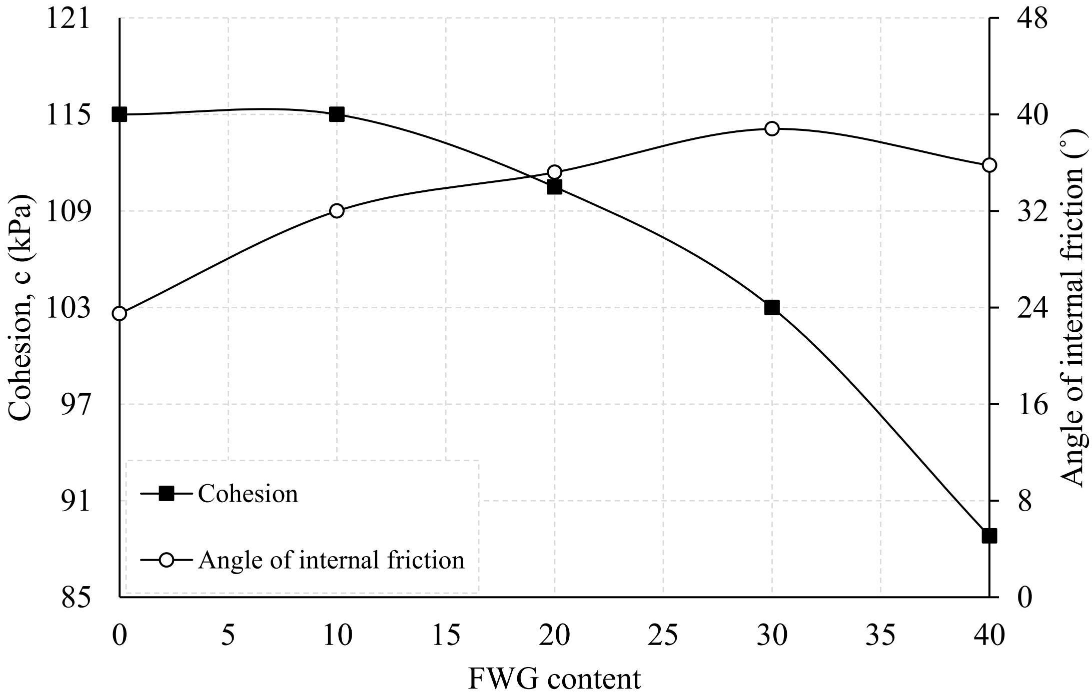

(b)

Figure 4.40. Direct shear testing results of bentonite with various amounts of FWG (a) peak shear stress values (b) cohesion and angle of internal friction values.

The stress-strain values of the tested specimens are presented in Figure 4.41. The figure shows that with WG additions up to 30%, the stress values of the mixtures increased at a given strain. However, once the 30% mixing ratio was exceeded the stress value decreased at a given strain. Unconfined compressive strength (q_u) values were presented in Figure 4.41. The q_u values of bentonite increased until 30% of WG addition, followed by a decrease at 40% WG. Such a transition was also observed in the direct shear testing results. This behavior could be explained by the transitional zone theory between fine and coarse mixtures (Lupini et al. 1981; Monkul and Ozden, 2007; Cabalar et al., 2013). While the transitional phase is a concept, it has been discussed for the soil mixtures over a long time (Lupini et al., 1981; Kuerbis and White 1989, Thevanayagam, 1998; Simoni and Housbly, 2006; Monkul and Ozden, 2007; Rahman et al., 2008; Cabalar, 2011; Cabalar et al., 2013: Mohammadi and Qadimi, 2015; Cabalar et al., 2021; Cabalar et al., 2022; Wang et al., 2022). The theory discusses three phases of fine-coarse mixtures. In the first phase, the coarse soil content is low and the coarse soil floats within the voids between the fine-grained soil. In this region, there is no contact between coarse-grained soil, therefore fine-grained soil controls the mechanical behavior of the soil matrix. Increasing the coarse content resulted in grain-to-grain contact of grains which leads to a coarse-soil-dominated soil mixture. In this phase, fine grains are floating within the voids of granular soil, therefore reducing the number of contacts between the coarse grains. The transition phase is a specific phase between these two phases. The transition content is believed to have a specific granular content where the e_s of the mixture is equal to the e_{max} of the host material (Monkul and Ozden, 2007). The optimum response of such mixtures is generally observed at the transition phase between coarse and fine grains. This theory has been used to explain a variety of geotechnical responses of different geomaterials, such as liquefaction, undrained shear response, stiffness, and wave propagation (Lade and Yamamuro, 1997; Kang and Bate, 2016; Kwa and Airey, 2017; Cabalar and Demir, 2019; Shi et al., 2020; Cabalar and Alosman, 2021). According to the UC testing results, the transitional WG content in this study was found to be around 30%. Ibrahim et al. (2021) observed that the peak q_u value of the kaolin-WG mixture was found at kaolin with 27% of WG. Furthermore, Disfani et al. (2009) show that the shear strength of WG-biosolid mixtures peaked at the range of 30%-50% WG content depending on the normal stress of the test. This study proposes a 56% increase in q_u value of clean bentonite with 30% WG additions.

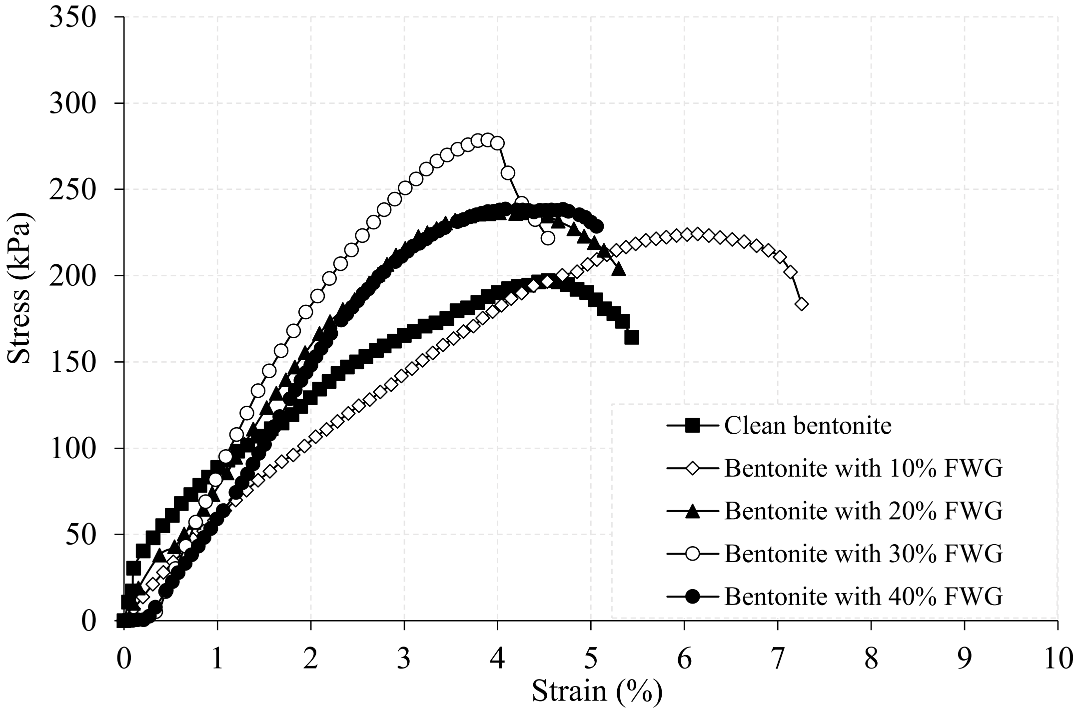

(a)

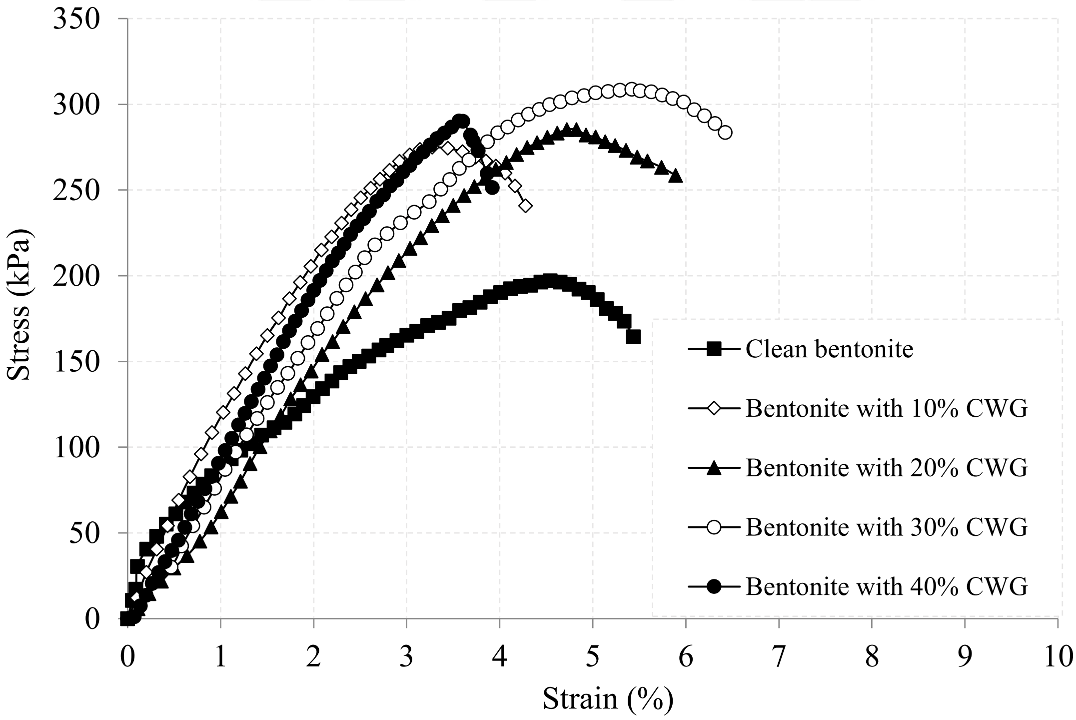

(b)

Figure 4.41. UC testing results of bentonite with different amounts of (a) FWG and (b) CWG.

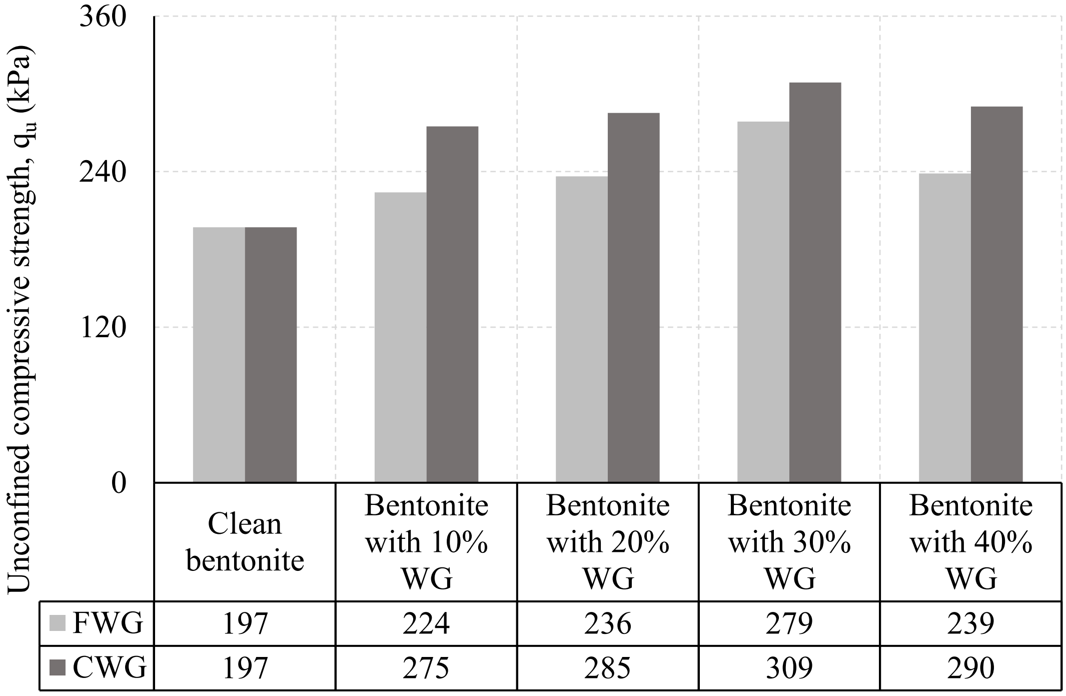

	Clean bentonite	Bentonite with 10% WG	Bentonite with 20% WG	Bentonite with 30% WG	Bentonite with 40% WG
FWG	197	224	236	279	239
CWG	197	275	285	309	290

Figure 4.42. The q_u values of bentonite with different amounts of FWG and CWG.

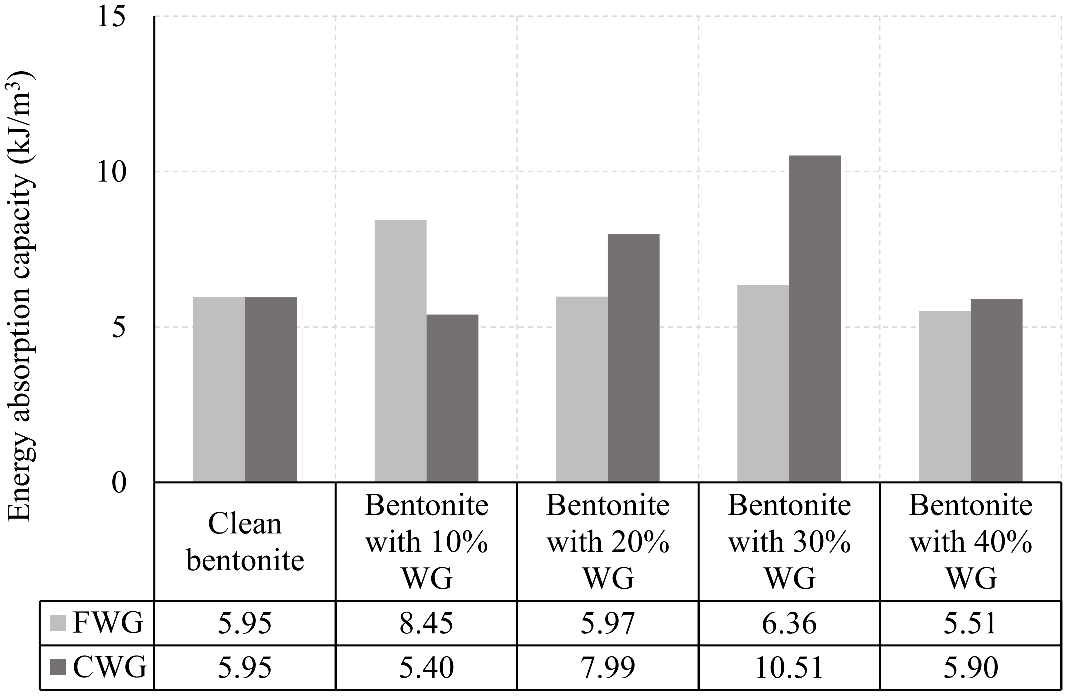

	Clean bentonite	Bentonite with 10% WG	Bentonite with 20% WG	Bentonite with 30% WG	Bentonite with 40% WG
FWG	5.95	8.45	5.97	6.36	5.51
CWG	5.95	5.40	7.99	10.51	5.90

Figure 4.43. The energy absorption capacity of bentonite with different amounts of FWG and CWG.

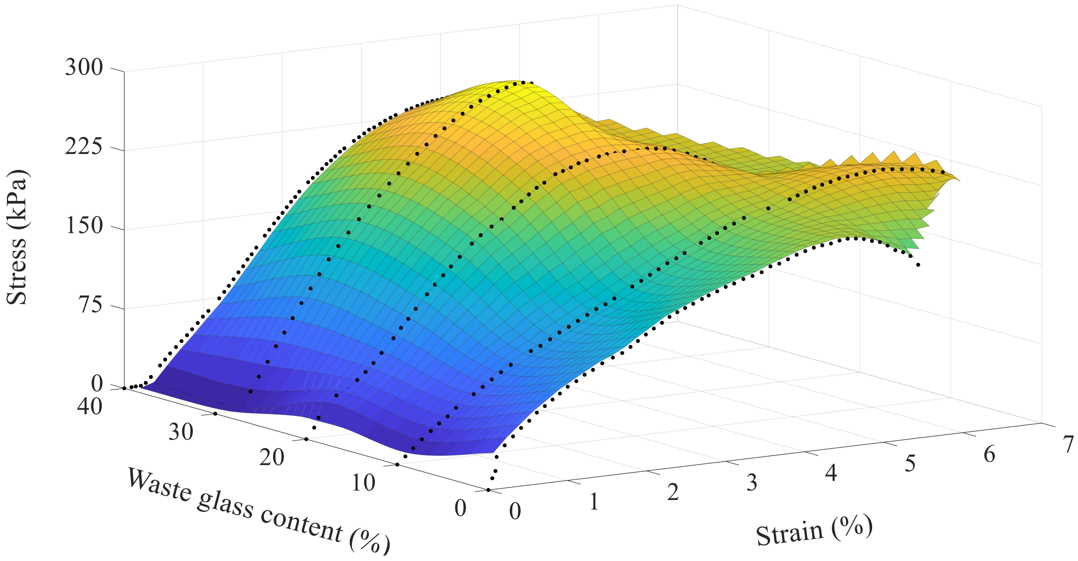

Figure 4.44. The 3D surface of the UC test result.

Figure 4.42 also shows that the q_u value of specimens containing the CWG is greater than that of specimens containing the FWG at a given WG concentration. In comparison, the q_u values of bentonite with FWG and CWG at a 20% content were found to be around 236 kPa and 285 kPa, respectively. According to Disfani et al. (2011), medium WG (0.01 mm-9.5 mm) has a greater friction angle value than fine WG (0.01 mm-4.75 mm). Their study also showed that clean CWG specimens have higher CBR, shear strength, and deviatoric stress than clean FWG specimens. Figure 4.42 shows the q_u values of the specimens in a bar chart format. This graph leads to the following conclusions: The q_u value has increased significantly with both the FWG and the CWG, and (ii) the q_u values of all specimens treated with the CWG are greater than those treated with the FWG. These findings are consistent with previous research on the effect of the amount and size of WG on the stress-strain response of the specimens (Disfani et al., 2011; Ibrahim et al., 2021). The energy absorption capacity of the tested specimens is shown in Figure 4.43. The area under the stress-strain curves of the specimens tested is used to calculate the energy absorption capacity values. The values ranged between 5.50 and 10.51 kJ/m^3. Bentonite with 30% CWG had the highest energy absorption capacity, with a 76% increase over clean clay. The impact of WG on energy absorption capacity is due to the angularity and stiffness properties of WG (Arabani et al., 2012). Figure 4.44 shows a three-dimensional surface of stress-strain behavior generated by a polynomial function. This also demonstrates that the previously mentioned transition behavior is visible and was observed during UCS tests at various strain levels.

4.2.9 Bender Element Testing Results

The deformation characteristics in engineering designs ranging from very small to large strain levels are important for various soil types, including clay. Simpson et al. (1979) propose a non-linear stiffness model for accurately estimating the deformation and stiffness characteristics observed in field measurements. This non-linear soil stiffness was supported by the laboratory tests of numerous researchers (Costa-Filho and Vaughan 1980; Jardine et al. 1985; Burland, 1989; Simpson, 1992; Mair, 1993; Lancellotta, 2008; Benz et al., 2009; Clayton, 2011; Cudny and Truty, 2020). The stiffness model shown in Figure 2.23 was widely accepted to quantify the behaviour of the soils. Many aspects of nonlinear soil stiffness have been thoroughly studied. They have been successfully used in geotechnical design after being incorporated into numerical models. Many of these nonlinear models and numerical assessments are extremely complex, requiring much testing and calculation. However, in some applications, complex models and analyses are unnecessary and using the small strain behaviour is sufficient (Atkinson, 2000, Clayton, 2011). One of the semi-analytical approaches to analyzing such problems is to simulate the characteristics in well-designed tests and incorporate curve-fitting equations for small strain behaviour into the classical elastoplastic soil model. This method simulates the characteristics of well-designed testing. This pragmatic scheme enables accurate field behavior prediction (Jardine et al., 1991; Jardine, 1992). The BE tests were performed on the mixtures to investigate stiffness properties at small strain levels. The importance of stiffness at small strain levels was given above and in the literature review part of the thesis. To obtain v_s, v_p, G_{max}, M_{max}, and υ, both S wave and P wave velocity tests were performed on the specimens.

The BE tests with various input frequencies from 30 kHz to 50 kHz were performed on the specimens. The testing results are presented in Tables 4.2 and 4.3. The v_s values of the soil mixtures tested at various frequency levels are presented in Figure 4.45. The bentonite-FWG specimens ranged from 127 m/s to 175 m/s, while the bentonite-CWG specimens ranged from 127 m/s to 194 m/s (see Figure 4.45a). Furthermore, the v_s

values of clean bentonite ranged from 127 to 130 m/s depending on the frequency employed during the test. The first important result is that the v_s of treated bentonite (bentonite with WG additions) was higher than clean bentonite. For example, with the addition of 40% CWG, the improvement rate of v_s values reached up to 52% over clean clay. The second notable feature of the results is that the v_s values of the bentonite increased with WG additions up to 25-30% and then decreased. For example, at 40 kHz, the v_s value of bentonite was 127 m/s, which increased to 194 m/s with the addition of 30% CWG and then decreased to 176 m/s with the addition of 40% CWG. This behavior was thought to support the previously discussed UCS testing results: the response of clean bentonite determined by BE improved until a certain level of WG content was reached, then decreased as more WG was added. To summarize the behavior, bentonite clay governs the response of the mixture until a specific mixing ratio is reached, at which point WG starts to dominate the mixture. Numerous studies describe such an approach in soil mixtures (Thevanayagam and Mohan 2000; Rahman et al. 2008; Watabe et al. 2017; Monkul et al. 2020). Similar trends were obtained by several researchers who presented the v_s values of various clay types with several admixture materials including fly ash, and zeolite. The optimal admixture contents in these studies range from 20% to 60%. Such a variation could depend on the type of soils employed by different studies (Vallejo and Lobo-Guerrero 2005; Kang and Bate 2016; Kordnaeij et al. 2019).

Regarding the effect of grain size of WG in bentonite, the v_s values of the specimen with CWG were found to be greater than the v_s values of the specimen with FWG. At 20 kHz, the v_s value of bentonite with CWG and FWG were 192 and 180 m/s, respectively. The v_s values of bentonite with CWG were found to be 8%-15% higher than those of FWG. This pattern could be explained by the fact that increasing the particle size of WG leads to a drop in contact counts. When the contact number decreases it is known that travel time decreases and therefore v_s values increase according to equation 5 (Bui, 2009).

Table 4.2. Summary of UCS and BE testing results for S wave test.

Specimens	WG contents (%)	γ_{dmax} (kN/m^3)	w_{opt} (%)	e_0	q_u (kPa)	v_s (m/s)			G_{max} (MPa)		
						30 kHz	40 kHz	50 kHz	30 kHz	40 kHz	50 kHz
Clean Bentonite	0	13.6	21.5	0.931	197	130	127	128	23	22	23
Bentonite with FWG	10	13.9	20.4	0.901	224	178	173	176	45	42	44
	20	14.0	19.7	0.896	236	180	175	178	46	43	45
	30	14.2	18.6	0.884	278	178	173	176	46	43	45
	40	14.5	17.4	0.857	238	168	165	164	41	40	40
Bentonite with CWG	10	14.1	20.2	0.871	274	171	169	173	42	41	43
	20	14.4	19.1	0.840	285	192	192	192	54	54	54
	30	15.0	17.9	0.788	308	194	194	194	57	57	57
	40	15.1	16.5	0.776	290	182	176	180	51	48	50

Table 4.3. Summary of BE testing results for P wave test

Specimens	WG contents (%)	v_p (m/s)			M_{max} (MPa)		
		30 kHz	40 kHz	50 kHz	30 kHz	40 kHz	50 kHz
Clean Bentonite	0	317	317	297	138	138	122
Bentonite with FWG	10	356	380	365	179	204	188
	20	407	380	396	237	206	224
	30	411	427	400	245	263	231
	40	356	345	365	187	176	197
Bentonite with CWG	10	364	353	359	190	179	185
	20	411	427	436	249	268	280
	30	416	388	404	263	229	248
	40	364	388	373	204	232	214

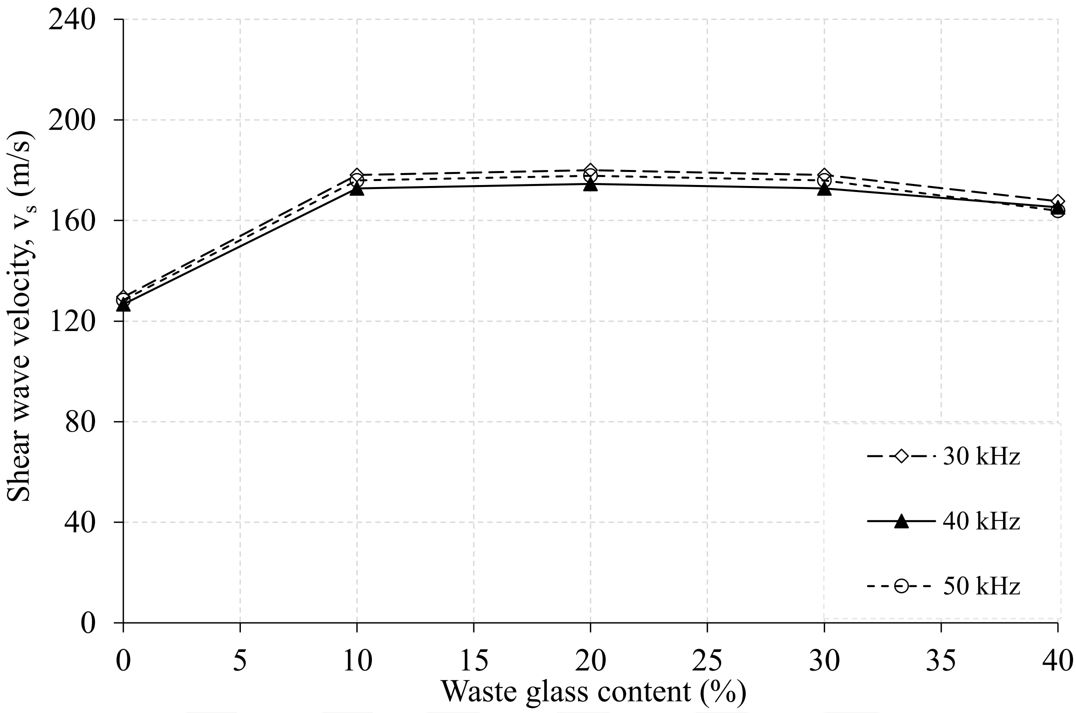

(a)

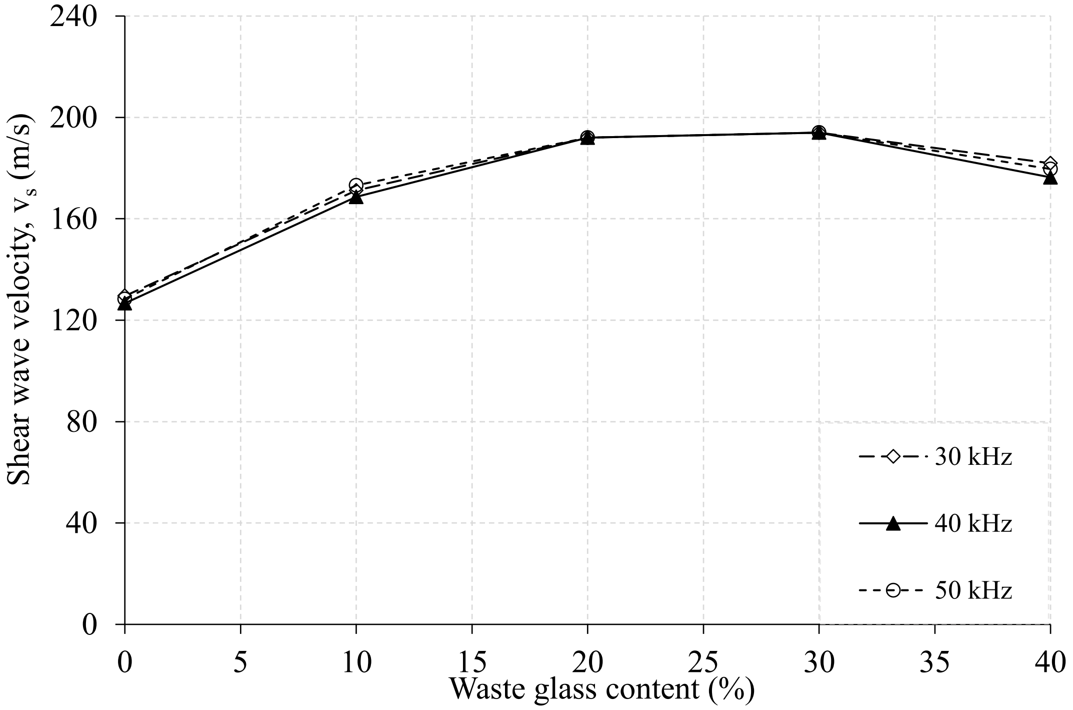

(b)

Figure 4.45. The v_s values of bentonite with different amounts of (a) FWG and (b) CWG for various frequencies.

The v_p values of all specimens ranged from 300 m/s to 440 m/s as indicated in Figure 4.46. The v_p value of bentonite varied around 310 m/s in different frequency ranges, while maximum v_p values were observed with 30% WG additions which ranged between 400 and 427 m/s. Similar to the v_s values, the v_p value of bentonite with 30% is higher than that of bentonite with 40%.

Figure 4.47 shows the G_{max} values of the specimens, which ranged from 22 to 57 MPa. At 40 kHz, the G_{max} value for clean bentonite was 22 MPa, while this value increased to around 57 MPa and 51 MPa for bentonite specimens containing 30% and 40% CWG, respectively. As previously mentioned, these trends could be related to the reaction between WG and the water and the transitional WG content (Bate et al., 2014; Kang and Bate 2016). Furthermore, a peak value of around 30% could be related to a combination of different micromechanics of bentonite and WG. Although both forces are available for bentonite and WG, the main factors governing the response of the stiffness mechanism of bentonite clay are non-contact forces, whereas contact forces govern the behaviour of WG (Mitchell and Soga, 2005). This means, repulsive and attractive forces play the main role in governing the response of bentonite clay whereas grain contact forces, as previously mentioned, control the behavior of these soils in WG (i.e., cohesionless soil) (Santamarina, 2003). When WG content was around 30%, the stiffness of the mixture reached the maximum value due to the transition mode between both soils. The behaviour of WG and bentonite was found to be similar to that of sand-clay mixtures. Such interpretation of the interplay between bentonite and sand was investigated by Sun et al. (2015). The researcher discussed that below critical sand content, the bentonite takes the external load while once the critical sand content is exceeded the sand skeleton bears the external load.

Regarding the effect of the grain size of WG on the testing results, the G_{max} value of the specimens with CWG in the same proportions was greater than that of the specimens with FWG. For example, at a constant input frequency of 50 kHz, the G_{max} value of a specimen containing 20% FWG was 45 MPa, whereas the bentonite with 20% CWG exhibited a G_{max} value of 54 MPa.

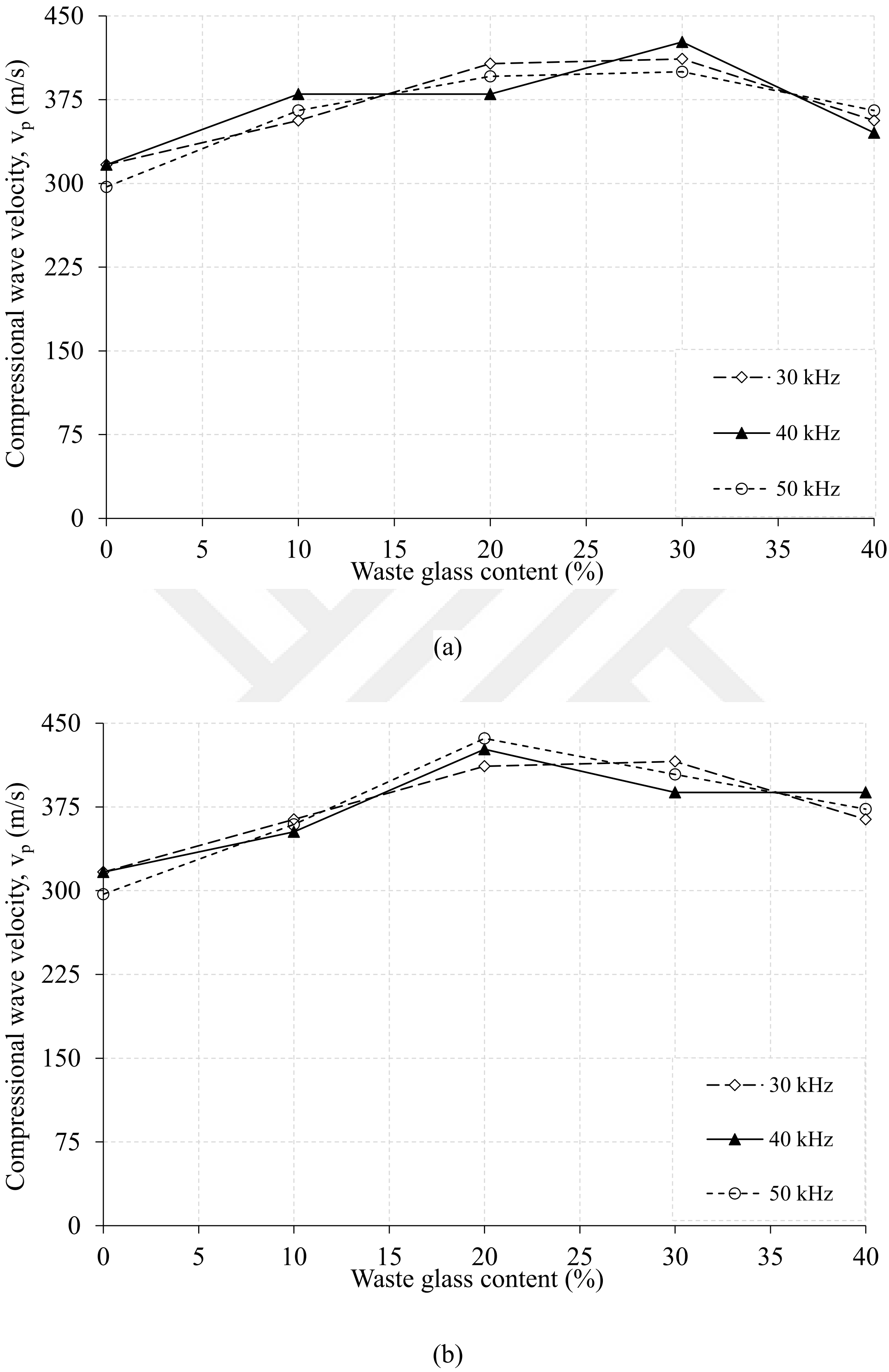

Figure 4.46. The v_p values of bentonite with different amounts of (a) FWG and (b) CWG for various frequencies.

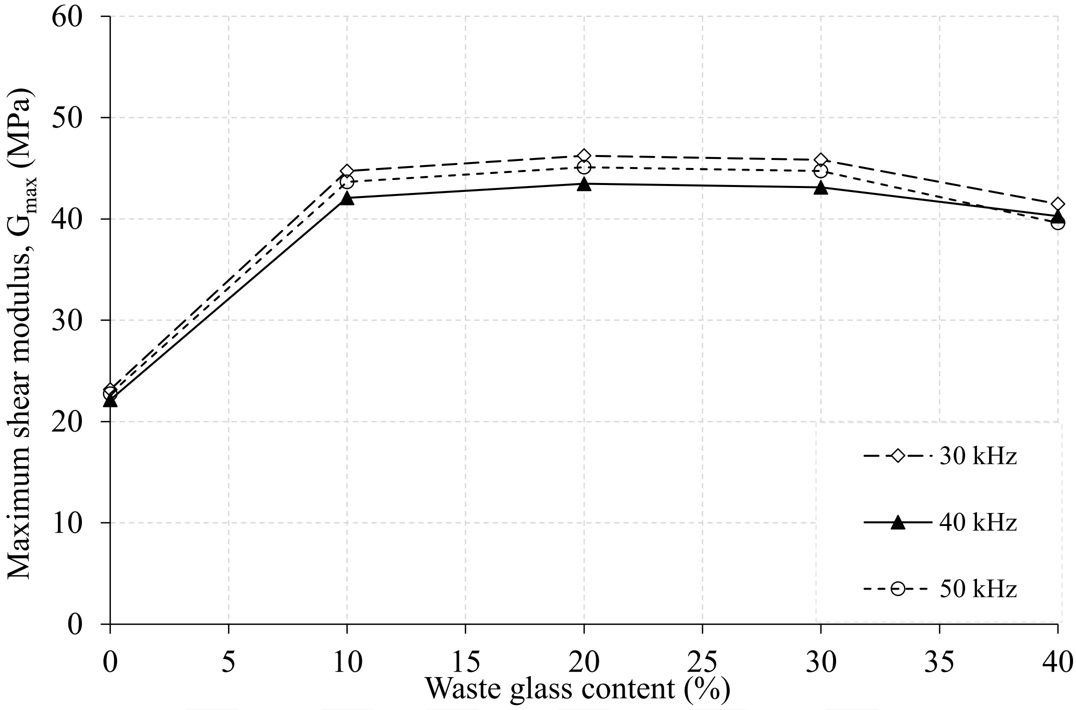

(a)

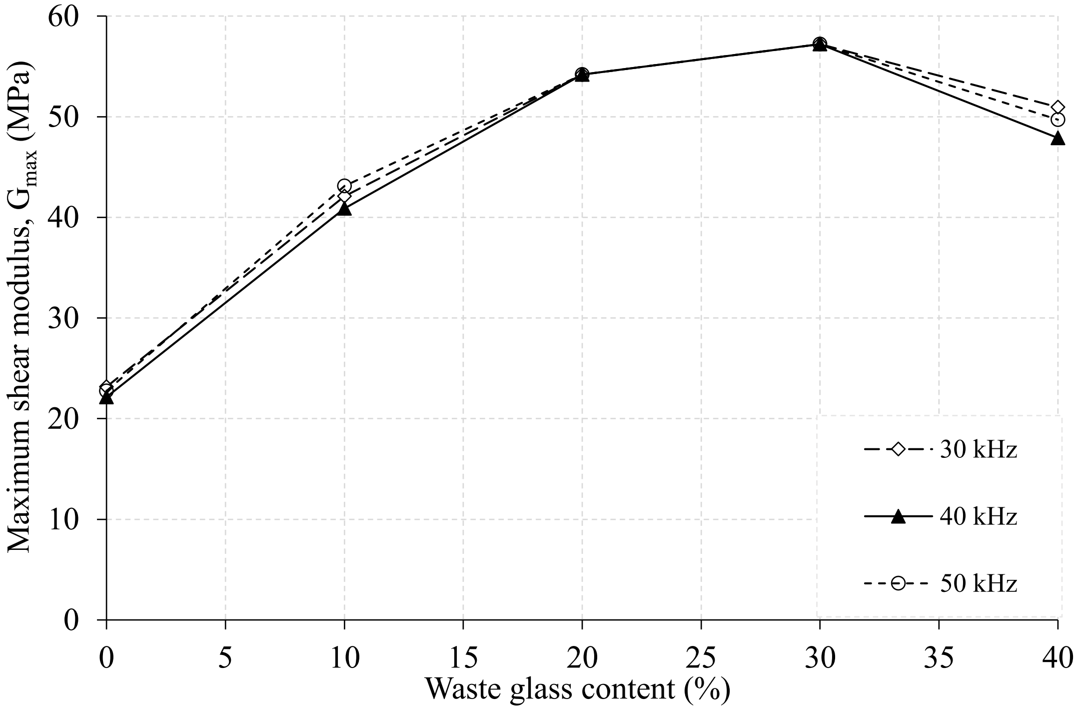

(b)

Figure 4.47. The G_{max} values of bentonite with different amounts of (a) FWG and (b) CWG for various frequencies.

The M_{max} values for all specimens are presented in Figure 4.48. The values ranged from 128 to 280 MPa. The effect of WG content on the M_{max} values was found to be consistent with the trend obtained in v_s and G_{max} values. The M_{max} of clean bentonite increased with WG additions, peaked at 30% WG additions, and then decreased at 40%. Regarding the particle size effect, the M_{max} of CWG-containing specimens is higher than that of FWG-containing specimens at a constant mixture ratio. M_{max} values for bentonite-30% FWG were found to be around 260 MPa and 280 MPa for bentonite-20% CWG. The small strain stiffness response of geomaterials is known to be dependent on interparticle contact stiffness (Clayton, 2011; Gu and Yang, 2013). According to Hertz's contact stiffness theory, such a trend could be explained by the effect of the size of the soil on the contact force. According to the theory, increasing the size of the grains leads to an increase in the contact area and contact force (Johnson and Johnson, 1987). This resulted in an increase in friction strength and thus contact stiffness (Bui, 2009). According to several DEM and experimental studies, coarse grains have a greater stiffness than fine grains because they have fewer contact points and, as a result, a higher contact force when subjected to a given load (Liu et al., 2020).

BE test is also used to obtain the Poisson's ratio (υ) values. The υ value is the ratio of the deformation of a material in the perpendicular direction of loading to the deformation in the specific direction of loading. It is commonly used to characterize the deformation property of a material. The υ value in isotropic cases is important to relate the below parameters. The relation between such parameters using the υ value is presented as follows (Clayton, 2011).

$$E_u = 2G_0(1+\upsilon_u)$$
$$\mathrm{K}^u = \frac{E^u}{3(1-2\upsilon^u)} \tag{4.1}$$

Where E^u, υ^u and K^u are undrained Young's modulus, undrained Poisson's ratio, and undrained Bulk modulus, respectively. Furthermore, the υ value is required as an input in a range of analytical and numerical models for saturated and unsaturated soils (Lu and Likos, 2004; Oh and Vanapalli, 2018). For an isotropic, elastic and homogenous material, the υ value of compacted soil specimen was obtained using equation 4.4 which is widely used to estimate the υ values of specimens at small strain levels (Ohsaki and Iwasaki 1973; Lee and Santamarina 2005; Arroyo et al. 2006; Kumar and

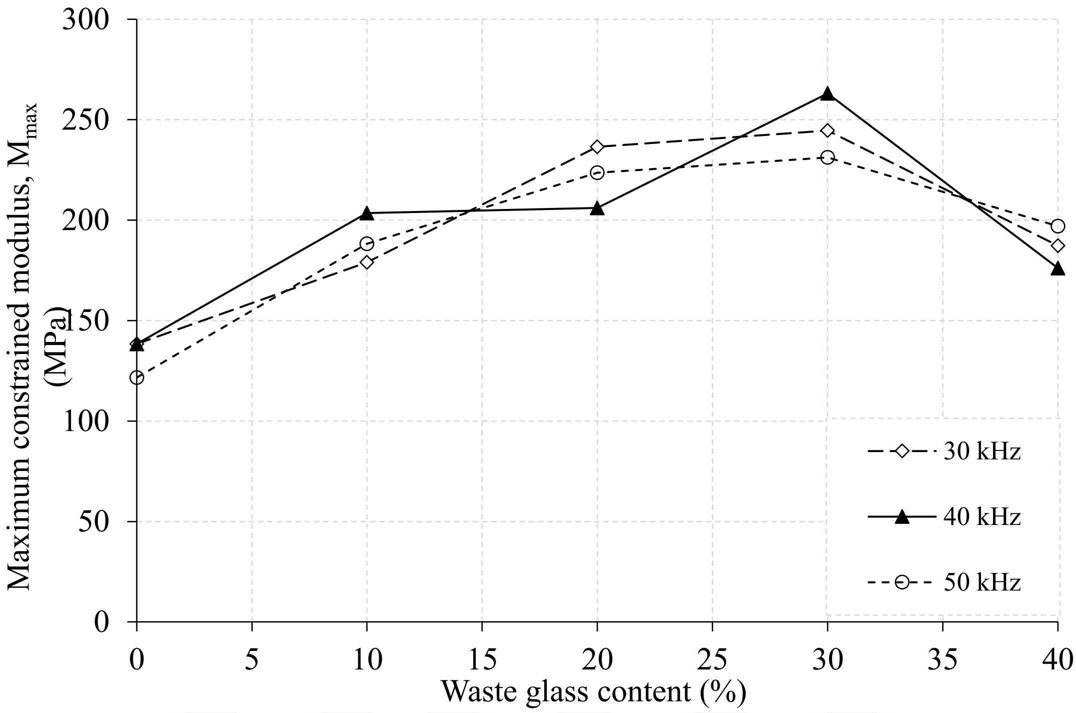

(a)

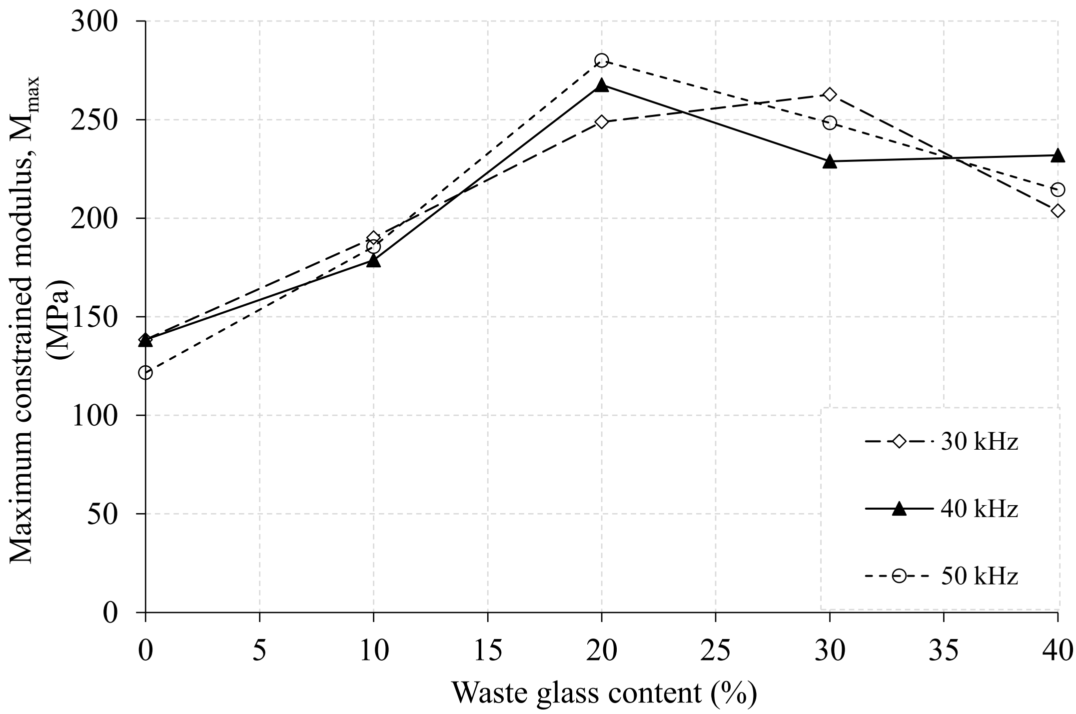

(b)

Figure 4.48. The M_{max} values of bentonite with different amounts of (a) FWG and (b) CWG for various frequencies.

Madhusudhan 2010; Ruan et al. 2021; He et al. 2021). This equation is used by numerous researchers to obtain υ value of compacted specimens (Sawangsuriya et al., 2008; Amaral et al., 2011; Oh and Vanapalli, 2011; Patel et al., 2018; Thota et al., 2021; Silva et al., 2022)

$$\upsilon = \frac{(v_p / v_s)^2 - 2}{2[(v_p / v_s)^2 - 1]} \tag{4.2}$$

Figure 4.49 shows the variation of the υ values at different frequencies as a function of the WG ratio. Table 4.4 also presents the υ values of the specimens. The values range between 0.35 and 0.4. The υ value of bentonite was found to be in the range of 0.39-0.4, depending on the input frequency. The lowest υ value was obtained at bentonite with 30% CWG, which ranged between 0.342 and 0.35. Figure 4.50 shows the range of v_p/v_s and the υ values of the specimens. The figure shows that the v_p/v_s ratios of the specimens ranged between 2.00 and 2.5, while the υ values ranged between 0.35 and 0.40. The v_p/v_s range and υ values presented in this study are comparable to those found in many studies for clean clay/clay-dominated soil mixtures (Gasparre et al., 2007; Uyanik, 2019; Balagosa et al., 2020).

Table 4.4. The υ values of the specimens obtained from BE testing

Specimens	WG contents (%)	υ		
		30 kHz	40 kHz	50 kHz
Clean Bentonite	0	0.400	0.405	0.385
Bentonite with FWG	10	0.333	0.370	0.349
	20	0.379	0.366	0.374
	30	0.385	0.402	0.380
	40	0.358	0.352	0.374
Bentonite with CWG	10	0.358	0.352	0.349
	20	0.361	0.373	0.380
	30	0.361	0.333	0.350
	40	0.333	0.370	0.349

4.2.10 The Relationship Between q_u and G_{max}

The relationships between the G_{max} (kPa) and q_u (kPa) values for the soil specimens tested in this study are shown in Figure 4.51. The results showed that increasing the q_u value increased the G_{max} values, but the rate of increase varied linearly. A linear equation was applied to the values, and two curves covered 90% of the values. Furthermore, Figure 4.51b shows a 3D surface of the G_{max} as a function of WG content and qu. The G_{max} values increase with WG content up to a range of roughly 20-30% and then decrease. G_{max} values of treated bentonite were found to be greater than that of untreated bentonite. The linear increasing trend of G_{max} values with the q_u shows that both variables show a similar response to the microstructure of bentonite-WG mixtures. Such a trend between two variables was obtained by several researchers in the literature (Consoli et al., 2020; Yao et al., 2020; Consoli et al., 2021).

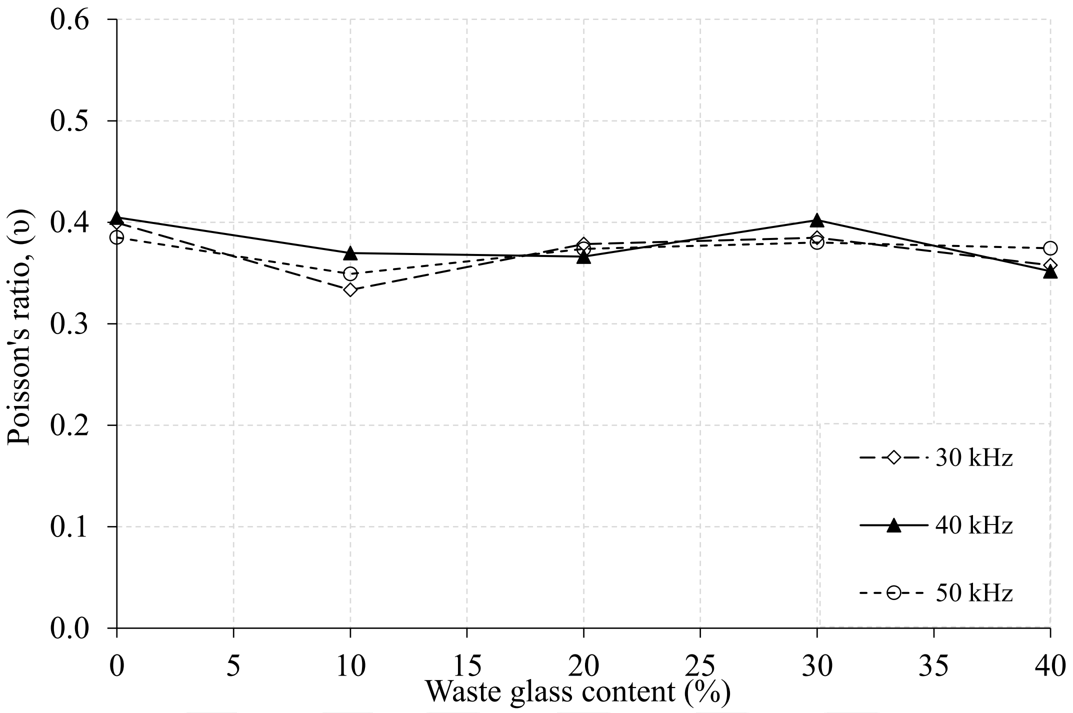

(a)

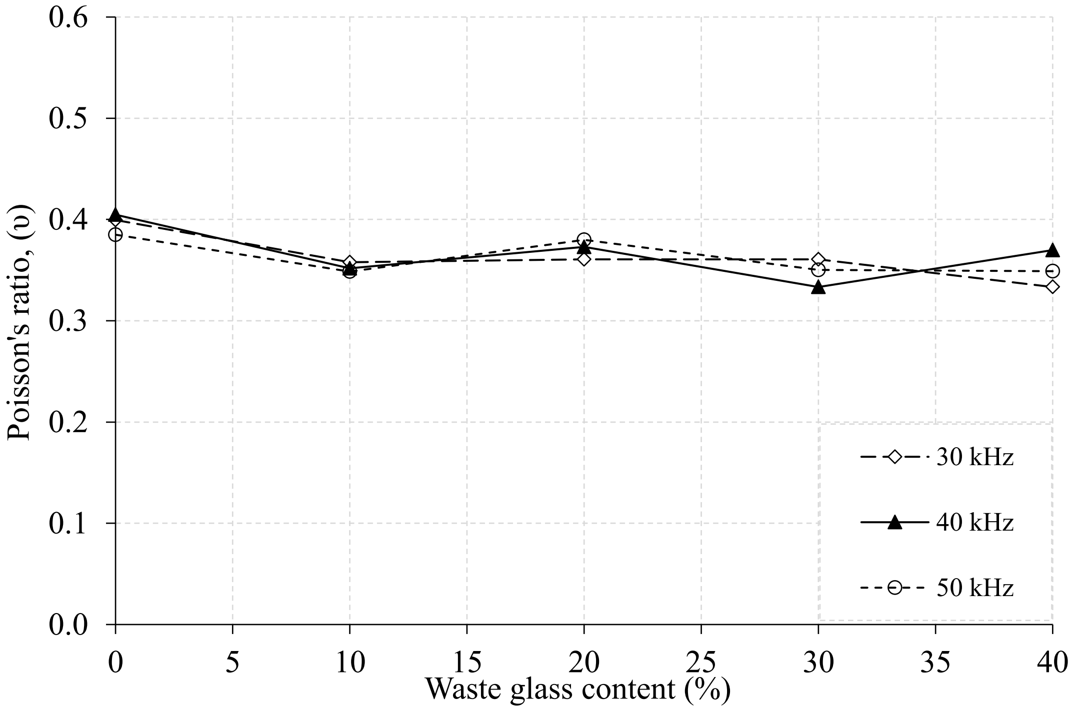

(b)

Figure 4.49. The υ values of bentonite with different amounts of (a) FWG and (b) CWG for various frequencies.

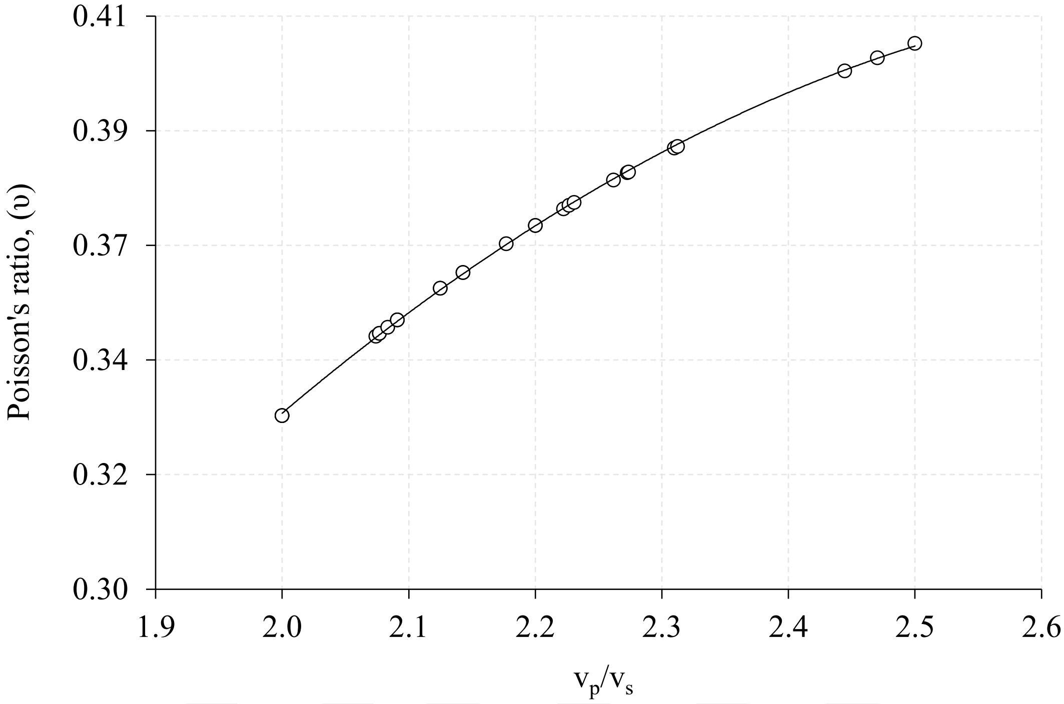

Figure 4.50. The υ values of the tested soil specimens as a function of v_p/v_s.

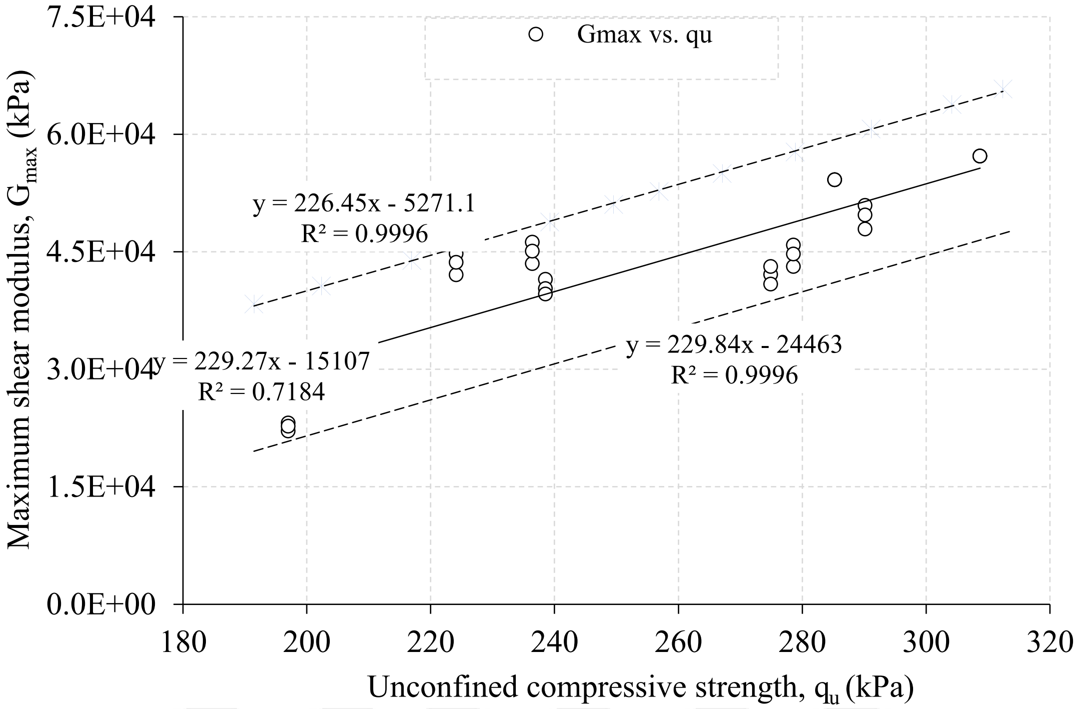

(a)

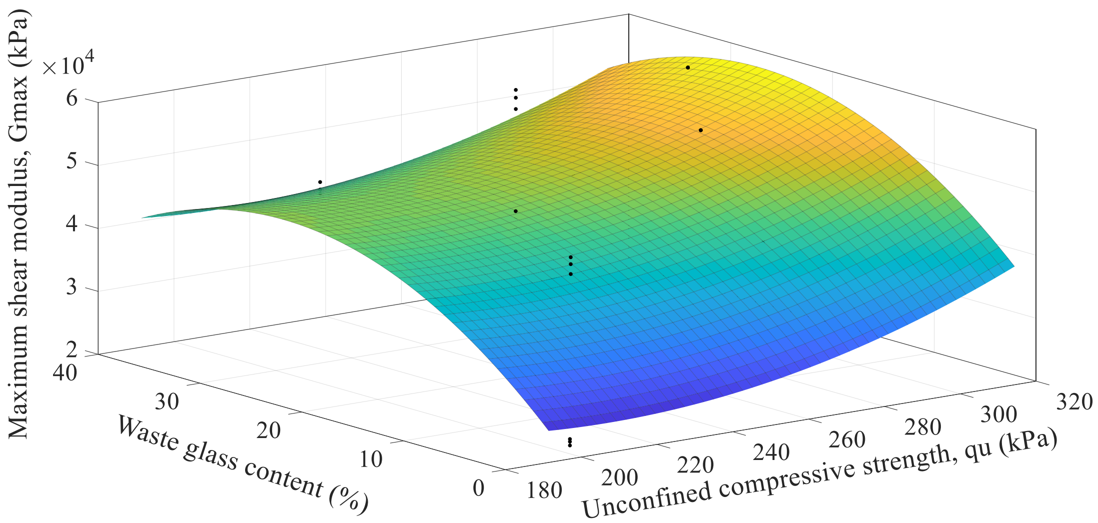

(b)

Figure 4.51. Variation of G_{max} as a function of (a) q_u (b) WG content and q_u.

4.3 Testing Results of Sand-Silt Mixtures

4.3.1 Effect of Effective Consolidation Stress

Figure 4.52 shows the e_{min} and e_{max} values of the mixtures. The results show that both indices decreased until 20% ML addition and then increased. The e_g values presented in 4.53 showed that e_g values increased with the ML additions. The strain results presented as average local strain (ε) calculated as the average strain readings from two LVDTs. The stress values presented as deviatoric stress (q) calculated as $q=\sigma'_1-\sigma'_3$ where the σ'_1 and σ'_3 are the effective major principal stress and effective minor principal stress. The strain from LVDTs is calculated by dividing the displacement readings by the center gauge length between the upper mouth and lower mount of the LVDT. The effective stress path of the tested specimens was presented using the Cambridge p'-q' formula, where p' is the mean effective stress determined as $(2\sigma'_1+\sigma'_3)/3$. The stiffness values at each point on the stress-strain curve are shown as secant modulus ($E_u=q/\varepsilon$).

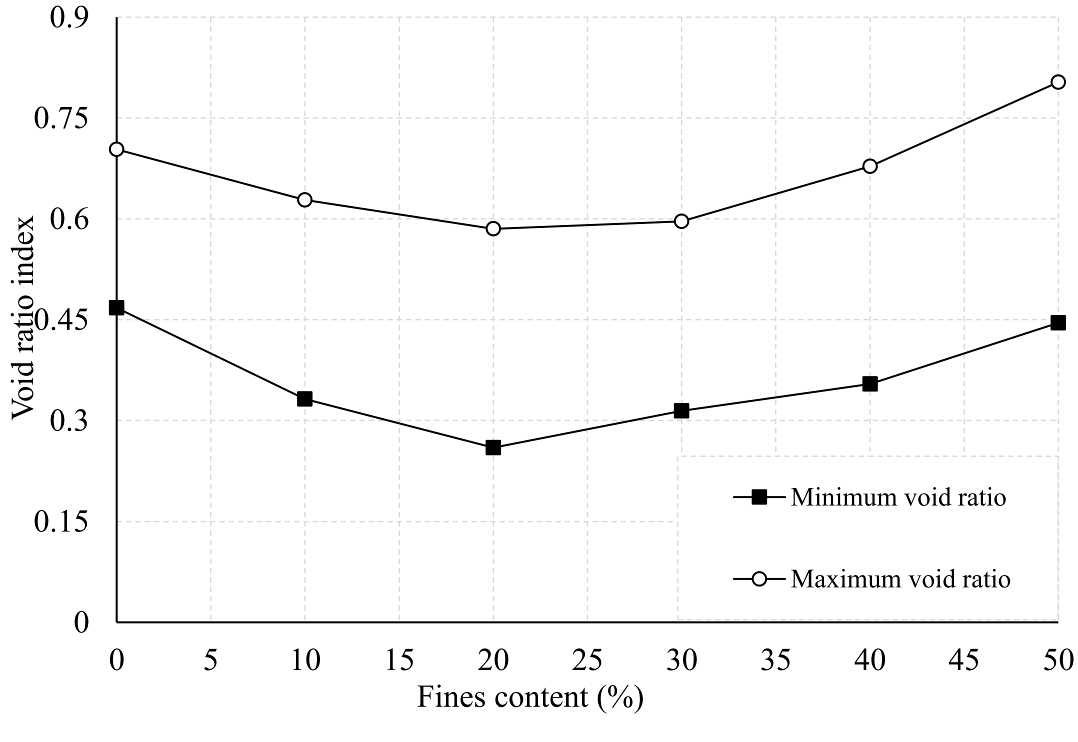

Figure 4.52. Variation of e_{max}, e_{min}, and the e values of the specimens

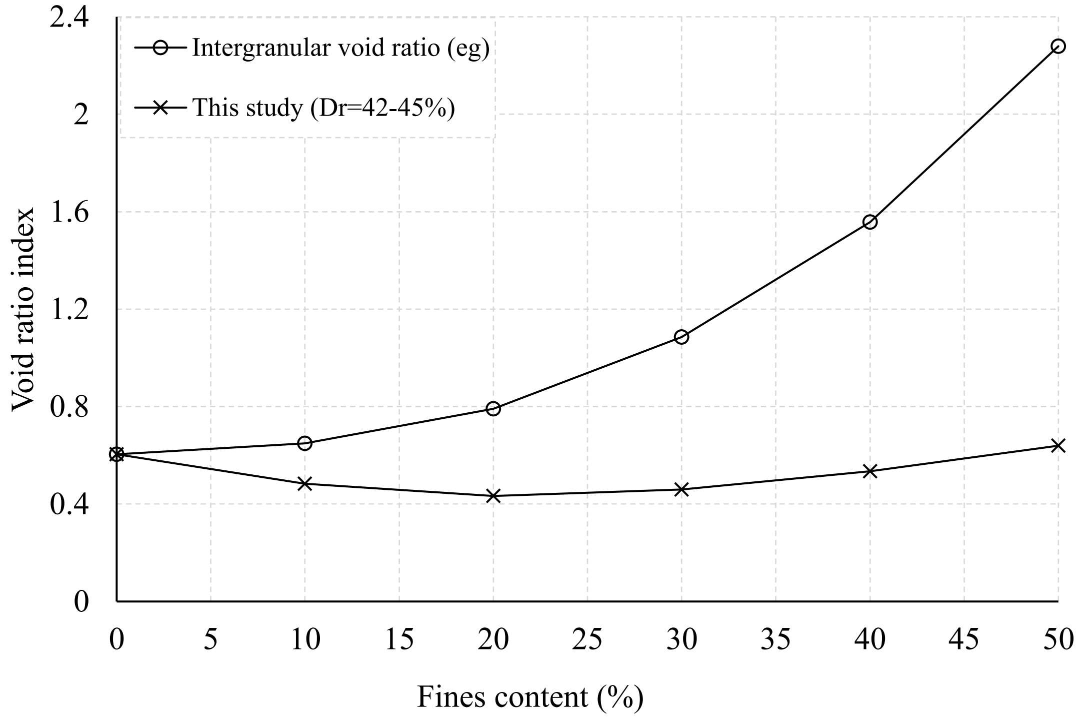

Figure 4.53. Variation of e and e_g values of the specimens

Figure 4.54 provides testing results for clean NS at 50 kPa effective confining stress (ECS). Figure 4.54a presents the strain readings from the LDS, the pair of LVDTs and the average strain of LVDTs throughout testing. The findings showed that at low strain levels, the readings from LVDTs are smaller than that of LDS. Figure 4.54b extends such a comparison to the stress-strain response up to 35 kPa deviatoric stress. A clear difference between the slope of the curve values obtained from LDS and LVDTs was realized in this range. According to the literature, such a difference is caused by the stiffness of the apparatus (e.g., the compression of the load cell, porous stone, filter papers, and device ends) (Clayton and Katrush, 1986). Some findings in the literature support these differences (Clayton and Khatrush, 1986; Burland, 1989; Cabalar and Clayton, 2010; Kumar et al., 2021). It is worth noting that because of such a difference in the small strain levels, the stiffness values obtained in triaxial tests were found to be inaccurate in the 1980s, and local strain transducers were developed to accurately measure the stiffness over small strain ranges in triaxial testing.

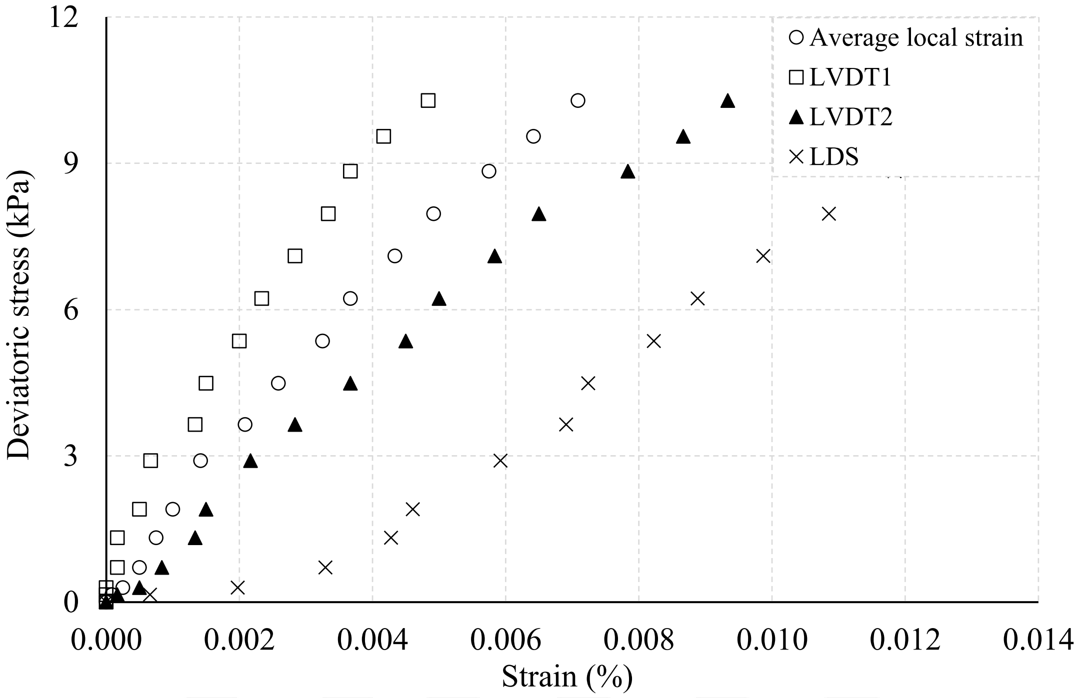

Average local strain
LVDT1
LVDT2
LDS
Deviatoric stress (kPa)
Strain (%)
0
3
6
9
12
0.000
0.002
0.004
0.006
0.008
0.010
0.012
0.014

(a)

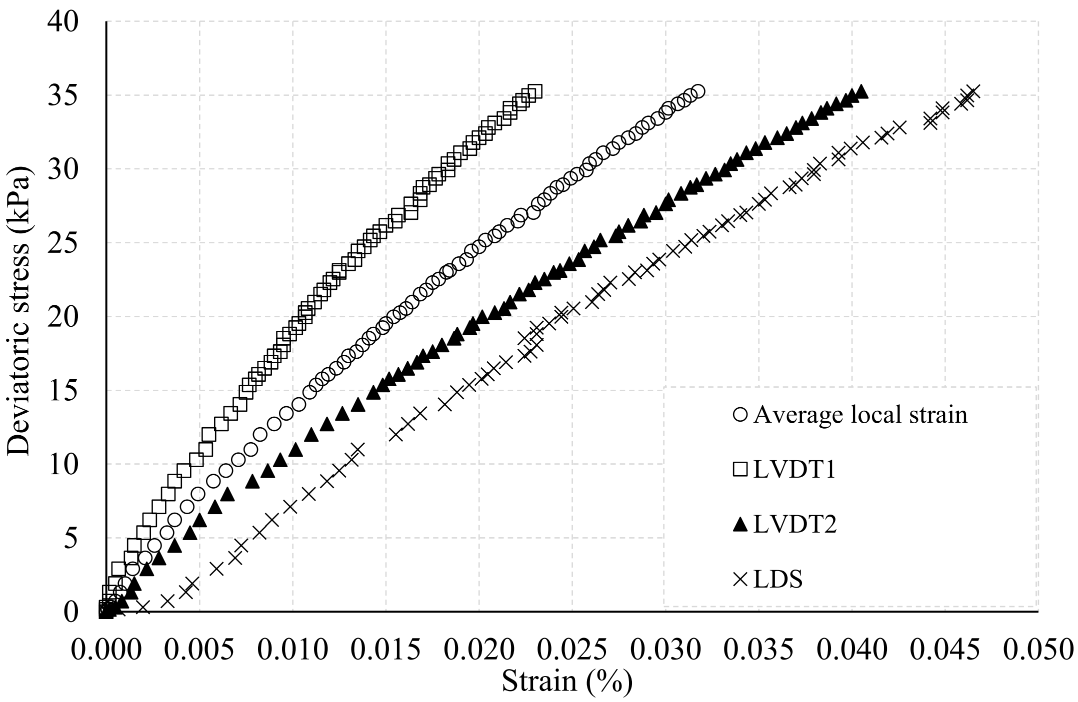

Average local strain
LVDT1
LVDT2
LDS
Deviatoric stress (kPa)
Strain (%)
0
5
10
15
20
25
30
35
40
0.000
0.005
0.010
0.015
0.020
0.025
0.030
0.035
0.040
0.045
0.050

(b)

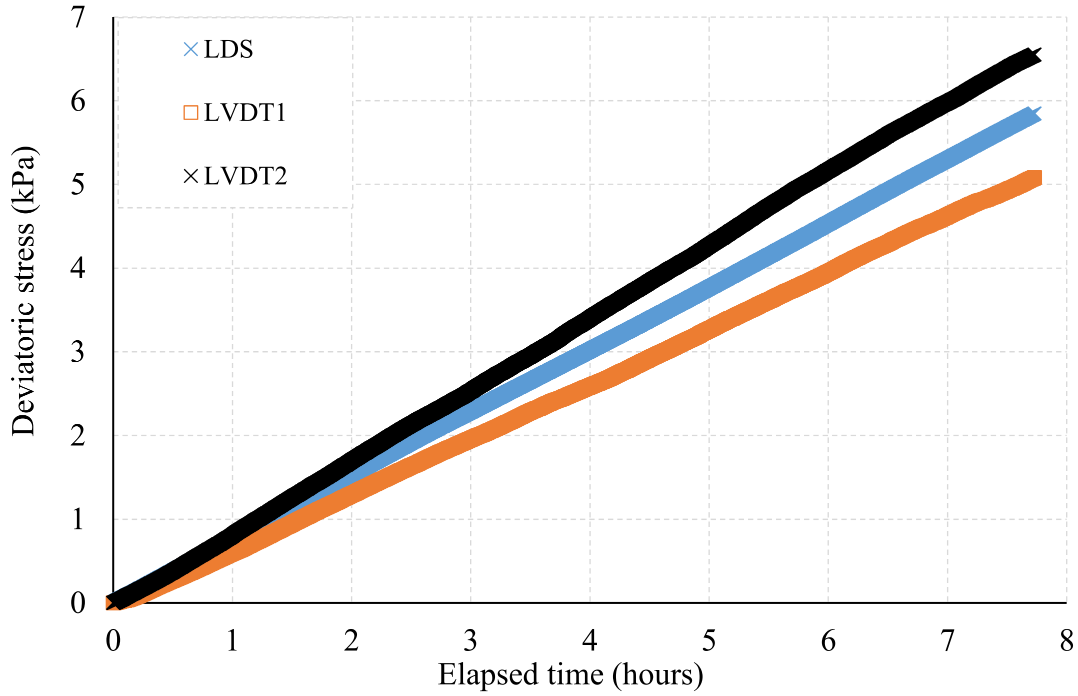

(c)

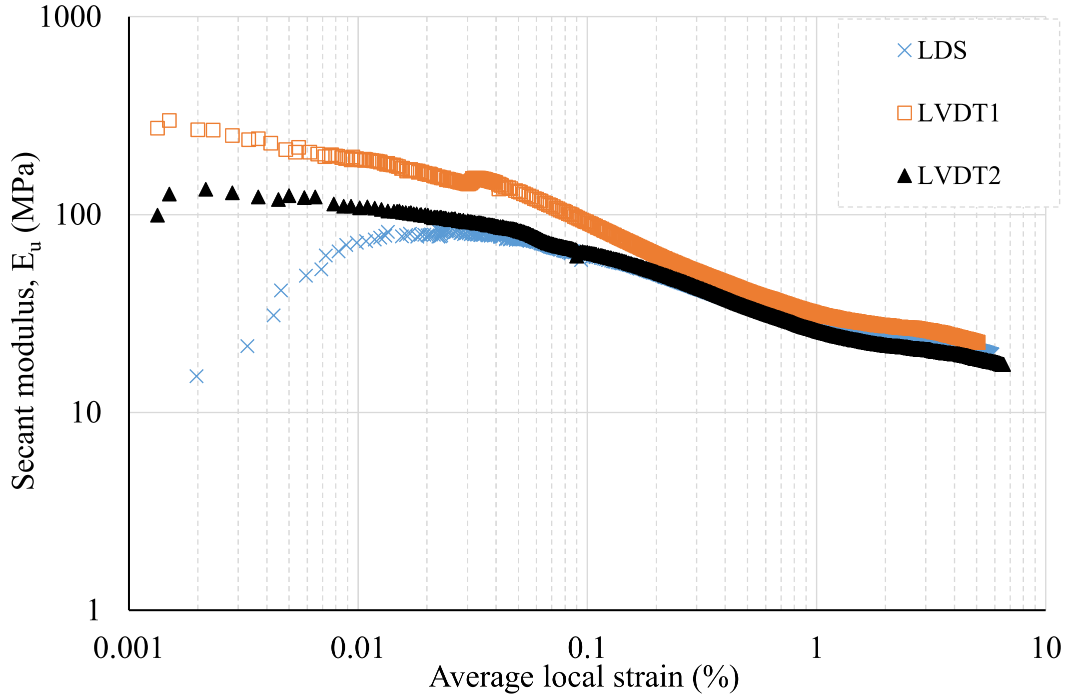

(d)

Figure 4.54. Response of the clean NS at 50 kPa ECS (a) and (b) strains from LDS and LVDTs at the small strain levels (c) stress-strain response throughout test (d) secant modulus of the specimen based on LDS and LVDTs

Figure 4.54c shows strain readings from LVDTs and the LDS. The strain reading from LDS was found to be around the average of that obtained from two LVDTs. Figure 4.54d shows the secant modulus of the specimen calculated using the strain values both from LDS and LVDTs. The figure clearly shows the difference in E_u values obtained from LVDTs and the LDS. Such a difference was also shown by Kumar et al. (2021) who presented the secant modulus of sandy soils calculated LVDTS and LDS. The strain values in the testing results are therefore calculated as the average reading from the LVDTs. Taking the average of the two LVDTs will eliminate any tilting or bedding error that may have occurred in the specimen.

Figure 4.55-4.59 presents the effect of ECS on the testing results of each mixture. Figure 4.55 presents the testing results of clean NS at 50, 100, and 150 kPa ECS. Figure 4.55a indicates the deviatoric stress trend with the average local strain. The results show a non-flow response of stress trend; the deviatoric stress values continuously increased with increasing strain. The testing results also showed that deviatoric stress values increased with increasing average local strain levels. Such a response is explained by the increasing contact stiffness of sand grains with increasing ECS. The excess pore water pressure during the shear is presented in Figure 4.55b. At low strain levels, the results show a slight contractive response (increase in excess pore water pressure during the test), followed by a continuous dilatancy (decrease in excess pore water pressure during the test). The contractiveness at the beginning of the shear increased with the increasing ECS. The beginning of a shear state in which some grains create little contractiveness by sliding or rotating with one another could be related to initial contractiveness. The maximum increase in the excess pore water pressures for NS at 50, 100, and 150 kPa were 5 kPa, 16 kPa, and 32 kPa, respectively. Once a peak pore water pressure was observed, the excess pore water pressure values started to decrease. Once the all grains exhibited little contractiveness the sand grains exhibited a dilative tendency. This is due to better contact between the sand grains. The stress path testing results at the p’ and q’ values are presented in Figure 4.55c. The mean effective stress increased and eventually reached the same critical state line for all tests. Secant modulus (E_u) is presented in Figure 4.55d. The results revealed a maximum E_u value for small strain levels, which gradually decreased. Such a stiffness response is consistent with the non-linear stiffness response of geomaterials proposed by Simpson et al. (1979) which has been confirmed by numerous studies (Atkinson, 2000; Clayton and Heymann, 2001; Clayton, 2011; Cabalar and Karabash, 2019; Kumar et al., 2021; Bozyigit and Altun, 2023). Regarding the factors controlling the E_u values, the values were primarily influenced by the ECS values of the test. Increasing the ECS of a given mixture increased the E_u values in all strain levels. At 0.01% of the local average strain, the E_u values for clean sand at 50, 100, and 150 kPa were around 103, 200, and 358 MPa. Such a response could be attributed to increasing isotropic ECS to cause better stiffness of the soil grains.

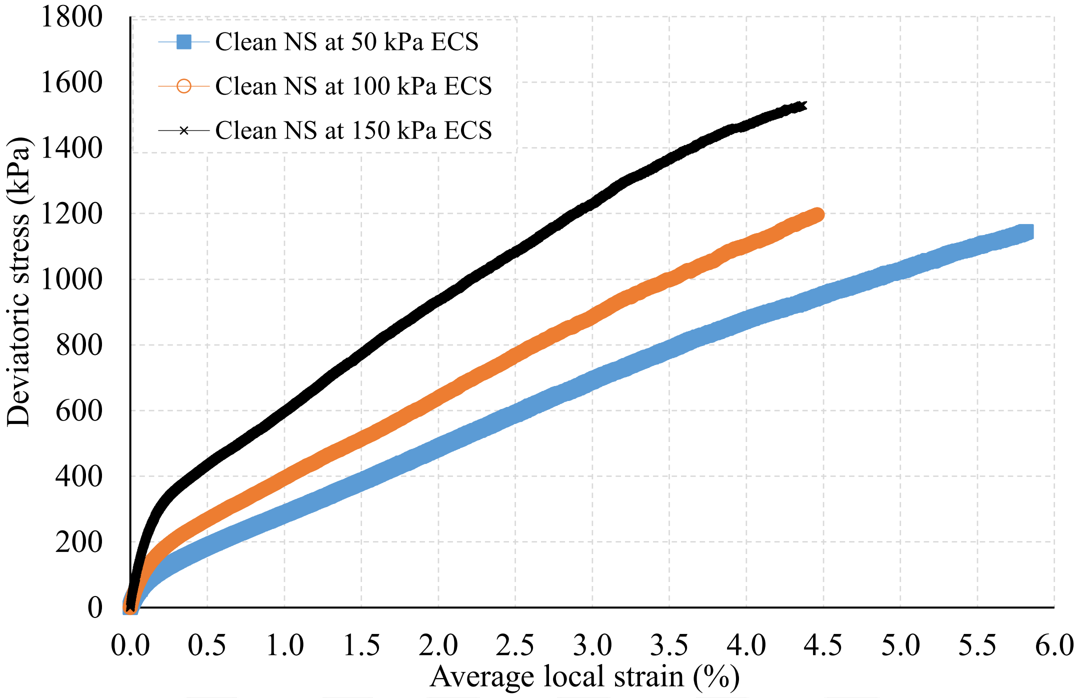

1800
1600
1400
1200
1000
800
600
400
200
0
Deviatoric stress (kPa)
Clean NS at 50 kPa ECS
Clean NS at 100 kPa ECS
Clean NS at 150 kPa ECS
0.0 0.5 1.0 1.5 2.0 2.5 3.0 3.5 4.0 4.5 5.0 5.5 6.0
Average local strain (%)

(a)

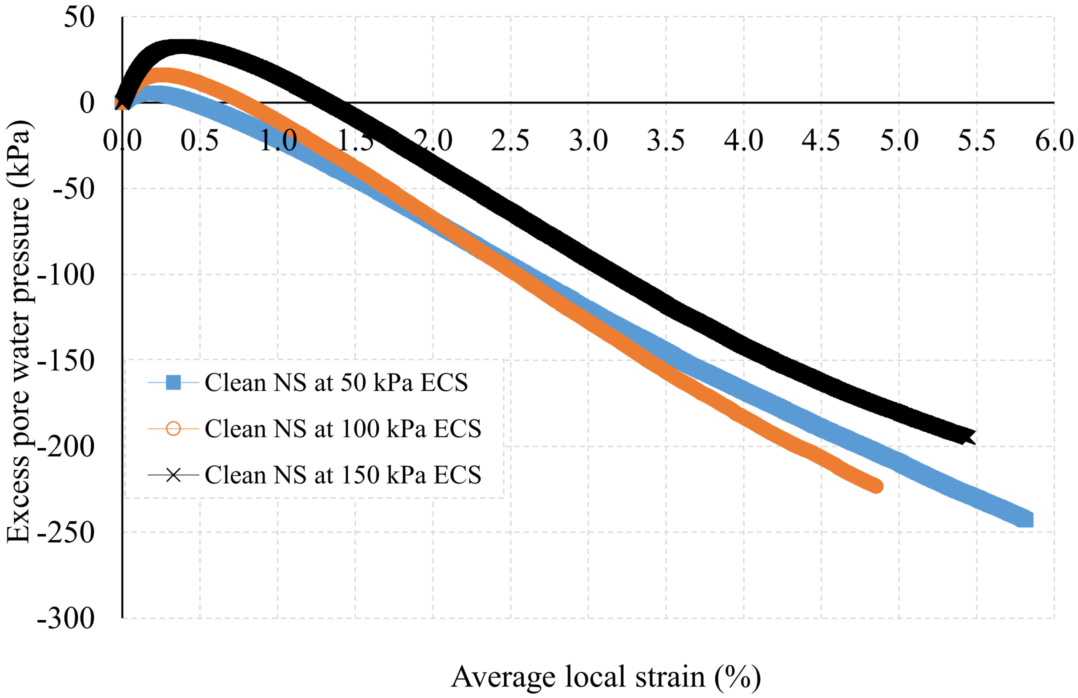

50
0
-50
-100
-150
-200
-250
-300
Excess pore water pressure (kPa)
0.0 0.5 1.0 1.5 2.0 2.5 3.0 3.5 4.0 4.5 5.0 5.5 6.0
Clean NS at 50 kPa ECS
Clean NS at 100 kPa ECS
Clean NS at 150 kPa ECS
Average local strain (%)

(b)

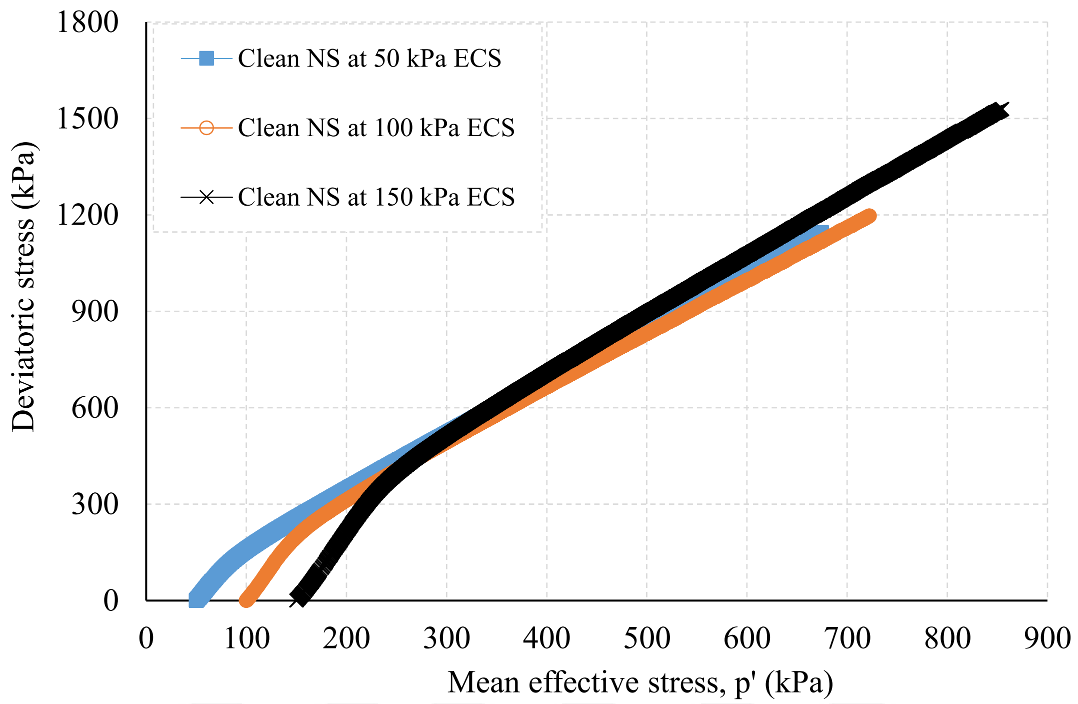

(c)

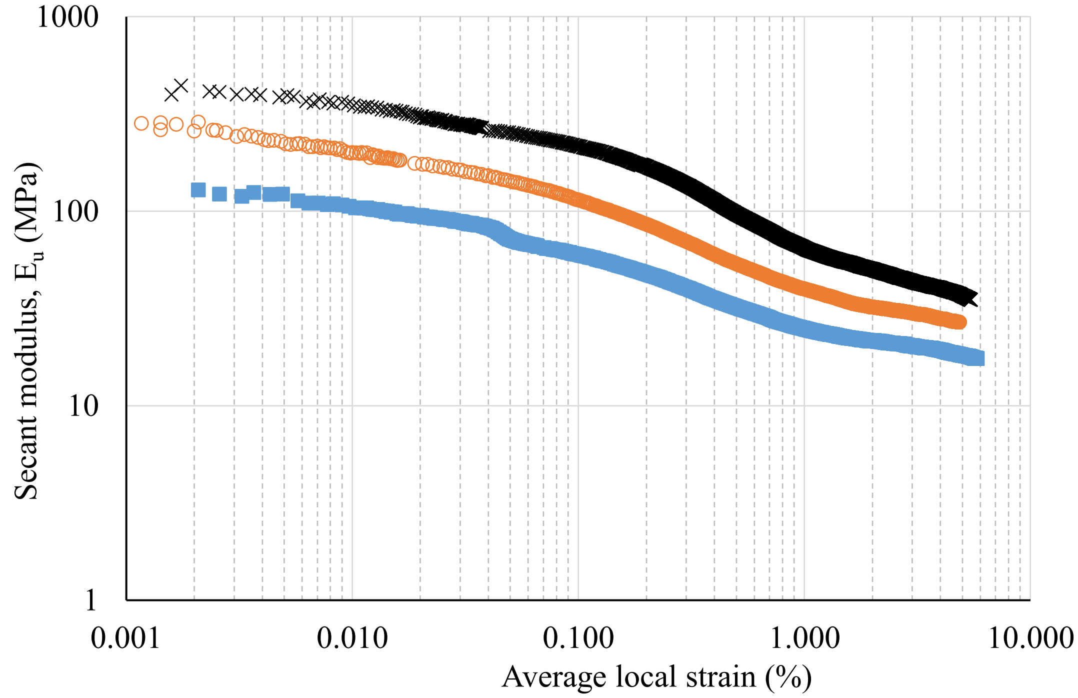

(d)

Figure 4.55. Undrained response of the clean NS at different ECS (a) stress-strain (b) pore water pressure (c) stress path (d) secant modulus

Figure 4.56 presents the testing results of NS with 10% ML at 50, 100, and 150 kPa ECS. Figure 4.56a indicates the deviatoric stress trend with the average local strain. The results showed that the deviatoric stress values continuously increased with increasing strain. The testing results also showed that deviatoric stress values increased with increasing ECS. The excess pore water pressure during the shear is presented in Figure 4.56b. The results show a contractive response during the small strain levels, and then a continuous dilatancy was observed. The excess pore water pressures at the end of the test stayed on the dilative tendency (i.e., the negative pore water pressure) of the graph. The contractiveness at the beginning of the shear increased with the increasing ECS. The maximum increase in the excess pore water pressures for NS with 10% ML at 50, 100, and 150 kPa were 9 kPa, 28 kPa, and 41 kPa. Such an increase in pore water pressure values was found to be increased with clay content as a result of the compressibility of clay particles. Once a peak pore water pressure was observed during the test, the values then started to decrease showing a sign of dilatancy. Overall, the results showed that increasing ECS decreases the dilative tendency of the mixtures. The stress path testing results at the p' and q' values are presented in Figure 4.56c. The mean effective stress increased and eventually reached the same critical state line for all tests. The E_u values are presented in Figure 4.56d.

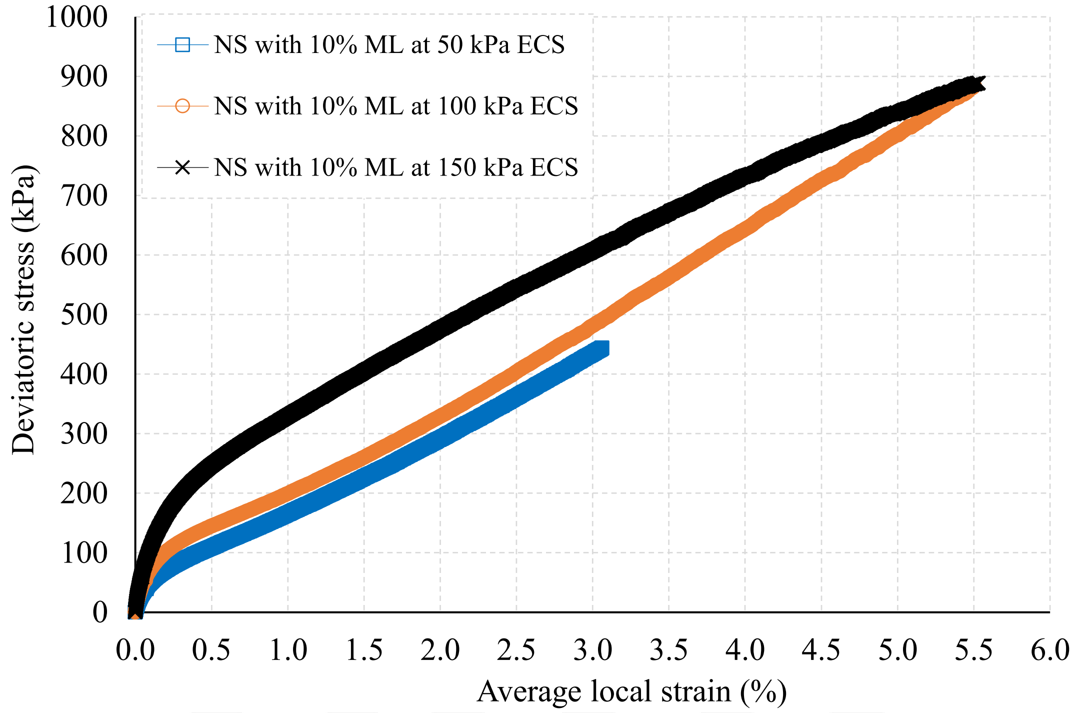
Deviatoric stress (kPa)
Average local strain (%)
NS with 10% ML at 50 kPa ECS
NS with 10% ML at 100 kPa ECS
NS with 10% ML at 150 kPa ECS

(a)

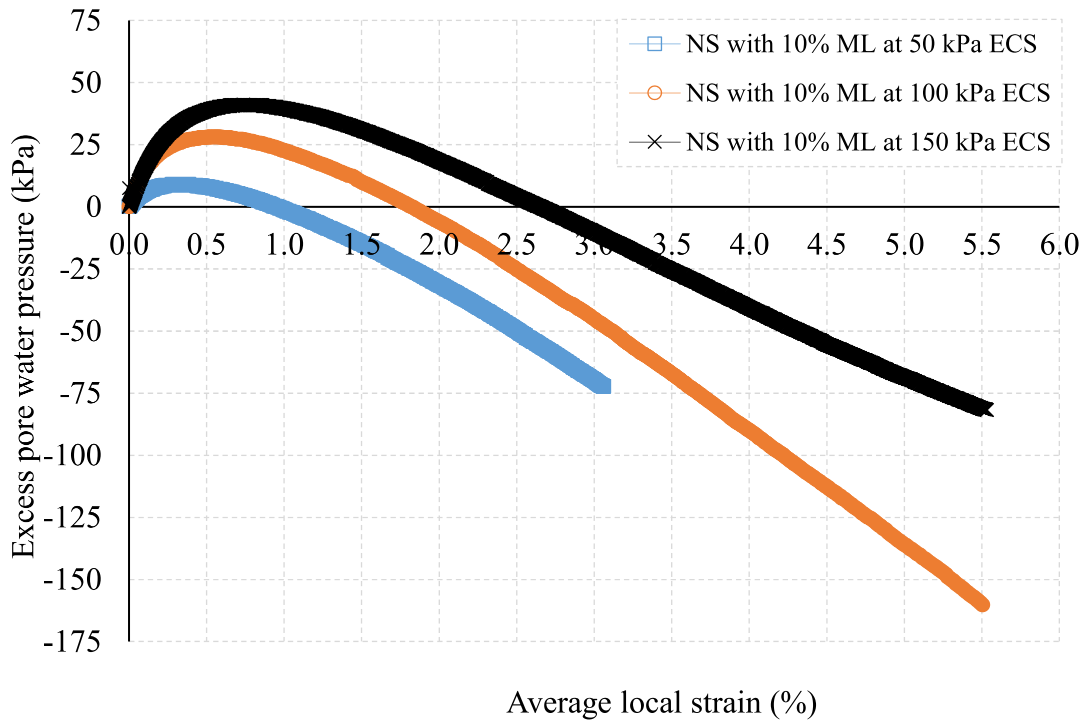
Excess pore water pressure (kPa)
Average local strain (%)
NS with 10% ML at 50 kPa ECS
NS with 10% ML at 100 kPa ECS
NS with 10% ML at 150 kPa ECS

(b)

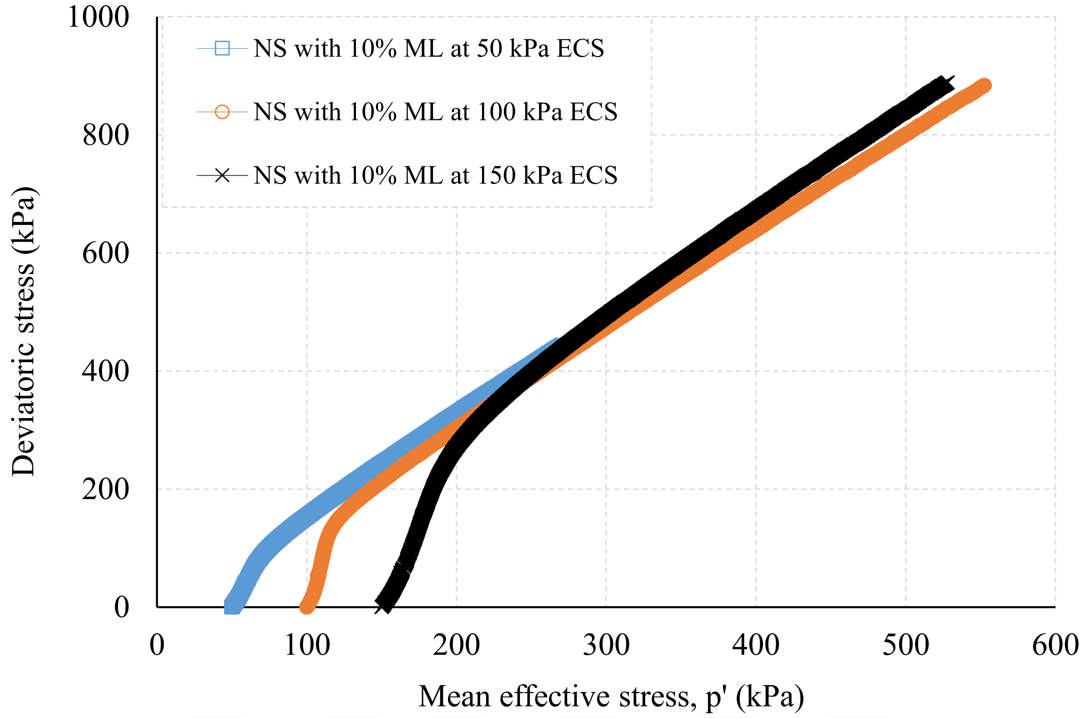

(c)

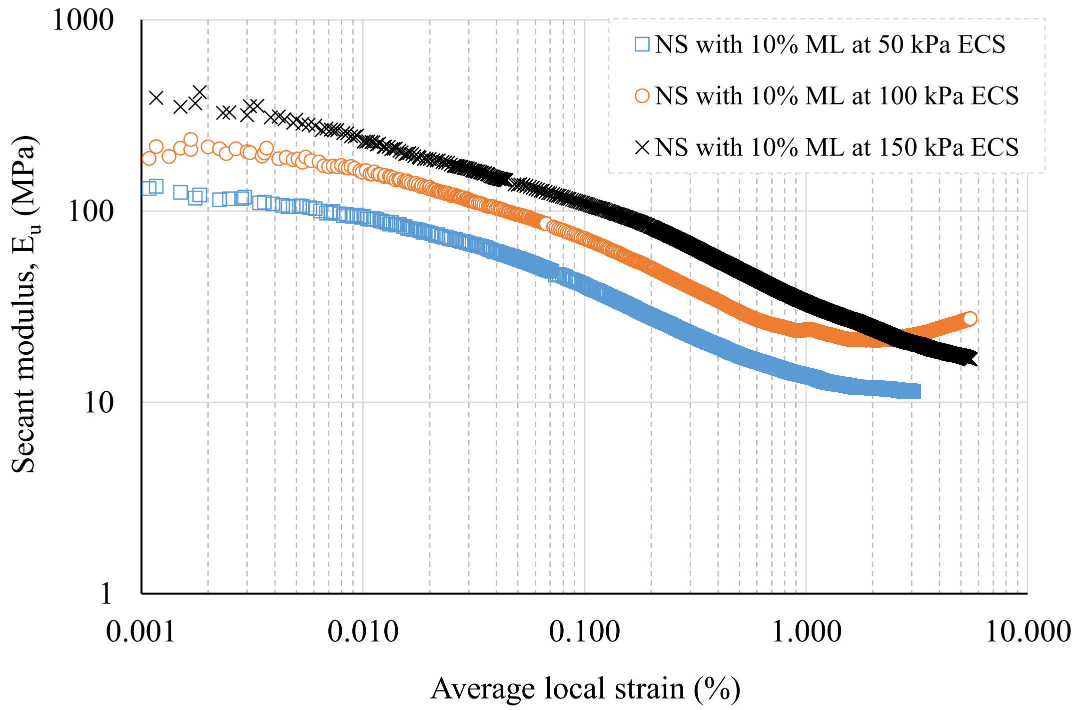

(d)

Figure 4.56. Undrained response of the NS with 10% ML at different ECS (a) stress-strain (b) pore water pressure (c) stress path (d) secant modulus

The E_u values were mainly influenced by the ECS value of the specimen. Increasing the ECS of a given mixture increased the E_u values in all strain levels. At 0.01% of the local average strain, the E_u values for clean sand at 50, 100, and 150 kPa were around 92, 155, and 230 MPa. Such a response could be described by increasing isotropic ECS, resulting in increased soil grain stiffness. Figure 4.57 presents the testing results of NS with 20% ML at 50, 100, and 150 kPa ECS. Figure 4.57a indicates the deviatoric stress trend with the average local strain. The testing results also showed that deviatoric stress values increased with increasing ECS. The excess pore water pressure during the shear is presented in Figure 4.57b. The results show a contractive response during the small strain levels, and then a continuous dilatancy was observed. The excess pore water pressures at the end of the test stayed on the dilative tendency (i.e., the negative pore water pressure) of the graph. The contractiveness at the beginning of the shear increased with the increasing ECS. The maximum increase in the excess pore water pressures for NS with 20% ML at 50, 100, and 150 kPa was 23 kPa, 48 kPa, and 65 kPa. The results showed that the dilative behaviour of the soil decreases with increasing ECS. The stress path testing results at the p' and q' values are presented in Figure 4.57c. The mean effective stress decreased and then increased to reach the same critical state line for all ECS. The E_u values are presented in Figure 4.57d. Increasing the ECS of a given mixture increased the E_u values in all strain levels. At 0.01% of the local average strain, the E_u values for clean sand at 50, 100, and 150 kPa were around 111, 151, and 208 MPa.

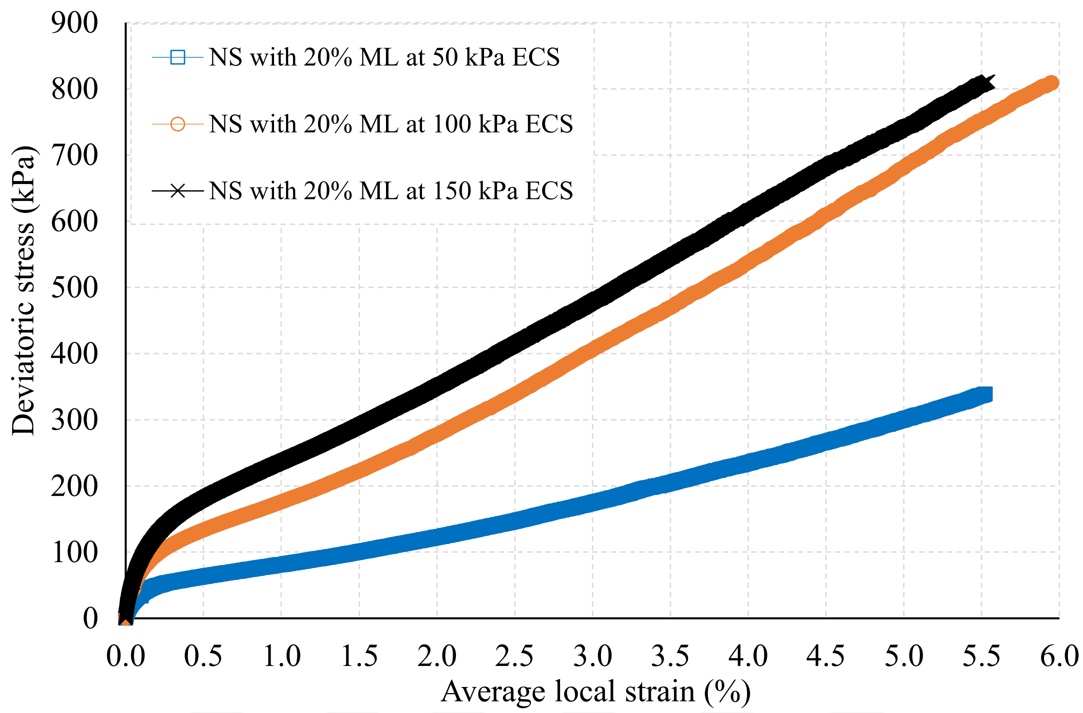

900
800
700
600
500
400
300
200
100
0
Deviatoric stress (kPa)
NS with 20% ML at 50 kPa ECS
NS with 20% ML at 100 kPa ECS
NS with 20% ML at 150 kPa ECS
0.0
0.5
1.0
1.5
2.0
2.5
3.0
3.5
4.0
4.5
5.0
5.5
6.0
Average local strain (%)

(a)

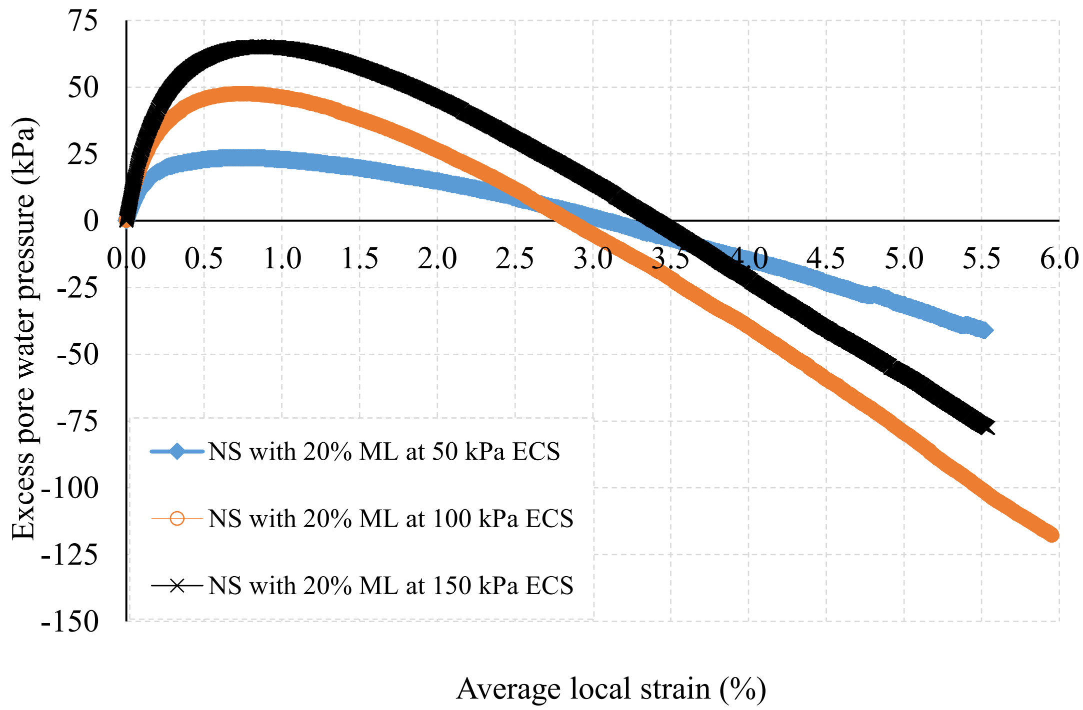

75
50
25
0
-25
-50
-75
-100
-125
-150
Excess pore water pressure (kPa)
0.0
0.5
1.0
1.5
2.0
2.5
3.0
3.5
4.0
4.5
5.0
5.5
6.0
NS with 20% ML at 50 kPa ECS
NS with 20% ML at 100 kPa ECS
NS with 20% ML at 150 kPa ECS
Average local strain (%)

(b)

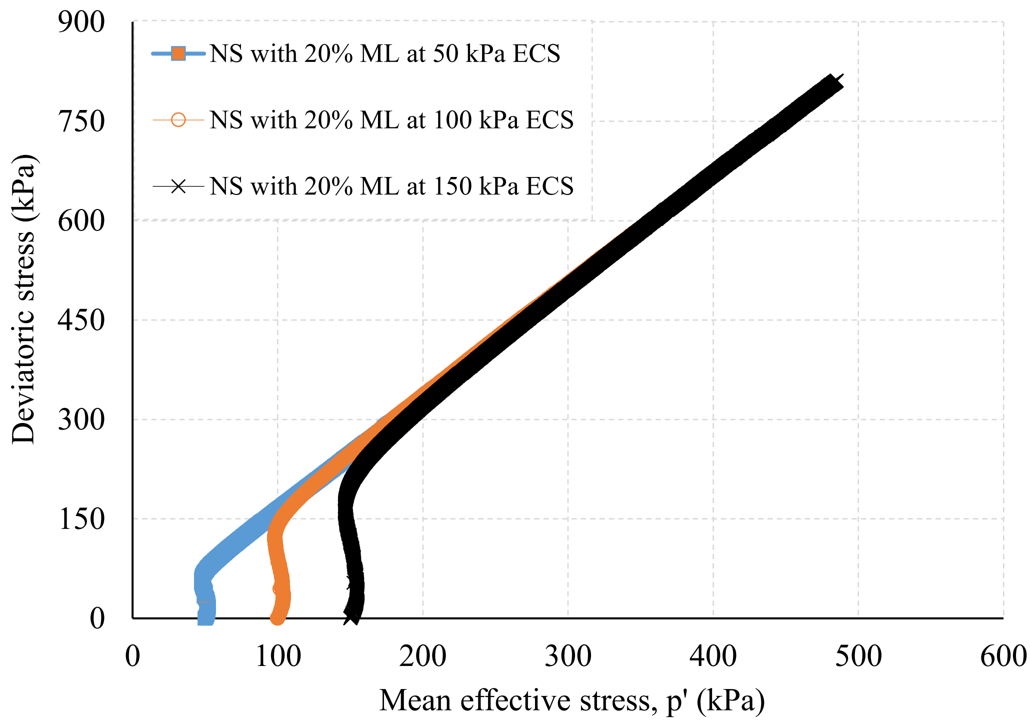

(c)

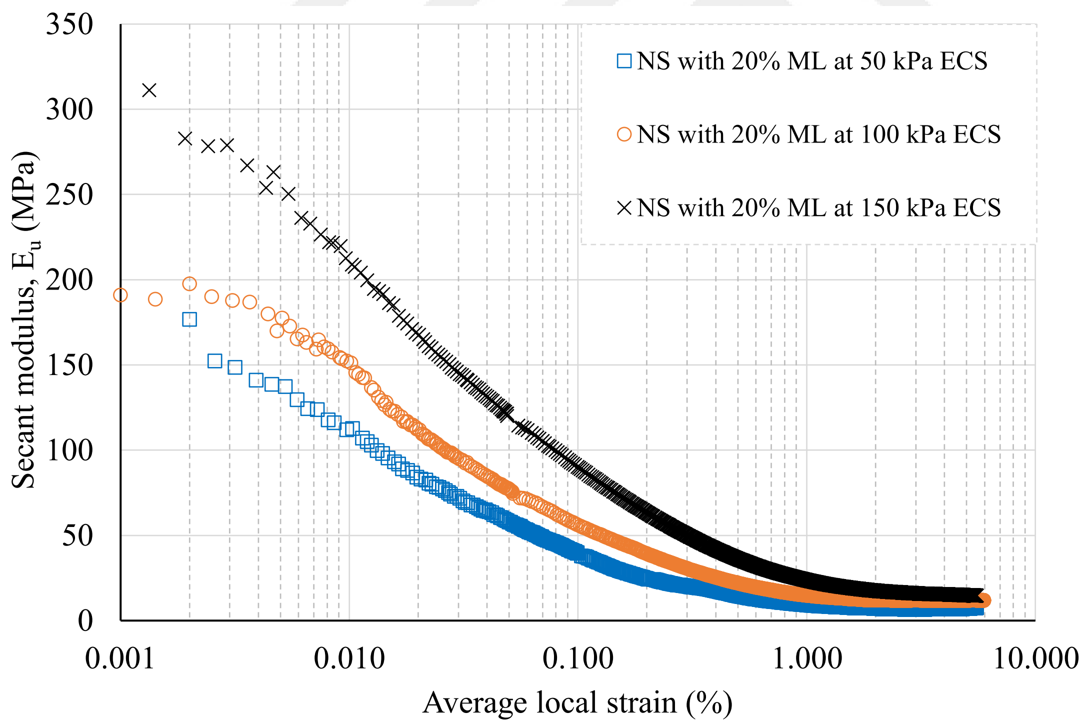

(d)

Figure 4.57. Undrained response of NS with 20% ML at different ECS (a) stress-strain (b) pore water pressure (c) stress path (d) secant modulus

Figure 4.58 presents the testing results of NS with 30% ML at 50, 100, and 150 kPa ECS. Figure 4.58a indicates the deviatoric stress trend with the average local strain. At a given strain, the deviatoric stress increased with ECS. The excess pore water pressure during the shear is presented in Figure 4.58b. The excess pore water pressure values exhibited a positive value during all stages of the test. The values increased at the small strain of the test and then showed a peak before decreasing at the end of the test. The maximum increase in the excess pore water pressures for NS with 30% ML at 50, 100, and 150 kPa was 29 kPa, 69 kPa, and 116 kPa. Such a high contractiveness of the specimens was also observed in the p-q space in Figure 4.58c. The mean effective stress first decreased and reached a minimum value before increasing. The E_u values are presented in Figure 4.58d. Increasing the ECS of a given mixture increased the E_u values in all strain levels. At 0.01% of the local average strain, the E_u values for clean sand at 50, 100, and 150 kPa were around 74, 148, and 171 MPa. Figure 4.59 presents the testing results of NS with 40% ML at 50, 100, and 150 kPa ECS. Figure 4.59a indicates the deviatoric stress trend with the average local strain. The results show that the deviatoric stress values increased relatively high at small strain levels and then showed a slight increment. At a given strain, the deviatoric stress of the soil specimens increased with the ECS. The excess pore water pressure during the shear is presented in Figure 4.59b. The excess pore water pressure values exhibited a positive value during all stages of the test. The pore water pressure values increased at the small strain of the test and then reached a plateau until the end of the test. The maximum increase in the excess pore water pressures for NS with 40% ML at 50, 100, and 150 kPa was 34 kPa, 80 kPa, and 127 kPa. Such a high contractiveness of the specimens was also observed in the p'-q space in Figure 4.59c. The mean effective stress first decreased and reached a minimum value before showing a slight increase. The E_u values are presented in Figure 4.59d. Increasing the ECS of a given mixture increased the E_u values in all strain levels. At 0.01% of the local average strain, the E_u values for clean sand at 50, 100, and 150 kPa were around 89, 122, and 173 MPa.

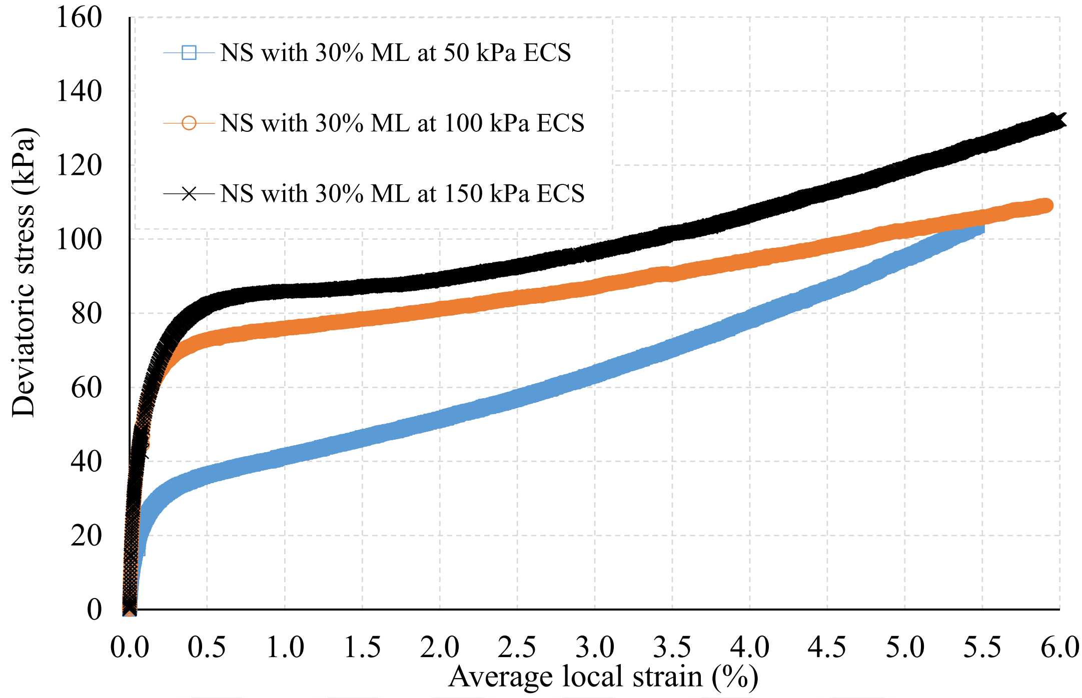
NS with 30% ML at 50 kPa ECS
NS with 30% ML at 100 kPa ECS
NS with 30% ML at 150 kPa ECS
Deviatoric stress (kPa)
Average local strain (%)
160
140
120
100
80
60
40
20
0
0.0
0.5
1.0
1.5
2.0
2.5
3.0
3.5
4.0
4.5
5.0
5.5
6.0

(a)

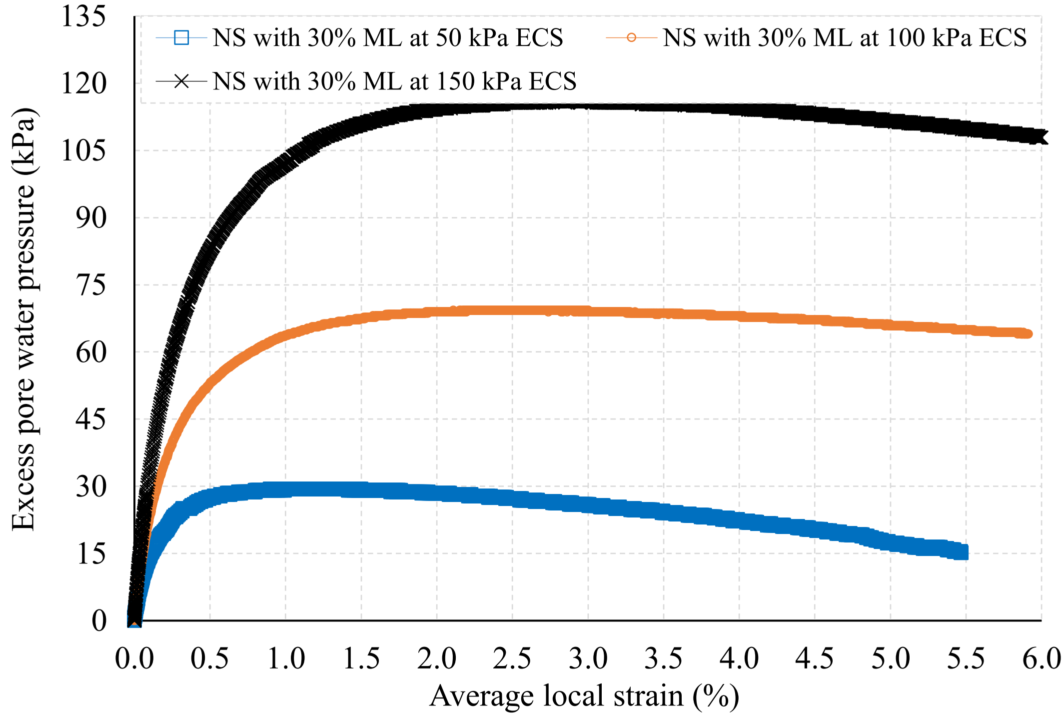
NS with 30% ML at 50 kPa ECS
NS with 30% ML at 100 kPa ECS
NS with 30% ML at 150 kPa ECS
Excess pore water pressure (kPa)
Average local strain (%)
135
120
105
90
75
60
45
30
15
0
0.0
0.5
1.0
1.5
2.0
2.5
3.0
3.5
4.0
4.5
5.0
5.5
6.0

(b)

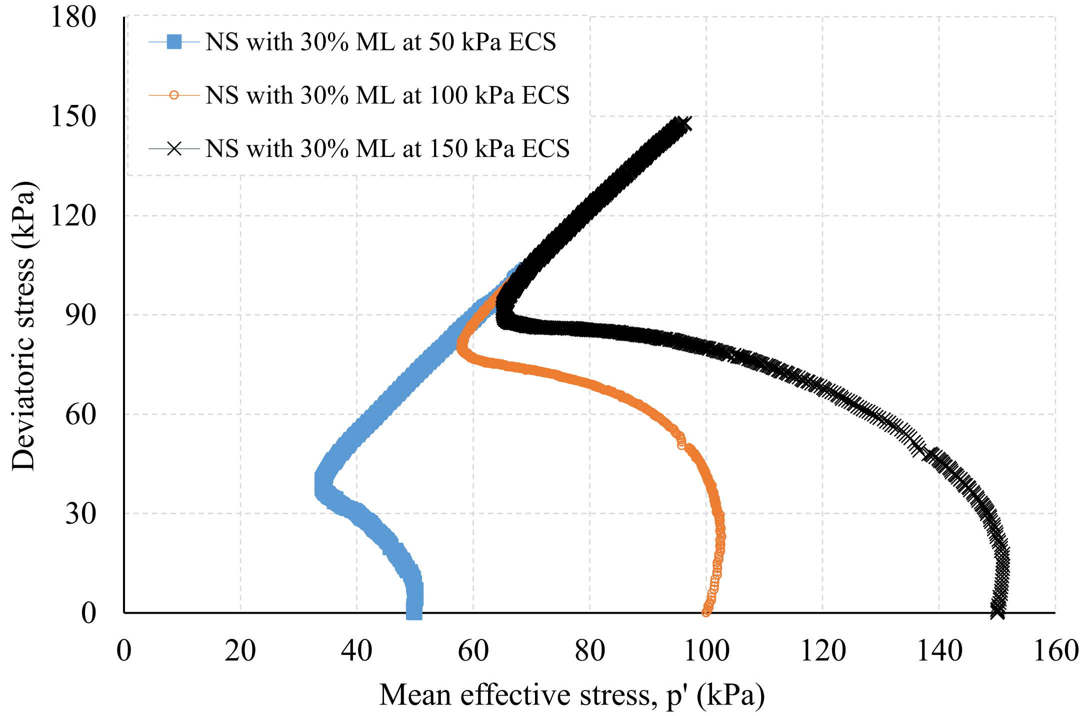

(c)

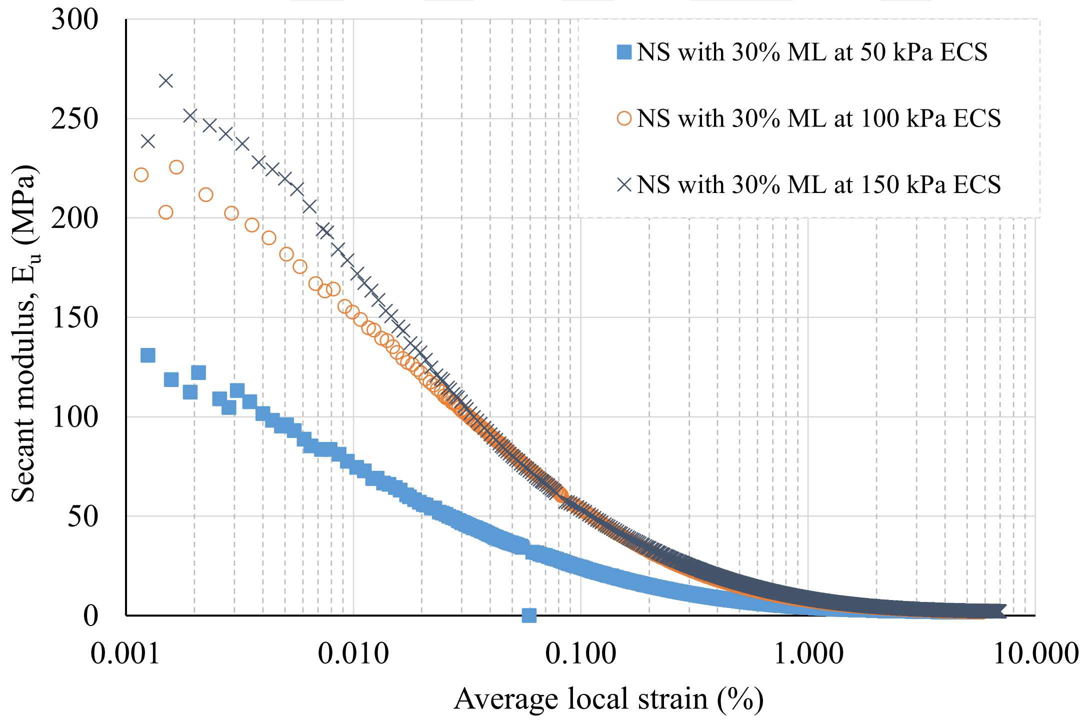

(d)

Figure 4.58. Undrained response of NS with 30% ML at different ECS (a) stress-strain (b) pore water pressure (c) stress path (d) secant modulus

Figure 4.60 presents the testing results of NS with 50% ML at 50, 100, and 150 kPa ECS. Figure 4.60a indicates the deviatoric stress values with the average local strain. The results show that the deviatoric stress values increased relatively high and small strain levels and then with the effect of contractiveness this increased ratio decreased. At a given strain, the deviatoric stress increased with ECS. The excess pore water pressure during the shear is presented in Figure 4.60b. The excess pore water pressure values exhibited a positive value during all stages of the test. The pore water pressure values increased at the small strain of the test and then reached a plateau until the end of the test. The maximum increase in the excess pore water pressures for NS with 50% ML at 50, 100, and 150 kPa was 35.8 kPa, 90 kPa, and 122 kPa. Such a high contractiveness of the specimens was also observed in the p'-q space in Figure 4.60c. The mean effective stress first decreased and reached a minimum value. The E_u values are presented in Figure 4.60d. E_u values were primarily influenced by the ECS value of the specimen. Increasing the ECS of a given mixture increased the E_u values in all strain levels. At 0.01% of the local average strain, the E_u values for clean sand at 50, 100, and 150 kPa were around 76, 144, and 190 MPa.

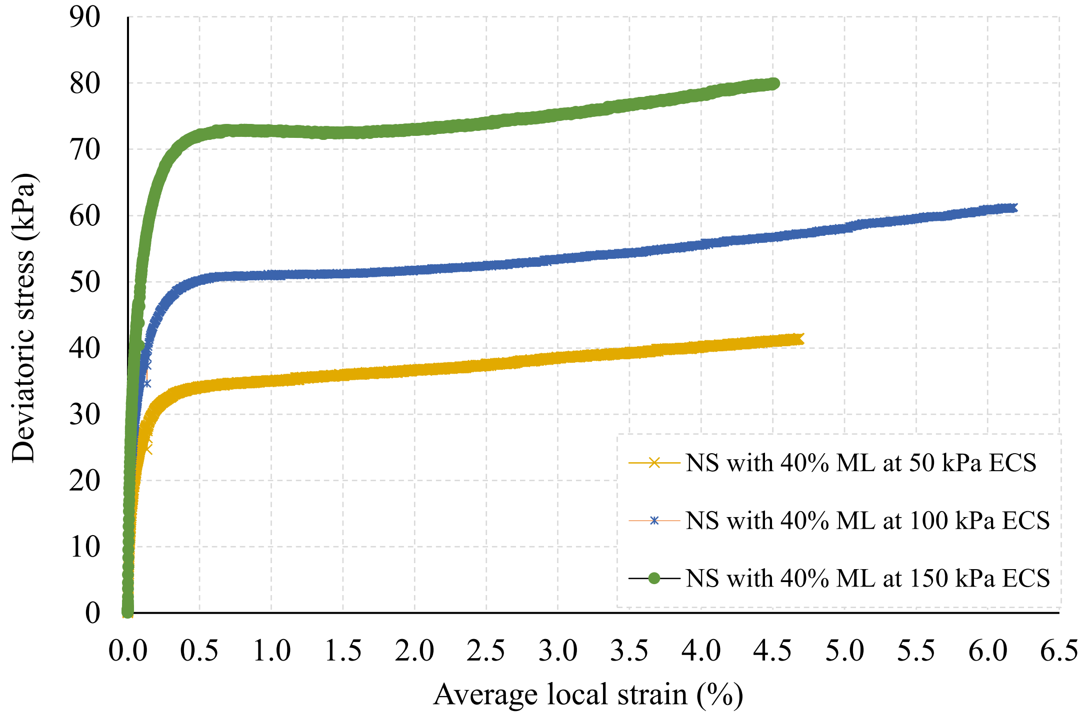
90
80
70
60
50
40
30
20
10
0
0.0
0.5
1.0
1.5
2.0
2.5
3.0
3.5
4.0
4.5
5.0
5.5
6.0
6.5
Deviatoric stress (kPa)
Average local strain (%)
NS with 40% ML at 50 kPa ECS
NS with 40% ML at 100 kPa ECS
NS with 40% ML at 150 kPa ECS

(a)

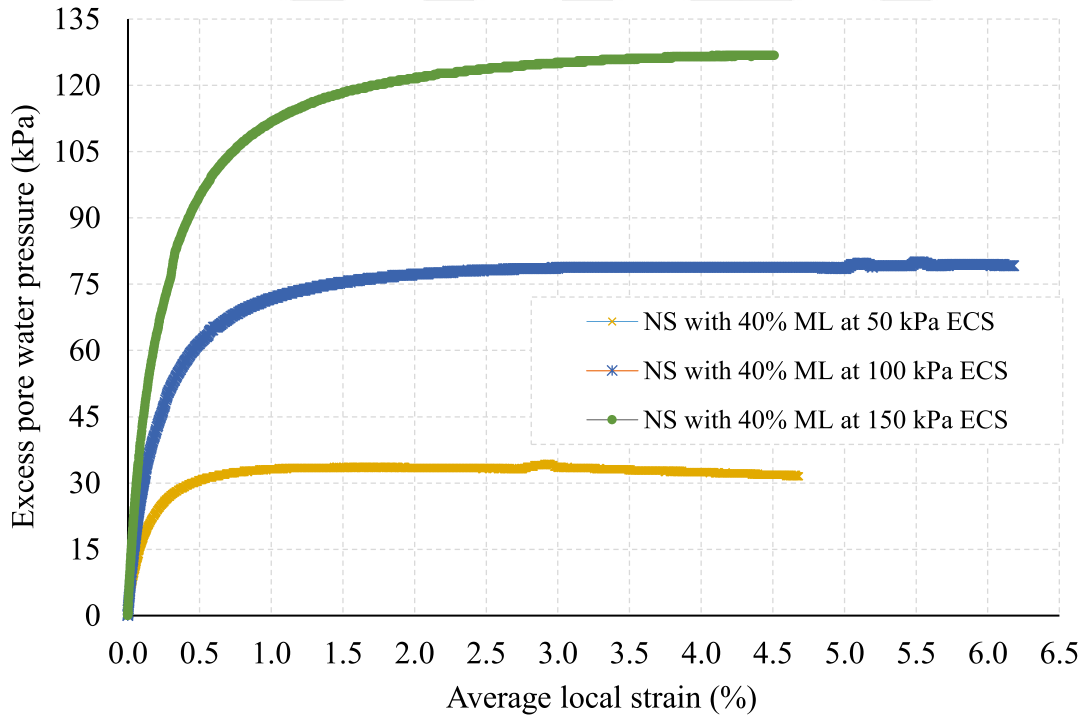
135
120
105
90
75
60
45
30
15
0
0.0
0.5
1.0
1.5
2.0
2.5
3.0
3.5
4.0
4.5
5.0
5.5
6.0
6.5
Excess pore water pressure (kPa)
Average local strain (%)
NS with 40% ML at 50 kPa ECS
NS with 40% ML at 100 kPa ECS
NS with 40% ML at 150 kPa ECS

(b)

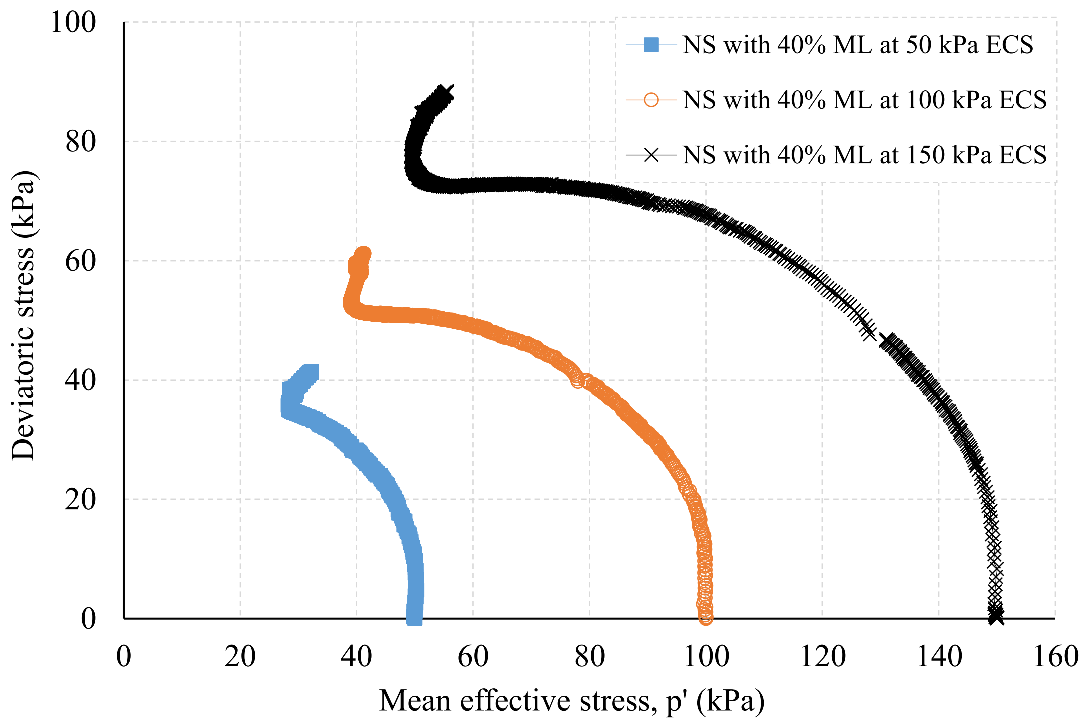

(c)

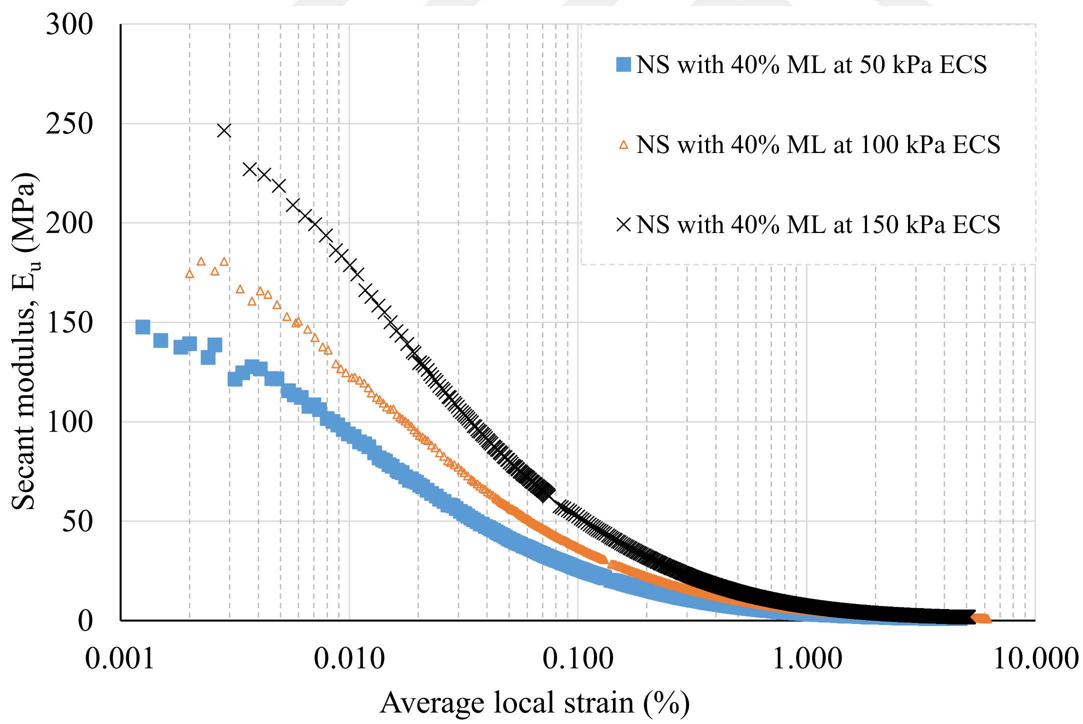

(d)

Figure 4.59. Undrained response of the NS with 40% ML at different ECS (a) stress-strain (b) pore water pressure (c) stress path (d) secant modulus

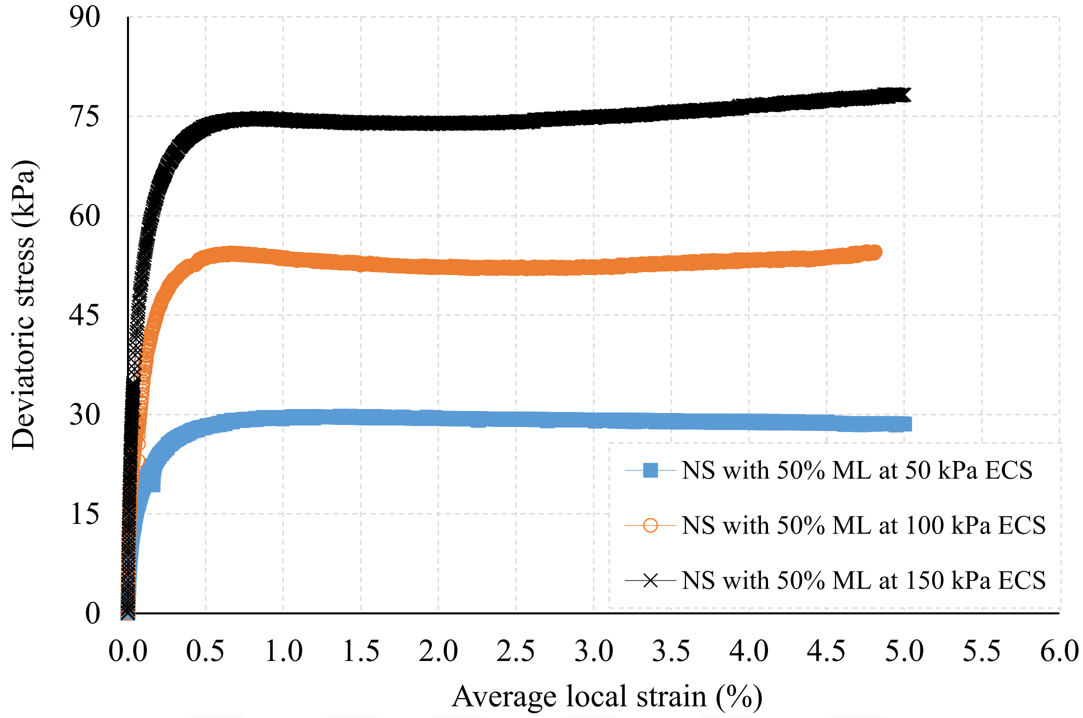

90
75
60
45
30
15
0
Deviatoric stress (kPa)
0.0 0.5 1.0 1.5 2.0 2.5 3.0 3.5 4.0 4.5 5.0 5.5 6.0
Average local strain (%)
NS with 50% ML at 50 kPa ECS
NS with 50% ML at 100 kPa ECS
NS with 50% ML at 150 kPa ECS

(a)

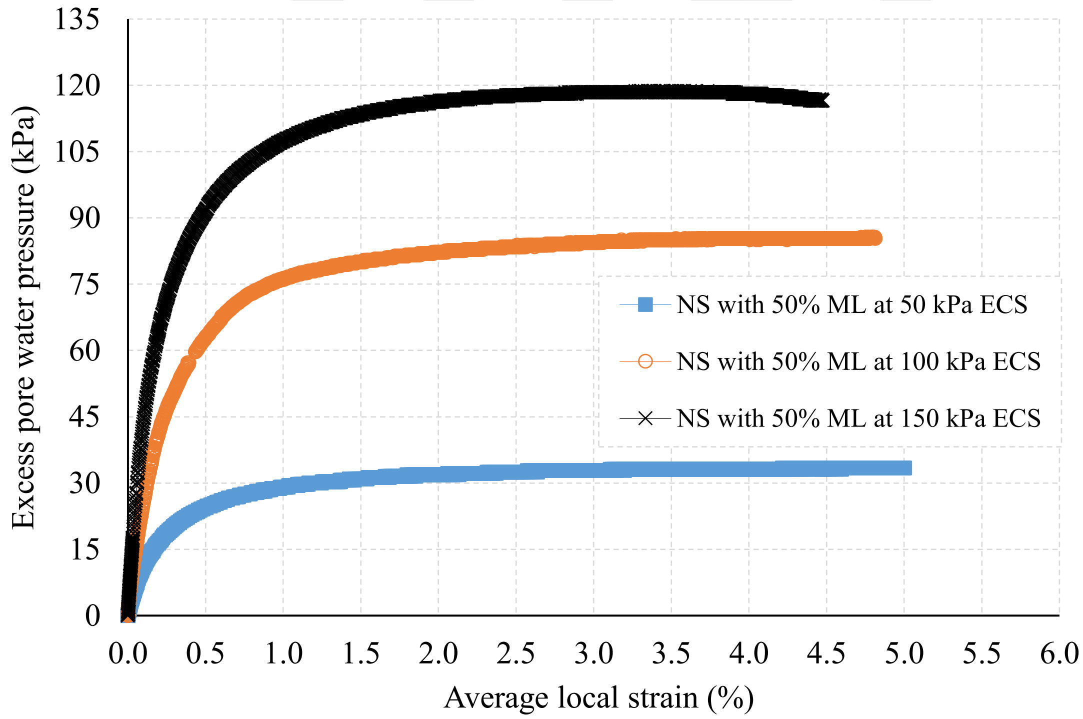

135
120
105
90
75
60
45
30
15
0
Excess pore water pressure (kPa)
0.0 0.5 1.0 1.5 2.0 2.5 3.0 3.5 4.0 4.5 5.0 5.5 6.0
Average local strain (%)
NS with 50% ML at 50 kPa ECS
NS with 50% ML at 100 kPa ECS
NS with 50% ML at 150 kPa ECS

(b)

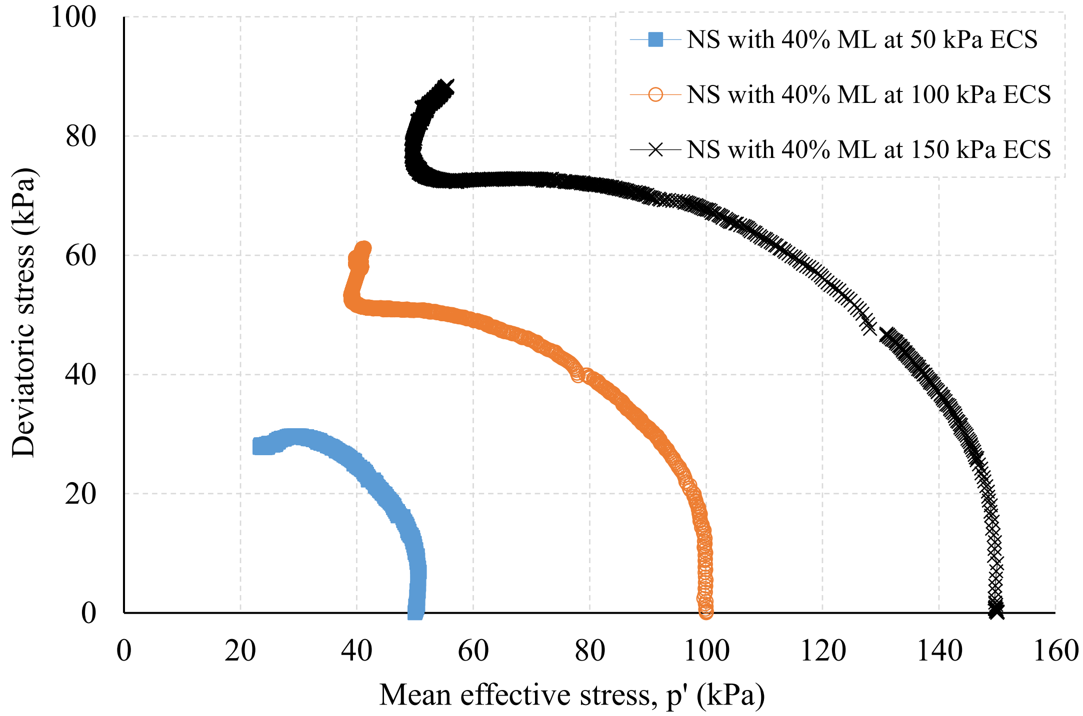

(c)

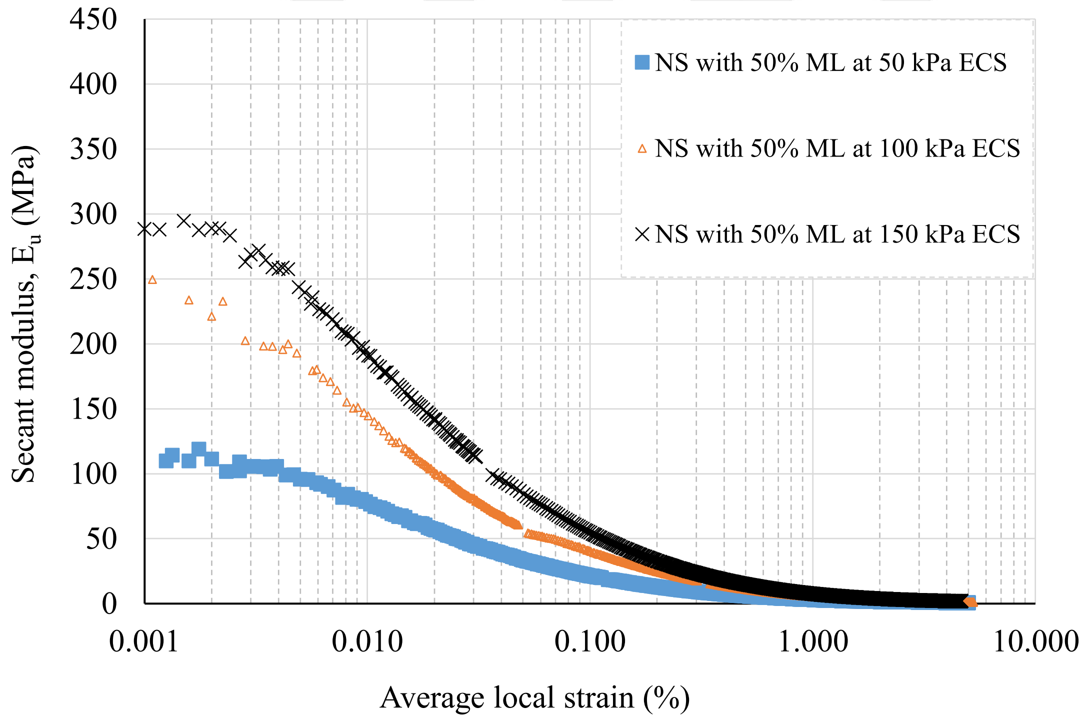

(d)

Figure 4.60. Undrained response of the NS with 50% ML at different ECS (a) stress-strain (b) pore water pressure (c) stress path (d) secant modulus

4.3.2 Effect of Clay Content

Figure 4.61-4.64 shows the testing results at constant ECS of the specimens to see the effect of clay. At each graph, the testing results for 50, 100, and 150 kPa were presented at different clay contents. Figure 4.61 shows the stress-strain results of mixtures at a given ECS. The results showed that at a given strain, the deviatoric stress value of sand decreased with increasing ML content. Such a difference could be explained by a difference in stiffness between sand and silt. Increasing silt content decreases the sand content which in turn decreases the stiffness of the mixtures. Considering a sand-dominated soil structure, fines additions up to a transitional fines content would position either in the voids of sand grains or the contacts between sand grains. Such a structure leads to little or no contribution of fines to the force chain which is governed by sand grains in such cases. Fines particles on the other hand decrease the mechanical behaviour of mixtures by negatively affecting the contact stiffness between sand grains. Similar results were obtained by Georgiannou et al. (1990) who showed that medium plastic kaolin additions increased the instability of host sand grains. Ni et al. (2004) also showed that the contribution of plastic fines to the strength of normally-consolidated soil mixture is negative as the considerable difference in hardness and size between sand and plastic fines particles. Similar testing results were also obtained by Goudarzy et al. (2022). The researcher presented the effect of kaolin and bentonite on the undrained behaviour of clean sand. The testing results presented by Goudarzy et al. (2022) showed that both fine additions decreased the undrained shear strength of the sand.

Figure 4.62 shows the pore water pressure trends of the mixtures at different ECS. At each ECS, the initial increase in pore water pressure values increased with increasing clay content. At the end of the test, NS with 30% and 40% ML showed a positive pore water pressure evaluation during the test. Furthermore, with increasing clay content dilatancy of the mixture decreases. The initial contractive response increased while and overall dilative response decreased with increasing ML content. It was noted that the initial contractive response of silty sand was due to the contractive response of silt grains at the contacts between sand grains. When the shear was commenced silt grains were forced to move into voids of sand grains due to the lack of stiffness of fine grains and such a response resulted in an initial contractive response. As the silt content increases such contractiveness increases meaning that there were more fine grains accumulating between the sand grains. When the silt grains were moved into voids between sand grains the response of soil was dilative due to better contact quality and dilative characteristics of sand grains. The mixtures having 30%, 40%, and 50% fines (i.e., ML) show almost no dilative response due to the high presence of fines in the mixtures. Such an effect of plastic fines on the host sand was also observed by numerous researchers who worked on non-plastic fine-sand mixtures (Zlatović and Ishihara, 1995; Yamamuro and Lade, 1997; Yamamuro and Lade, 1998; Murthy et al., 2007; Yang and Wei, 2012; Mahmoudi et al., 2022a; Mahmoudi et al., 2022b).

Stress path testing results of the mixtures in Figure 4.63 show a similar critical state angle for the mixtures. The sand mixed with 30%, 40%, and 50% ML mixtures showed a strong contractive response, and the other mixtures with 0%, 10%, and 20% ML contents exhibited a dilative response. The results showed that the addition of silt grains decreased the mean effective stress by increasing the pore water pressure or contractiveness of the mixtures. The reasons for such behaviour are given above. E_u values were compared in Figure 4.64. The E_u values of the mixtures at a given strain decrease with increasing silt contents. The difference in stiffness values confirms the testing results of deviatoric stress and pore water pressure. Such behaviour could be explained by the increasing presence of clay particles between the sand grains as explained above. Moreover, a significant difference in stiffness of coarse and fine grains led to such a difference. The main reason for such a difference is that sand grains are governed mainly by contact forces whereas non-contact (i.e., electro-chemical) forces govern the response of medium plastic or plastic fines. Also, a significant difference in the size of the particles between two grains was one of the main reasons to affect such a response. It can be discussed that the small size of the fines resulted in the fact that fine grains are little affected by the gravity forces. Considering such effect combined with the non-contact forces (e.g., repulsive and attractive forces) between the particles, the fine particles possess relatively little contact forces therefore low stiffness and high compressibility. In contrast, sand grains are relatively composed of large grains with a high influence of gravity due to their grain size. Such properties of sand grains led to a contact force-dominated mechanical response. Therefore, sand grains generally possess high stiffness compared to clay (Santamarina, 2003; Mitchell and Soga, 2005). Figure 4.65 presents the critical state line for all mixtures. All mixtures show similar critical state lines with a stress ratio at the critical state (M_{CS})

value of 1.69. The friction angle at the critical state (ϕ_{CS}) was also obtained as 41.24° using the following equation. Such a result is consistent with Murthy et al. (2007), Porcino et al. (2020) and Goudarzy et al. (2021).

$$\sin\phi_{CS} = \frac{3M_{CS}}{6+M_{CS}} \tag{4.3}$$

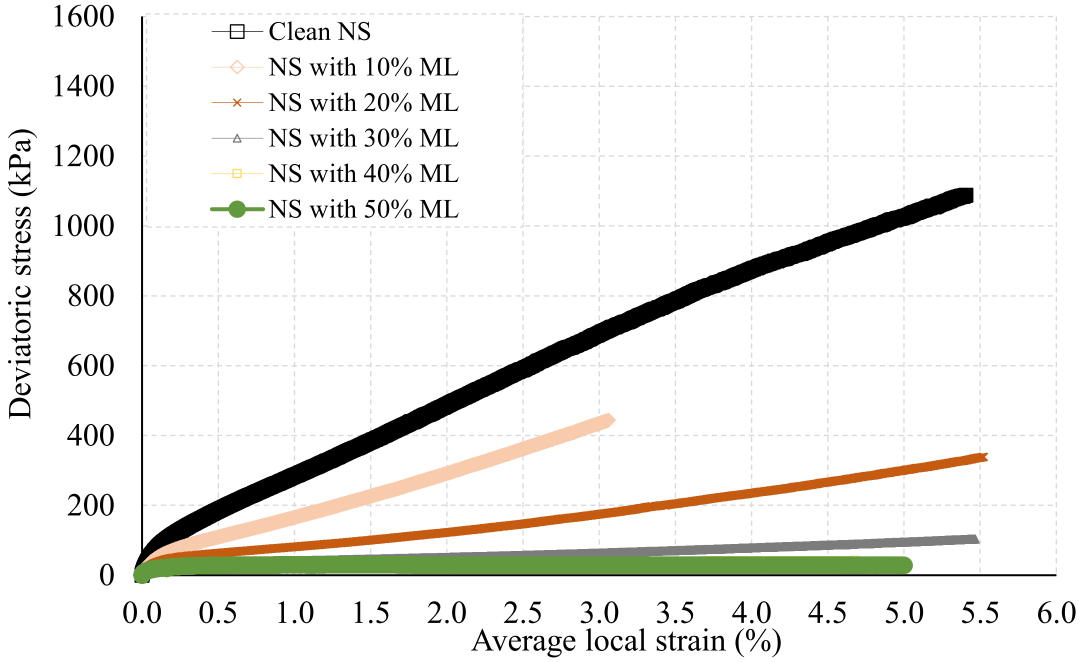

(a)

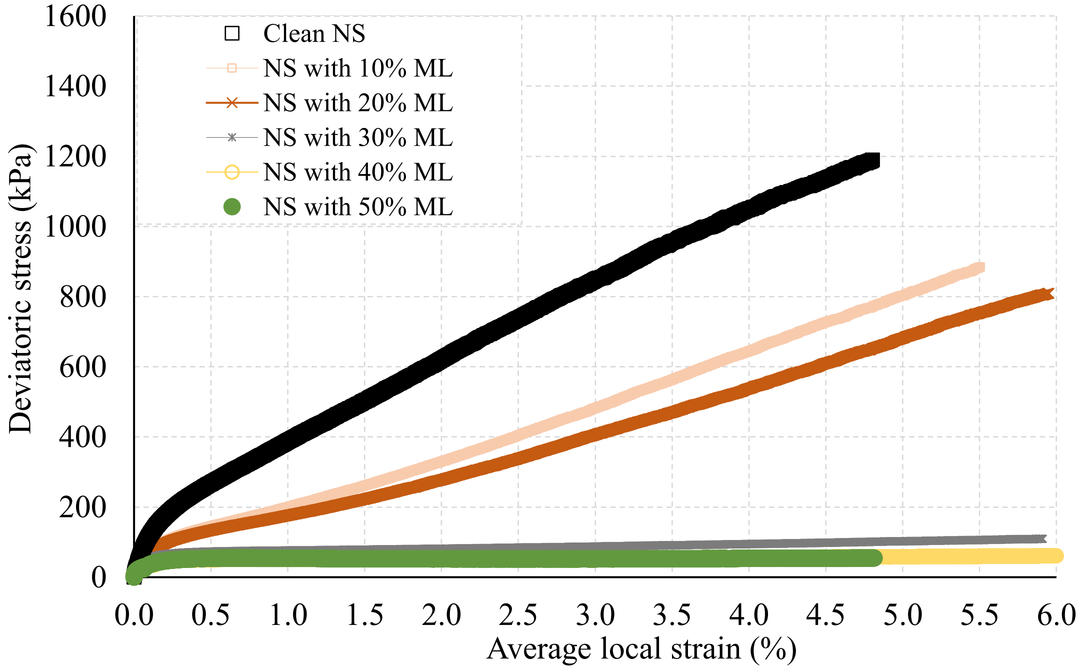

(b)

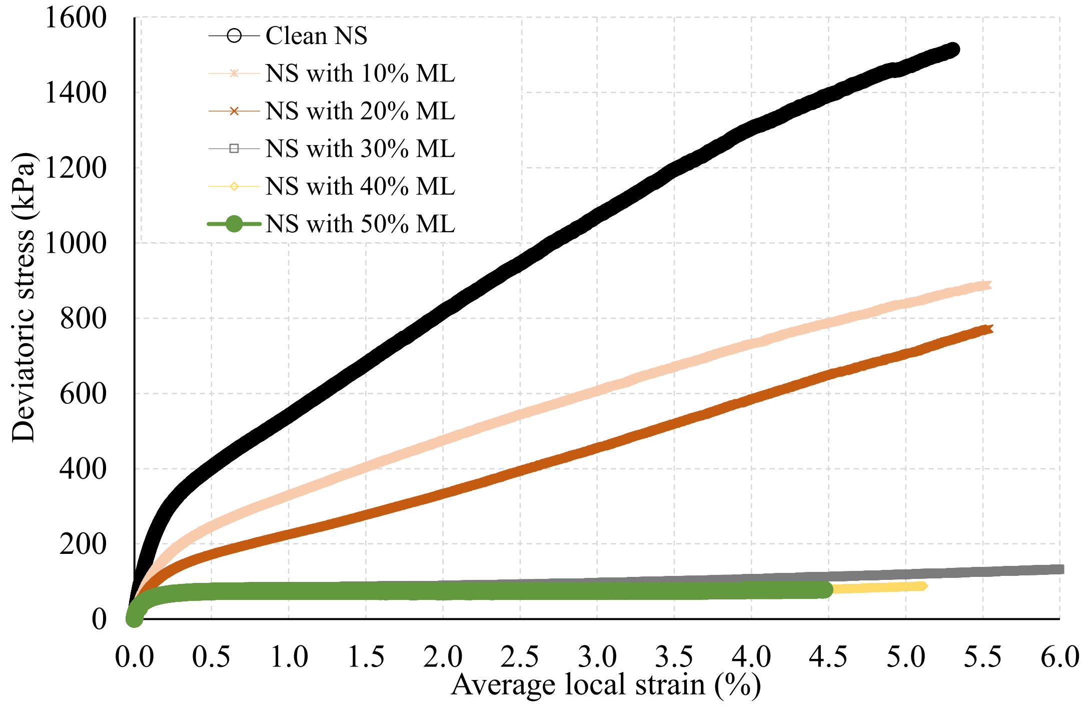

(c)

Figure 4.61. Stress-strain response of NS with various amounts of ML at (a) 50 kPa (b) 100 kPa and (c) 150 kPa ECS.

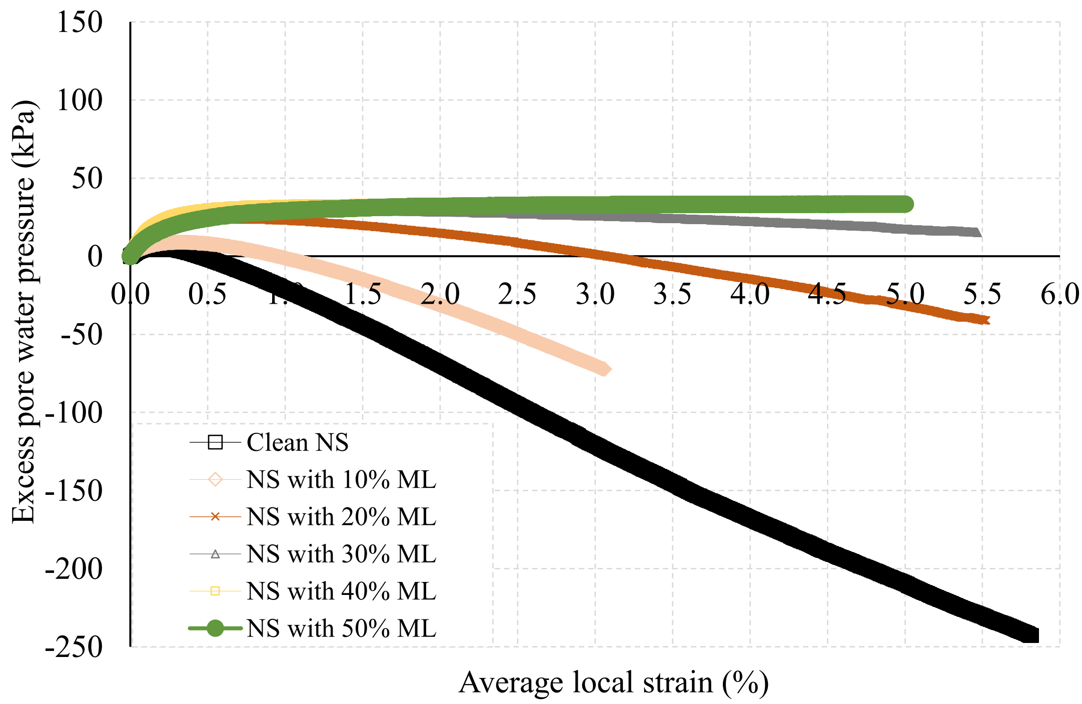

(a)

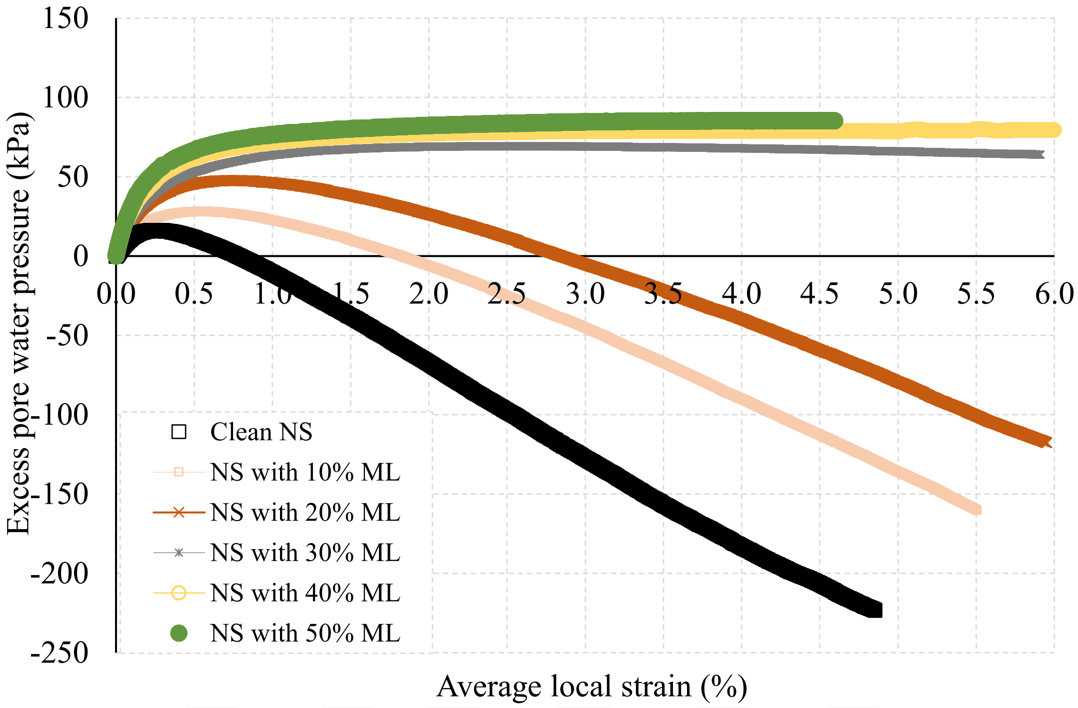

(b)

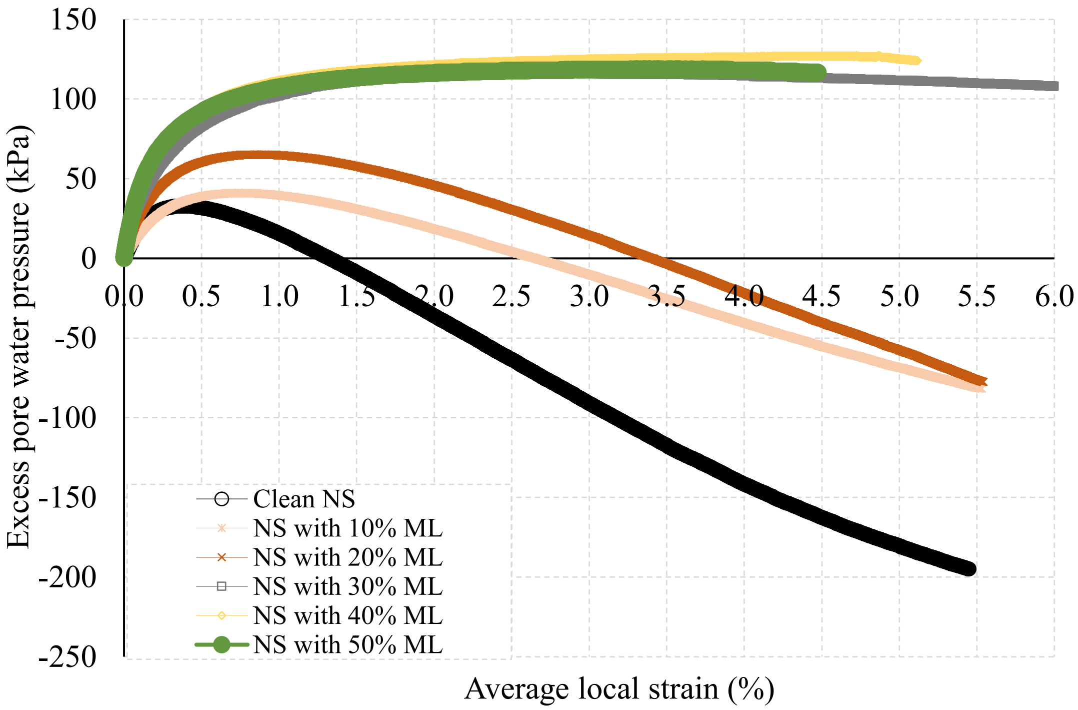

(c)

Figure 4.62. Pore water pressure response of NS with various amounts of ML at (a) 50 kPa (b) 100 kPa and (c) 150 kPa ECS.

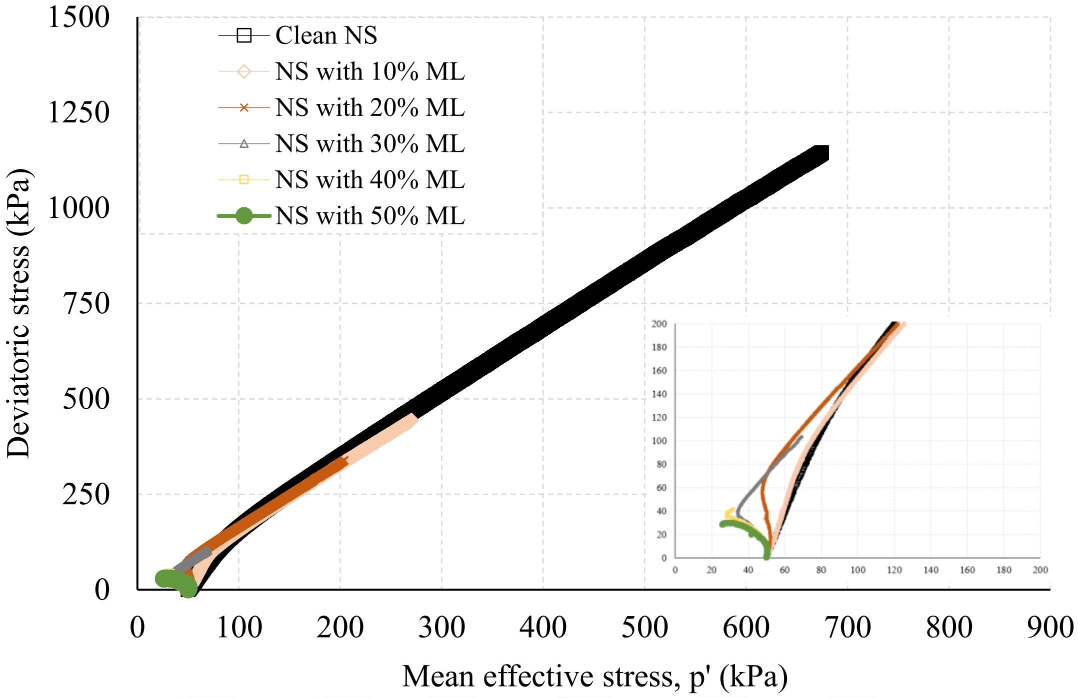

Clean NS
NS with 10% ML
NS with 20% ML
NS with 30% ML
NS with 40% ML
NS with 50% ML
Deviatoric stress (kPa)
Mean effective stress, p' (kPa)

(a)

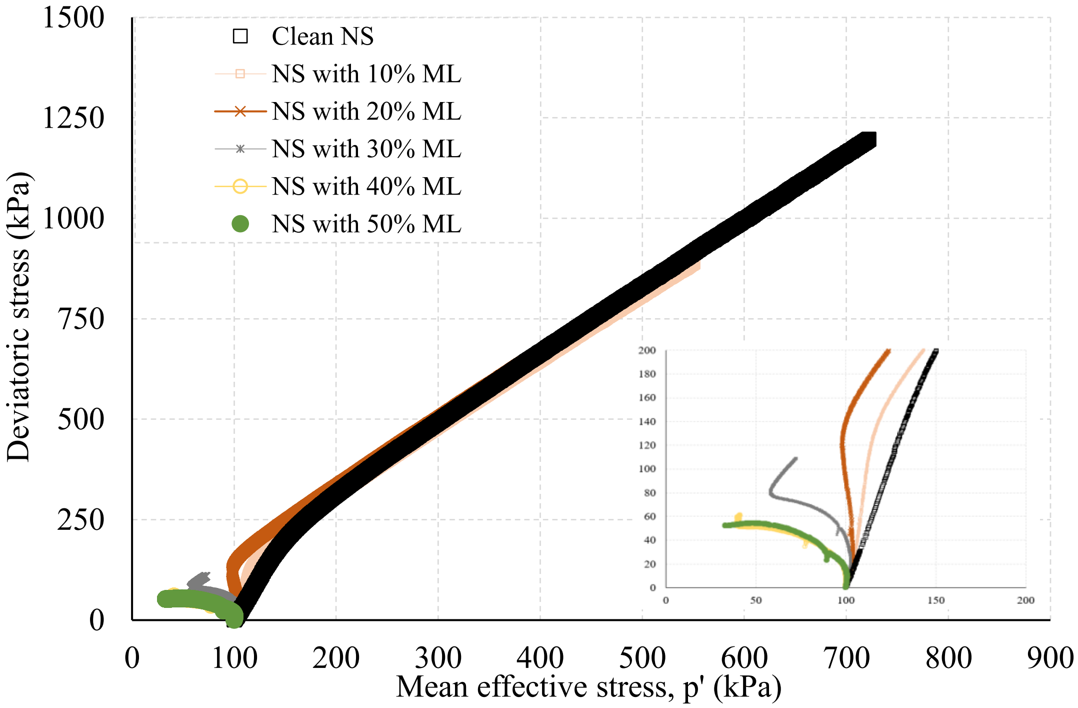

Clean NS
NS with 10% ML
NS with 20% ML
NS with 30% ML
NS with 40% ML
NS with 50% ML
Deviatoric stress (kPa)
Mean effective stress, p' (kPa)

(b)

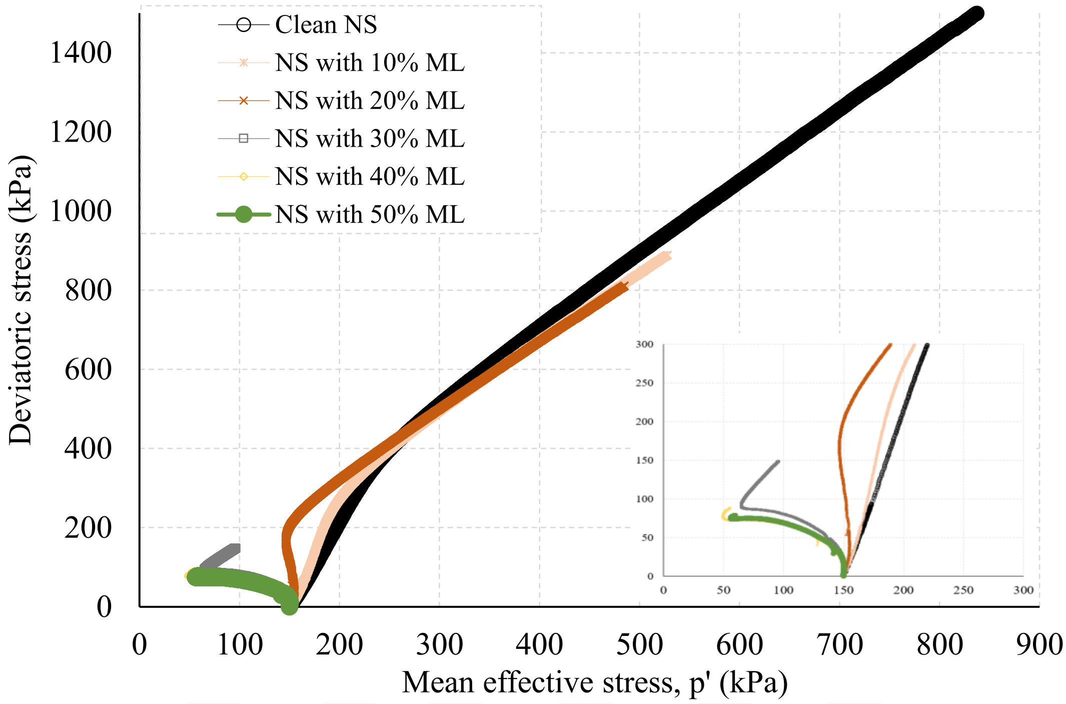

(c)

Figure 4.63. Stress paths of NS with various amounts of ML at (a) 50 kPa (b) 100 kPa and (c) 150 kPa ECS.

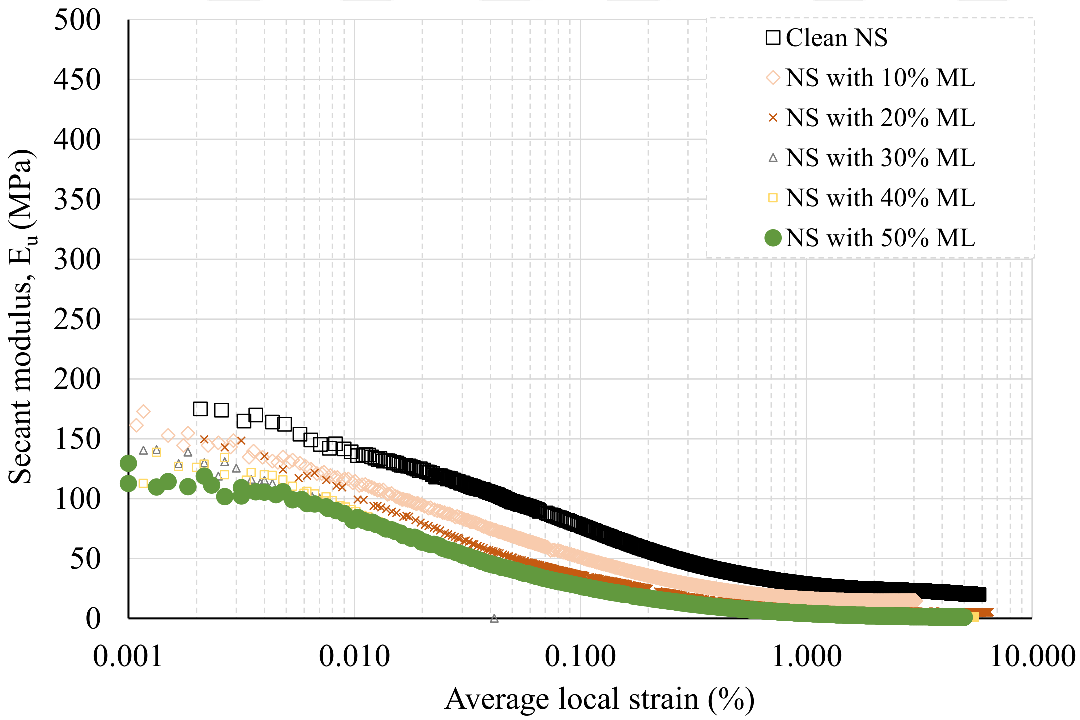

(a)

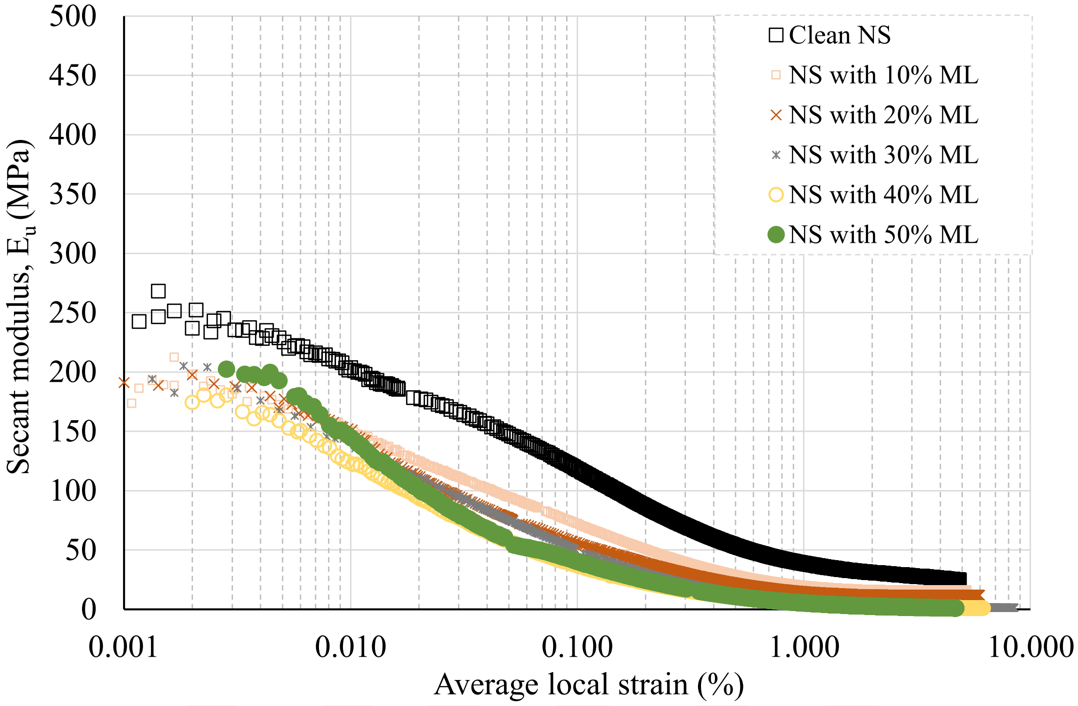

(b)

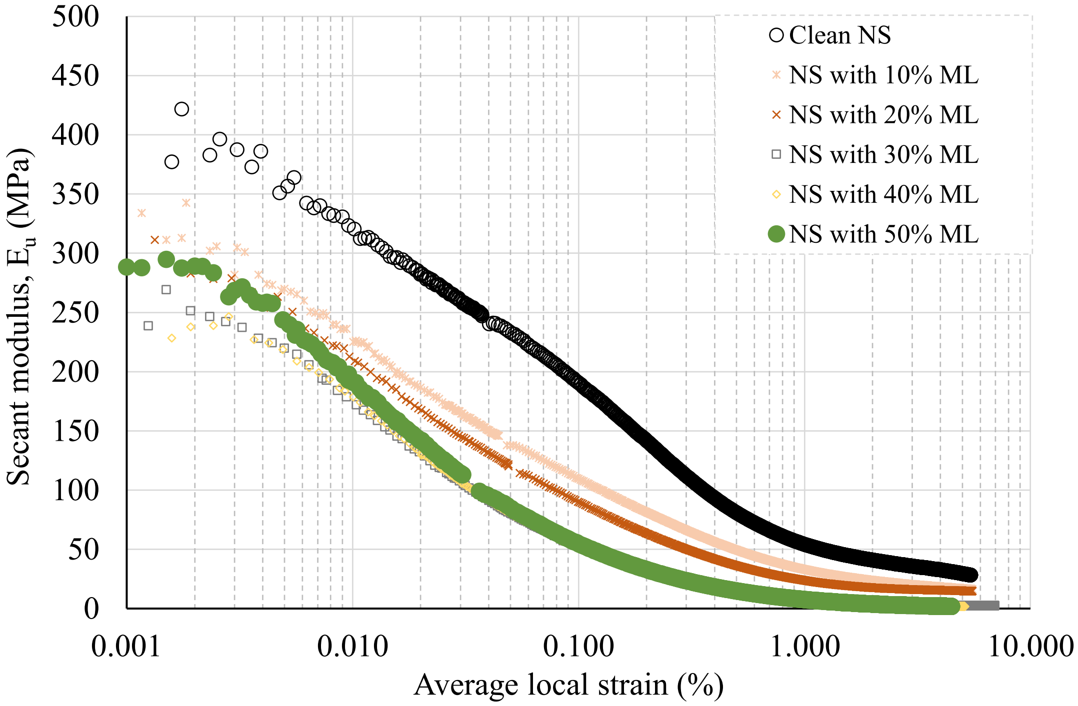

(c)

Figure 4.64. The E_u values of the NS with various amounts of ML at (a) 50 kPa (b) 100 kPa and (c) 150 kPa ECS.

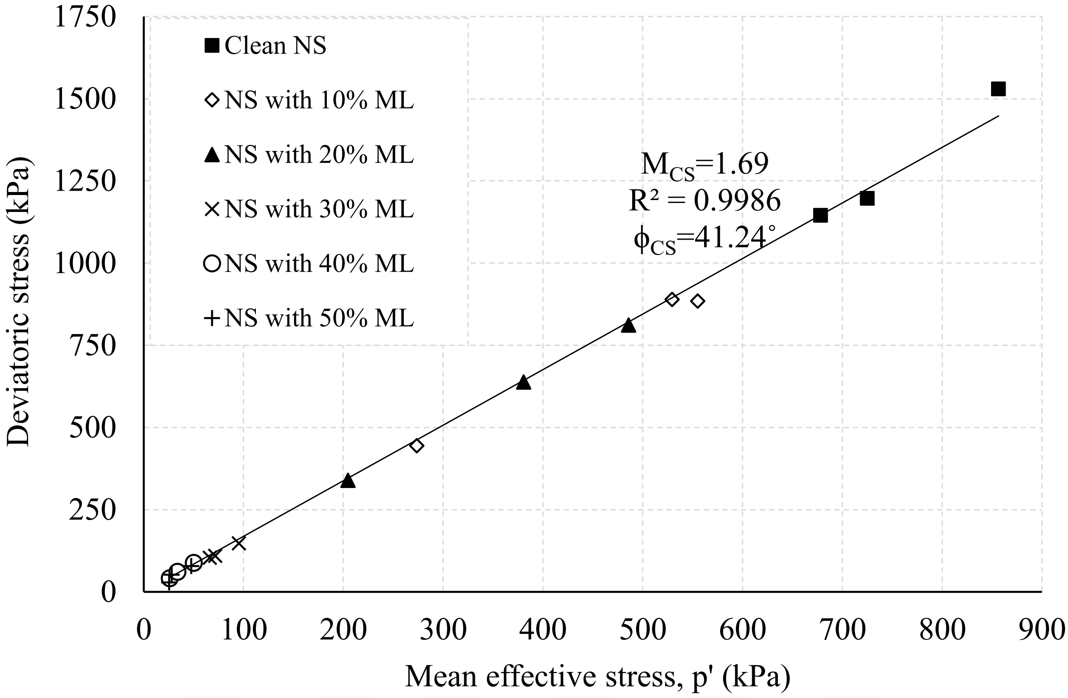

Figure 4.65. Critical state line in q–p’ space for NS with various fines contents

CHAPTER 5
CONCLUSIONS

This thesis aimed to investigate the geotechnical properties of bentonite-glass mixtures. In the first part of the thesis waste glass (WG) grains of two distinct sizes were mixed with bentonite with mixing ratios of 0%, 10%, 20%, 30%, and 40%. A laboratory testing program including compaction, fall cone, consolidation, direct shear crumb, double hydrometer, viscosity, unconfined compression (UC), and bender element (BE) tests were performed on the mixtures. The thesis also focused on the undrained triaxial response of Narlı sand (NS). In this part, medium plastic silt (ML) particles are mixed with NS with 0%, 10%, 20%, 30%, 40%, and 50%. A series of CU tests at 50 kPa, 100 kPa, and 150 kPa were performed on the mixtures. The results of the thesis can be summarized below.

- The compaction results show that the γ_{dmax} clean bentonite increased with WG addition, whereas the w_{opt} decreased with WG grains.
- The laboratory fall-cone testing results indicate that at a given water content, WG additions in bentonite led to an increase in the penetration which leads to an increase in the undrained shear strength (s_u) values of the mixtures. With WG additions, the s_u and liquid limit values of the bentonite decreased. The liquid limit values obtained from fall-cone tests showed that the liquid limit of clean bentonite decreased with both FWG and CWG additions.
- The compressibility index (c_c), swelling index (c_s), and coefficient of volume change (m_v) decreased with WG additions.
- The direct shear testing results show that cohesion values of bentonite decreased with WG additions. The angle of internal friction of bentonite increased until 30% WG content and then decreased at 40% of WG content.
- The UC testing results show that the q_u of bentonite samples increased up to 30% WG content, then decreased at 40% of WG content. The addition of 30% FWG and CWG increased the q_u values of clean bentonite by 41% and 56%, respectively.

- Dispersibility tests (i.e., crumb, double hydrometer) suggested that the dispersion ratio of bentonite decreased with WG additions. According to crumb tests, 90% WG additions changed the dispersive potential of clean bentonite from Grade 1 (High reaction) to Grade 4 (No reaction).
- The viscosity tests at various rotational speeds indicated that an increase in rotational speed resulted in a decrease in the viscosity values of the mixtures. The addition of WG in bentonite at a given rotational speed resulted in a decrease in the viscosity values of the mixtures. A maximum decrement in the viscosity values of the bentonite was obtained by 40% of CWG addition by 70%.
- The BE testing results showed that v_s values of the bentonite increased up to 30% of WG and then decreased at 40%. Similar trends were obtained in v_p, G_{max} and M_{max} values. Maximum v_p and v_s values in bentonite with 30% CWG were found to be around 436 m/s and 195 m/s, respectively, which are 40% and 54% higher than those of clean bentonite.
- The Poisson's ratio (υ) values obtained using equation 3 show that the values vary from 0.35 to 0.40, while the v_p/v_s ratios were found to be between 2.0 and 2.5. The minimum υ values were obtained at bentonite with 30% of WG.
- The bentonite and WG mixtures can be classified into three distinct regions based on their overall behavior. The first was the bentonite-dominated form, in which bentonite dominated the behavior and WG grains floated between bentonite voids. In the third region, increasing WG grain content resulted in a WG-dominated mixture at WG content greater than around 30%. The second category can be named "transitional WG content." In the transitional WG content, because both soil types contributed to the mechanical behaviour of the soil matrix in this region, the bentonite and WG mixtures had the highest q_u, v_s, v_p, G_{max}, and M_{max} values.
- CU testing results on NS-ML mixtures showed that increasing the ECS of the test increased the deviatoric stress, contractive behaviour, and secant modulus (E_u) of the mixtures. Increasing clay content at a given ECS decreased the deviatoric stress of the sand.
- ML additions increased the excess pore water pressure (i.e., contractiveness) of the mixtures. Excess pore water pressure values during the test were found

to be on the contractive side (i.e., positive excess pore water pressure) for the sand mixed with 30, 40, and 50% ML. The Narlı sand with low ML contents (0, 10, and 20%) showed negative pore water pressure at the end of the tests.

- Stress path results showed increasing contractiveness and decreasing mean effective stress and deviatoric stress of the mixtures with the ML additions.
- The E_u values of sand continuously decreased with the ML additions until 40%. Compared to the 40% ML addition, an increase in the E_u values at small strain was observed with the addition of 50% ML.

CHAPTER 6
RECOMMENDATION FOR FUTURE WORKS

The following recommendation is suggested by the author.

1. Suggesting an alternative material to be used in a bentonite-based mixture also requires investigating the unsaturated and thermal properties of the mixture. Therefore, the author suggests investigating the hydro-mechanical behaviour of bentonite-WG mixtures. Investigating the temperature effect would be interesting for such mixtures. Thermo-mechanical constitutive models can be applied to the use of WG grains for these areas.

3. Another additive material for bentonite-WG mixtures can be tested to create better cementation between these two materials. Biopolymers are one example of such additive materials.

4. Micromechanics of the bentonite-WG mixtures can be detailed with some images and pore size distribution graphs.

5. The effect of different sizes/shapes and plasticity of the host and additive soils on transitional fines content is required to improve the equation given by Rahman (2008).

6. A relatively slow loading rate of 0.02 mm/min was used in the triaxial tests, effect of different loading rates on the undrained behaviour of the mixtures is useful for further research.

REFERENCES

Abbaslou, H, Hadifard, H, & Ghanizadeh, A. R. (2020). Effect of cations and anions on flocculation of dispersive clayey soils. *Heliyon*, *6*(2), e03462. https://doi.org/10.1016/j.heliyon.2020.e03462

Adedokun, S. I., Oluremi, J. R., & Obebe, D. S. (2019). Effects of Glass Fines on the Geotechnical Properties of Cement Stabilized Lateritic Soil, *International Journal of Engineering Research in Africa*, *45*, 42-52. https://doi.org/10.4028/www.scientific.net/JERA.45.42

Ahmadi-Naghadeh, R., & Toker, N. K. (2018). A new isotropic specimen preparation method from slurry for both saturated and unsaturated triaxial testing of a low-plasticity silt. *Geotechical Testing Journal*, 42(4). https://doi.org/10.1520/GTJ20170269

Akgun, H., & Kockar, M. K. (2018). Evaluation of a sand bentonite mixture as a shaft/borehole sealing material, *Applied Clay Science*, *164*, 34-43. https://doi.org/10.1016/j.clay.2017.12.043

Alarcon-Guzman, A., Leonards, G. A., & Chameau, J. L. (1988). Undrained monotonic and cyclic strength of sands, *Journal of Geotechnical Engineering*, *114*(10), 1089-1109. https://doi.org/10.1061/(ASCE)0733-9410(1988)114:10(1089)

Amaral, M. F., Da Fonseca, A. V., Arroyo, M., Cascante, G., & Carvalho, J. (2011). Compression and shear wave propagation in cemented-sand specimens, *Géotechnique Letters*, *1*(3), 79-84. https://doi.org/10.1680/geolett.11.00032

Anisimov, O. A. (2007). Potential feedback of thawing permafrost to the global climate system through methane emission, *Environmental Research Letters*, *2*(4), 045016. https://doi.org/10.1088/1748-9326/2/4/045016

Arabani, M., Sharafi, H., Habibi, M. R., & Haghshenas, E. (2012). Laboratory evaluation of cement stabilized crushed glass-sand blends, *Electronic Journal of Geotechnical Engineering*, *17*, 1777-1792.

Arroyo, M., D. Muir Wood, P. D. Greening, L. Medina, & J. Rio. (2006). Effects of sample size on bender-based axial G_0 measurements, Géotechnique, *56*(1): 39-52. https://doi.org/10.1680/geot.2006.56.1.39

Arulrajah, A., Ali, M. M. Y., Disfani, M. M., Piratheepan, J., & Bo, M. W. (2012b). Geotechnical performance of recycled glass-waste rock blends in footpath bases, *Journal of Materials in Civil Engineering*, *25*(5), 653-661. https://doi.org/10.1061/(ASCE)MT.1943-5533.0000617

Arulrajah, A., Piratheepan, J., Disfani, M. M., & Bo, M. W. (2012a). Geotechnical and geoenvironmental properties of recycled construction and demolition materials in pavement subbase applications, *Journal of Materials in Civil Engineering*, *25*(8), 1077-1088. https://doi.org/10.1061/(ASCE)MT.1943-5533.0000617

Asl, M. T., & Taherabadi, E. (2018). Modification of silty clay strength in cold region's pavement using glass residue, *Cold Regions Science and Technology*, *154*, 111-119. https://doi.org/10.1016/j.coldregions.2018.06.005

ASTM D1557 (2012). Standard test methods for laboratory compaction characteristics of soil using modified effort. West Conshohocken, USA,

ASTM D2166 (2016). Standard test method for unconfined compressive strength of cohesive soil. West Conshohocken, USA, 2016.

ASTM D4221-18 (2018). Standard Test Method for Dispersive Characteristics of Clay Soil by Double Hydrometer. Conshohocken, USA.

ASTM D4253-16e1 (2019) Standard Test Methods for Maximum Index Density and Unit Weight of Soils Using a Vibratory Table, Conshohocken, USA.

ASTM D4254-16 (2016) Standard Test Methods for Minimum Index Density and Unit Weight of Soils and Calculation of Relative Density, Conshohocken, USA.

ASTM D6528-17 (2017) Standard Test Method for Consolidated Undrained Direct Simple Shear Testing of Fine Grain Soils. Conshohocken, USA.

ASTM D6572-21 (2019). Standard Test Methods for Determining Dispersive Characteristics of Clayey Soils by the Crumb Test. West Conshohocken, USA,

ASTM D7928-21e1. Standard Test Method for Particle-Size Distribution (Gradation) of Fine-Grained Soils Using the Sedimentation (Hydrometer) Analysis. Conshohocken, USA, 2021.

ASTM D4767-11. Standard Test Method for Consolidated Undrained Triaxial Compression Test for Cohesive Soils. Conshohocken, USA, 2020.

ASTM D2166 (2006). Standard test method for unconfined compressive strength of cohesive soil. Conshohocken, USA.

ASTM D8295-19 (2018). Standard test method for determination of shear wave velocity and initial shear modulus in soil specimens using bender elements. ASTM International, West Conshohocken, USA.

Atkinson, J. H. (2000). Non-linear soil stiffness in routine design, *Géotechnique*, *50*(5), 487-508. https://doi.org/10.1680/geot.2000.50.5.487

Attom, M. (2018). The use of WG material to control soil swelling pressure. International Conference on Technological Challenges for Better World;. Philippines.

Balagosa, J., Yoon, S., & Choo, Y. W. (2020). Experimental investigation on small-strain dynamic properties and unconfined compressive strength of gyeongju compacted bentonite for nuclear waste repository, *KSCE Journal of Civil Engineering*, *24*(9), 2657-2668. https://doi.org/10.1007/s12205-020-0372-z

Baldi, G., Hight, D. W., & Thomas, G. E. (1988). A reevaluation of conventional triaxial test methods. Advanced triaxial testing of soil and rock, ASTM STP, 977, 219-263.

Bate, B., Zhao, Q., & Burns, S. E. (2014). Impact of organic coatings on frictional strength of organically modified clay. *Journal of Geotechnical and Geoenvironmental*

Engineering, *140*(1), 228-236. https://doi.org/10.1061/(ASCE)GT.1943-5606.0000980

Bekhiti, M., Trouzine, H., & Rabehi, M. (2019). Influence of waste tire rubber fibers on swelling behavior, unconfined compressive strength and ductility of cement stabilized bentonite clay soil, *Construction and Building Materials*, *208*, 304-313. https://doi.org/10.1016/j.conbuildmat.2019.03.011

Belkhatir, M., Arab, A., Della, N., & Schanz, T. (2012). Experimental study of undrained shear strength of silty sand: effect of fines and gradation, *Geotechnical and Geological Engineering*, *30*, 1103-1118. https://doi.org/10.1007/s10706-012-9526-1

Bentz, D. P., Ferraris, C. F., Galler, M. A., Hansen, A. S., & Guynn, J. M. (2012). Influence of particle size distributions on yield stress and viscosity of cement–fly ash pastes, *Cement and Concrete Research*, *42*(2), 404-409. https://doi.org/10.1016/j.cemconres.2011.11.006

Benz, T., Schwab, R., & Vermeer, P. (2009). Small-strain stiffness in geotechnical analyses, *Bautechnik*, *86*(S1). 16-27. https://doi.org/10.1002/bate.200910038

Bilgen, G. (2020). Utilization of powdered glass as an additive in clayey soils, *Geotechnical and Geological Engineering*, *38*(3), 3163-3173. https://doi.org/10.1007/s10706-020-01215-7

Bilgen, G. (2022). Long-term compressive strength and microstructural appraisal of seawater, lime, and WG powder–treated clay soils, *Arabian Journal of Geosciences*, *15*(9), 1-18. https://doi.org/10.1007/s12517-022-10167-6

Bilondi, M. P., Toufigh, M. M., & Toufigh, V. (2018). Using calcium carbide residue as an alkaline activator for glass powder–clay geopolymer, *Construction and Building Materials*, *183*, 417-428. https://doi.org/10.1016/j.conbuildmat.2018.06.190

Bishop, A. W. (1959) The principle of effective stress. *Teknisk ukeblad*, *39*: 859-863.

Bjerrum, L. (1967) Engineering geology of Norwegian normally consolidated marine clays as related to settlements of buildings. *Geotechnique, 17*, 81–118. https://doi.org/10.1680/geot.1967.17.2.83

Blanchard, O. (1992). Energy consumption and modes of industrialization: four developing countries, *Energy Policy*, *20*(12), 1174-1185. https://doi.org/10.1016/0301-4215(92)90096-K

Bozyigit, I., & Altun, S. (2023). Small-strain behavior and post-cyclic characteristics of low plasticity silts. *Bulletin of Earthquake Engineering*, *21*(2), 791-810. https://doi.org/10.1007/s10518-022-01561-2

Brookfield, D. *Viscometer Operating Instructions Manual No*. M13-2100-A0415.

Brooks, R., Udoeyo, F. F., & Takkalapelli, K. V. (2010). Geotechnical properties of problem soils stabilized with fly ash and limestone dust in Philadelphia, *Journal of Materials in Civil Engineering*, *23*(5), 711-716. https://doi.org/10.1061/(ASCE)MT.1943-5533.0000214

Brown, S. F., & Snaith, M. S. (1974). The measurement of recoverable and irrecoverable deformations in the repeated load triaxial test, *Geotechnique*, *24*(2), 255-259. https://doi.org/10.1680/geot.1974.24.2.255

Bui, M. T. (2009). *Influence of some particle characteristics on the small strain response of granular materials* (Doctoral dissertation, University of Southampton).

Burland, J. (1989). Nintlı Laurits Bjerrum Memorial Lecture:“Small is beautiful"–the stiffness of soils, *Canadian Geotechnical Journal*, *26*(4), 499-516. https://doi.org/10.1139/t89-064

Burland, J. B., & Symes, M. J. P. R. (1982). A simple axial displacement gauge for use in the triaxial apparatus, *Geotechnique*, *32*(1), 62-65. https://doi.org/10.1680/geot.1982.32.1.62

Cabalar, A. F. (2011). The effects of fines on the behaviour of a sand mixture, *Geotechnical and Geological Engineering*, *29*(1), 91-100. https://doi.org/10.1007/s10706-010-9355-z

Cabalar, A. F. (2015). Stress fluctuations in granular material response during cyclic direct shear test, Granular Matter, *17*(4), 439-446. https://doi.org/10.1007/s10035-015-0568-y

Cabalar, A. F., & Alosman, S. O. (2021). Influence of rock powder on the behaviour of an organic soil, *Bulletin of Engineering Geology and the Environment*, *80*(11), 8665-8676. https://doi.org/10.1007/s10064-021-02457-2

Cabalar, A. F., & Clayton, C. R. I. (2010). Some observations of the effects of pore fluids on the triaxial behaviour of a sand, *Granular Matter*, *12*, 87-95. https://doi.org/10.1007/s10035-009-0164-0

Cabalar, A. F., & Demir, S. (2019). Fall-cone testing of unsaturated sand–clay mixtures, *Proceedings of the Institution of Civil Engineers-Geotechnical Engineering*, *172*(5), 432-441. https://doi.org/10.1680/jgeen.18.00155

Cabalar, A. F., & Demir, S. (2022). Geotechnical properties of a bentonite treated with WG grains. *Arabian Journal of Geosciences*, *15*(9), 880. https://doi.org/10.1007/s12517-022-10169-4

Cabalar, A. F., & Demir, S., Khalaf, M. M. (2021). Liquefaction resistance of different size/shape sand-clay mixtures using a pair of bender element–mounted molds, *Journal of Testing and Evaluation*, *49*(1), 509-524. https://doi.org/10.1520/JTE20180677

Cabalar, A. F., & Karabash, Z. (2019). Influence of cement type and sample preparation on the small-strain behaviour of sands, *Arabian Journal for Science and Engineering*, *44*, 8835-8848. https://doi.org/10.1007/s13369-019-04070-8

Cabalar, A. F., & Mustafa, W. S. (2015). Fall cone tests on clay–sand mixtures. *Engineering Geology*, *192*, 154-165. https://doi.org/10.1016/j.enggeo.2015.04.009

Cabalar, A. F., Dulundu, K., & Tuncay, K. (2013). Strength of various sands in triaxial and cyclic direct shear tests, *Engineering Geology*, *156*, 92-102. https://doi.org/10.1016/j.enggeo.2013.01.011

Cabalar, A. F., Hama, S. O., & Demir, S. (2022). Behaviour of a Clay and Gravel Mixture, *The Baltic Journal of Road and Bridge Engineering*, *17*(1), 98-116. https://doi.org/10.7250/bjrbe.2022-17.553

Cai, Y., Dong, Q., Wang, J., Gu, C., & Xu, C. (2015). Measurement of small strain shear modulus of clean and natural sands in saturated condition using bender element test, *Soil Dynamics and Earthquake Engineering*, *76*, 100-110. https://doi.org/10.1016/j.soildyn.2014.12.013

Camacho-Tauta, J., Ali, H., Cascante, G., & Viana da Fonseca, A. (2015, December). Frequency domain method in bender element testing–experimental observations. In Deformation Characteristics of Geomaterials, Proceedings of the 6th International Symposium on Deformation Characteristics of Geomaterials, VA Rinaldi et al.(Eds.), IOS Press,(1) (pp. 398-406).

Carraro, J. A. H., Prezzi, M., & Salgado, R. (2009). Shear strength and stiffness of sands containing plastic or nonplastic fines. *Journal of Geotechnical and Geoenvironmental Engineering*, *135*(9), 1167-1178. https://doi.org/10.1061/(ASCE)1090-0241(2009)135:9(1167)

Castro, G. (1969). Liquefaction of sands, Harvard soil mechanics series No. 81, Harvard University, Cambridge, Mass.

Castro, G. (1975). Liquefaction and cyclic mobility of saturated sands, *Journal of the Geotechnical Engineering Division*, *101*(6), 551-569. https://doi.org/10.1061/AJGEB6.0000173

Castro, G., & Poulos, S. J. (1977). Factors affecting liquefaction and cyclic mobility, *Journal of the Geotechnical Engineering Division*, *103*(6), 501-516. https://doi.org/10.1061/AJGEB6.0000433

Chang, C. S., Deng, Y., & Meidani, M. (2018). A multi-variable equation for relationship between limiting void ratios of uniform sands and morphological characteristics of their particles, *Engineering Geology*, *237*, 21-31. https://doi.org/10.1016/j.enggeo.2018.02.003

Cherif Taiba, A., Belkhatir, M., Kadri, A., Mahmoudi, Y., & Schanz, T. (2016). Insight into the effect of granulometric characteristics on the static liquefaction susceptibility of silty sand soils, *Geotechnical and Geological Engineering*, *34*, 367-382. https://doi.org/10.1007/s10706-015-9951-z

Chidiac, S. E., & Federico, L. M. (2007). Effects of WG additions on the properties and durability of fired clay brick, *Canadian Journal of Civil Engineering*, *34*(11), 1458-1466. https://doi.org/10.1139/L07-120

Cho, G. C., Dodds, J., & Santamarina, J. C. (2006). Particle shape effects on packing density, stiffness, and strength: natural and crushed sands, *Journal of Geotechnical and Geoenvironmental Engineering*, *132*(5), 591-602. https://doi.org/10.1061/(ASCE)1090-0241(2006)132:5(591)

Clayton, C. R. I. (2011). Stiffness at small strain: research and practice, *Géotechnique*, *61*(1), 5-37. https://doi.org/10.1680/geot.2011.61.1.5

Clayton, C. R. I., & Khatrush, S. A. (1986). A new device for measuring local axial strains on triaxial specimens, *Géotechnique*, *36*(4), 593-597. https://doi.org/10.1680/geot.1986.36.4.593

Cokca, E., & Yilmaz, Z. (2004). Use of rubber and bentonite added fly ash as a liner material, *Waste Management*, *24*(2), 153-164. https://doi.org/10.1016/j.wasman.2003.10.004

Cole, C., Gnanapragasam, A., Cooper, T., & Singh, J. (2019). An assessment of achievements of the WEEE Directive in promoting movement up the waste hierarchy: experiences in the UK, *Waste Management*, *87*, 417-427. https://doi.org/10.1016/j.wasman.2019.01.046

Cole, K. W., & Burland, J. B. (1972). Observation of retatining wall movements associated with a large excavation, In *Fifth Eur Conf on Soil Proc/Sp/* (No. Conf Paper).

Consoli, N. C., da Silva Carretta, M., Festugato, L., Leon, H. B., Tomasi, L. F., & Heineck, K. S. (2021). Ground WG–carbide lime as a sustainable binder stabilising three different silica sands, *Géotechnique*, *71*(6), 480-493. https://doi.org/10.1680/jgeot.18.P.099

Consoli, N. C., Winter, D., Leon, H. B., & Scheuermann Filho, H. C. (2018). Durability, strength, and stiffness of green stabilized sand, *Journal of Geotechnical* *and Geoenvironmental Engineering*, *144*(9), 04018057. https://doi.org/10.1061/(ASCE)GT.1943-5606.0001928

Costa Filho, L. M. (1980). A laboratory investigation of the small strain behaviour of London clay. PhD thesis, University of London.

Cuccovillo, T., & Coop, M. R. (1997). The measurement of local axial strains in triaxial tests using LVDTs, *Géotechnique*, *47*(1), 167-171.

Cudny, M., & Truty, A. (2020). Refinement of the Hardening Soil model within the small strain range, Acta Geotechnica, 15(8), 2031-2051.

Cui, S. L., Zhang, H. Y., & Zhang, M. (2012). Swelling characteristics of compacted GMZ bentonite–sand mixtures as a buffer/backfill material in China, *Engineering Geology*, *141*, 65-73. https://doi.org/10.1016/j.enggeo.2012.05.004

Daramola, O. (1978). The influence of stress-history on the deformation of a sand, PhD thesis, University of London.

Das, B. M., & Sivakugan, N. (2016). *Fundamentals of geotechnical engineering*. Cengage Learning.

Delage, P., Marcial, D., Cui, Y. J., & Ruiz, X. (2006). Ageing effects in a compacted bentonite: a microstructure approach, *Géotechnique*, *56*(5), 291-304. https://doi.org/10.1680/geot.2006.56.5.291

Demirbas, A. (2011). Waste management, waste resource facilities and waste conversion processes, *Energy Conversion and Management*, *52*(2), 1280-1287. https://doi.org/10.1016/j.enconman.2010.09.025

Deng, Y., Zhang, T., Cui, Y., Chen, Y., Deng, T., & Zhou, X. (2018). Pore water salinity effect on the intrinsic compression behaviour of artificial soft soils, *Applied Clay Science*, *166*, 299-306. https://doi.org/10.1016/j.clay.2018.09.027

Disfani, M. M., Arulrajah, A., Bo, M. W., & Hankour, R. J. W. M. (2011). Recycled crushed glass in road work applications, *Waste Management*, *31*(11), 2341-2351. https://doi.org/10.1016/j.wasman.2011.07.003

Disfani, M. M., Arulrajah, A., Bo, M. W., & Sivakugan, N. (2012). Environmental risks of using recycled crushed glass in road applications, *Journal of Cleaner Production*, *20*(1). 170-179. https://doi.org/10.1016/j.jclepro.2011.07.020

Disfani, M. M., Arulrajah, A., Suthagaran, V., & Bo, M. W. (2009). Geotechnical characteristics of recycled glass-biosolid mixtures, *In Proceedings of the 17th International Conference on Soil Mechanics and Geotechnical Engineering*, Alexandria, Egypt, 5-9. https://doi.org/10.3233/978-1-60750-031-5-201

Dutta, J., & Mishra, A. K. (2016). Consolidation behaviour of bentonites in the presence of salt solutions, *Applied Clay Science*, *120*, 61-69. https://doi.org/10.1016/j.clay.2015.12.001

Dyvik, R., & Madshus, C. (1985). Lab measurements of Gmax using bender elements. Proc. ASCE Annual Convention on Advances in the Art of Testing Soils under Cyclic Conditions, Detroit, MI, 186–196.

Dyvik, R., & Olsen, T. S. (1989). Gmax measured in consolidation and DSS tests using bender elements. Proc. Proceedings of the 12th International Conference on Soil Mechanics and Foundation Engineering, 1, 39–42.

El Mohtar, C. S., Bobet, A., Drnevich, V. P., Johnston, C. T., & Santagata, M. C. (2014). Pore pressure generation in sand with bentonite: from small strains to liquefaction, *Géotechnique*, *64*(2), 108-117. https://doi.org/10.1680/geot.12.P.169

El Mountassir, G., Sánchez, M., & Romero, E. (2014). An experimental study on the compaction and collapsible behaviour of a flood defence embankment fill, *Engineering Geology*, *179*, 132-145. https://doi.org/10.1016/j.enggeo.2014.06.023

Eriksson, O., Reich, M. C., Frostell, B., Björklund, A., Assefa, G., Sundqvist, J. O., Granath, J., Baky, A., & Thyselius, L. (2005). Municipal solid waste management from a systems perspective, *Journal of Cleaner Production*, *13*(3), 241-252. https://doi.org/10.1016/j.jclepro.2004.02.018

Fauzi, A., Djauhari, Z., & Fauzi, U. J. (2016). Soil engineering properties improvement by utilization of cut waste plastic and crushed WG as additive, *International Journal of Engineering and Technology*, *8*(1), 15.

Fell, R., MacGregor, P., & Stapledon, D. (1992). Geotechnical engineering of embankment dams (p. 675). Rotterdam: Balkema.

Fredlund, D. G., Rahardjo, H., & Fredlund, M. D. (2012) Unsaturated Soil Mechanics in Engineering Practice. John Wiley & Sons, Hoboken,

Garlanger, J. E. (1972) The consolidation of soils exhibiting creep under constant effective stress. *Geotechnique*, *22*(1), 71–78. https://doi.org/10.1680/geot.1972.22.1.71

Gasparre, A., Nishimura S., Minh N. A., Coop M. R., & Jardine R. J. (2007). The stiffness of natural london clay. *Géotechnique*, *57*(1), 33-47. https://doi.org/10.1680/geot.2007.57.1.33

Geng, Y, Fu J, Sarkis, J, & Xue, B., (2012) Towards a national circular economy indicator system in China: an evaluation and critical analysis, *Journal of Cleaner Production*, *23*(1), 216-224. https://doi.org/10.1016/j.jclepro.2011.07.005

Georgiannou, V. N. (2006). The undrained response of sands with additions of particles of various shapes and sizes. *Géotechnique*, *56*(9), 639-649.

Georgiannou, V. N., Burland, J. B., & Hight, D. W. (1990). The undrained behaviour of clayey sands in triaxial compression and extension. *Geotechnique*, *40*(3), 431-449.

Goto, S., Tatsuoka, F., Shibuya, S., Kim, Y., & Sato, T. (1991). A simple gauge for local small strain measurements in the laboratory, *Soils and Foundations*, *31*(1), 169-180. https://doi.org/10.3208/sandf1972.31.169

Goudarzy, M., Sarkar, D., Lieske, W., & Wichtmann, T. (2021). Influence of plastic fines content on the liquefaction susceptibility of sands: monotonic loading, *Acta Geotechnica*, 1-19. https://doi.org/10.1007/s11440-021-01283-w

Grubb, D. G., Gallagher, P. M., Wartman, J., Liu, Y., & Carnivale III, M. (2006). Laboratory evaluation of crushed glass–dredged material blends, *Journal of*

Geotechnical and Geoenvironmental Engineering, *132*(5), 562-576. https://doi.org/10.1061/(ASCE)1090-0241(2006)132:5(562)

Gu, X. Q., & Yang, J. (2013). A discrete element analysis of elastic properties of granular materials. *Granular Matter*, *15*(2), 139-147. https://doi.org/10.1007/s10035-013-0390-3

Gupt, C. B., Bordoloi, S., Sahoo, R. K., & Sekharan, S. (2021). Mechanical performance and micro-structure of bentonite-fly ash and bentonite-sand mixes for landfill liner application, *Journal of Cleaner Production*, *292*, 126033. https://doi.org/10.1016/j.jclepro.2021.126033

Hansbo, S. (1957). New approach to the determination of the shear strength of clay by the fall-cone test.

Harrou, A., Gharibi, E. K., Taha, Y., Fagel, N., & El Ouahabi, M. (2020). Phosphogypsum and black steel slag as additives for ecological bentonite-based materials: Microstructure and characterization, *Minerals*, *10*(12), 1067. https://doi.org/10.3390/min10121067

He, H., Payan, M., & Senetakis K. (2021). The behaviour of a recycled road base aggregate and quartz sand with bender/extender element tests under variable stress states, *European Journal of Environmental and Civil Engineering*, *25*(1): 152-169. https://doi.org/10.1080/19648189.2018.1521749

Hird, C. C., & Yung, P. C. Y. (1989). The use of proximity transducers for local strain measurements in triaxial tests, *Geotechnical Testing Journal*, *12*(4), 292-296.

Ibrahim, H. H., Mawlood, Y. I., & Alshkane, Y. M. (2019). Using WG powder for stabilizing high-plasticity clay in Erbil city-Iraq, *International Journal of Geotechnical Engineering*, 1-8. https://doi.org/10.1080/19386362.2019.1647644

Ikara, I. A., Kundiri, A. M., & Mohammed, A. (2015). Effects of WG (WG) on the Strength Characteristics of Cement Stabilized Expansive Soil, *American Journal of Engineering Research*, *4*, 33-41.

Ishihara, K. (1993). Liquefaction and flow failure during earthquakes, The 33rd Rankine Lecture. *Geotechnique, 43*(3), 351–415.

Ishihara, K., Tatsuoka, F., & Yasuda, S. (1975). Undrained deformation and liquefaction of sand under cyclic stresses, *Soils and Foundations*, *15*(1), 29-44. https://doi.org/10.3208/sandf1972.15.29

Jalal, F. E., Mulk, S., Memon, S. A., Jamhiri, B., & Naseem, A. (2021). Strength, hydraulic, and microstructural characteristics of expansive soils incorporating marble dust and rice husk ash, *Advances in Civil Engineering*, 2021, 1-18. https://doi.org/10.1155/2021/9918757

Jardine, R. J. (1991). Some practical applications of a non-linear ground model, In Proc. of 10th European Regional Conference on SMFE, Firenze, 1991, 223-228.

Jardine, R. J. (1992). Some observations on the kinematic nature of soil stiffness, *Soils and Foundations*, *32*(2), 111-124. https://doi.org/10.3208/sandf1972.32.2_111

Jardine, R. J., Fourie, A., Maswoswe, J., & Burland, J. B. (1985). Field and laboratory measurements of soil stiffness. In *International conference on soil mechanics and foundation engineering, 11*, 511-514.

Jardine, R. J., Symes, M. J., & Burland, J. B. (1984). The measurement of soil stiffness in the triaxial apparatus, *Géotechnique*, *34*(3), 323-340. https://doi.org/10.1680/geot.1984.34.3.323

Johnson, K. L., & Johnson, K. L. (1987). Contact mechanics. Cambridge university press.

Kang, X., & Bate, B. (2016). Shear wave velocity and its anisotropy of polymer modified high-volume class-F fly ash–kaolinite mixtures, *Journal of Geotechnical and Geoenvironmental Engineering*, *142*(12), 04016068. https://doi.org/10.1061/(ASCE)GT.1943-5606.0001562

Karakan, E., & Demir, S. (2018). Effect of fines content and plasticity on undrained shear strength of quartz-clay mixtures. *Arabian Journal of Geosciences*, *11*, 1-12. https://doi.org/10.1007/s12517-018-4114-1

Kaza, S., Yao, L., Bhada-Tata, P., & Van Woerden, F. (2018). What a waste 2.0: a global snapshot of solid waste management to 2050.

Kazmi, D., Serati, M., Williams, D. J., Qasim, S., & Cheng, Y. P. (2021). The potential use of crushed WG as a sustainable alternative to natural and manufactured sand in geotechnical applications, *Journal of Cleaner Production*, *284*, 124762. https://doi.org/10.1016/j.jclepro.2020.124762

Khan, M. S., Tufail, M., & Mateeullah, M. (2018). Effects of WG powder on the geotechnical properties of loose subsoils, *Civil Engineering Journal*, *4*(9), 2044-2051.

Khatib, J. (2016). Sustainability of construction materials. Woodhead Publishing.

Kordnaeij, A., Moayed, R. Z., Soleimani, M. (2019). Shear wave velocity of zeolite-cement grouted sands, *Soil Dynamics and Earthquake Engineering*, *122*, 196-210. https://doi.org/10.1016/j.soildyn.2019.03.026

Kuerbis, R. H., & Vaid, Y. P. 1989. Undrained behaviour of clean and silty sands. In Proceedings of Discussion Session on Influence of Local Conditions on Seismic Response. 12th International Conference on Soil Mechanics and Foundation Engineering, Rio de Janeiro. Eclirecl by the ICSMFE Committee. A.A. Balkema, Rotterdam. pp. 91-100.

Kumar, G. V., & Wood M. D. (1999) Fall cone and compression tests on clay–gravel mixtures. *Geotechnique*, *49*(6), 727–739. https://doi.org/10.1680/geot.1999.49.6.727

Kumar, J., & Madhusudhan B. N. 2010. Effect of relative density and confining pressure on Poisson ratio from bender and extender elements tests, *Géotechnique*, *60* (7), 561-567. https://doi.org/10.1680/geot.9.T.003

Kumar, S. S., Dey, A., & Murali Krishna, A. (2021). Evaluation of monotonic and dynamic shear modulus of sand using on-sample transducers in cyclic triaxial apparatus, *Acta Geotechnica*, *16*, 221-236. https://doi.org/10.1007/s11440-020-01035-2

Kwa, K. A., & Airey, D. W. (2017). Effects of fines on liquefaction behaviour in well-graded materials, *Canadian Geotechnical Journal*, *54*(10), 1460-1471. https://doi.org/10.1139/cgj-2017-0016

Lade, P. V., & Yamamuro, J. A. (1997). Effects of nonplastic fines on static liquefaction of sands, *Canadian Geotechnical Journal*, *34*(6), 918-928. https://doi.org/10.1139/t97-052

Lade, P. V., Yamamuro, J. A., & Liggio Jr, C. D. (2009). Effects of fines content on void ratio, compressibility, and static liquefaction of silty sand, *Geomechanics and Engineering*, *1*(1), 1-15.

Lancellotta, R. (2008). Geotechnical engineering. CRC Press.

Le, T. M., Fatahi, B., & Khabbaz, H. (2012). Viscous behaviour of soft clay and inducing factors. *Geotechnical and Geological Engineering*, *30*, 1069-1083. https://doi.org/10.1007/s10706-012-9535-0

Lee, J. S., & Santamarina. J. C. 2005. Bender elements: performance and signal interpretation, *Journal of Geotechnical and Geoenvironmental Engineering*, *131*(9): 1063-1070. https://doi.org/10.1061/(ASCE)1090-0241(2005)131:9(1063)

Lee, P. Y. (1976). Study of irregular compaction curves, *ASTM International*, 278-288.

Lee, P. Y., & Hsu, D. C. (1973). Temperature effect on irregularly shaped compaction curves of soils, *Highway Research Record*, 438.

Lee, P. Y., & Suedkamp, R. J. (1972). Characteristics of irregularly shaped compaction curves of soils, *Highway Research Record*, *381*, 1-9.

Likos, W. J. (2000). Total suction-moisture content characteristics for expansive soils, *2000-2009-Mines Theses & Dissertations*.

Likos, W. J., & Jaafar, R. (2014). Laboratory fall cone testing of unsaturated sand. *Journal of Geotechnical and Geoenvironmental Engineering*, *140*(8), 04014043. https://doi.org/10.1061/(ASCE)GT.1943-5606.0001143

Lings, M. L., & Greening, P. D. (2001). A novel bender/extender element for soil testing, *Géotechnique*, *51*(8), 713-717. https://doi.org/10.1680/geot.2001.51.8.713

Liu, X., Zou, D., Liu, J., Zhou, C., & Zheng, B. (2020). Experimental study to evaluate the effect of particle size on the small strain shear modulus of coarse-grained soils. *Measurement*, *163*, 107954. https://doi.org/10.1016/j.measurement.2020.107954

Lu, N., & Likos. W. J. (2004). Unsaturated soil mechanics. New York: Wiley

Lupini, J. F., Skinner, A. E., & Vaughan, P. R. (1981). The drained residual strength of cohesive soils. *Geotechnique*, *31*(2), 181-213.

Mahmoudi, Y., Cherif Taiba, A., Belkhatir, M., Arab, A., & Schanz, T. (2018). Laboratory study on undrained shear behaviour of overconsolidated sand–silt mixtures: effect of the fines content and stress state, *International Journal of Geotechnical Engineering*, *12*(2), 118-132. https://doi.org/10.1080/19386362.2016.1252140

Mahmoudi, Y., Cherif Taiba, A., Belkhatir, M., Baille, W., & Wichtmann, T. (2022b). Characterization of mechanical behavior of binary granular assemblies through the equivalent void ratio and equivalent state parameter, *European Journal of Environmental and Civil Engineering*, *26*(7), 2869-2897. https://doi.org/10.1080/19648189.2020.1775708

Mahmoudi, Y., Cherif Taiba, A., Hazout, L., & Belkhatir, M. (2022a). Comprehensive laboratory study on stress–strain of granular soils at constant global void ratio: combined effects of fabrics and silt content, *Acta Geotechnica*, *17*(8), 3269-3292. https://doi.org/10.1007/s11440-022-01480-1

Mair, R. J. (1993). Developments in geotechnical engineering research: applications to tunnels and deep excavations. Unwin Memorial Lecture, *Proceedings of the Institution of Civil Engineers - Civil Engineering*, 1, 27–41.

Marcial, D., Delage, P., & Cui, Y. J. (2002). On the high stress compression of bentonites, *Canadian Geotechnical Journal*, *39*(4), 812-820. https://doi.org/10.1139/t02-019

Miller, S. A., John, V. M., Pacca, S. A., & Horvath, A. (2018). Carbon dioxide reduction potential in the global cement industry by 2050, *Cement and Concrete Research*, *114*, 115-124. https://doi.org/10.1016/j.cemconres.2017.08.026

Mitchell, J. K., & Soga, K. (2005). Fundamentals of soil behavior (Vol. 3, p. USA). New York: John Wiley & Sons.

Modarres, A., & Nosoudy, Y. M. (2015). Clay stabilization using coal waste and lime—Technical and environmental impacts, *Applied Clay Science*, *116*, 281-288. https://doi.org/10.1016/j.clay.2015.03.026

Mohamad, R., & Dobry, R. (1986). Undrained monotonic and cyclic triaxial strength of sand, *Journal of Geotechnical Engineering*, *112*(10), 941-958. https://doi.org/10.1061/(ASCE)0733-9410(1986)112:10(941)

Mohammadi, A., & Qadimi, A. (2015). A simple critical state approach to predicting the cyclic and monotonic response of sands with different fines contents using the equivalent intergranular void ratio, *Acta Geotechnica*, *10*(5), 587-606. https://doi.org/10.1007/s11440-014-0318-z

Mohammed, M. K., Al-Hadithi, A. I., & Mohammed, M. H. (2019). Production and optimization of eco-efficient self compacting concrete SCC with limestone and PET, *Construction and Building Materials*, *197*, 734-746. https://doi.org/10.1016/j.conbuildmat.2018.11.189

Mollamahmutoglu, M., & Yilmaz, Y. (2001). Potential use of fly ash and bentonite mixture as liner or cover at waste disposal areas, *Environmental Geology*, *40*(11), 1316-1324. https://doi.org/10.1007/s002540100355

Monkul, M. M., & Ozden, G. (2007). Compressional behavior of clayey sand and transition fines content, *Engineering Geology*, *89*(3-4), 195-205. https://doi.org/10.1016/j.enggeo.2006.10.001

Morselli, L., De Robertis, C., Luzi, J., Passarini, F., & Vassura, I. (2008). Environmental impacts of waste incineration in a regional system (Emilia Romagna, Italy) evaluated from a life cycle perspective, *Journal of Hazardous Materials*, *159*(2-3), 505-511. https://doi.org/10.1016/j.jhazmat.2008.02.047

Mujah, D., Ahmad, F., Hazarika, H., & Safari, A. (2013). Evaluation of the mechanical properties of recycled glass fibers-derived three dimensional geomaterial for ground improvement, *Journal of Cleaner Production*, *52*, 495-503. https://doi.org/10.1016/j.jclepro.2013.03.035

Mukherjee, K., & Mishra, A. K. (2020). Undrained performance of sustainable compacted sand-bentonite–glass fiber composite for landfill application, *Journal of Cleaner Production*, *244*, 118662. https://doi.org/10.1016/j.jclepro.2019.118662

Mukherjee, K., & Mishra, A. K. (2021a). Impact of glass fibre on hydromechanical behaviour of compacted sand–bentonite mixture for landfill application, *European Journal of Environmental and Civil Engineering*, *25*(7), 1179-1200. https://doi.org/10.1080/19648189.2019.1572541

Mukherjee, K., & Mishra, A. K. (2021b). Recycled waste tire fiber as a sustainable reinforcement in compacted sand–bentonite mixture for landfill application, *Journal of Cleaner Production*, *329*, 129691. https://doi.org/10.1016/j.jclepro.2021.129691

Murray, H. H. (1991). Overview—clay mineral applications. *Applied clay science*, *5*(5-6), 379-395. https://doi.org/10.1016/0169-1317(91)90014-Z

Murthy, T. G., Loukidis, D., Carraro, J. A. H., Prezzi, M., & Salgado, R. (2007). Undrained monotonic response of clean and silty sands, *Géotechnique*, *57*(3), 273-288. https://doi.org/10.1680/geot.2007.57.3.273

Nevels Jr, J. B. (1993). Dispersive clay embankment erosion: a case history. Transportation Research Record, (1406).

Ni, Q. T. S. T., Tan, T. S., Dasari, G. R., & Hight, D. W. (2004). Contribution of fines to the compressive strength of mixed soils. *Géotechnique*, *54*(9), 561-569.

Oh, W. T., & Vanapalli, S. K. (2011). Relationship between Poisson's ratio and soil suction for unsaturated soils. In Proc., 5th Asia-Pacific Conf. on Unsaturated Soils (pp. 239-245). Bangkok, Thailand: Kasetsart Univ.

Oh, W. T., & Vanapalli, S. K. (2018). Modeling the stress versus settlement behavior of shallow foundations in unsaturated cohesive soils extending the modified total stress approach, Soils and Foundations, *58*(2), 382-397. https://doi.org/10.1016/j.sandf.2018.02.008

Ohsaki, Y., & Iwasaki. R. (1973). On dynamic shear moduli and Poisson's ratios of soil deposits, Soils and Foundations, *13*(4): 61-73. https://doi.org/10.3208/sandf1972.13.4_61

Olson, R. E. (1963). Effective stress theory of soil compaction, *Journal of the Soil Mechanics and Foundations Division*, *89*(2), 27-45. https://doi.org/10.1061/JSFEAQ.0000503

Olufowobi, J., Ogundoju, A., Michael, B., & Aderinlewo, O. (2014). Clay soil stabilisation using powdered glass, *Journal of Engineering Science and Technology*. *9*(5), 541-558.

Ooi, P. S., Li, M. M., Sagario, M. L., & Song, Y. (2008). Shear strength characteristics of recycled glass, *Transportation Research Record*, *2059*(1), 52-62. https://doi.org/10.3141/2059-06

Ouhadi, V. R., & Goodarzi, A. R. (2006). Assessment of the stability of a dispersive soil treated by alum. *Engineering Geology*, *85*(1-2), 91-101. https://doi.org/10.1016/j.enggeo.2005.09.042

Ozhan, H. O. (2021). Determination of mechanical and hydraulic properties of polyacrylamide-added bentonite-sand mixtures, *Bulletin of Engineering Geology and the Environment*, *80*(3), 2557-2571. https://doi.org/10.1007/s10064-020-02062-9

Pan, S. Y., Du, M. A., Huang, I. T., Liu, I. H., Chang, E. E., & Chiang, P. C. (2015). Strategies on implementation of waste-to-energy (WTE) supply chain for circular economy system: a review, *Journal of Cleaner Production*, *108*, 409-421. https://doi.org/10.1016/j.jclepro.2015.06.124

Papo, A., Piani, L., & Ricceri, R. (2010). Rheological properties of very high-strength Portland cement pastes: influence of very effective superplasticizers, *International Journal of Chemical Engineering*, 2010. https://doi.org/10.1155/2010/682914

Patel, A., Ingale, R., & Bhanarkar, K. B. (2018). Effect of compaction states and the confining pressure on Poisson's ratio of stratified and non-stratified soils, *Arabian Journal for Science and Engineering*, *43*, 1983-1999. https://doi.org/10.1007/s13369-017-2846-y

Patel, S. K., & Singh, B. (2017). Experimental Investigation on the Behaviour of Glass Fibre-Reinforced Cohesive Soil for Application as Pavement Subgrade Material, *International Journal of Geosynthetics and Ground Engineering*, *3*(2), 13. https://doi.org/10.1007/s40891-017-0090-x

Patel, S. K., & Singh, B. (2019). Shear strength response of glass fibre-reinforced sand with varying compacted relative density, *International Journal of Geotechnical Engineering*, *13*(4), 339-351. https://doi.org/10.1080/19386362.2017.1352157

Pillai, R. G., Gettu, R., Santhanam, M., Rengaraju, S., Dhandapani, Y., Rathnarajan, S., & Basavaraj, A. S. (2019). Service life and life cycle assessment of reinforced concrete systems with limestone calcined clay cement (LC3). *Cement and Concrete Research*, *118*, 111-119. https://doi.org/10.1016/j.cemconres.2018.11.019

Pitman, T. D., Robertson, P. K., & Sego, D. C. (1994). Influence of fines on the collapse of loose sands, *Canadian Geotechnical Journal*, *31*(5), 728-739. https://doi.org/10.1139/t94-084

Porcino, D. D., Diano, V., Triantafyllidis, T., & Wichtmann, T. (2020). Predicting undrained static response of sand with non-plastic fines in terms of equivalent granular state parameter. *Acta Geotechnica*, *15*(4), 867-882. https://doi.org/10.1007/s11440-019-00770-5

Quinonez Samaniego, R. A., Scheuermann Filho, H. C., de Araújo, M. T., Bruschi, G. J., Festugato, L., & Consoli, N. C. (2023). Key parameters controlling strength and resilient modulus of a stabilised dispersive soil. *Road Materials and Pavement Design*, *24*(1), 279-294. https://doi.org/10.1080/14680629.2021.2013937

Rahman, M. M. (2009). Modelling the influence of fines on liquefaction behaviour. University of New South Wales, Australian Defence Force Academy, School of Engineering and Information Technology.

Rahman, M. M., Lo, S. R., & Gnanendran, C. T. (2008). On equivalent granular void ratio and steady state behaviour of loose sand with fines, *Canadian Geotechnical Journal*, *45*(10), 1439-1456. https://doi.org/10.1139/T08-064

Rawat, M., Singh, U. K., Mishra, A. K., & Subramanian, V. (2008). Methane emission and heavy metals quantification from selected landfill areas in India, *Environmental Monitoring and Assessment*, *137*(1-3), 67-74. https://doi.org/10.1007/s10661-007-9729-8

Ren, Q., Tao, Y., Jiao, D., Jiang, Z., Ye, G., & De Schutter, G. (2021). Plastic viscosity of cement mortar with manufactured sand as influenced by geometric features and particle size, *Cement and Concrete Composites*, *122*, 104163. https://doi.org/10.1016/j.cemconcomp.2021.104163

Richards, K. S., & Reddy, K. R. (2007). Critical appraisal of piping phenomena in earth dams. *Bulletin of Engineering Geology and the Environment*, *66*, 381-402. https://doi.org/10.1007/s10064-007-0095-0

Roscoe, K. H., Schofield, A., & Wroth, A. P. (1958). On the yielding of soils, *Geotechnique*, *8*(1), 22-53. https://doi.org/10.1680/geot.1958.8.1.22

Ruan, B., Miao, Y., Cheng, K., & Yao, E. L. (2021). Study on the small strain shear modulus of saturated sand-fines mixtures by bender element test. *European Journal of Environmental and Civil Engineering*, *25*(1), 28-38. https://doi.org/10.1080/19648189.2018.1513870

Sabbar, A. S., Chegenizadeh, A., & Nikraz, H. (2017). Static liquefaction of very loose sand–slag–bentonite mixtures, *Soils and Foundations*, *57*(3), 341-356. https://doi.org/10.1016/j.sandf.2017.05.003

Saberian, M., Li, J., & Cameron, D. (2019). Effect of crushed glass on behavior of crushed recycled pavement materials together with crumb rubber for making a clean green base and subbase, *Journal of Materials in Civil Engineering*, *31*(7), 04019108. https://doi.org/10.1061/(ASCE)MT.1943-5533.0002765

Sadeghi, H., Kiani, M., Sadeghi, M., & Jafarzadeh, F. (2019). Geotechnical characterization and collapsibility of a natural dispersive loess. *Engineering Geology*, *250*, 89-100. https://doi.org/10.1016/j.enggeo.2019.01.015

Sakai, S. I., Yoshida, H., Hirai, Y., Asari, M., Takigami, H., Takahashi, S., ... & Chi, N. K. (2011). International comparative study of 3R and waste management policy developments. *Journal of Material Cycles and Waste Management*, *13*, 86-102. https://doi.org/10.1007/s10163-011-0009-x

Salamatpoor, S., & Salamatpoor, S. (2017). Evaluation of adding crushed glass to different combinations of cement-stabilized sand, *International Journal of Geo-Engineering*, *8*(1), 1-12. https://doi.org/10.1186/s40703-017-0044-0

Santamarina, J. C. (2003). Soil behavior at the microscale: particle forces. In Soil behavior and soft ground construction (pp. 25-56). https://doi.org/10.1061/40659(2003)2

Sawangsuriya, A., Fall, M., & Fratta, D. (2008). Wave-based techniques for evaluating elastic modulus and Poisson's ratio of laboratory compacted lateritic soils, *Geotechnical and Geological Engineering*, *26*, 567-578. https://doi.org/10.1007/s10706-008-9190-7

Shaikh, S. M., Nasser, M. S., Hussein, I. A., & Benamor, A. (2017). Investigation of the effect of polyelectrolyte structure and type on the electrokinetics and flocculation behavior of bentonite dispersions, *Chemical Engineering Journal*, *311*, 265-276. https://doi.org/10.1016/j.cej.2016.11.098

Sharma, L. K., Singh, R., Ahmad, M., Umrao, R. K., & Singh, T. N. (2017, June). Experimental Evaluation of Geomechanical Behaviour of Bentonite-Sand Mixture for Nuclear Waste Disposal, In *ISRM European Rock Mechanics Symposium-EUROCK 2017*. OnePetro.

Shen, Y., Zhu, Y., Liu, H., Li, A., & Ge, H. (2018). Macro-meso effects of gradation and particle morphology on the compressibility characteristics of calcareous sand, *Bulletin of Engineering Geology and the Environment*, *77*(3), 1047-1055. https://doi.org/10.1007/s10064-017-1157-6

Shi, J., Haegeman, W., & Xu, T. (2020). Effect of non-plastic fines on the anisotropic small strain stiffness of a calcareous sand, *Soil Dynamics and Earthquake Engineering*, *139*, 106381. https://doi.org/10.1016/j.soildyn.2020.106381

Shirley, D. J. (1978). An improved shear wave transducer. *The Journal of the Acoustical Society of America*, *63*(5), 1643-1645. https://doi.org/10.1121/1.381866

Silva, J. P. D. S., Cacciari, P. P., Ribeiro, L. F., & Jefferies, M. (2022). Influence of compaction on small-strain shear modulus of iron ore tailings, *Proceedings of the Institution of Civil Engineers-Geotechnical Engineering*, *175*(2), 247-260. https://doi.org/10.1680/jgeen.21.00036

Simoni, A., & Houlsby, G. T. (2006). The direct shear strength and dilatancy of sand–gravel mixtures, *Geotechnical & Geological Engineering*, *24*(3), 523-549. https://doi.org/10.1007/s10706-004-5832-6

Simpson, B. (1992). Thirty-second Rankine Lecture: Retaining structures: displacement and design, *Geotechnique*, *42*(4), 541-576. https://doi.org/10.1680/geot.1992.42.4.541

Simpson, B., O'riordan, N. J., & Croft, D. D. (1979). A computer model for the analysis of ground movements in London Clay, *Géotechnique*, *29*(2), 149-175. https://doi.org/10.1680/geot.1979.29.2.149

Singh, J., Laurenti, R., Sinha, R., & Frostell, B. (2014). Progress and challenges to the global waste management system, *Waste Management Research*, *32*(9), 800-812. https://doi.org/10.1177/0734242X14537868

Skempton, A. W., & Jones, O. T. (1944). Notes on the compressibility of clays, *Quarterly Journal of the Geological Society*, *100*(1-4), 119-135. https://doi.org/10.1144/GSL.JGS.1944.100.01-04.08

Sobolev, K., Türker, P., Soboleva, S., & Iscioglu, G. (2007). Utilization of WG in ECO-cement: strength properties and microstructural observations, *Waste Management*, *27*(7), 971-976. https://doi.org/10.1016/j.wasman.2006.07.014

Sridharan, A, & Nagaraj, H. B., (1999). Absorption water content and liquid limit of soils. *Geotechnical Testing Journal*, *22*(2), 127-133.

Sridharan, A., & Nagaraj, H. B. (2000). Compressibility behaviour of remoulded, fine-grained soils and correlation with index properties, *Canadian Geotechnical Journal, 37*(3), 712-722. https://doi.org/10.1139/t99-128

Sun, W. J., Wei, Z. F., Sun, D. A., Liu, S. Q., Fatahi, B., &Wang, X. Q. (2015). Evaluation of the swelling characteristics of bentonite–sand mixtures. *Engineering Geology*, *199*, 1-11. https://doi.org/10.1016/j.enggeo.2015.10.004

Tan, R. B., & Khoo, H. H. (2006). Impact assessment of waste management options in Singapore, *Journal of the Air Waste Management Association*, *56*(3), 244-254. https://doi.org/10.1080/10473289.2006.10464463

Terzaghi, K. (1941) Undisturbed clay samples and undisturbed clays. *Journal of the Boston Society of Civil Engineers*, *29*(3), 211–231

Thevanayagam, S. (1998). Effect of fines and confining stress on undrained shear strength of silty sands, *Journal of Geotechnical and Geoenvironmental Engineering*, *124*(6), 479-491. https://doi.org/10.1061/(ASCE)1090-0241(1998)124:6(479)

Thevanayagam, S. (2000). Liquefaction potential and undrained fragility of silty soils. In *proceedings of the 12th world conference earthquake engineering*. New Zealand Society of Earthquake Engineering, Wellington, New Zealand.

Thevanayagam, S., & Mohan, S. (2000). Intergranular state variables and stress–strain behaviour of silty sands, *Geotechnique*, *50*(1), 1-23. https://doi.org/10.1680/geot.2000.50.1.1

Thevanayagam, S., Shenthan, T., Mohan, S., & Liang, J. (2002). Undrained fragility of clean sands, silty sands, and sandy silts. *Journal of Geotechnical and Geoenvironmental Engineering*, *128*(10), 849-859. https://doi.org/10.1061/(ASCE)1090-0241(2002)128:10(849)

Ural, N. (2018). The importance of clay in geotechnical engineering (p. 83). London, UK: IntechOpen.

Uyanık, O. (2019). Estimation of the porosity of clay soils using seismic P-and S-wave velocities. *Journal of Applied Geophysics*, *170*, 103832. https://doi.org/10.1016/j.jappgeo.2019.103832

Vadlamudi, S., & Mishra, A. K. (2018). Consolidation characteristics of sand–bentonite mixtures and the influence of sand particle size, *Journal of Hazardous, Toxic, and Radioactive Waste*, *22*(4), 06018001. https://doi.org/10.1061/(ASCE)HZ.2153-5515.0000409

Vallejo, L. E., & Lobo-Guerrero, S. (2005). The elastic moduli of clays with dispersed oversized particles, *Engineering Geology*, *78*(1-2), 163-171. https://doi.org/10.1016/j.enggeo.2004.12.003

Van Impe, W. F. (1989). Soil improvement techniques and their evolution. Balkema, Rotterdam, the Netherlands, 110-111.

Villar, M. V. (2021). Thermo-hydro-mechanical characterisation of a bentonite from Cabo de Gata. A study applied to the use of bentonite as sealing material in high level radioactive waste repositories.

Villar, M. V., Iglesias, R. J., García-Siñeriz, J. L., Lloret, A., & Huertas, F. (2020). Physical evolution of a bentonite buffer during 18 years of heating and hydration. *Engineering Geology*, *264*, 105408. https://doi.org/10.1016/j.enggeo.2019.105408

Wakeling, T. R. (1970). A Comparison of the results of standard site investigations methods against the results of a detailed geotechnical investigation in middle chalk at mundford, norfolk.

Wang, D. W., Zhu, C., Tang, C. S., Li, S. J., Cheng, Q., Pan, X. H., & Shi, B. (2021). Effect of sand grain size and boundary condition on the swelling behavior of bentonite–sand mixtures, *Acta Geotechnica*, *16*(9), 2759-2773. https://doi.org/10.1007/s11440-021-01194-w

Wang, F. C., Feng, X. N., Gong, H., & Zhao, H. Y. (2017). Study of permeability of glass-sand soil, *Archives of Civil Engineering*, *63*(3), 175-190. https://doi.org/10.1515/ace-2017-0036

Wang, J. (2010). High-level radioactive waste disposal in China: update 2010. *Journal of Rock Mechanics and Geotechnical Engineering*, *2*(1), 1-11. https://doi.org/10.3724/SP.J.1235.2010.00001

Wang, T., Liu, S., Wautier, A., & Nicot, F. (2022). Updated skeleton void ratio for gravelly sand mixtures considering effect of grain-size distribution, *Canadian Geotechnical Journal*, *59*(1), 12-23. https://doi.org/10.1139/cgj-2020-0570

Wang, Y., Benahmed, N., Cui, Y. J., & Tang, A. M. (2017b). A novel method for determining the small-strain shear modulus of soil using the bender elements technique, *Canadian Geotechnical Journal*, *54*(2), 280-289. https://doi.org/10.1139/cgj-2016-0341

Wartman, J., Grubb, D. G., & Nasim, A. S. M. (2004a). Select engineering characteristics of crushed glass, *Journal of Materials in Civil Engineering*, *16*(6), 526-539. https://doi.org/10.1061/(ASCE)0899-1561(2004)16:6(526)

Wartman, J., Grubb, D. G., & Strenk, P. (2004b). Engineering properties of crushed glass-soil blends. In Geotechnical engineering for transportation projects, 732-739.

Watabe, Y., Sassa, S., Kaneko, T., & Nakata, Y. (2017). Mechanical characteristics of undisturbed coral gravel soils: The intergranular void ratio as a common governing parameter. *Soils and Foundations*, *57*(5), 760-775. https://doi.org/10.1016/j.sandf.2017.08.007

Xiang, G. S., Ye, W. M., Zhou, Y., & Jalal, F. E. (2021). Combined effects of temperature and salt solution on swelling of GMZ01 bentonite–sand mixtures, *Bulletin of Engineering Geology and the Environment*, *80*(9), 6677-6688. https://doi.org/10.1007/s10064-021-02342-y

Xu, Y., Zeng, Z., & Lv, H. (2019). Temperature dependence of apparent thermal conductivity of compacted bentonites as buffer material for high-level radioactive waste repository. *Applied Clay Science*, *174*, 10-14. https://doi.org/10.1016/j.clay.2019.03.017

Yaghoubi, E., Arulrajah, A., Yaghoubi, M., & Horpibulsuk, S. (2020). Shear strength properties and stress–strain behavior of waste foundry sand, *Construction and Building Materials*, *249*, 118761. https://doi.org/10.1016/j.conbuildmat.2020.118761

Yamamuro, J. A., & Lade, P. V. (1997). Static liquefaction of very loose sands, *Canadian Geotechnical Journal*, *34*(6), 905-917. https://doi.org/10.1139/t97-057

Yamamuro, J. A., & Lade, P. V. (1998). Steady-state concepts and static liquefaction of silty sands, *Journal of Geotechnical and Geoenvironmental Engineering*, *124*(9), 868-877. https://doi.org/10.1061/(ASCE)1090-0241(1998)124:9(868)

Yang, J., & Wei, L. M. (2012). Collapse of loose sand with the addition of fines: the role of particle shape, *Géotechnique*, *62*(12), 1111-1125. https://doi.org/10.1680/geot.11.P.062

Yang, J., Wei, L. M., & Dai, B. B. (2015). State variables for silty sands: Global void ratio or skeleton void ratio?, *Soils and Foundations*, *55*(1), 99-111. https://doi.org/10.1016/j.sandf.2014.12.008

Yong, R. N., Boonsinsuk, P., & Wong, G. (1986). Formulation of backfill material for a nuclear fuel waste disposal vault, *Canadian Geotechnical Journal*, *23*(2), 216-228. https://doi.org/10.1139/t86-031

Yuan, C., & Chareyre, B. (2022). Transitioning from the funicular to the pendular regime in granular soils. *Géotechnique*, *72*(9), 825-831. https://doi.org/10.1680/jgeot.20.P.141

Zhang, J. R., Xu, M. D., Christidis, G. E., & Zhou, C. H. (2020). Clay minerals in drilling fluids: functions and challenges. *Clay Minerals*, *55*(1), 1-11. https://doi.org/10.1180/clm.2020.10

Zheng, X., Li, X., & Xu, Y. (2022). Study on the shear strength and micro-structure of Gaomiaozi bentonite under chemical conditions in a repository, *Environmental Earth Sciences*, *81*(13), 1-11. https://doi.org/10.1007/s12665-022-10461-2

Zlatović, S., & Ishihara, K. (1995). On the influence of nonplastic fines on residual strength. First international conference on earthquake geotechnical engineering, 95, 239-244.

CURRICULUM VITAE

Name: Süleyman Demir

EDUCATION

2015-2017 MSc in Geotechnical Engineering, University of Gaziantep, Turkey.

2011-2015 BSc in Civil Engineering, Selçuk University, Turkey

EMPLOYMENT

Kilis 7 Aralık University- 2017 - Research assistant

Publications

A. Journal Papers (International)

A.10 Demir, S., Cabalar, A. F., Dispersion, viscosity, unconfined compression and bender element testing of bentonite-waste glass mixtures. European Journal of Environmental and Civil Engineering. https://doi.org/10.1080/19648189.2023.2231527

A.9 Cabalar, A. F., Akbulut, N., Demir, S., Yildiz, O. (2023). Use of a biopolymer for road pavement subgrade. Sustainability, 15(10), 8231. https://doi.org/10.3390/su15108231

A.8 Cabalar, A. F., Demir, S. (2022). Geotechnical properties of a bentonite treated with waste glass grains. Arabian Journal of Geosciences, 15(9), 1-9. https://doi.org/10.1007/s12517-022-10169-4

A.7 Cabalar, A. F., Hama, S. O., Demir, S. (2022). Behaviour of a clay and gravel mixture. The Baltic Journal of Road and Bridge Engineering, 17(1), 98-116. https://doi.org/10.7250/bjrbe.2022-17.553

A.6 Cabalar, A. F., Demir, S., Khalaf, M. M. (2021). Liquefaction resistance of different size/shape sand-clay mixtures using a pair of bender element–mounted molds. Journal of Testing and Evaluation, 49(1), 509-524. https://doi.org/10.1520/JTE20180677

A.5 Cabalar, A. F., Demir, S. (2020). Fall-cone testing of different size/shape sands treated with a biopolymer. Geomechanics and Engineering, 22(5), 441-448. https://doi.org/10.12989/gae.2020.22.5.441

A.4 Karakan, E., Demir, S. Observations and findings on mechanical and plasticity behavior of sand-clay mixtures. Arabian Journal of Geosciences, 13, 983 (2020). https://doi.org/10.1007/s12517-020-05762-4

A.3 Cabalar, A.F., Demir, S. (2019). Fall-cone testing of unsaturated sand-clay mixtures. Proceedings of the Institution of Civil Engineers-Geotechnical Engineering, 172 (5), 432-441. https://doi.org/10.1680/jgeen.18.00155.

A.2 Karakan E., Demir, S. (2018) "Effect of fines content and plasticity on undrained shear strength of quartz-clay mixtures", Arabian Journal of Geosciences 11, 743. https://doi.org/10.1007/s12517-018-4114-1.

A.1 Demir, S., Çabalar, A.F. (2017) "Sewage sludge ash in soil improvement", The International Journal of Energy & Engineering Sciences, 3(2), 4-9.

B. Journal Papers (National)

B.4 Karakan E., Demir, S. (2018) "Liquid limit determination of various sand clay mixtures by Casagrande and fall cone test methods", Balıkesir Üniversitesi Fen Bilimleri Enstitüsü Dergisi, 20(2) 1-11.

B.3 Cabalar, A.F., Demir, S., Akbulut N. (2018). Kil-kum Karışımlarının Bazı Geoteknik Özellikleri", Dicle Üniversitesi Mühendislik Fakültesi Dergisi, 9(2), 871-879.

B.2 Karabash Z., Cabalar, A.F., Demir, S. (2018) "Narlı kumunun üç eksenli kayma davranışı", Çukurova Üniversitesi Mühendislik Mimarlık Fakültesi Dergisi, 33(2), 177-188.

B.1 Karakan E., Demir, S. (2018) "Relationship between undrained shear strength with atterberg limits of kaolinite/bentonite–Quartz Mixtures" Uluslararası Mühendislik Araştırma ve Geliştirme Dergisi, 10 (3), 92-102.

C. International Conference Papers:

C.12. Demir, S., Cabalar, A. F (2023). Fall-cone testing of the waste glass-bentonite Mixtures, 12th International İstanbul Scientific Research Congress on Life, Engineering, and Applied Sciences, 56-62.

C.11. Demir, S., Cabalar, A. F (2023). Dispersive potential of the waste glass-bentonite Mixtures, 12th International İstanbul Scientific Research Congress on Life, Engineering, and Applied Sciences, 51-55.

C.10 Demir, S., Cabalar, A. F (2019). Undrained shear strength values of clay-sewage sludge ash mixtures, International Conference on Innovation, Sustainability, Technology and Education in Civil Engineering, 314-318

C.9 Karakan E., Demir, S. (2019), "Stress–Strain relation and strength characteristics of sand clay mixtures" International Civil Engineering and Architecture Conference, Trabzon, Turkey, 509-513.

C.8 Karakan E., Demir, S. (2019), "Gradation effects on the strength properties of bentonite sand mixtures" International Civil Engineering and Architecture Conference Trabzon, Turkey, 504-508.

C.7 Demir, S., Karakan E., (2018), "Strength properties of bentonite-quartz mixtures, II. International Scientific and Vocational Studies Congress, Nevşehir, Turkey, 1300-1305.

C.6 Demir, S., Cabalar, A.F. (2018), "Effect of sewage sludge ash on the strength of a clay, The International Conference on Sustainable Energy and Environment Sensing, University of Cambridge, Cambridge, United Kingdom.

C.5 Demir, S., Karakan E., (2018), "Plastic limit estimation from fall-cone test method, II.International Scientific and Vocational Studies Congress, Nevsehir, Turkey, 1295-1299.

C.4 Demir, S., Cabalar, A.F. (2018), “Some geotechnical properties of clays in Gaziantep Turkey”. International Congress on Engineering and Architecture (ENAR), 2104-2107.

C.3 Karakan E., Demir, S. (2018), “Relationship between undrained shear strength and Atterberg limits of clay soils” II. International Scientific and Vocational Studies Congress, Nevşehir, Turkey.

C.2. Alosman S., Demir S., Cabalar A.F. (2018). Effect of stone powder on Atterberg’s limits of an organic soil. International Congress on Engineering and Architecture (ENAR), Turkey, 2108-2111.

C.1 Karakan E., Demir, S. (2018), “Relationship between cone penetration and undrained shear strength of Sand-Clay Mixtures” II. International Scientific and Vocational Studies Congress, Nevşehir, Turkey, 673-676.

D. National Conference Papers:

D.1 Demir S., Cabalar A.F., Akbulut N. (2016) Kum kil karışımlarının şişme özellikleri, Zemin Mekaniği ve Geoteknik Mühendisliği 16. Ulusal Kongresi, 1051-1056.